ANALYSIS OF SINGLE PHASE CONVECTIVE HEAT TRANSFER IN MICROCHANNELS WITH VARIABLE THERMAL CONDUCTIVITY AND VARIABLE VISCOSITY

A THESIS SUBMITTED TO
THE GRADUATE SCHOOL OF NATURAL AND APPLIED SCIENCES
OF
MIDDLE EAST TECHNICAL UNIVERSITY

BY

ARİF CEM GÖZÜKARA

IN PARTIAL FULLFILLMENT OF THE REQUIREMENTS
FOR
THE DEGREE OF MASTER OF SCIENCE
IN
MECHANICAL ENGINEERING

FEBRUARY 2010

Approval of the thesis:

ANALYSIS OF SINGLE PHASE CONVECTIVE HEAT TRANSFER IN MICROCHANNELS WITH VARIABLE THERMAL CONDUCTIVITY AND VARIABLE VISCOSITY

submitted by **ARİF CEM GÖZÜKARA** in partial fulfillment of the requirements for the degree of **Master of Science in Mechanical Engineering Department, Middle East Technical University** by,

Prof. Dr. Canan Özgen _____
Dean, Graduate School of **Natural and Applied Sciences**

Prof. Dr. Suha Oral _____
Head of Department, **Mechanical Engineering**

Asst. Prof. Dr. Almıla Güvenç Yazıcıoğlu _____
Supervisor, **Mechanical Engineering Dept., METU**

Prof. Dr. Sadık Kakaç _____
Co-Supervisor, **Mechanical Engineering Dept., TOBB-ETU**

Examining Committee Members:

Asst. Prof. Dr. Derek K. Baker _____
Mechanical Engineering Dept., METU

Asst. Prof. Dr. Almıla Güvenç Yazıcıoğlu _____
Mechanical Engineering Dept., METU

Asst.Prof. Dr. Merve Erdal _____
Mechanical Engineering Dept., METU

Asst. Prof. Dr. Cüneyt Sert _____
Mechanical Engineering Dept., METU

Asst. Prof. Dr. Selin Aradağ _____
Mechanical Engineering Dept., TOBB-ETU

Date: 01.02.2010

I hereby declare that all information in this document has been obtained and presented in accordance with academic rules and ethical conduct. I also declare that, as required by these rules and conduct, I have fully cited and referenced all material and results that are not original to this work.

Name, Last Name : Arif Cem Gözükara

Signature :

ABSTRACT

ANALYSIS OF SINGLE PHASE CONVECTIVE HEAT TRANSFER IN MICROCHANNELS WITH VARIABLE THERMAL CONDUCTIVITY AND VARIABLE VISCOSITY

Gözükara, Arif Cem

M.Sc. Department of Mechanical Engineering

Supervisor: Asst. Prof. Dr. Almıla Güvenç Yazıcıoğlu

Co-Supervisor: Prof. Dr. Sadık Kakaç

February 2010, 243 Pages

In this study simultaneously developing single phase, laminar and incompressible flow in a micro gap between parallel plates is numerically analyzed by including the effect of variation in thermal conductivity and viscosity with temperature. Variable property solutions for continuity, momentum and energy equations are performed in a coupled manner, for air as a Newtonian fluid. In these analyses the rarefaction effect, which is important for the slip flow regime, is taken into account by imposing slip velocity and temperature jump boundary conditions to the wall boundaries. Mainly, the influence of viscous dissipation, axial conduction, geometric parameters and rarefaction on the property variation effect is aimed to be discussed in detail. Therefore, the effects of variable thermal conductivity and viscosity are investigated simultaneously with the effects of rarefaction, geometric parameters, viscous dissipation and axial conduction. The difference between constant and variable solutions in terms of heat transfer characteristics is related to the effects of viscous dissipation axial conduction and rarefaction. According to results, property variation is substantially effective in

the entrance region where temperature and velocity gradients are high. On the other hand, property variation effects are not significant for fully developed air flows in microchannel.

Keywords: Heat transfer, microchannel, thermal conductivity variation, viscosity variation, slip flow

ÖZ

TEK FAZLI MİKROKANAL AKIŞINDA KONVEKSİYONEL ISI TRANSFERİNİN DEĞİŞKEN ISIL İLETKENLİK KATSAYISI VE DEĞİŞKEN VİSKOZİTE İLE İNCELENMESİ

Gözükara, Arif Cem

Yüksek Lisans Makine Mühendisliği

Tez Yöneticisi: Yard. Doç. Dr. Almıla Güvenç Yazıcıoğlu

Ortak Tez Yöneticisi: Prof. Dr. Sadık Kakaç

Şubat 2010, 243 Sayfa

Bu çalışmada hidrodinamik ve ısıl olarak gelişmekte olan, laminar, tek fazlı ve sıkıştırılamaz mikrokanal akışında değişken özniteliklerin etkisi incelenmiştir. Paralel plakalar arasındaki mikrokanallardaki akışın modellenmesinde sayısal yöntemlerden faydalanılmıştır. Kaygan akış rejiminin incelendiği çalışmada sabit duvar sıcaklığı sınır koşulu kullanılmıştır. Değişken özniteliklerin hesaba katılabilmesi amacıyla hareket ve enerji denklemleri birlikte çözülmüştür. Momentum ve enerji denklemlerinin birlikte çözümüne ek olarak, basınç ve hız değişkenlerinin de çözümü eşlenerek gerçekleştirilmiştir. Kaygan akış rejimi, duvar kayması ve sıcaklık sıçraması duvar sınır koşulları kullanılarak modellenmiştir. Seyrelme, sürtünme kaybı, eksen boyunca ısı iletiminin etkileriyle birlikte, değişken ısıl iletkenlik katsayısı ve viskozitenin akışkanın ısı transferi karakteristiğine etkileri detaylı olarak tartışılmıştır. Değişken ısıl iletkenlik katsayısı ve viskozitenin etkilerinin anlaşılabilmesi amacıyla hem değişken hem de sabit ısıl iletkenlik ve viskozite için çözümler gerçekleştirilmiştir. Elde edilen sonuçlar değerlendirildiğinde değişken ısıl

iletkenlik katsayısı ve viskozitenin giriş bölgesinde kayda değer bir farka sebep olduğu, fakat tam gelişmiş akış için sabit özniteliklerden ciddi bir fark göstermediği görülmüştür.

Anahtar Kelimeler: Isı transferi, mikrokanal, değişken ısıl iletkenlik katsayısı, değişken viskozite, kaygan akış

to my family…

ACKNOWLEDGEMENTS

I like to thank to my supervisor Asst. Prof. Dr. Almıla GÜVENÇ YAZICIOĞLU for the endless support, encouragement and patience during my research activities.

I would also like to express my sincere appreciation to my co-supervisor, Prof. Dr. Sadık KAKAÇ for his boundless support, excellent supervision and endless patience in addition to invaluable comments and contributions. I am also grateful to him for his perfect supervision in the every aspect of life.

I am thankful to my superior Dr. Ali ÇOLAKOĞLU for the encouragement guidance and mentoring. His invaluable advices helped me a lot to gain a foresight about both academic and professional life.

I would like to state my thanks to Murat BARIŞIK for his technical support and intimate friendship.

I would like to thank to Başar BULUT and Barbaros ÇETİN for their support, help and friendship.

I owe a sincere appreciation to my ancestors, who had survived through misery, poverty and wars, for the inspiration to overcome the difficulties that I had came across.

I would like to express my appreciation to my colleagues Ahmet Levent AVŞAR, Berkan BÜYÜKDAĞLIOĞLU, Gökhan CÜYLAN, Kaan Kubilay ÖZSOY, and

Derya AKKUŞ for providing me the necessary computational power and the patience during the day long runs.

I also would like to thank Güvenç CANBALOĞLU and Kamil Mert ÇAKAR for their useful comments and their continuous support beyond their ingenuous friendship.

I would like to thank to my colleagues Berkan ERDOĞMUŞ and Mustafa OCAK for their devoted work which makes everything to proceed hassle-free during my absence in the company.

I wish to express my deepest gratitude to my family who had endlessly and unconditionally supported me throughout my life. Especially I would like to state my sincere appreciation to my grandmother for her endless love, encouragement, and support. Unfortunately, words would be inconclusive to express my feelings toward my family.

Also I would like to thank to ASELSAN Inc. for supporting my research activities and providing the necessary computational power.

Also I would like to thank to TÜBİTAK for the financial support throughout this work.

TABLE OF CONTENTS

LIST OF TABLES

TABLES

LIST OF FIGURES

FIGURES

NOMENCLATURE

Br	Brinkman number, $Br = \mu U / k\,(T_i - T_w)$
c_p	constant pressure specific heat, *J/kgK*
D_h	hydraulic diameter
F_M	tangential momentum accommodation factor
F_T	thermal accommodation factor
H	half channel spacing
h	convective heat transfer coefficient, W/m^2K
k	thermal conductivity, *W/mK*
Kn	Knudsen number, $Kn = \lambda / L$
L	channel length, *m*
Nu	Nusselt number
P	pressure, *Pa*
Pe	Péclet number, $Pe = Re.Pr$
Pr	Prandtl number, $Pr = \mu\, c_p / k$
Re	Reynolds number, $Re = \rho\, U\, L / \mu$
T	temperature, *K*
u	velocity in axial direction, m/s
u_s	slip velocity, *m/s*
v	velocity in longitudinal direction
x	axial coordinate axis
y	vertical coordinate axis

Greek Symbols

α	thermal diffusivity, m^2/s
γ	weighting factor
μ	dynamic viscosity, kg/ms
ρ	density, kg/m^3
λ	mean free path, m
θ	dimensionless temperature
τ	dimensionless time

Subscripts

i	axial node values
j	vertical node values
imax	last axial node value
jmax	last vertical node value
boundary	values at the boundary
mean	mean values
wall	wall values
x	local values
∞	free stream parameter
vp	temperature variable thermophysical property
cp	constant thermophysical property

Superscripts

*	Non-dimensional parameter
n	time step

CHAPTER 1

INTRODUCTION

The need for maximizing the performance of micro mechanical systems and electronic components urges the minimization of dimensions. Minimized dimensions come along with a complex heat transfer and fluid flow problem within these devices and components. This newly introduced phenomenon is called “Microscale fluid flow and heat transfer” because of related dimensional magnitudes. It is important to point out that, fluid flow and heat transfer in microscale cannot be characterized by the macroscale approaches. For instance, the early transition from laminar to turbulent regime, friction factors a few times higher than expected, and higher heat transfer coefficients observed in the laminar rather than the turbulent regime, are some of the indications that conventional theories used in macroscale fluid flow and heat transfer become inadequate for modeling in microscale. An observation of the studies in the field and related reviews on the subject give the impression that every result obtained by the researchers was considered as surprising. Additionally, a small percentage of the results converge to a point where microflow is subjected to discussion. On the other hand, the miniaturization trend in manufacturing micro devices and electrical components increases every year. For a variety of fields in which these micro devices are used; such as, biomedical, micro fabrication, and optics, fluid flow and heat transfer need to be understood and modeled with an acceptable reliability. This urgent need for comprehending the mechanisms behind heat transfer and fluid flow phenomena in microscale canalized the researchers to the

issue. Since the fluid flow and heat transfer characteristics of microflow cannot be modeled with the conventional theoretical models, some new methods have been introduced by different researchers. In general, some extensions are made to conventional methods by including the scaling effects that become important for modeling microflows. On the other hand, some researchers prefer using models that are used for molecular gas flow, which are probabilistic and deterministic methods. The major effects that become important for microscale flow and usually negligible for macroscale flow can be listed as follows:

- Surface roughness effect
- Electrokinetic forces between fluid and wall boundaries-for liquids
- Rarefaction effects-for gases

By considering the dominance of these effects, it is possible to make a distinction between micro and macro flows. Unfortunately there is no existing common definition for "micro" scale. Therefore it is appropriate to follow the dimensional scale offered by Kandlikar and Grande [1] for classifying channel flows in micro scale.

1 μm $< C_D <$ 10 μm	: Transitional Microchannels
10 μm $< C_D <$ 200 μm	: Microchannels
200 μm $< C_D <$ 3 mm	: Minichannels
3 mm $< C_D$	: Conventional passages

C_D represents the minimum dimension of the microchannel. This classification is used for gaseous flows in channels, which is the main point of interest in this study. Numerous extensive studies in the field of micro scale fluid flow and heat transfer continue to move towards converging to common results as the time passes.

1.1 Modeling

As stated by Gad-el-Hak [2] and as shown in Figure 1.1, the flow field can be modeled in two different ways. In the first one the flow field is treated as a collection of particles and this approach is named as molecular approach. The second one is continuum approach, in which the flow field is assumed to be infinitely divisible and continuous [2]. Macro scale flow problems are associated with the continuum model. In this model, the flow variables such as velocity, pressure, and density are defined for every point in space and time [2].

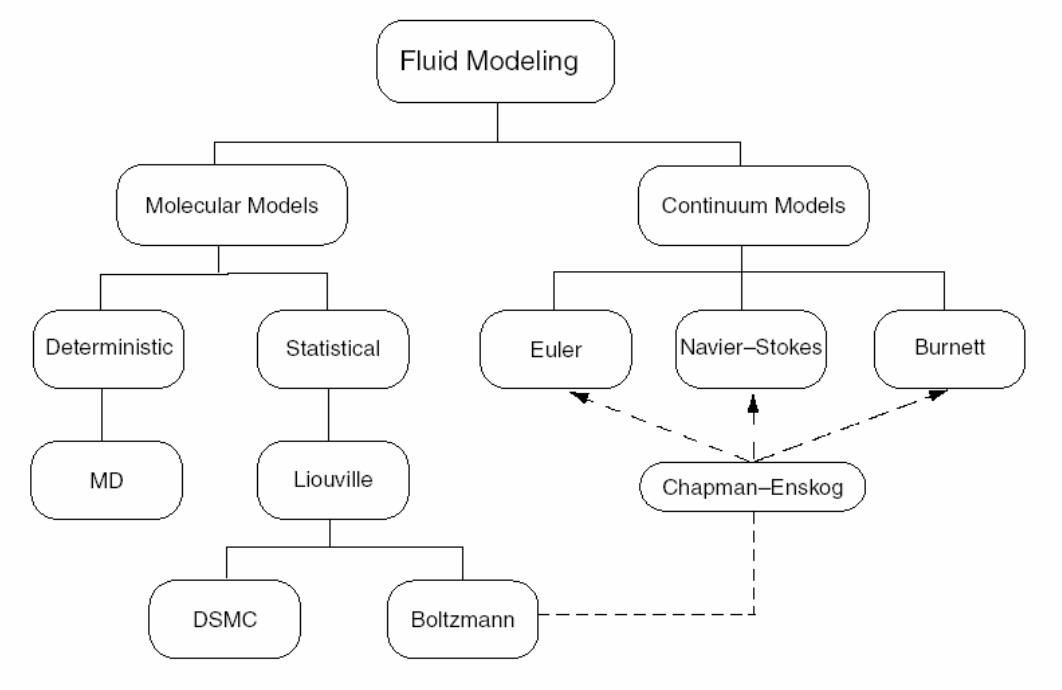

Figure 1.1 Molecular and continuum flow models [2]

Using the conservation principles, continuum can be modeled in terms of mass, momentum, and energy. Partial differential equations based on mass and

momentum conservation are named as Navier-Stokes equations. Likewise the partial differential form of the energy conservation equation is named as energy equation. The ease of handling these equations mathematically makes them a preferable tool for modeling flow fields, as long as the continuum approach is applicable. On the other hand, these equations disregard the molecular nature of gases and it is not possible to model dilute and rarefied gas flows, which are far from being a continuous media. Additionally, it should be noted here that the classical no-slip boundary condition between fluid-solid interfaces is likely to fail before the flow becomes free-molecular. Since the area of interest in this study is gases, discussions will be based on gaseous flows.

To make a further distinction between continuous media and free-molecular flow, another parameter, "mean free path" is needed to be introduced. Mean free path represents the average distance traveled by gas molecules before they collide with each other. However, a distinction cannot be made for the flow by just considering the mean free path. For this purpose this mean free path should be compared with the characteristic dimension of the flow. Continuum model can be valid when mean free path of the gas is much smaller than the characteristic dimension of the flow. The ratio of mean free path and characteristic dimension of the flow is defined as Knudsen number characterizing the flow.

$$Kn = \frac{\lambda}{D_h} \tag{1.1}$$

Where λ is the mean free path and D_h is the characteristic dimension of the flow. Furthermore a classification of flow regimes based on Knudsen number is available in various resources. A scale proposed by Gad-el-Hak [3] is given in Figure 1.2.

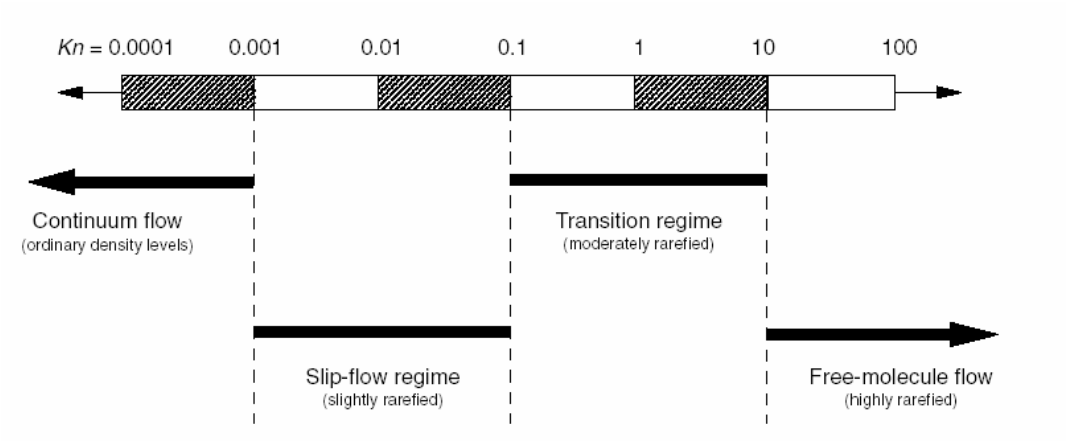

Figure 1. 2 Knudsen number regimes [3]

The region in which Knudsen number varies between 0.1 and 0.001 is named as slip-flow regime in Figure 1.2. The range of Knudsen number will be within these limits throughout this study, and therefore the area of interest will be the slip-flow regime. In this flow regime, the collisions between wall and fluid particles are not as frequent as the collisions taking place in continuum flow. The amount of collisions in slip-flow regime will not be enough to establish a thermodynamic equilibrium between wall and fluid particles. Thus, no-slip and no-temperature jump boundary conditions that are used in continuum regime, will no longer be valid in the absence of thermodynamic equilibrium.

The reflection of fluid molecules from the wall after a collision may occur in two different ways. The first one is specular reflection, in which fluid molecules conserve their tangential momentum. The second one is diffuse reflection, which is completely random and uncorrelated. In the second type, for balancing the tangential momentum, a finite slip velocity will exist at the wall. Expression for

the slip velocity for Cartesian coordinates is given below. Background of the subject is discussed in detail by Larrode *et al.* [4].

$$u_{gas} - u_{wall} = \frac{2-\sigma_v}{\sigma_v}\lambda\left(\frac{\partial u}{\partial y}\right)_w + \frac{3}{4}\frac{\mu}{\rho T_{gas}}\left(\frac{\partial u}{\partial x}\right)_w \tag{1.2}$$

The σ_v is tangential momentum accommodation factor, λ is mean free path of the fluid, μ is dynamic viscosity and ρ is the density of the fluid in Equation 1.2. This equation is derived by Maxwell [5] for an isothermal wall based on the kinetic theory. The tangential momentum accommodation coefficient basically refers to the fraction of diffusely reflected molecules. This coefficient varies from 0 to 1 for different solid-fluid combinations. This experimentally determined coefficient is usually taken as 1 for most of the applications [6]. Additionally the second term in the equation is named as thermal creep, which represents the portion of slip velocity in the direction opposite to the tangential heat flux. After non-dimensionalization is applied to the slip velocity equation, the thermal creep term becomes a function of the second order of Knudsen number, which makes this term insignificant for small Knudsen numbers. Detailed explanation and formulation is given by Gad-el Hak [2]. A similar expression for the temperature jump boundary condition at the wall is proposed by von Smoluchowski [7].

$$T_s - T_{wall} = \frac{2-\sigma_T}{\sigma_T}\left[\frac{2\gamma}{\gamma+1}\right]\frac{\lambda}{\mathrm{Pr}}\left(\frac{\partial T}{\partial y}\right)_w \tag{1.3}$$

In Equation 1.3, σ_v is the thermal accommodation coefficient, the ratio of energy accommodated by the diffusely reflected molecules. This coefficient varies between 0 and 1. It is also determined experimentally and the value depends on the solid-fluid combination, surface roughness, and temperature difference at the

fluid-solid interface. According to various sources (e.g. [8] and [9]), thermal accommodation coefficients are taken as unity in most analyses.

1.2 Scope of the study

In addition to those mentioned in the previous section, there are some other effects usually neglected in the macroscale flows that may become significant for the microscale. One of these is the effect of axial heat conduction in the fluid, which is generally insignificant for the macro scale flows where effect of conductive heat transfer is relatively high. Since the Reynolds and Péclet numbers become smaller, axial conduction is significant in micro flows. Another term that is usually neglected in macro-flow modeling is the viscous dissipation. According to Shah and London [10], one of the cases where viscous dissipation becomes significant is the microscale duct flow with low flow velocities and low temperature differences at the wall-fluid interface. At this point Brinkman number needs to be introduced, which is a measure of the relative significance of the viscous dissipation in a flow [11]. Additionally Brinkman number can be related with the temperature-variable property effects on convective heat transfer [12]. The dimensionless numbers mentioned here will be discussed in detail in the following Chapters.

In this study, the effects of temperature-variable viscosity and thermal conductivity will be investigated in two-dimensional rarefied microchannel flows. Therefore momentum equations will be solved fully coupled with the energy equation to include the effects of thermal conductivity and viscosity variation in the flow field and temperature field calculations. Additionally, axial conduction and viscous dissipation terms will be included in the numerical model, since these terms become significant for microscale heat transfer. Velocity and pressure variables will be solved in coupled manner, since flow is simultaneously

developing. An explicit method is preferred in numerical solution for being simple and not very costly in terms of computational load.

In Chapter 2, previous studies related with microchannels will be summarized to comprehensively outline the issue. Analytical, numerical, and experimental studies will be discussed. The studies related to property variation microchannel flows available in the literature, will also be discussed in this part. Chapter 3 is dedicated to the formulation and numerical solution methods for parallel plate microchannels for both constant and variable thermophysical properties. Detailed explanation for the formulation and numerical modeling will be presented in this chapter. The results will include two different flow conditions, which are fluid heating and cooling. In Chapter 4 the obtained results for both flow conditions and the effects of rarefaction, viscous heating, and axial conduction on temperature-variable properties, will be discussed in detail. Discussions will be made for both constant and variable property solutions in combination with the related parameters. Finally in Chapter 5, the study will be summarized and concluded with final remarks.

CHAPTER 2

LITERATURE SURVEY

Research on heat transfer in microchannels and microtubes is mainly driven by the developments in the electronics technology. The need for maximizing the performance of electronic components urges the minimization of dimensions. Minimized dimensions come along with a complex heat transfer problem. This newly introduced heat transfer phenomenon is called “microscale heat transfer” because of related dimensional magnitudes. It is important to point out that, fluid flow and heat transfer in microscale may not be characterized by the macroscale approach. The urgent need for comprehending the mechanisms behind the heat transfer and fluid flow behavior in microscale has forced researchers to focus on the issue. In this Chapter, mainly, previous studies related with microscale fluid flow and heat transfer will be reviewed. Available studies about variable property solution of fluid flow and heat transfer problems in microscale will also be discussed. It is possible to divide this chapter into four subsections regarding the subjects reviewed. In the first part, fundamental studies about microscale flow and property variation in macroscale will be reviewed briefly. In the second part, available studies about temperature variable property solutions in microscale will be discussed. The third part will be dedicated to studies related with the effects of viscous dissipation and rarefaction. In the final part studies combining experimental and numerical work about microscale flow will be discussed.

One of the well known earliest studies related to microchannels was conducted by Tuckerman and Pease [13] who investigated the convective cooling of electronic

components by using microchannel heat sinks. A significant result that can be driven out from their study is the observation of higher heat transfer coefficients in laminar regime rather than turbulent. This result increased the interest for the investigation of laminar convection in microchannels. In the middle of the 1990's Peng and Peterson [14] published the results of their experimental study about single phase convective heat transfer in microchannels. This study mainly focused on the classification of flow regimes in terms of Reynolds number and the investigation of the effect of geometry on fluid flow and heat transfer. It is stated that, laminar flow is observed for Reynolds numbers less than 400. In addition to these fundamental studies about microscale fluid flow and heat transfer, previous work on variable property solutions in both macro and microscale heat transfer problems should be mentioned. One of the earliest studies has been conducted by Deissler [15]. Fully developed laminar flow in tubes by considering the property variation along the radius was investigated in this study. A similar study was performed by Oskay and Kakaç [16] to examine the effect of viscosity variation with temperature in pipe flow.

Various scientists have been involved with the property variation in macroscale heat transfer. It is possible to say that in macroscale, property variation is a well understood concept and methods and correlations have been developed to account for property variation such as the property ratio method. In recent years, with the increasing importance of microscale heat transfer, effect of property variation became a point of interest in this field. Li *et al.* [17] studied variable thermophysical property effect on a three dimensional microchannel model. A finite difference code utilizing Tri-Diagonal Matrix Algorithm was developed for solving temperature and velocity fields. In their study, hydrodynamically fully developed, thermally developing liquid flow was investigated by neglecting viscous dissipation effects. Average Nusselt numbers were taken as a reference for comparison of the results. When the results are examined, it is possible to see

that the variation in liquid thermophysical properties with temperature, significantly affects the flow and heat transfer.

The effects of thermophysical property variation on heat transfer and fluid flow in microchannels has been comprehensively discussed by Gulhane and Mahulikar [18]. In this study, the researchers worked on a two-dimensional axisymmetrical numerical model. Two different cases were examined throughout the study, which are simultaneously developing flow and hydrodynamically fully developed, thermally developing pipe flow. In the modeling constant wall heat flux boundary condition is used with the laminar, incompressible flow assumptions. In addition to these assumptions, axisymmetric swirl terms in momentum equation, compressibility and viscous dissipation terms in energy equation are neglected. Variation of viscosity, density, specific heat, and thermal conductivity is taken as a function of temperature during the formulation. The role of each thermophysical property variation is discussed separately and in combination with each other for two different cases. The results of their study can be summarized in Figure 2.1.

Thermophysical properties	Effect on	
	Velocity field	Temperature field
Density (ρ)	Direct effect. Flattens axial profile (significant)	Direct effect (significant)
Specific heat (C_p)	Indirect effect (insignificant)	Direct effect. Reduces ($T_w - T_m$) at high temperature (significant)
Viscosity (μ)	Direct effect. Sharpens axial profile (significant)	Indirect effect (insignificant)
Thermal conductivity (k)	Indirect effect. Flattens axial profile (significant)	Direct effect. Flattens temperature profile (significant)

Figure 2.1 Effect of thermo physical property variation on flow and temperature field [18]

Another important study was performed by Peng *et al.* [12] who had investigated the variable property effect for hydrodynamically fully developed, thermally developing flow with a two dimensional model. In their model, Peng and his colleagues assumed that the flow is laminar and incompressible. Moreover, they assumed that specific heat of the fluid is constant. Viscosity and thermal conductivity are taken as single variable functions of temperature. In their mathematical formulation viscous dissipation terms in the energy equation are not neglected.

Temperature dependent viscosity of liquid water is expressed by Peng *et al.* [12] as follows

$$\mu(T) = \mu(T_{ref})\left(\frac{T}{T_{ref}}\right)^{n} \exp\left[B\left(T^{-1} - T_{ref}^{-1}\right)\right] \tag{2.1}$$

In Equation (2.1) T_{ref} is taken as 293 K, n 8.9, and B 4700. Similarly, the thermal conductivity of water is expressed as a cubic polynomial function of temperature, which is given as follows.

$$k(T) = a_0 + a_1 T + a_2 T^2 + a_3 T^3 \tag{2.2}$$

Nusselt number increase and velocity profile change along the channel are discussed in detail. It is stated that the increase in Nusselt number resulting from variable property solution becomes significant for high heat flux values. Moreover, a formula is proposed for predicting Nusselt number obtained with the variable property solution. The formula presented is given below.

$$\frac{Nu_{vp}}{Nu_{cp}} = 1 + \varepsilon K_k \bar{h}_B + \left[K_\rho \left(\frac{206}{605} - \frac{232}{1815} \frac{1}{\mathrm{Pr}_0} \right) - K_\mu \frac{13}{121} + K_k \frac{148}{605} + K_C \frac{309}{1210} \right] + O\left(\varepsilon^2\right) \tag{2.3}$$

Here,

$$\varepsilon = (11/24)(q_w'' R / k_0 T_0) \tag{2.4}$$

$$\bar{h}_B = (48/11\mathrm{Pr}_0)x \tag{2.5}$$

$$K_\alpha = \left(\frac{T}{\alpha}\right)\left(\frac{\partial \alpha}{\partial T}\right)_0 \tag{2.6}$$

Another important research, closely related with the property variation in microchannels was conducted by Nonino *et al.* [19]. In their work Nonino and his colleagues investigated the effect of viscous dissipation and variable dynamic viscosity in microchannels with arbitrary cross-sections for simultaneously and thermally developing flows. They developed a finite element based numerical solver for solving Navier Stokes equations for three dimensional and axisymmetrical geometries. Constant wall temperature boundary condition was used in calculations. Dynamic viscosity variation with temperature was considered in a range, in which, the ratio of the viscosity value at the inlet temperature to the viscosity value at the wall temperature is between 2 and 0.5. The research focused on the variation of Nusselt number with viscosity variation and viscous dissipation. In addition to Nusselt number they also investigated pressure drop and friction coefficient variations with Brinkman number and viscosity variation.

Formerly a similar study was performed by Koo and Kleinstreuer [20]. They comprehensively investigated the significance of viscous dissipation in micro-scale convective heat transfer, in addition to fluid property, geometrical, and flow regime effects. Their numerical model was capable of solving hydrodynamically fully developed and thermally developing incompressible laminar flow. Main point of discussion in their research was change in the significance of viscous dissipation with channel size, aspect ratio, Reynolds numbers and viscosity variation. The results of this study point out that the variation of viscosity has stronger effects on viscous dissipation for comparatively small channel size. In addition to this, they proposed that viscous dissipation strongly affects the friction factor calculations and should be accounted for in micro flows.

Temperature dependent fluid properties in micro flows was investigated by Mahulikar *et al.* [21] by solving one dimensional numerical model for momentum and energy equations with variable thermophysical properties. They stated that it is possible to simulate the decrease in Nusselt number with increasing Reynolds number in microchannels with a one dimensional analysis by including the thermoproperty variation effect.. Based on this Herwig and Mahulikar [22] extended the scope of their investigation. In their work, the importance of variable property effects in micro-sized geometries was discussed by using an order of magnitude approach. Additionally numerical solutions were performed to visualize the effect of temperature variable thermophysical properties. There are four different models proposed in their study. The first is one is the constant property model, in which the property in consideration has a single value along the solution domain. The second is the quasi-constant properties model, in which the properties vary with the mean temperature of the fluid at a given axial position. The third model was named as weakly-variable property model. In this model, the property variation in radial/longitudinal direction is directly included and quasi-constant property model is used for the variation in axial direction. The last one is called as strongly-variable property model, which should be used when

property variations in both radial and axial directions is equally strong. It is stated that, for micro-sized geometries, axial temperature gradients are as large as the radial ones, so the fourth one is the most appropriate method for modeling property variation. The strongly-variable property model enforces the fully coupled solution of energy and momentum equations. The working fluid in their study was water and the variation of specific heat and density with temperature was negligible. Thus, only the variation of viscosity and thermal conductivity was accounted for. The authors solved laminar, incompressible, steady micro pipe flow by neglecting viscous dissipation, numerically. According to the results, Nusselt number differs up to %30 when property variation is included. This study is one of the most fundamental works that justifies the significance of variable property solution in microscale fluid flow heat transfer.

El-Genk and Yang [23] numerically investigated the effects of viscous dissipation, slip wall boundary condition, and viscosity variation on pressure drop and friction factors in microchannel flow. In the study mainly, the effect of flow variables on fluid flow is discussed. However, energy equation is also solved for determining the effect of viscous dissipation and viscosity variation with temperature. Experimentally determined slip length values are used for imposing the slip wall boundary condition. Results of their study point out that it is important to include the effect of viscosity variation for accurately determining the friction factors in a thermally developing microchannel flow. A study related with the application was performed by Li *et al.* [24], about thermal property variations in rectangular microchannels. They proposed that conventional macroscale theories are capable of predicting the flow and heat transfer characteristics for the dimensions and Reynolds numbers used in their work. The hydraulic diameter of the channel used is 0.333 mm and Reynolds number changes between 101 and 1775. The results of their numerical work agree well with the Sieder and Tate correlation [25] and the results of experiments.

Unfortunately when Reynolds number range and dimensions are considered, the flow can be classified as a macro-sized flow.

As is has been previously stated in the introduction, rarefaction is an important phenomenon for microscale flows. Wang and Yang [26] investigated slip flow in microchannels by using lattice-Boltzmann method. The results of the study agree well with the results of modified Navier-Stokes solutions. Barron *et al.* [27] made an extension to the Graetz problem by including slip flow effects. Since viscous dissipation and axial conduction terms are neglected in the Graetz problem, they were neglected in their study as well. Some correlations relating Nusselt number with Graetz and Knudsen number were proposed in the study. A brief result that can be derived from the study is the increase of Nusselt number with increasing Knudsen number for a given Graetz number. Jeong and Jeong [28] investigated the effects of viscous dissipation and axial conduction in, hydrodynamically fully developed, thermally developing microscale flow analytically by using eigenfunction expansion. They worked on simple flow model in two dimensions for both constant wall heat flux and constant wall temperature cases. Considering their results, it is possible to say that Nusselt number decreases with increasing Knudsen and Brinkman numbers, while it increases with increasing Péclet number.

Extended Graetz problem was also studied by Çetin *et al.* [29]. Eigenfunction expansion method was used for the analytical solution of the energy equation. The conclusion drawn from the study about the effects of Brinkman, Peclet and Knudsen number was same with the Jeong and Jeong's work. However in this study it was reported that thermal entrance length increases with decreasing Peclet number. An additional remark in this study is the reduction in the effect of Brinkman number on local Nusselt number with increasing rarefaction. A similar problem was also solved numerically by Çetin *et al.* later [30]. Most of the results were consistent with the results of their analytical work. The authors claimed that

the numerical model can be extended to more complex boundary conditions and solutions. In this study they overcame the instability problem introduced by the axial conduction terms in the thermally developing flow by extending the axial dimensionless length of solution domain from $+\infty$ to $-\infty$. For more information one may refer to [10].

Another important contribution in this area was made by Morini *et al.* [31] who investigated the effect of rarefaction on pressure drop and friction factor. They analyzed the rarefaction effect in trapezoidal, double trapezoidal, and rectangular silicon microchannels numerically and experimentally. Finite difference solution was made for incompressible flow with constant fluid properties. They concluded that friction factor reduction increases with increasing Knudsen numbers as expected. In addition to this, friction factor reduction increases with increasing aspect ratio for three different geometries. They stated that for gas flow in microchannels, the rarefaction effect can be analyzed separate from the compressibility effect, as long as the flow is incompressible. Similar results were obtained by Zhang *et al.* [32] who investigated slip flow characteristics of compressible gas flow. Zhang and his colleagues found out that compressibility effects become less significant and rarefaction effects become dominant for the low Reynolds number flows. According to the results of their study, slip velocity boundary condition defined at the walls makes the flow more incompressible than the no slip wall boundaries. Significance of compressibility effects for low Reynolds number flows are illustrated in Figure 2.2, where fRe is plotted versus the hydraulic diameter D_h (in μm) for Re = 10.

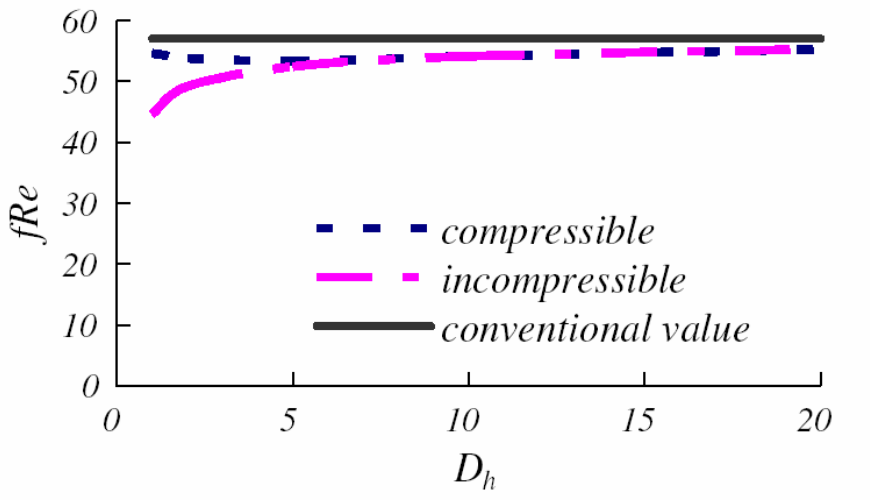

Figure 2.2 Variation of *f*Re with hydraulic diameter. Re =10 [32]

Compressibility and slip flow effects are also discussed by Hong *et al.* [33]. The study is mainly dedicated to investigate the characteristics of gaseous parallel-plate micro flows with no slip boundary condition, but they also presented the results of runs for slip wall boundary condition. Only constant wall heat flux case is studied by using ALE (Arbitrary Lagrangian-Eulerian) based numerical method. Similar to other studies, they proposed that as the flow velocity increases, slip flow effects become insignificant relative to compressibility effects. Moreover, velocity slip and temperature jump effects in microchannels were investigated in detail by Yu and Ameel [34]. They used an analytical model for solving the hydrodynamically fully developed, thermally developing flow by using integral transform technique. The main focus of their study was to investigate the effects of slip-flow parameters on heat transfer and fluid flow. Tunc and Bayazıtoğlu [35] studied the effect of aspect ratio and Knudsen number on heat transfer and fluid flow in rectangular microchannels. They made an analytical solution by using integral transform method. Only fully developed

conditions were considered in conjunction with constant wall heat flux boundary conditions in the study.

The effects of rarefaction and viscous dissipation in compressible gaseous flows were studied by Rij *et al.* [36]. They included slip velocity and temperature jump boundary conditions in their numerical model. Both constant temperature and constant wall heat flux boundary conditions were used as different cases. Effects of aspect ratio, Brinkman number, Knudsen number, Péclet number, and momentum and thermal accommodation factors were discussed in simultaneously developing flow. It is stated that for simultaneously developing flow, viscous dissipation and axial conduction effects should be accounted for. Another remarkable study on simultaneously developing flow in microchannels belongs to Nizamand *et al.* [37]. They investigated simultaneously developing flow in trapezoidal microchannels with Reynolds numbers ranging between 0.1 and 1 and Knudsen number changing between 0 and 0.1. In their study, both friction and heat transfer coefficients are inversely proportional with the Knudsen number in fully developed flow sections. On the other hand, Nusselt and Poiseuelle number reaches an asymptotic value as a result of high levels of velocity slip and temperature jump at the entrance region of the trapezoidal channels.

Tso and Mahulikar [11] aimed to explain the unusual behavior of convective heat transfer by understanding the effect of viscous dissipation. Throughout their study the main point of focus is to discuss physical meaning and significance of Brinkman number. They claimed that the unusual decrease in Nusselt number with increasing Reynolds number in laminar flow can be explained by the significance of viscous dissipation, thus with Brinkman number. In addition, the study includes correlations relating Brinkman number with the experimentally obtained Nusselt values. Simultaneously developing slip flow in rectangular microchannels was also discussed by Renskizbulut *et al.* [38]. They mainly focused on determining the effects of Reynolds number, aspect ratio, and

Knudsen number on simultaneously developing flow. In their study, only constant wall temperature boundary condition is used. Slip velocity at walls are modeled by Maxwell's [5] slip velocity theorem. The temperature jump boundary condition is defined by using the von Smoluchowski's [7] model. Constant fluid properties were used and viscous dissipation was neglected in numerical model. Throughout the study Reynolds numbers varied between 0.1 and 10. One of the interesting results they reached is the independence of Nusselt number from the geometry at the inlet section. This phenomenon can be seen in Fig. 2.3. Here, x* denotes the dimensionless axial distance, while α* denotes the channel aspect ratio.

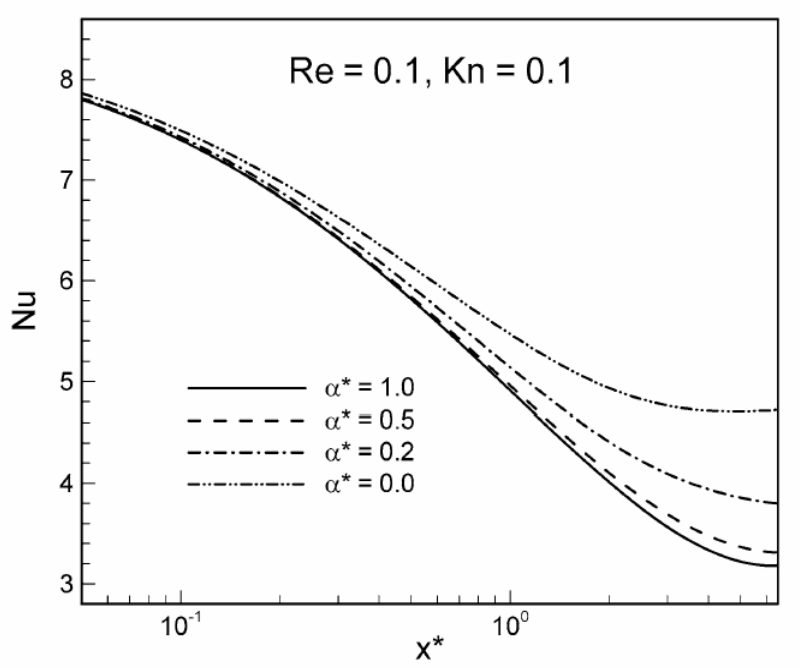

Figure 2.3 Axial variation of Nusselt number at Re=0.1 and Kn=0.1 for different aspect ratios [38].

At the very beginning of the channel Nusselt numbers are very close to each other for all aspect ratios. However, as the aspect ratio decreases toward the parallel-plate limit, dependence of Nusselt number on Knudsen number increases. Worek *et al.* [39] also investigated slip flow in rectangular microchannels. The study is based on a finite-volume numerical model. Mainly the variation of entrance length, friction coefficient, average fluid temperature, and Nusselt number with changing Knudsen and Péclet numbers, and aspect ratio is investigated. The flow is assumed to be steady, single phase, incompressible, and laminar. The fluid properties are assumed to be constant and viscous dissipation terms are neglected. Slip velocity and temperature jump at wall-fluid interface is accounted for in the model .They preferred solving an elliptic type momentum and energy equation. As a computational domain, quarter of a rectangular channel is used since boundaries are symmetrical. The slip velocity and temperature jump boundary conditions are imposed on the numerical model by using first order approximations. Pressure velocity coupling method is chosen as SIMPLE (by Patankar and Spalding [40]). They derived a correlation from the results of their analyses for fully developed friction factor as a function of Knudsen number and aspect ratio. The effect of Brinkman number and Prandtl number for slip flow regime in microtubes is studied by Sun *et al.* [41]. Their numerical model was validated with the analytical results of [35]. Hydrodynamically fully developed, thermally developing flow is analyzed for different Knudsen, Brinkman and Prandtl numbers. Three different wall boundary conditions are used in the study, which are constant wall temperature, constant wall heat flux and linearly varying wall temperature. They remarked that, temperature jump at wall boundary should be used together with the slip velocity boundary condition, for not overestimating heat transfer. The numerical solutions show that local Nusselt number decreases up to a point with the axial distance, and then it jumps to a final value. The phenomenon is related with the viscous dissipation, and this jump occurs earlier in the entrance region with increasing Brinkman number. The variation of Nusselt number with Brinkman number can be observed in Figure 2.4.

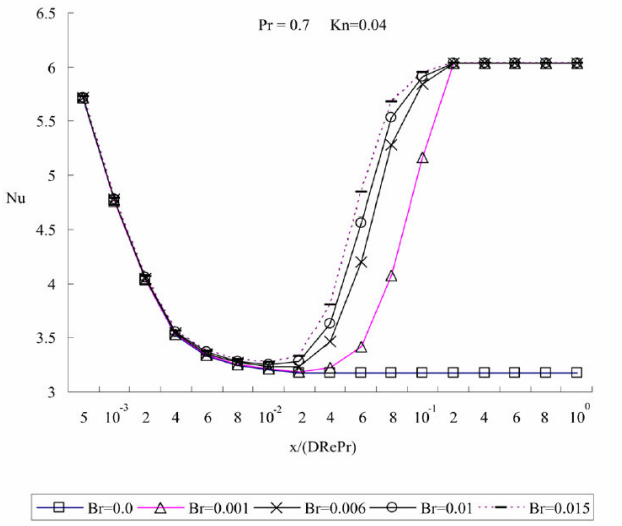

Figure 2.4 Variation of Nusselt number with Brinkman number in the thermal entrance region, with temperature jump boundary condition [41].

Effect of Prandtl number on heat transfer and Nusselt number is reported to be directly proportional. In the study it can be seen that, linearly varying temperature wall boundary condition yields nearly the same results with the constant wall heat flux boundary condition.

Morini [42] investigated the effect of viscous heating in microchannels and tried to explain the results of experimental data. Basically, Morini developed a model to predict the viscous dissipation in microchannels. For this purpose, effects of viscous heating and consequent viscosity decrease imposed on the conventional Navier-Stokes equations. This approach provided an explanation for the experimental observations in which friction factor decreases with the increasing Reynolds number. Kroeker *et al.* [43] investigated the heat transfer and pressure drop of heat sinks with circular microchannels. In their analytical work, they used the continuum model and classical Navier-Stokes equations. The effects of geometrical parameters and material properties on heat transfer characteristics are

investigated. As a result of the comparison they made, they reported that the thermal resistance of heat sinks with rectangular channels is lower than the ones with circular channels.

Mishan *et al.* [44] compared the experimental results of their microchannel test setup, by using Infrared (IR) imaging technology and numerical modeling. Infrared imaging technique is used for observing the temperature distribution in the test setup. The results obtained are compared with the results of CFD analysis. They validated the conventional theory proposed by Shah and London [10] after superimposition of entrance region effects for a microchannel with 410 μm hydraulic diameter. A study comparing the correlations, numerical analyses and experimental results is performed by Lee *et al.* [45]. They investigated the validity of conventional Navier-Stokes equations for predicting the thermal behavior of single phase flow through microchannels. In addition, the results of the experiment they have conducted are compared with both recent correlations and the numerical simulation results of commercial codes. Moreover, the importance of entrance and boundary conditions for more accurate numerical analyses is stressed. According to this study, numerical simulations carried out have a better agreement with the experimental results than the correlations. Wang and Zhixin [46] proposed that conventional computational fluid mechanics is deficient in modeling microscale fluid flow and heat transfer when continuum approach is no more valid. The deficiency of classical Navire-Stokes equations is also observed by Toh *et al.* [47], who also performed numerical analysis in microscale.

Numerous, experimental research has also been conducted in the area of microscale heat transfer. One of the most extensive reviews on the comparison of theoretical and experimental studies in microscale heat transfer is prepared by Morini [48]. This study contains experimental setup data, the results obtained from experiments of different researchers, and the empirical correlations derived. The valuable work of Morini shows that experimental results are not converging

to a common point but with the improvements in the technology and measurement techniques, results are becoming more reliable. Another study focused on comparison of the conventional theory and the experiment results is performed by Hetsroni *et al.* [49]. They analyzed rectangular, trapezoidal, circular and triangular micro-channels with hydraulic diameters ranging from 60 μm and 2000 μm. They concluded that simple one-dimensional models have a significant discrepancy with the experimental results. Also they proposed that classical Navier-Stokes and energy equations are inadequate to explain the experimental results. They claim to explain experimental results by including axial conduction effects, non-adiabatic inlet and outlet boundary conditions, and viscous dissipation to their numerical model. Experimental data correlated fairly well by using this model. On the other hand, they stated that effect viscous dissipation is negligible due to the experimental results obtained. The study of Gamrat *et al.* [50] also contains both experimental and numerical work. In the experiments, they investigated high aspect ratio channels with spacing ranging between 0.1 and 0.3 mm. Reynolds number for water flow in the experiments changed between 200 and 3000. Their numerical model assumes that the flow is incompressible, steady, and laminar. Additionally, property variation and viscous dissipation is neglected in the numerical model. The researchers claimed that the main difference between experimentally and numerically estimated Nusselt numbers arose from neglecting viscous dissipation and property variation. Also they stated that for their case, results of two dimensional and three dimensional numerical models are in good agreement, so it would be more advantageous to use two dimensional numerical models when computation costs are considered. One of the important results they converged to is the dependence of entrance effects on Reynolds number and channel spacing separately, as it was not the case denoted by Shah and London [10]. Shah and London proposed that Poiseuelle number for different channel spacing is a function of Reynolds number.

Another experimental study was performed by Mokrani *et al.* [51] who investigated the convective heat transfer in rectangular microchannels with channel spacing varying in the 0.0001 to 1 mm range. According to the results of their study, they proposed that the conventional continuum mechanics laws and correlations are valid for the dimensions and Reynolds numbers that they examined. Celata *et al.* [52] performed an interesting study in which, viscous heating is used to predict the friction factors. They also discussed occurrence of viscous heating, its significance for micro flows, and verification of its presence experimentally. They prepared an analytical model relating viscous heating with friction factors and claimed to validate this model with the experimental results. In addition to this, they proposed a limit, beyond which viscous dissipation cannot be neglected. The expression for the limit is given in the equation below.

$$\frac{Ec}{\mathrm{Re}}\left[f \,\mathrm{Re}\, L^{*} \right] \geq 1 \tag{2.7}$$

The L* in Equation 2.4 represents dimensionless channel length. Ec is the Eckert number.

Mala and Li [53] reported that predictions of conventional theory are incapable of defining micro-channel flows, as a result of their experimental work. As Reynolds number increases and micro tube diameter decreases, the experimentally found pressure drop and friction factors significantly deviate from the conventional theory. Researchers draw attention to two possible reasons of higher flow resistance than the conventionally estimated value. The first one may be an early transition from laminar to turbulent flow regime. The second may be the roughness effects. Therefore, they used roughness viscosity model for explaining the discrepancy between theoretical and experimental results. The results of roughness viscosity model and experiment were in good agreement.

CHAPTER 3

SINGLE PHASE HEAT TRANSFER IN PARALLEL PLATE MICROCHANNELS WITH CONSTANT WALL TEMPERATURE

3.1 Introduction

Chapter 3 is dedicated to formulation, numerical model and results of single phase laminar flow and heat transfer in parallel plate microchannels with constant wall temperature. Flow inside the channel is assumed to be laminar and incompressible. The thermophysical properties are also assumed to be constant for the analyses in this chapter. Pressure and velocity are solved in a coupled manner for observing the entrance effects. The rarefaction effects are included in the model due to the investigated Knudsen number range.

3.2 Variable Thermal Conductivity and Viscosity

Main focal point of this study is the effect of viscosity and thermal conductivity variation with temperature. These variations can be modeled with different approaches. Two different approaches are commonly used. According to these approaches, modeling can be based on the empirical data or can be based on the theoretical derivation. Many researchers prefer using empirically produced data in their studies. However, in some cases this kind of approach may introduce certain errors and it may be incapable for predicting the property variation correctly. Actually, the characteristics of thermal conductivity and viscosity differ from the

empirical relations significantly for the “dilute gas” density range. Lemmon and Jacobsen [54] extensively summarized the literature and available data for the thermal conductivity and viscosity variation with temperature in dilute gases. For our study, fluid density is close to the range in which empirical data is produced. Therefore, especially thermal conductivity variation is modeled by using the empirical based correlation [55]. On the other hand, variation of viscosity is modeled by using the “Sutherlands law of viscosity” which is based on the kinetic theory of gases. [56]

Sutherland’s formula for air can be written as follows,

$$\frac{\mu}{\mu_0} = \left(\frac{T}{T_0}\right)^{\frac{3}{2}} \frac{T_0 + S}{T + S} \qquad (3.1)$$

In Equation (3.1) the S is Sutherland’s constant which is equal to 111 K for air and T_0 μ_0 are the reference temperature and viscosity respectively. In this study reference temperature T_0 is taken as 273 K and the reference viscosity μ_0 is equal to 1.716E-5 N.s/m^2.

Both Gulhane and Mahulikar [18] and Herwig and Mahulikar [22], who had studied property variation effects in microchannels, used empirical based correlations. However, these researchers used water as working fluid. Additionally, researchers investigating the effects of property variation in air flow also used empirically produced data. The correlations used by Hernandez and Zamora [57], and Jaluria *et al.* [58] are given in Figure 3.1 in comparison with the empirical data taken from [55]. The data is non-dimensionalized by using the reference conductivity at 273 K.

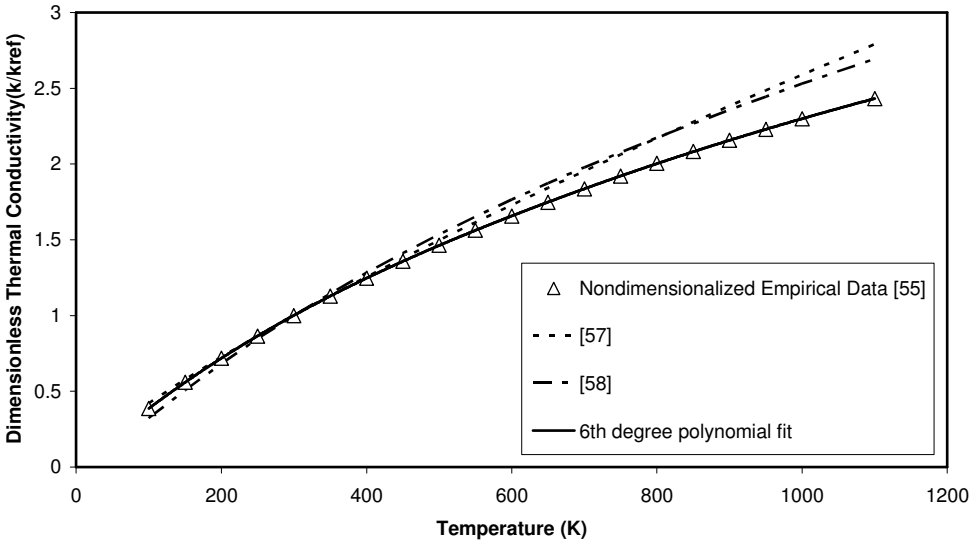

Figure 3.1 Dimensionless thermal conductivity plotted against temperature, data taken from references [55],[57] and [58]

The 6th degree polynomial fit, based on the empirical data of [63] can be expressed as follow,

$$k(T) = 1.035\cdot10^{-18}T^6 - 3.447\cdot10^{-15}T^5 + 3.627\cdot10^{-12}T^4 - 1.071\cdot10^{-10}T^3 - 2.985\cdot10^{-6}T^2 + 4.178\cdot10^{-3}T - 2.212\cdot10^{-3} \quad (3.2)$$

To be able to reduce the errors resulted from truncation; ten decimal places are used while expressing the coefficients of the polynomial function. The temperature scale used is Kelvin.

Similar to Figure 3.1 also the viscosity values obtained from Sutherlands formula are given in comparison with the empirical data in Figure 3.2. The data is non-dimensionalized by using reference viscosity value at 273K.

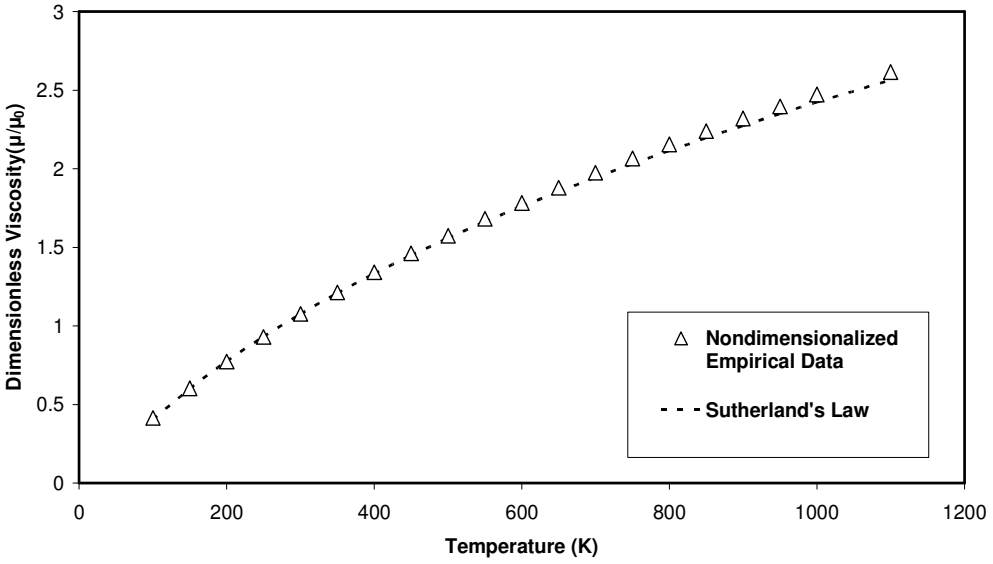

Figure 3.2 Dimensionless viscosity plotted against temperature, empirical data taken from [55] compared with Sutherlands Law

As can be seen from Figure 3.2, the viscosity values estimated from Sutherlands Law are in good agreement with the empirical data.

3.3 Formulation of the Problem

Analyzed geometry and governing equations for the problem will be discussed in this section. Schematic view of the geometry is given in Figure 3.3.

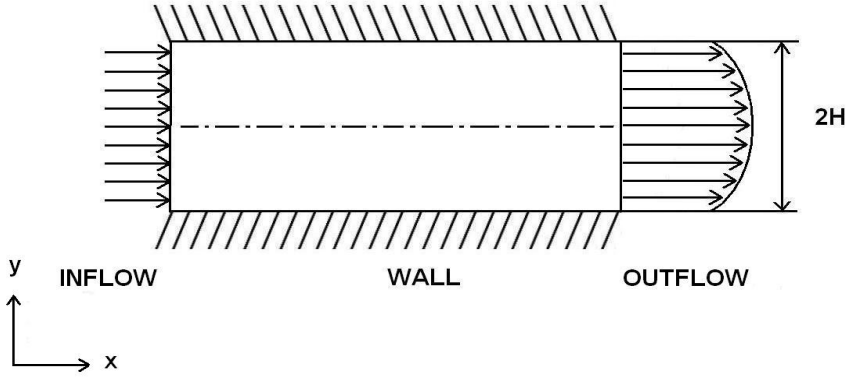

Figure 3.3 Schematic view of the parallel plate microchannel

Two dimensional flow and heat transfer problem will be expressed in terms of differential equations. The governing equations will be written for the Cartesian coordinates, for the given reference frame in Figure 3.3. The equations for the defined geometry and flow conditions will be as follows [59].

Continuity equation:

$$\frac{\partial u}{\partial x}+\frac{\partial v}{\partial y}=0 \tag{3.3}$$

Momentum equations:

x-momentum equation

$$\frac{\partial(\rho u)}{\partial t}+\frac{\partial(\rho u^2)}{\partial x}+\frac{\partial(\rho uv)}{\partial y}=-\frac{\partial p}{\partial x}+\frac{\partial}{\partial x}\left(\lambda\nabla\cdot\vec{V}+2\mu\frac{\partial u}{\partial x}\right)+\frac{\partial}{\partial y}\left[\mu\left(\frac{\partial v}{\partial x}+\frac{\partial u}{\partial y}\right)\right]+\rho f_x \tag{3.4}$$

y-momentum equation

$$\frac{\partial(\rho v)}{\partial t}+\frac{\partial(\rho uv)}{\partial x}+\frac{\partial(\rho v^2)}{\partial}=-\frac{\partial p}{\partial y}+\frac{\partial}{\partial x}\left[\mu\left(\frac{\partial v}{\partial x}+\frac{\partial u}{\partial y}\right)\right]+ \\ \frac{\partial}{\partial y}\left(\lambda\nabla\cdot\vec{V}+2\mu\frac{\partial v}{\partial y}\right)+\rho f_y \tag{3.5}$$

Equations (3.3), (3.4) and (3.5) are the equations for flow field. Before continuing with the derivations, these equations are should be simplified and non-dimensionalized. First of all, since the flow is incompressible, the divergence of velocity will be equal to zero. Moreover the body forces will be neglected throughout the analyses, and this will drop the last term from Equations (3.4) and (3.5). Simplified form of these equations can be written as follows.

$$\rho\cdot\left(\frac{\partial u}{\partial t}+\frac{\partial(u^2)}{\partial x}+\frac{\partial(uv)}{\partial y}\right)=-\frac{\partial p}{\partial x}+2\frac{\partial}{\partial x}\left(\mu\frac{\partial u}{\partial x}\right)+\frac{\partial}{\partial y}\left(\mu\frac{\partial v}{\partial x}\right)+\frac{\partial}{\partial y}\left(\mu\frac{\partial u}{\partial y}\right) \tag{3.6}$$

$$\rho\cdot\left(\frac{\partial v}{\partial t}+\frac{\partial(uv)}{\partial x}+\frac{\partial(v^2)}{\partial y}\right)=-\frac{\partial p}{\partial y}+\frac{\partial}{\partial x}\left(\mu\frac{\partial v}{\partial x}\right)+\frac{\partial}{\partial x}\left(\mu\frac{\partial u}{\partial y}\right)+2\frac{\partial}{\partial y}\left(\mu\frac{\partial v}{\partial y}\right) \tag{3.7}$$

Energy equation for Cartesian coordinates can be written as follows.

$$\rho\frac{D}{Dt}\left(h+\frac{V^2}{2}\right)=\rho\dot{q}+\frac{\partial}{\partial x}\left(k\frac{\partial T}{\partial x}\right)+\frac{\partial}{\partial y}\left(k\frac{\partial T}{\partial y}\right)-\frac{\partial(up)}{\partial x}-\frac{\partial(vp)}{\partial y}+ \\ \frac{\partial(u\tau_{xx})}{\partial x}+\frac{\partial(u\tau_{yx})}{\partial y}+\frac{\partial(v\tau_{xy})}{\partial x}+\frac{\partial(v\tau_{yy})}{\partial y}+\rho\vec{f}\cdot\vec{V} \tag{3.8}$$

The left hand side of Equation (3.8) can be expressed as follows.

$$\rho\frac{Dh}{Dt}+\rho\frac{D}{Dt}\left(\frac{u^2}{2}+\frac{v^2}{2}\right)=\rho\frac{Dh}{Dt}-u\frac{\partial p}{\partial x}-v\frac{\partial p}{\partial y}+u\left(\frac{\partial \tau_{xx}}{\partial x}+\frac{\partial \tau_{yx}}{\partial y}\right)+ v\left(\frac{\partial \tau_{xy}}{\partial x}+\frac{\partial \tau_{yy}}{\partial y}\right) \tag{3.9}$$

After subtracting Equation (3.9) from Equation (3.8) one will obtain a convenient expression for the energy equation in the form given below.

$$\rho\frac{Dh}{Dt}=\rho\dot{q}-\frac{\partial}{\partial x}\left(k\frac{\partial T}{\partial x}\right)+\frac{\partial}{\partial y}\left(\frac{\partial T}{\partial y}\right)-p\left(\frac{\partial u}{\partial x}+\frac{\partial v}{\partial y}\right)+\tau_{xx}\frac{\partial u}{\partial x}+\tau_{yy}\frac{\partial v}{\partial y}+ \tau_{yx}\left(\frac{\partial u}{\partial y}+\frac{\partial v}{\partial x}\right) \tag{3.10}$$

Since flow is incompressible, divergence of velocity will be zero. Additionally there will be no internal heat generation and body force in the flow. Also for an ideal gas enthalpy h can be expressed as $h=c_pT$. Similarly viscous stress terms for a Newtonian fluid can be expressed in terms of velocity gradients. After making the mentioned simplifications, Equation (3.10) can be written as;

$$\rho c_p\left(\frac{\partial T}{\partial t}+u\frac{\partial T}{\partial x}+v\frac{\partial T}{\partial y}\right)=\frac{\partial}{\partial x}\left(k\frac{\partial T}{\partial x}\right)+\frac{\partial}{\partial y}\left(k\frac{\partial T}{\partial y}\right)+ \left[2\mu\left(\left(\frac{\partial u}{\partial x}\right)^2+\left(\frac{\partial v}{\partial y}\right)^2+\left(\frac{\partial u}{\partial y}+\frac{\partial v}{\partial x}\right)\right)\right] \tag{3.11}$$

After simplification and rearrangement of the momentum and energy equations, they should be non-dimensionalized by using appropriate non-dimensional variables. In the non-dimensionalization following parameters will be used.

$$t^* = \frac{tU_\infty}{H} \tag{3.12}$$

$$p^* = \frac{p - p_\infty}{\rho_\infty U_\infty^2} \tag{3.13}$$

$$x^* = \frac{x}{H} \tag{3.14}$$

$$y^* = \frac{y}{H} \tag{3.15}$$

$$u^* = \frac{u}{U_\infty} \tag{3.16}$$

$$v^* = \frac{v}{U_\infty} \tag{3.17}$$

$$\mu^* = \frac{\mu}{\mu_\infty} \tag{3.18}$$

$$\mathrm{Re} = \frac{\rho_\infty U_\infty H}{\mu_\infty} \tag{3.19}$$

The non-dimensionalized x-momentum equation by the variables above can be written as follows.

$$\frac{\partial u^*}{\partial t^*}+\frac{\partial (u^{*2})}{\partial x^*}+\frac{\partial (u^* v^*)}{\partial y^*}=-\frac{\partial p^*}{\partial x^*}+ \\ \frac{1}{\mathrm{Re}}\left(\frac{\partial^2 u^*}{\partial x^{*2}}+\frac{\partial^2 u^*}{\partial y^{*2}}+2\frac{\partial \mu^*}{\partial x^*}\frac{\partial u^*}{\partial x^*}+\frac{\partial \mu^*}{\partial y^*}\frac{\partial v^*}{\partial x^*}+\frac{\partial \mu^*}{\partial y^*}\frac{\partial u^*}{\partial y^*}\right) \tag{3.20}$$

Similarly the non-dimensional form of the y-momentum equation is given below.

$$\frac{\partial v^*}{\partial t^*}+\frac{\partial (u^* v^*)}{\partial x^*}+\frac{\partial (v^{*2})}{\partial y^*}=-\frac{\partial p^*}{\partial y^*}+ \\ \frac{1}{\mathrm{Re}}\left(\frac{\partial^2 v^*}{\partial x^{*2}}+\frac{\partial^2 v^*}{\partial y^{*2}}+2\frac{\partial \mu^*}{\partial y^*}\frac{\partial v^*}{\partial y^*}+\frac{\partial \mu^*}{\partial x^*}\frac{\partial v^*}{\partial x^*}+\frac{\partial \mu^*}{\partial x^*}\frac{\partial u^*}{\partial y^*}\right) \tag{3.21}$$

Additionally, energy equation also needs to be non-dimensionalized. All of the non-dimensional variables defined above will be used in non-dimensionalization of energy equation except the non-dimensional pressure term defined in Equation (3.13) .In addition to the previously defined variables, some new variables will be introduced. These parameters are given below.

$$\theta=\frac{T-T_w}{T_i-T_w} \tag{3.22}$$

$$k^*=\frac{k}{k_\infty} \tag{3.23}$$

$$\mathrm{Pr}=\frac{c_p \mu_\infty}{k_\infty} \tag{3.24}$$

$$Br=\frac{\mu_\infty U_\infty^2}{k_\infty (T_i-T_w)} \tag{3.25}$$

After non-dimensionalization energy equation takes the following form

$$\frac{\partial\theta}{\partial t^*}+u^*\frac{\partial\theta}{\partial x^*}+v^*\frac{\partial\theta}{\partial y^*}=\frac{1}{\mathrm{Re}\,\mathrm{Pr}}\left(\frac{\partial k^*}{\partial x^*}\frac{\partial\theta}{\partial x^*}+k^*\frac{\partial^2\theta}{\partial x^{*2}}+\frac{\partial k^*}{\partial y^*}\frac{\partial\theta}{\partial y^*}+ k^*\frac{\partial^2\theta}{\partial y^{*2}}\right)+\frac{Br}{\mathrm{Re}\,\mathrm{Pr}}\left[2\mu^*\left(\left(\frac{\partial u^*}{\partial x^*}\right)^2+\left(\frac{\partial v^*}{\partial y^*}\right)^2+\left(\frac{\partial u^*}{\partial y^*}+\frac{\partial v^*}{\partial x^*}\right)\right)\right] \tag{3.26}$$

The spatial domain is chosen as a half of the channel as a result of symmetry. The boundary conditions and reference frame can be seen in Figure 3. 4.

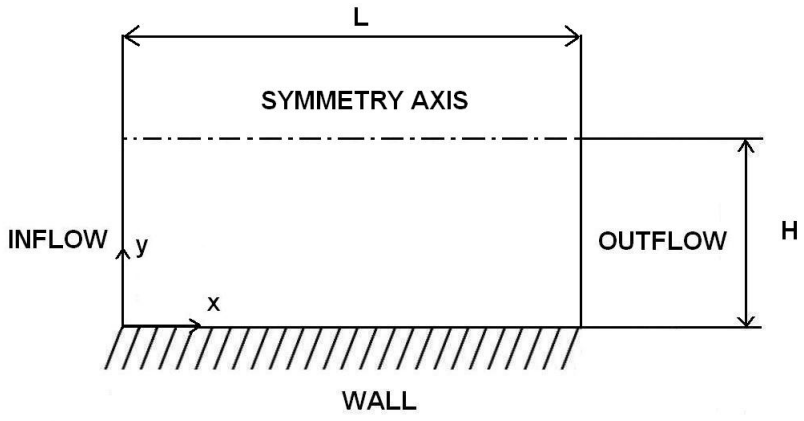

Figure 3. 4 Schematic representation of spatial solution domain and reference axes.

The channel length is denoted as L, and half channel width is denoted as H in the figure. Solution domain is surrounded by four different boundaries. The boundary conditions that will be used in the solution of momentum and energy equations can be written as follows.

In x and y-momentum equations, u and v velocity components at the boundaries will be defined as:

$$y = 0 \qquad u = u_s = \lambda \left(\frac{\partial u}{\partial y} \right)_{y=0} \tag{3.27}$$

$$y = 0 \qquad v = 0 \tag{3.28}$$

$$y = H \qquad \frac{\partial u}{\partial y} = 0 \tag{3.29}$$

$$y = H \qquad v = 0 \tag{3.30}$$

$$x = 0 \qquad u = U_\infty \tag{3.31}$$

$$x = 0 \qquad v = 0 \tag{3.32}$$

$$x = L \qquad \frac{\partial u}{\partial x} = 0 \tag{3.33}$$

$$x = L \qquad \frac{\partial v}{\partial x} = 0 \tag{3.34}$$

As the x-momentum equation, these boundary conditions should also be non-dimensionalized before using with the non-dimensional equations. Then the non-dimensional boundary conditions for momentum equations can be written as follows.

$$y^* = 0 \qquad u^* = u_s^* = 4Kn \left(\frac{\partial u^*}{\partial y^*} \right)_{y^*=0} \tag{3.35}$$

Knudsen number is the ratio of mean free path of fluid to the characteristic dimension of flow. The hydraulic diameter D_h for parallel plates will be the twice of the plate spacing (4H) which is used as characteristic dimension throughout this study.

$$y^* = 0 \qquad v^* = 0 \tag{3.36}$$

$$y^* = 1 \qquad \frac{\partial u^*}{\partial y^*} = 0 \tag{3.37}$$

$$y^* = 1 \qquad v^* = 0 \tag{3.38}$$

$$x^* = 0 \qquad u^* = 1 \tag{3.39}$$

$$x^* = 0 \qquad v^* = 0 \tag{3.40}$$

$$x^* = \frac{L}{H} \qquad \frac{\partial u^*}{\partial x^*} = 0 \tag{3.41}$$

$$x^* = \frac{L}{H} \qquad \frac{\partial v^*}{\partial x^*} = 0 \tag{3.42}$$

Boundary conditions also need to be defined for the energy equation. The temperature values at boundaries can be expressed as:

$$y = 0 \qquad T = T_s = \frac{\lambda}{\kappa}\left(\frac{\partial T}{\partial y}\right)_{y=0} \tag{3.43}$$

Where $\kappa = \dfrac{\Pr(\gamma+1)}{2\gamma}$ (3.44)

$$y = H \qquad \frac{\partial T}{\partial y} = 0 \tag{3.45}$$

$$x = 0 \qquad T = T_i \tag{3.46}$$

$$x = L \qquad \frac{\partial T}{\partial x} = 0 \tag{3.47}$$

The boundary conditions should be written in non-dimensional form before using in solution of non-dimensional energy equation.

$$y^* = 0 \qquad \theta = \theta_s = \frac{4Kn}{\kappa}\left(\frac{\partial \theta}{\partial y^*}\right)_{y^*=0} \tag{3.48}$$

$$y^* = 1 \qquad \frac{\partial \theta}{\partial y^*} = 0 \tag{3.49}$$

$$x^* = 0 \qquad \theta = 0 \tag{3.50}$$

$$x^* = \frac{L}{H} \qquad \frac{\partial \theta}{\partial x^*} = 0 \tag{3.51}$$

In the analyses, another frequently used dimensionless number is the Nusselt number. This dimensionless parameter is directly related with heat transfer coefficient. Before continuing with the expression of Nusselt number, first local heat transfer coefficient for the parallel plate geometry will be defined. The energy balance at the wall interface can be written as follows,

$$h_x(T_{mean} - T_{wall}) = -k\left(\frac{\partial T}{\partial y}\right)_{y=0} \tag{3.52}$$

by rearranging Equation (3.52), it is possible to obtain the expression for local heat transfer coefficient

$$h_x = \frac{-k}{(T_{mean} - T_{wall})}\left(\frac{\partial T}{\partial y}\right)_{y=0} \tag{3.53}$$

By using the expression for local heat transfer coefficient, local Nusselt number can be written as,

$$Nu_x = \frac{h_x D_h}{k} = \frac{-4H}{(T_{mean} - T_{wall})}\left(\frac{\partial T}{\partial y}\right)_{y=0} \tag{3.54}$$

Where, mean temperature of the flow is defined as a function of axial position, as follows:

$$T_{mean}(x) = \int_0^H u(x,y)T(x,y)dy \tag{3.55}$$

D_h is taken as 4H which is the hydraulic diameter of parallel plates as mentioned above. As all other expressions it is possible to express the local Nusselt number in terms of non-dimensional parameters, for convenience.

$$Nu_x = \frac{-4\left(\frac{\partial \theta}{\partial y^*}\right)_{y^*=0}}{\theta_{mean}} \tag{3.56}$$

Similarly, the mean temperature can be expressed non-dimensionally as,

$$\theta_{mean}(x) = \int_0^1 u^*(x^*, y^*)\theta(x^*, y^*)dy^* \tag{3.57}$$

Equations, non-dimensional parameters, boundary conditions and the dimensionless numbers that are used in the analyses for constant wall temperature case are defined above. Momentum and energy equations are rearranged and extended to account for the thermophysical property variation. Moreover, axial conduction, viscous dissipation terms and all convective terms are included in the mathematical model. Unfortunately it is not possible to solve these equations analytically, for this reason numerical methods will be utilized to approximate the solution. Before solving the equations numerically, equations must be discretized in spatial and time domain. The next subsection is dedicated to discretization of equations and numerical solution.

3.4 Numerical Model

Since the effect of thermophysical property variation is desired to be observed in this study, momentum equations (Equations (3.6), (3.7)) and the energy equation (Equation (3.11)) need to be solved in a coupled manner. As mentioned before, the analytical solution for these partial differential equations do not exist. Therefore solution of the momentum and energy equations will be approximated numerically [60].In this problem, solution domain is simple and uncomplicated. Boundaries lie parallel to the reference axes and this eliminates the need for transformation. In addition to the geometric conformity, momentum and energy equations are also expressed in transient form for the sake of mathematical simplicity and computational convenience. Actually the heat transfer and fluid flow problem subject to discussion is a steady state problem. However, steady state momentum and energy equations will be elliptical partial differential equations which require more sophisticated numerical methods for being solved.

On the other hand parabolic partial differential equations can be solved explicitly which is relatively simple and computationally straightforward.

Implicit methods require simultaneous solution of the equations at the same solution step and this may require inversion of large matrices, additionally, the iterative procedure increases the computational cost. Nevertheless, implicit methods do not have a time step size limitation as a convergence criterion. On the other hand explicit methods needs a divergence free time step size.

In the explicit solution procedure of the parabolic differential equation, each variable at a node is computed for the next time step by using the values obtained in the previous time step. However, transient solution converges to the steady state solution as the time goes to infinity.

As it is stated above, chosen time step should satisfy the convergence criteria. This convergence criterion involves the flow variables and grid spacing, which is known as Courant-Friedrichs-Lewy (CFL) condition. Since an adaptive time stepping scheme is used for the solution of our problem, the time steps are chosen automatically to satisfy this condition. The details of this procedure can be found in [60]

3.4.1 Geometry Discretization

Numerical solution will be carried out on a finite number of grid points which will be called as mesh. Since our geometry conformed on Cartesian coordinates, it is possible to use uniformly distributed grid points for the solution. Also, symmetry of the problem geometry reduces the number of required grid points in solution domain.

Since pressure and velocity parameters will be coupled throughout the study, a staggered grid arrangement is used for the spatial discretization. Actually the method of using staggered grid for spatial discretization is based on the finite volume method. In finite volume method, mass balance is tried to be established for a cell by using the velocities defined at the cell boundaries. Similarly for the staggered grid used here, different unknown variables are defined at different grid points of a cell. Staggered grid and cell structure for a Cartesian grid is given in Figure 3.5.

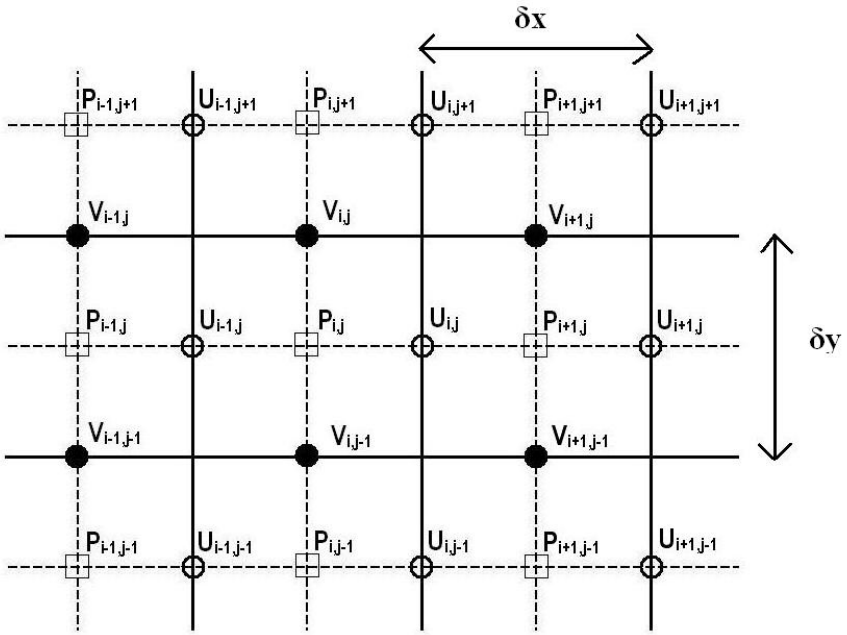

Figure 3.5 Schematic representation of staggered grid for Cartesian coordinates

In a uniformly distributed staggered grid, a cell is a rectangular region, surrounded by velocity nodes. Each cell has a node at the center where pressure and temperature values of the cell are assigned. In a cell, horizontal velocity

components are located at the center of vertical cell edges and the vertical velocity components are defined for the nodes at the center of horizontal cell edges. Cells are defined with the corresponding index (*i,j*) where *i* stands for the horizontal coordinate of the cell and likewise *j* denotes the vertical coordinate. Thus, for the cell (*i,j*) coordinates of the center node can be expressed as $((i-0.5)\delta x,((j-0.5)\ \delta y)$ parametrically. It is possible to locate the node coordinates for horizontal and vertical velocity components as long as the cell index is known.

Since the velocity and pressure values are defined at different locations on our staggered grid it can be said that there exist three separate cells which are shifted by half grid spacing, for these three different variables.

On staggered grid, all nodes can not be aligned with the domain boundary, for this reason boundary condition implementation will be slightly complicated. To overcome this problem actual domain is encircled with an extra boundary strip made up of grid cells. The boundary strip around the problem domain can be seen in Figure 3.6.

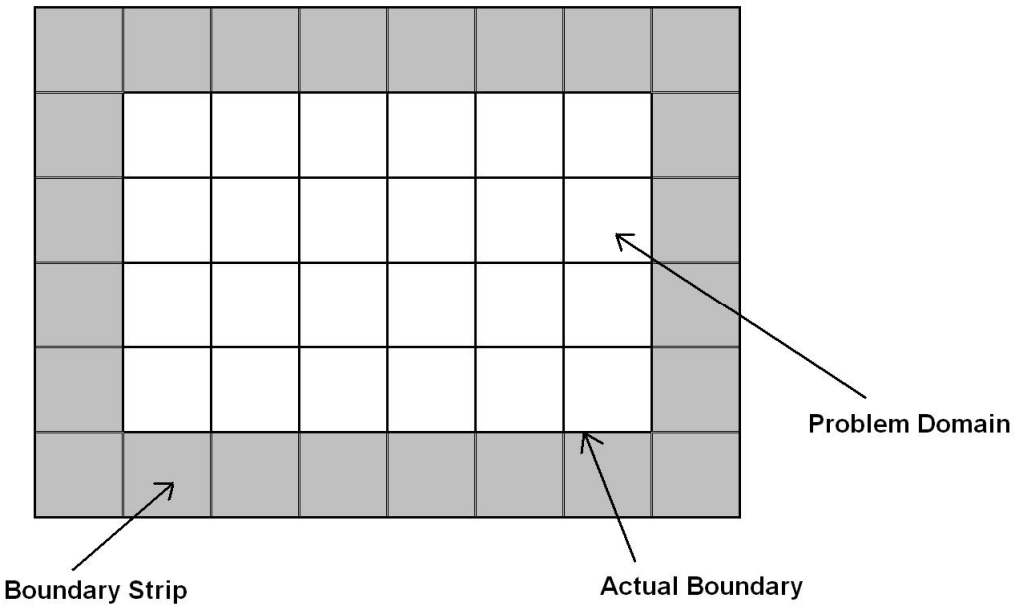

Figure 3.6 Sketch of problem domain and boundary strip

The cells in the boundary strip will be used for averaging the required values at the boundary of the problem domain. The details of this implementation will be discussed later.

3.4.2 Equation Discretization

Discretization is the process of conversion of partial differential equations into linear algebraic ones on the given solution domain. Energy and momentum equations are composed of both spatial and time derivatives of temperature, velocity, and pressure terms. Throughout the study, spatial and time derivatives will be separately discretized. The details of the discretization in spatial domain will be discussed in detail in the following part.

3.4.2.1 Discretization of Momentum Equations

The momentum equation in x direction and the momentum equation in y direction will be discretized separately. In Figure 3.7 velocity nodes and the positions where equations will be discretized can be seen.

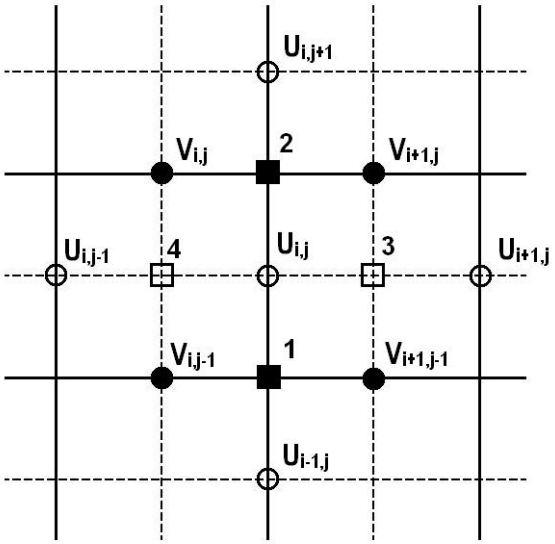

Figure 3.7 Velocity nodes and discretization locations

The terms in the x momentum equation will be discretized at the midpoints of the vertical edges of each cell. These locations are where u velocities are located in Figure 3.7.

Diffusive terms in the x momentum equation are given below,

$$\frac{\partial^2 u}{\partial x^2}\ ,\ \frac{\partial^2 u}{\partial y^2} \tag{3.58}$$

These terms can be directly discretized by using central differencing, which is second order accurate $O(\delta x^2)$. Discretization of the terms in Equation (3.58) is as follows,

$$\left[\frac{\partial^2 u^*}{\partial x^{*2}}\right]_{i,j} = \left(\frac{u^*_{i+1,j} - 2u^*_{i,j} + u^*_{i-1,j}}{(\delta x^*)^2}\right) \tag{3.59}$$

$$\left[\frac{\partial^2 u^*}{\partial y^{*2}}\right]_{i,j} = \left(\frac{u^*_{i+1,j} - 2u^*_{i,j} + u^*_{i-1,j}}{(\delta y^*)^2}\right) \tag{3.60}$$

On the other hand, convective terms, which can be seen below, introduce some difficulties in spatial discretization.

$$\frac{\partial(u^{*2})}{\partial x^*}, \frac{\partial(u^* v^*)}{\partial y^*} \tag{3.61}$$

Since $\partial(uv)/\partial y$ will be discretized at the point where $U_{i,j}$ is located in Figure 3.7. One will need to use the average values for v and u velocities at locations 3 and 4 for being able to use central differencing method for the product *uv*. The locations 3 and 4 can be seen in Figure 3.7. The discretized form of the $\partial(uv)/\partial y$ term will be in the following form,

$$\left[\frac{\partial(u^* v^*)}{\partial y^*}\right]_{i,j} = \frac{1}{\delta y^*}\left(\frac{\left(v^*_{i,j} + v^*_{i+1,j}\right)}{2}\frac{\left(u^*_{i,j} - u^*_{i+1,j}\right)}{2} - \frac{\left(v^*_{i,j-1} + v^*_{i+1,j-1}\right)}{2}\frac{\left(u^*_{i,j-1} - u^*_{i,j}\right)}{2}\right) \tag{3.62}$$

Similarly, the $\partial(u^2)/\partial x$ term can be discretized in terms of averaged values at locations 3 and 4, by using central differencing with half mesh width. The discretized form of $\partial(u^2)/\partial x$ term can be expressed as follows,

$$\left[\frac{\partial(u^{*2})}{\partial x^*}\right]_{i,j} = \frac{1}{\delta x^*}\left(\left(\frac{u^*_{i,j} + u^*_{i+1,j}}{2}\right)^2 - \left(\frac{u^*_{i-1,j} + u^*_{i,j}}{2}\right)^2\right) \tag{3.63}$$

Since, pure central differencing for the discretization of convective terms may cause problem in convergence where flow is reversed or rapidly changed direction, the convergence characteristics of the solution can be enhanced with the use of a different approach. However, using pure upwind differencing scheme in discretization may cause a diffusion problem for the convective terms which is also known as false diffusion. A more conservative form of the upwind differencing which is known as "donor cell" differencing scheme [60] will be utilized. In our problem, the variables are defined at different locations of a cell. Due to the need for relocating the parameters and derivatives, it would be appropriate to use donor cell differencing scheme. The conservative characteristic of donor cell discretization will slow down the convergence of solutions. Therefore, for the enhancement of convergence characteristics and stability of solution, convective terms are discretized with a weighted average of central differencing and donor cell differencing scheme. As mentioned above it is possible to relocate the variables by averaging in the donor cell discretization. For the discretization of the convective terms given in Equation (3.61) one of the two variables in the derivative should be defined at the interval midpoints. Thus, for the discretization of $\partial(u^2)/\partial x$ term donor cell variables will be the u velocity values averaged at location 3 and 4 defined in Figure 3.7. These donor cell variables will be in the following form,

$$donor-cell-\text{var}iable_3 = \frac{u^*_{i,j} + u^*_{i+1,j}}{2} \tag{3.64}$$

$$donor-cell-\text{var}iable_4 = \frac{u^*_{i-1,j} + u^*_{i,j}}{2} \tag{3.65}$$

Similarly for the discretization of $\partial(uv)/\partial y$ term in the x momentum equation, donor cell variables that are defined at location 3 and 4 will be as follows,

$$donor-cell-\text{var}iable_3 = \frac{v^*_{i,j} + v^*_{i+1,j}}{2} \tag{3.66}$$

$$donor-cell-\text{var}iable_4 = \frac{v^*_{i,j-1} + v^*_{i+1,j-1}}{2} \tag{3.67}$$

By using the weighted average of donor cell and central differencing schemes, discretization of $\partial(u^2)/\partial x$ will be,

$$\left[\frac{\partial(u^{*2})}{\partial x^*}\right]_{i,j} = \frac{1}{\delta x^*}\left(\left(\frac{u^*_{i,j} + u^*_{i+1,j}}{2}\right)^2 - \left(\frac{u^*_{i-1,j} + u^*_{i,j}}{2}\right)^2\right) + \gamma\frac{1}{\delta x^*}\left(\frac{\left|u^*_{i,j} + u^*_{i+1,j}\right|}{2}\frac{\left(u^*_{i,j} - u^*_{i+1,j}\right)}{2} - \frac{\left|u^*_{i-1,j} + u^*_{i,j}\right|}{2}\frac{\left(u^*_{i-1,j} - u^*_{i,j}\right)}{2}\right) \tag{3.68}$$

In Equation (3.68) γ stands for the weighting factor which lies between 0 and 1. Likewise discretized $\partial(uv)/\partial y$ term can be written as,

$$\left[\frac{\partial(u^* v^*)}{\partial y^*}\right]_{i,j} = \frac{1}{\delta y^*}\left(\frac{\left(v^*_{i,j} + v^*_{i+1,j}\right)}{2}\frac{\left(u^*_{i,j} - u^*_{i+1,j}\right)}{2} - \frac{\left(v^*_{i,j-1} + v^*_{i+1,j-1}\right)}{2}\frac{\left(u^*_{i,j-1} - u^*_{i,j}\right)}{2}\right) + \gamma\frac{1}{\delta y^*}\left(\frac{\left|v^*_{i,j} + v^*_{i+1,j}\right|}{2}\frac{\left(u^*_{i,j} - u^*_{i+1,j}\right)}{2} - \frac{\left|v^*_{i,j-1} + v^*_{i+1,j-1}\right|}{2}\frac{\left(u^*_{i,j-1} - u^*_{i,j}\right)}{2}\right) \tag{3.69}$$

The other terms in the x momentum equation will be discretized around the same grid point with the convective terms where $U_{i,j}$ lies in Figure 3.7. The equations in the discretized form can be written as,

$$\left[\frac{\partial^2 u^*}{\partial x^{*2}}\right]_{i,j} = \left(\frac{u^*_{i+1,j} - 2u^*_{i,j} + u^*_{i-1,j}}{(\delta x^*)^2}\right) \tag{3.70}$$

$$\left[\frac{\partial^2 u^*}{\partial y^{*2}}\right]_{i,j} = \left(\frac{u^*_{i+1,j} - 2u^*_{i,j} + u^*_{i-1,j}}{(\delta y^*)^2}\right) \tag{3.71}$$

Viscosity terms are defined at the cell centers where temperature values are also defined. The discretization of the spatial derivatives of viscosity terms are written as follows.

$$\left[\frac{\partial \mu^*}{\partial x^*}\right]_{i,j} = \left(\frac{\mu^*_{i+1,j} - \mu^*_{i,j}}{\delta x^*}\right) \tag{3.72}$$

$$\left[\frac{\partial u^*}{\partial x^*}\right]_{i,j} = \left(\frac{u^*_{i+1,j} - u^*_{i-1,j}}{2\delta x^*}\right) \tag{3.73}$$

$$\left[\frac{\partial \mu^*}{\partial y^*}\right]_{i,j} = \left(\frac{\left(\frac{\mu^*_{i+1,j+1} + \mu^*_{i,j+1}}{2}\right) - \left(\frac{\mu^*_{i+1,j-1} + \mu^*_{i,j-1}}{2}\right)}{2\delta y^*} \right) \tag{3.74}$$

$$\left[\frac{\partial v^*}{\partial x^*}\right]_{i,j} = \left(\frac{\left(\frac{v^*_{i+1,j} + v^*_{i+1,j-1}}{2}\right) - \left(\frac{v^*_{i,j} + v^*_{i,j-1}}{2}\right)}{2\delta x^*} \right) \tag{3.75}$$

$$\left[\frac{\partial u^*}{\partial y^*}\right]_{i,j} = \left(\frac{u^*_{i,j+1} - u^*_{i,j-1}}{2\delta y^*} \right) \tag{3.76}$$

Pressure values are defined at the cell centers and derivative of the pressure will be also discretized around the same grid point with the other terms. The discretized form of the pressure term is given below,

$$\left[\frac{\partial p^*}{\partial x^*}\right]_{i,j} = \left(\frac{p^*_{i+1,j} - p^*_{i,j}}{\delta x^*} \right) \tag{3.77}$$

In addition to spatial derivatives, there is also a time derivative term in the x momentum equation. As mentioned earlier the time discretization is separate from spatial discretization.

$$\left[\frac{\partial u^*}{\partial t^*}\right]^{(n+1)} = \left(\frac{u^{*(n+1)} - u^{*n}}{\delta t^*} \right) \tag{3.78}$$

In a similar manner the terms in the y momentum equation will also be discretized. These terms will be discretized for the cell *(i,j)* around the node

where velocity $V_{i,j}$ lies in Figure 3.7. Convective terms will be discretized similarly by using a weighted average of donor cell and central differencing schemes. The discretized terms for the y momentum equation can be expressed as follows,

$$\left[\frac{\partial(u^* v^*)}{\partial x^*}\right]_{i,j} = \frac{1}{\delta x^*}\left(\frac{\left(u^*_{i,j} + u^*_{i,j+1}\right)}{2}\frac{\left(v^*_{i,j} - v^*_{i+1,j}\right)}{2} - \frac{\left(u^*_{i-1,j} + u^*_{i-1,j+1}\right)}{2}\frac{\left(v^*_{i-1,j} - v^*_{i,j}\right)}{2}\right) + \gamma\frac{1}{\delta y^*}\left(\frac{\left|u^*_{i,j} + u^*_{i,j+1}\right|}{2}\frac{\left(v^*_{i,j} - v^*_{i+1,j}\right)}{2} - \frac{\left|u^*_{i-1,j} + u^*_{i-1,j+1}\right|}{2}\frac{\left(v^*_{i-1,j} - v^*_{i,j}\right)}{2}\right) \tag{3.79}$$

$$\left[\frac{\partial(v^{*2})}{\partial y^*}\right]_{i,j} = \frac{1}{\delta y^*}\left(\left(\frac{v^*_{i,j} + v^*_{i,j+1}}{2}\right)^2 - \left(\frac{v^*_{i,j-1} + v^*_{i,j}}{2}\right)^2\right) + \gamma\frac{1}{\delta x^*}\left(\frac{\left|v^*_{i,j} + v^*_{i,j+1}\right|}{2}\frac{\left(v^*_{i,j} - v^*_{i,j+1}\right)}{2} - \frac{\left|v^*_{i,j-1} + v^*_{i,j}\right|}{2}\frac{\left(v^*_{i,j-1} - v^*_{i,j}\right)}{2}\right) \tag{3.80}$$

$$\left[\frac{\partial^2 v^*}{\partial x^{*2}}\right]_{i,j} = \left(\frac{v^*_{i+1,j} - 2v^*_{i,j} + v^*_{i-1,j}}{(\delta x^*)^2}\right) \tag{3.81}$$

$$\left[\frac{\partial^2 v^*}{\partial y^{*2}}\right]_{i,j} = \left(\frac{v^*_{i+1,j} - 2v^*_{i,j} + v^*_{i-1,j}}{(\delta y^*)^2}\right) \tag{3.82}$$

$$\left[\frac{\partial \mu^*}{\partial y^*}\right]_{i,j} = \left(\frac{\mu^*_{i,j+1} - \mu^*_{i,j}}{\delta y^*}\right) \tag{3.83}$$

$$\left[\frac{\partial v^*}{\partial y^*}\right]_{i,j} = \left(\frac{v^*_{i,j+1} - v^*_{i,j-1}}{2\delta y^*}\right) \tag{3.84}$$

$$\left[\frac{\partial \mu^*}{\partial x^*}\right]_{i,j} = \left(\frac{\left(\frac{\mu^*_{i+1,j} + \mu^*_{i+1,j+1}}{2}\right) - \left(\frac{\mu^*_{i-1,j} + \mu^*_{i-1,j+1}}{2}\right)}{2\delta x^*}\right) \tag{3.85}$$

$$\left[\frac{\partial v^*}{\partial x^*}\right]_{i,j} = \left(\frac{v^*_{i+1,j} - v^*_{i-1,j}}{2\delta x^*}\right) \tag{3.86}$$

$$\left[\frac{\partial u^*}{\partial y^*}\right]_{i,j} = \left(\frac{\left(\frac{u^*_{i+1,j+1} + u^*_{i,j+1}}{2}\right) - \left(\frac{u^*_{i+1,j} + u^*_{i-1,j}}{2}\right)}{\delta y^*}\right) \tag{3.87}$$

Since viscosity terms in the y momentum equation cannot be discretized by using donor cell scheme, these terms are simply discretized by using central differencing which is again second order accurate.

$$\left[\frac{\partial p^*}{\partial y^*}\right]_{i,j} = \left(\frac{p^*_{i,j+1} - p^*_{i,j}}{\delta y^*}\right) \tag{3.88}$$

$$\left[\frac{\partial v^*}{\partial t^*}\right]^{(n+1)} = \left(\frac{v^{*(n+1)} - v^{*n}}{\delta t^*}\right) \tag{3.89}$$

The weighting factor in the discretized convective terms will be selected according to Hirt et al. [61] by using the given formula.

$$\gamma \geq \max\left(\left|\frac{u_{i,j}}{\delta x}\right|, \left|\frac{v_{i,j}}{\delta x}\right|\right) \tag{3.90}$$

After discretization of the momentum equations, also boundary values for these equations should be defined.

3.4.2.2 Discretization of Energy Equation

In the discretization of energy equation, spatial derivatives of thermal conductivity and viscosity are also considered, since these variables are changing spatially in accordance with the temperature change. Similar to the momentum equations, the discretization of the convective terms is made by using the mixture of donor cell and central differencing schemes. Additionally the conductive terms in the equations will also be discretized by using the same method. Main advantage regarding this type of discretization for the conductive terms is the improved convergence characteristics as a result of averaged donor cell differencing scheme. This discretization method enables to use weighted average of central differencing with the forward or backward differencing schemes, according to the temperature gradient. The differencing scheme becomes a weighted average of central and backward differencing, where temperature gradient is negative, in other words if the temperature is decreasing in the positive direction then a backward differencing scheme will be employed. The mechanism for differencing is the inverse of this one for the positive temperature gradient case.

Before presenting the discretized terms in the energy equation, it should be noted that the dimensionless temperature, thermal conductivity and the viscosity variables are defined at the cell center. Since viscosity and thermal conductivity

are directly related with temperature in our situation, defining these variables at the cell centers where temperature values are defined would be more convenient.

Discretized terms in the energy equation can be written as follows,

$$\left[\frac{\partial(u^*\theta)}{\partial x^*}\right]_{i,j} = \frac{1}{\delta x^*}\left(u^*_{i,j}\frac{(\theta_{i,j}-\theta_{i+1,j})}{2} - u^*_{i-1,j}\frac{(\theta_{i-1,j}-\theta_{i,j})}{2}\right) + \gamma\frac{1}{\delta x^*}\left(\left|u^*_{i,j}\right|\frac{(\theta_{i,j}-\theta_{i+1,j})}{2} - \left|u^*_{i-1,j}\right|\frac{(\theta_{i-1,j}-\theta_{i,j})}{2}\right) \tag{3.91}$$

$$\left[\frac{\partial(v^*\theta)}{\partial y^*}\right]_{i,j} = \frac{1}{\delta y^*}\left(v^*_{i,j}\frac{(\theta_{i,j}-\theta_{i,j+1})}{2} - v^*_{i,j-1}\frac{(\theta_{i,j-1}-\theta_{i,j})}{2}\right) + \gamma\frac{1}{\delta y^*}\left(\left|v^*_{i,j}\right|\frac{(\theta_{i,j}-\theta_{i,j+1})}{2} - \left|v^*_{i,j-1}\right|\frac{(\theta_{i,j-1}-\theta_{i,j})}{2}\right) \tag{3.92}$$

$$\left[\frac{\partial}{\partial x^*}\left(k^*\frac{\partial\theta}{\partial x^*}\right)\right]_{i,j} = \frac{1}{\delta x^*}\left(\frac{(k^*_{i,j}+k^*_{i+1,j})}{2}\frac{(\theta_{i+1,j}-\theta_{i,j})}{\delta x^*} - \frac{(k^*_{i,j}+k^*_{i-1,j})}{2}\frac{(\theta_{i,j}-\theta_{i-1,j})}{\delta x^*}\right) + \gamma\frac{1}{\delta x^*}\left(\frac{k^*_{i,j}-k^*_{i+1,j}}{2}\left|\frac{\theta_{i+1,j}-\theta_{i,j}}{\delta x^*}\right| - \frac{k^*_{i-1,j}-k^*_{i,j}}{2}\left|\frac{\theta_{i,j}-\theta_{i-1,j}}{\delta x^*}\right|\right) \tag{3.93}$$

$$\left[\frac{\partial}{\partial y^*}\left(k^*\frac{\partial\theta}{\partial y^*}\right)\right]_{i,j} = \frac{1}{\delta y^*}\left(\frac{(k^*_{i,j}+k^*_{i,j+1})}{2}\frac{(\theta_{i,j+1}-\theta_{i,j})}{\delta x^*} - \frac{(k^*_{i,j}+k^*_{i,j-1})}{2}\frac{(\theta_{i,j}-\theta_{i,j-1})}{\delta x^*}\right) + \gamma\frac{1}{\delta y^*}\left(\frac{k^*_{i,j}-k^*_{i,j+1}}{2}\left|\frac{\theta_{i,j+1}-\theta_{i,j}}{\delta y^*}\right| - \frac{k^*_{i-1,j}-k^*_{i,j}}{2}\left|\frac{\theta_{i,j}-\theta_{i,j-1}}{\delta y^*}\right|\right) \tag{3.94}$$

The viscous dissipation terms in the energy equation required to be discrtetized at the cell centers where other terms of the energy equations are also discretized. The viscous terms are given below.

$$\left[\frac{\partial u^*}{\partial x^*}\right]_{i,j} = \left(\frac{u^*_{i,j} - u^*_{i-1,j}}{\delta x^*}\right) \tag{3.95}$$

$$\left[\frac{\partial v^*}{\partial y^*}\right]_{i,j} = \left(\frac{v^*_{i,j} - v^*_{i,j-1}}{\delta y^*}\right) \tag{3.96}$$

$$\left[\frac{\partial u^*}{\partial y^*}\right]_{i,j} = \left(\frac{\frac{\left(u^*_{i,j+1} + u^*_{i-1,j+1}\right)}{2} - \frac{\left(u^*_{i,j-1} + u^*_{i-1,j-1}\right)}{2}}{2\delta y^*}\right) \tag{3.97}$$

$$\left[\frac{\partial v^*}{\partial x^*}\right]_{i,j} = \left(\frac{\frac{\left(v^*_{i-1,j} + v^*_{i-1,j-1}\right)}{2} - \frac{\left(v^*_{i+1,j1} + v^*_{i+1,j-1}\right)}{2}}{2\delta x^*}\right) \tag{3.98}$$

$$\left[\frac{\partial \theta}{\partial t^*}\right]^{(n+1)} = \left(\frac{\theta^{(n+1)} - \theta^n}{\delta t^*}\right) \tag{3.99}$$

3.4.2.3 Boundary Values for Discretized Equations

For being able to solve the discretized momentum equations, boundary values will be required for the unknowns. The velocity values on the domain boundaries in addition to the pressure and temperature values of the ghost cells will be required. The appropriate ghost cell values will be used for implementation of the desired values at the domain boundary. As mentioned above the values at the boundary of the problem domain will be defined by averaging the value of the ghost cells and

the adjacent fluid cells. The problem domain, ghost cells and the indexing of the cells are illustrated in Figure 3.8. There are four different type of boundary conditions used in this problem as stated above. These boundary conditions are; inlet, outlet, symmetry and wall with velocity slip and temperature jump. The details of the boundary conditions will be discussed in the following subsections. The positions and alignment of these boundaries in the computation domain can be seen in Figure 3.9.

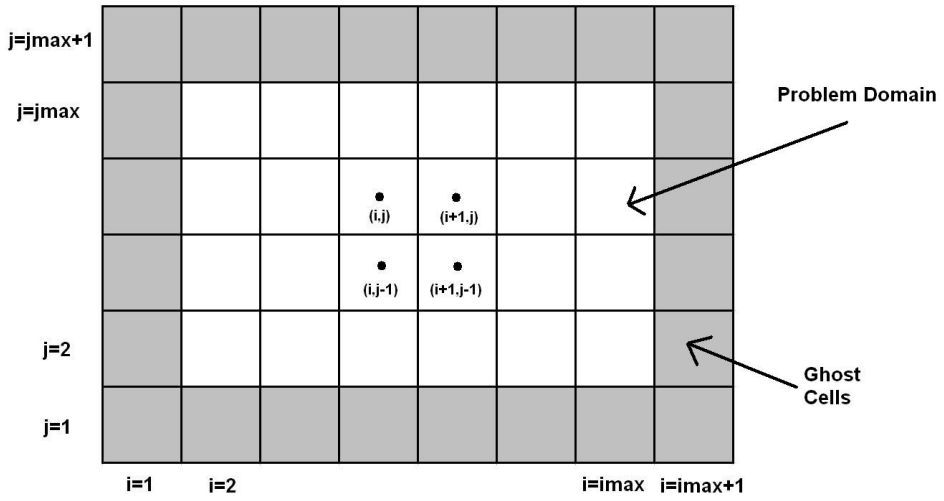

Figure 3.8 Problem domain ghost cells and the cell indexing

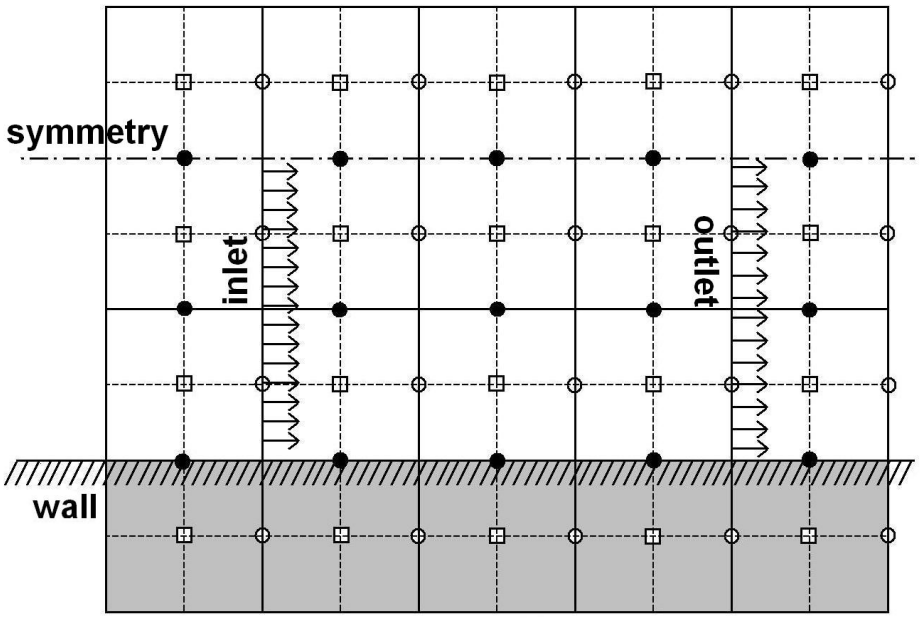

Figure 3.9 Boundary conditions and their alignment in the grid

3.4.2.3.1 Inlet

The required x velocity values for the channel inlet will be $u_{1,j}$ where j is ranging from 1 to j_{max}. Here j_{max} is standing as a placeholder for the number of cells in the longitudinal direction.

The y direction velocity nodes are not lying on the inlet boundary so the ghost cell values that should be defined for the implementation of inlet boundary values are $v_{1,j}$ where j is ranging from 1 to j_{max}. As stated above, by averaging with the adjacent fluid cells, ghost cell values will be used for obtaining the desired values at the boundary. Schematic view of the cells and y direction velocity nodes around the inlet boundary can be seen in Figure 3.10. Ghost cells are out of our problem domain as it is stated before. Averaged boundary values, which lie halfway between two y velocity nodes, can be calculated as,

$$v^*_{boundary,j} = \frac{v^*_{1,j} + v^*_{2,j}}{2} \tag{3.100}$$

in Equation (3.100) the j index is ranging from 1 to j_{max}. It is known that at the inlet boundary, vertical velocity component required to be set as zero. As a result, boundary condition for y velocity can be written as follows,

$$v^*_{boundary,j} = \frac{v^*_{1,j} + v^*_{2,j}}{2} = 0 \tag{3.101}$$

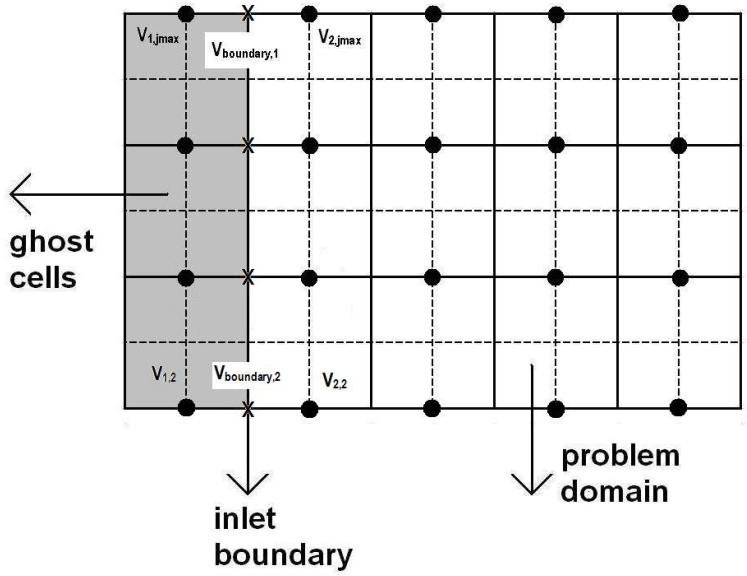

Figure 3.10 Schematic view of ghost cells of y velocity and inlet boundary

Similarly pressure and temperature boundary conditions can be imposed on the inlet boundary by using the ghost cells. The schematic view of the temperature and pressure nodes around that boundary can be seen in Figure 3.11. As it had

been shown above for the y-velocity values, temperature and pressure values at the boundary can be calculated by averaging the nodal values at both sides. Expressions for the pressure and temperature values at the inlet boundary can be written as follows.

$$p^*_{boundary,j} = \frac{p^*_{1,j} + p^*_{2,j}}{2} \tag{3.102}$$

$$\theta_{boundary,j} = \frac{\theta_{1,j} + \theta_{2,j}}{2} \tag{3.103}$$

Similar to Equation (3.101) in Equation (3.102) and (3.103) the index j varies from 1 to j_{max}, along the inlet boundary.

On the inlet boundary after setting the required velocity values, zero pressure gradient condition is also required to be set [60]. The pressure gradient at the inlet boundary can be expressed by using the ghost cell and adjacent fluid cell pressure values. The finite difference representation for the pressure gradient at the inlet is given below,

$$\left(\frac{\partial p^*}{\partial x^*}\right)_{boundary,j} = \frac{p^*_{2,j} - p^*_{1,j}}{\delta x^*} \tag{3.104}$$

Zero pressure gradient boundary condition is assured, by setting the appropriate values of the ghost cell nodes. Similarly desired temperature values at the inlet boundary are imposed by using ghost cells.

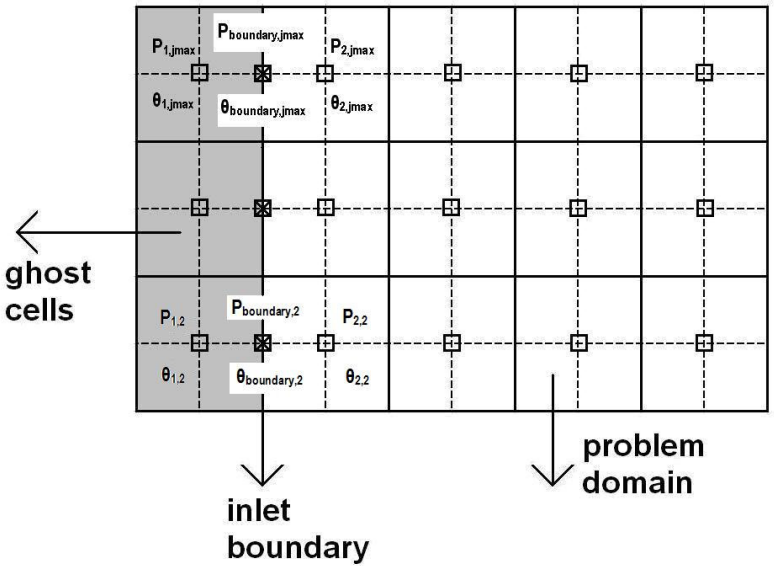

Figure 3.11 Schematic view of ghost cells for temperature and pressure at the inlet boundary

The x velocity nodes directly lie on the inlet boundary, as a result it is possible to define x velocity boundary values without using ghost cell values and averaging. The schematic representation of the x velocity nodes on the inlet boundary can be seen in Figure 3.12.

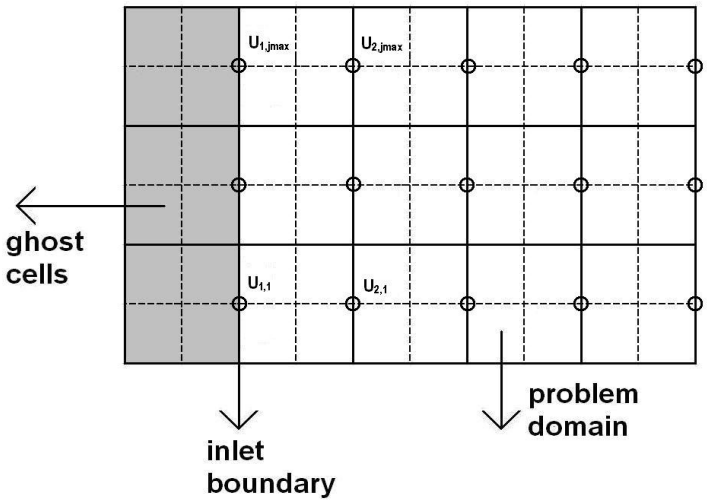

Figure 3.12 Schematic view of x velocity nodes at the inlet boundary

3.4.2.3.2 Wall

Wall boundary condition is imposed by using ghost cell method for temperature, pressure and x velocity. Procedure for defining temperature and pressure values on the wall boundary is similar to the procedure used for the inlet boundary. Again ghost cells values will be averaged with the adjacent fluid cell values on the boundary. The schematic view of ghost cells, problem domain, and pressure and temperature nodes is given in Figure 3.13

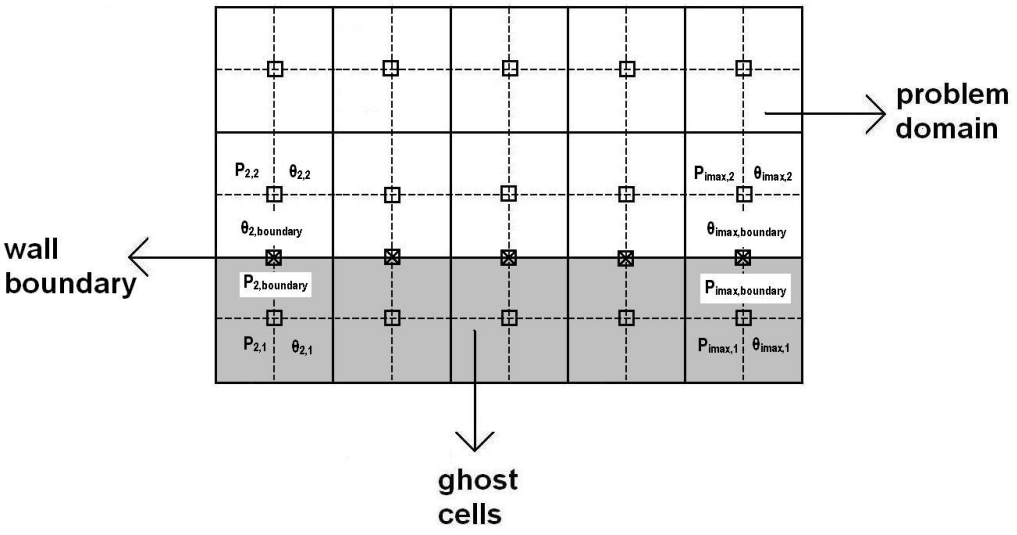

Figure 3.13 Schematic view of pressure and temperature nodes around the wall boundary

The index i will vary from 2 to i_{max}, for velocity, temperature and pressure values at wall boundary. Here, parameter i_{max} is a placeholder for the number of nodes in the x direction of problem domain. Likewise, pressure values will be implemented by averaging the two adjacent nodes to the boundary. The expression for the pressure values at the wall boundary can be written as follows.

$$p^*_{i,boundary} = \frac{p^*_{i,1} + p^*_{i,2}}{2} \tag{3.105}$$

Transverse pressure gradient at the wall boundary assumed to be zero. The representation for the pressure gradient $\left(\frac{\partial p^*}{\partial y^*}\right)_{i,boundaary}$ can be expressed as written below, by using central differencing with half mesh width.

$$\left(\frac{\partial p^*}{\partial y^*}\right)_{i,boundary} = \frac{p^*_{i,2} - p^*_{i,1}}{\delta y^*} \tag{3.106}$$

Another important issue is to define slip velocity at the wall boundary. Non-dimensional expression for the slip velocity after neglecting some of the terms can be written as follows,

$$u^* = u^*_s = 4Kn\left(\frac{\partial u^*}{\partial y^*}\right)_{y^*=0} \tag{3.107}$$

Similarly the expression for the temperature jump at the wall boundary can be written in non-dimensionalized form after simplification as,

$$\theta = \theta_s = \frac{4Kn}{\kappa}\left(\frac{\partial \theta}{\partial y^*}\right)_{y^*=0} \tag{3.108}$$

The temperature and velocity gradient given in Equation (3.107) and (3.108) can be represented in the following form by using the central differencing with half mesh width.

$$\left(\frac{\partial u^*}{\partial y^*}\right)_{i,boundary} = \frac{u^*_{i,2} - u^*_{i,1}}{\delta y^*} \tag{3.109}$$

$$\left(\frac{\partial \theta}{\partial y^*}\right)_{i,boundary} = \frac{\theta_{i,2} - \theta_{i,1}}{\delta y^*} \tag{3.110}$$

By using Equation (3.109) and (3.110), slip velocity and the temperature jump at the wall boundary can be expressed in terms of the adjacent node values. The

expressions for slip velocity and temperature jump in terms of node values are as follows,

$$u^*_{i,boundary} = u^*_s = 4Kn\left(\frac{u^*_{i,2} - u^*_{i,1}}{\delta y^*}\right) \tag{3.111}$$

$$\theta_{i,boundary} = \theta_s = \frac{4Kn}{\kappa}\left(\frac{\theta_{i,2} - \theta_{i,1}}{\delta y^*}\right) \tag{3.112}$$

In addition to Equation (3.111) and (3.112), one more algebraic relation is required for being able to define ghost node values. The required relation is obtained by averaging the values of nodes adjacent to boundary.

$$u^*_{i,boundary} = \frac{u^*_{i,1} + u^*_{i,2}}{2} \tag{3.113}$$

$$\theta_{i,boundary} = \frac{\theta_{i,1} + \theta_{i,2}}{2} \tag{3.114}$$

The arrangement of the nodes for x velocity values can be seen in Figure 3.14.

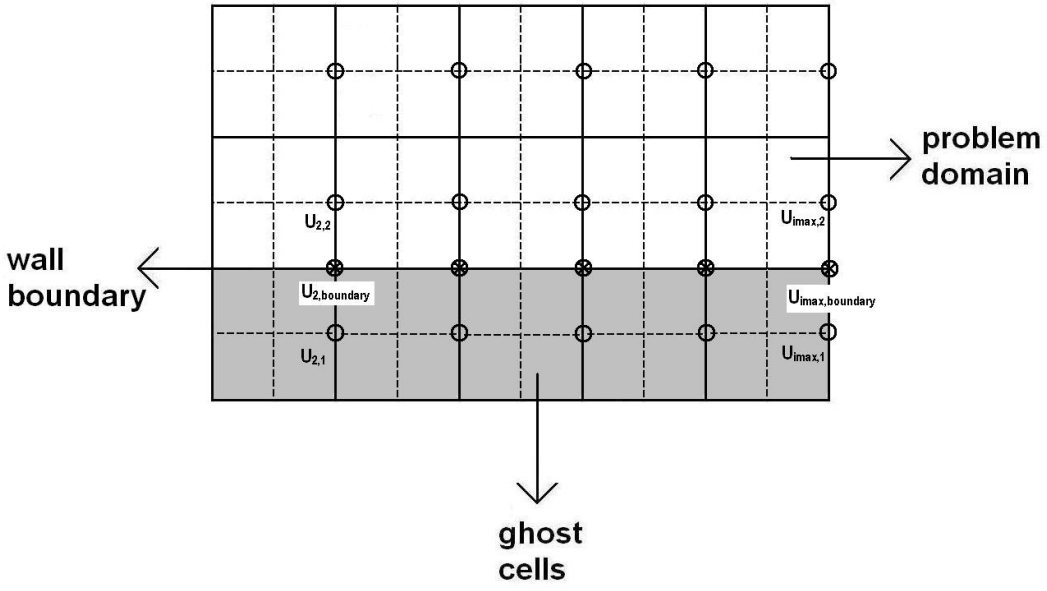

Figure 3.14 Schematic view of x velocity nodes around the wall boundary

By using the Equations (3.111), (3.112), (3.113), (3.114) it is possible to define the ghost cell values $\theta_{i,1}$ and $u^*_{i,1}$.

Since y velocity nodes lie on the wall boundary, values can be directly assigned to these nodes. The vertical component of velocity is equal to zero at the wall boundary. The schematic representation of y velocity node arrangement on the wall boundary is given in Figure 3.15.

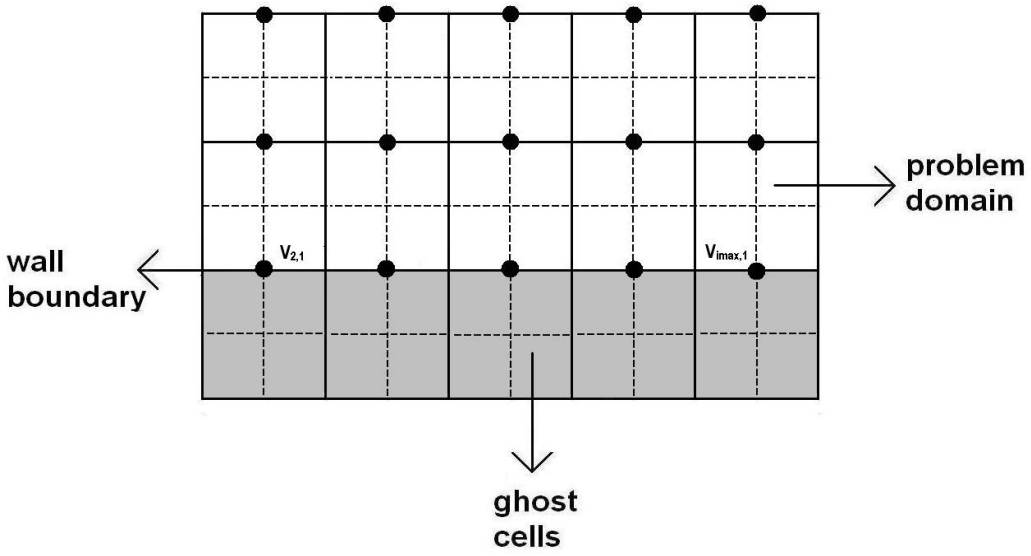

Figure 3.15 Schematic view of y velocity nodes around the wall boundary

3.4.2.3.3 Outlet

In our case, outlet boundary condition is located at the end of the channel where, flow reaches fully developed state. Gradients of the flow variables converge to zero as the flow is fully developed. For this reason at the outlet boundary, gradients of flow variables are set equal to zero. As it is utilized while defining other boundary conditions, ghost cell method is used for the outlet boundary. The alignment of pressure and temperature nodes around the outlet boundary can be seen in Figure 3.16.

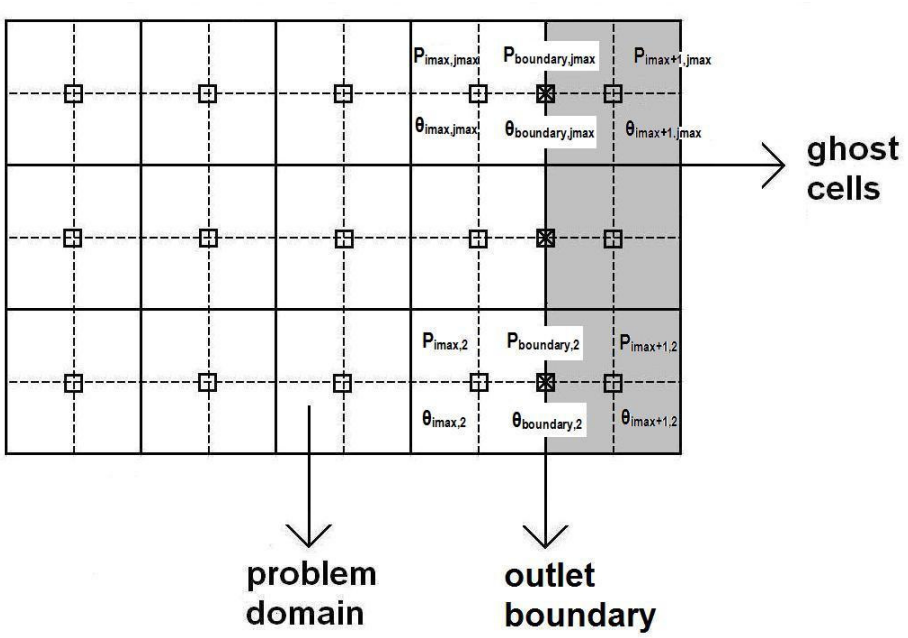

Figure 3.16 Schematic view of pressure and temperature nodes around the outlet boundary

Finite difference equations for pressure and temperature gradients at the boundary are discretized with half mesh width and central differencing. Discretized form of the pressure and temperature gradients will be as follows,

$$\left(\frac{\partial p^*}{\partial x^*}\right)_{boundary,j} = \frac{p^*_{i\max+1,j} - p^*_{\max i,j}}{\delta x^*} = 0 \tag{3.115}$$

$$\left(\frac{\partial \theta}{\partial x^*}\right)_{boundary,j} = \frac{\theta_{i\max+1,j} - \theta_{\max i,j}}{\delta x^*} = 0 \tag{3.116}$$

The x velocity gradient in the axial direction will be equal to zero also. The gradient can be expressed in terms of adjacent nodes, by using finite difference

method. The velocity gradient is discretized with central differencing and full mesh width around outlet boundary. The discretized boundary condition is written as follows.

$$\left(\frac{\partial u^*}{\partial x^*}\right)_{boundary,j} = \frac{u^*_{i\max+1,j} - u^*_{\max i-1,j}}{2\delta x^*} = 0 \tag{3.117}$$

The arrangement of x velocity cells around the outlet boundary can be seen in Figure 3.17.

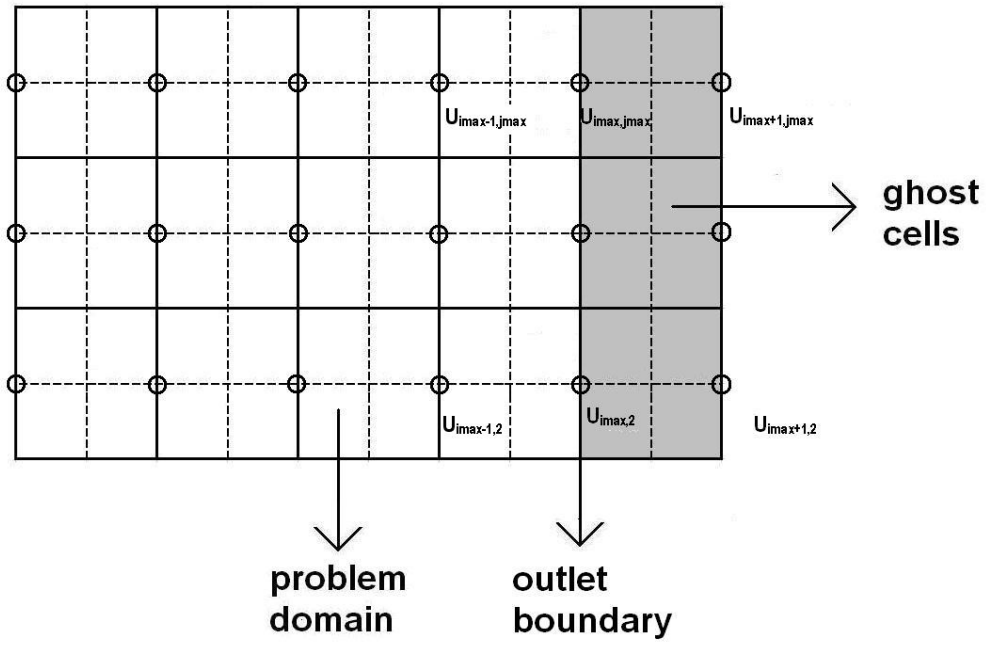

Figure 3.17 Schematic view of x velocity nodes around the outlet boundary

Similar to other flow variables also y velocity gradient will be equal to zero at the outlet boundary. The schematic view of y velocity nodes around the outlet boundary is given in Figure 3.18. The y velocity gradient at the boundary can discretized with half mesh width, as follows,

$$\left(\frac{\partial v^*}{\partial x^*}\right)_{boundary,j} = \frac{v^*_{i\max+1,j} - v^*_{\max i,j}}{\delta x^*} = 0 \tag{3.118}$$

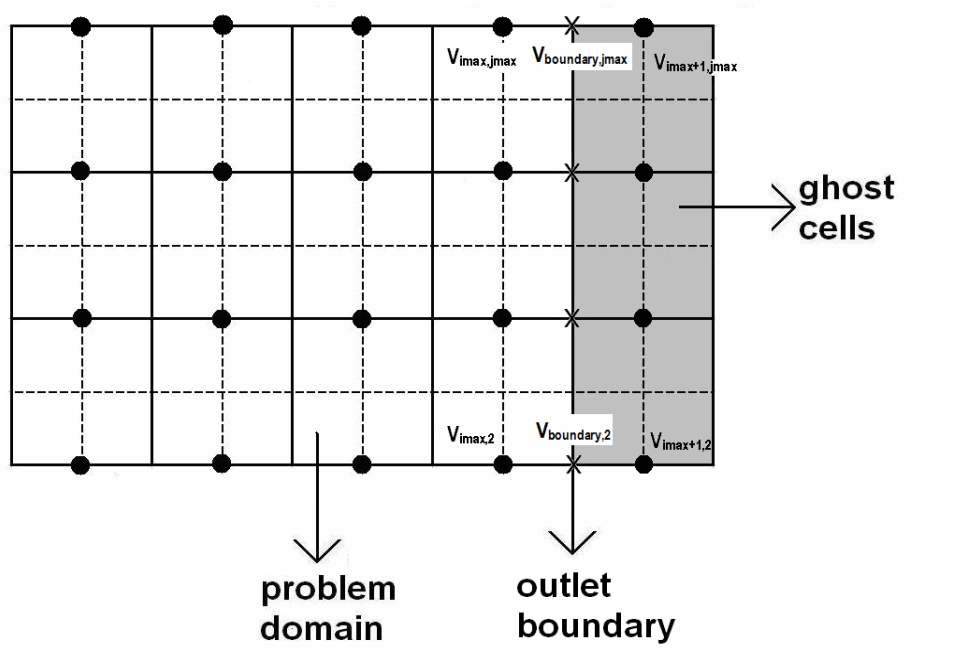

Figure 3.18 Schematic view of y velocity nodes around the outlet boundary

3.4.2.3.4 Symmetry

Since velocity and temperature profiles for the flowing fluid between parallel plates are symmetrical around the centerline, it would be convenient to use

symmetry boundary condition to reduce the computational domain size and computation time. Velocity temperature and pressure values are mirrored through the symmetry boundary. The alignment of pressure and temperature nodes around the symmetry boundary can be seen in Figure 3.19.

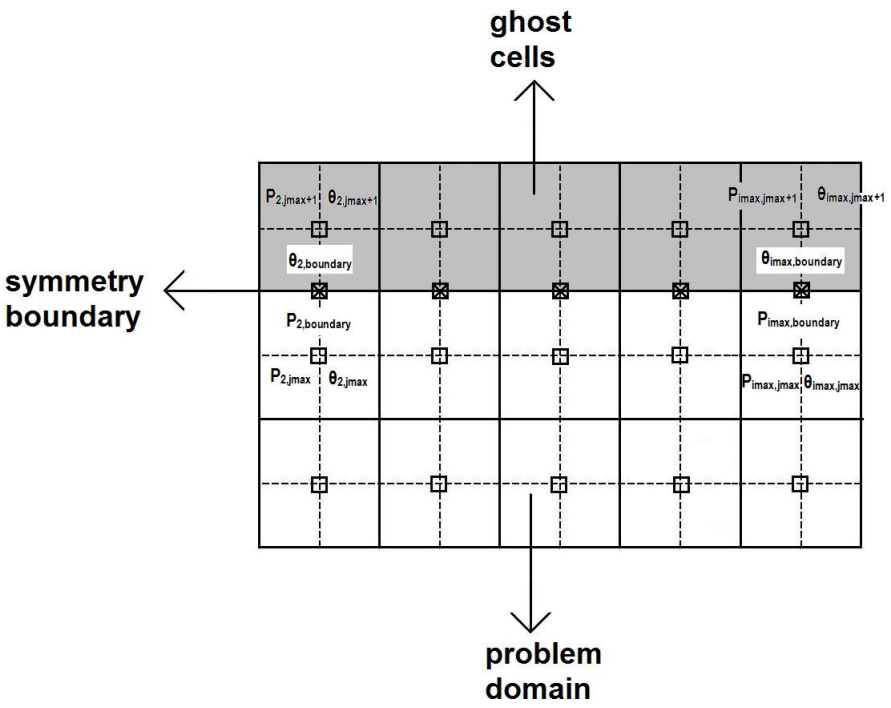

Figure 3.19 Schematic view of pressure and temperature nodes around the symmetry boundary

The ghost cell pressure and temperature values required to be set as follows,

$$p^*_{i,j\max+1} = p^*_{i,j\max} \tag{3.119}$$

$$\theta_{i,j\max+1} = \theta_{i,j\max} \tag{3.120}$$

Similar to pressure and temperature, x velocity values are also mirrored through symmetry boundary. Figure 3.20 shows the alignment of x velocity nodes around the symmetry boundary.

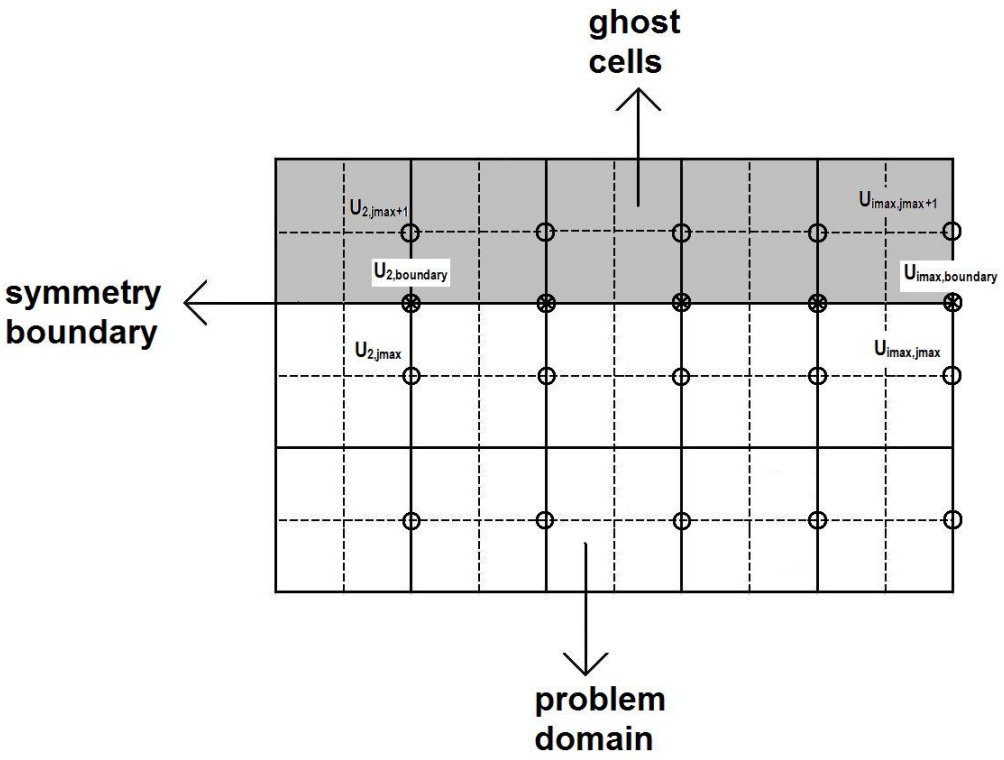

Figure 3.20 Schematic view of x velocity nodes around the symmetry boundary

The ghost cell values required to be set as follows, to assure symmetry boundary condition,

$$u^*_{i,j\max+1} = u^*_{i,j\max} \tag{3.121}$$

As it can be seen in Figure 3.21, y velocity nodes lie on the symmetry boundary, and it is known that at the symmetry point of flow, y velocity is equal to zero. Then y velocity values can be defined as zero, explicitly.

$$v^{*}_{i,j\max} = 0 \tag{3.122}$$

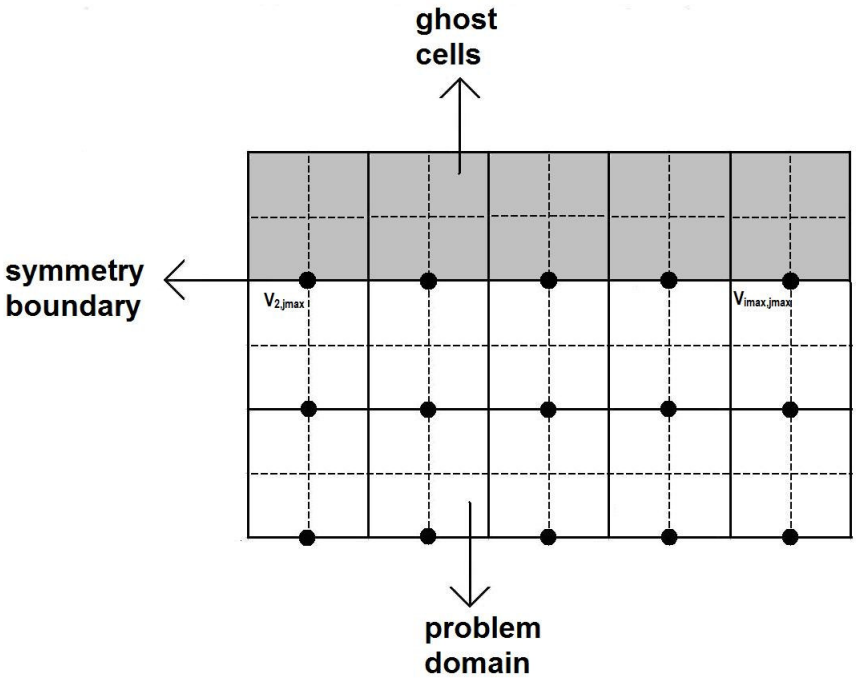

Figure 3.21 Schematic view of y velocity nodes on the symmetry boundary

3.5 Solution Method

Since the x momentum and y momentum equations are separate, sequential solution method is used throughout the study. In addition to x and y momentum

equation, to be able to solve pressure unknowns, continuity equation is also used. Additionally for analyzing heat transfer, energy equation is also employed. As stated earlier, investigation is focused on the effects of property variation on fluid flow and heat transfer. For this reason, beside continuity and momentum equations, energy equation is also required to be solved conjointly with both momentum and continuity equations. Due to the variation of viscosity with temperature, both temperature and velocity profile will be affected. In brief, momentum, continuity and energy equations are required to be solved at the same iteration.

The discretized equations will be solved in a transient manner by the solver. The solution begins at time t*=0. The initial values for the unknowns are set for the beginning of time. The time is incremented by δt, and at each time step, values of unknowns are updated. This time stepping loop is continued until certain variables become fixed in a definite precision range.

Before discussing the time stepping loop, procedure for solving velocity and pressure unknowns simultaneously, will be explained below.

First, discretized momentum equations are rearranged as follows. The superscripts in the parentheses are denoting the time step that, variable is calculated.

$$u^{*(n+1)} = u^{*(n)} + \delta t\left[-\frac{\partial(u^{*2})}{\partial x^*} - \frac{\partial(u^* v^*)}{\partial y^*} - \frac{\partial p^*}{\partial x^*} + \frac{1}{\mathrm{Re}}\left(\frac{\partial^2 u^*}{\partial x^{*2}} + \frac{\partial^2 u^*}{\partial y^{*2}} + 2\frac{\partial \mu^*}{\partial x^*}\frac{\partial u^*}{\partial x^*} + \frac{\partial \mu^*}{\partial y^*}\frac{\partial v^*}{\partial x^*} + \frac{\partial \mu^*}{\partial y^*}\frac{\partial u^*}{\partial y^*}\right)\right] \tag{3.123}$$

$$v^{*(n+1)} = v^{*(n+1)} + \delta t\left[-\frac{\partial(u^* v^*)}{\partial x^*} - \frac{\partial(v^{*2})}{\partial y^*} - \frac{\partial p^*}{\partial y^*} + \frac{1}{\mathrm{Re}}\left(\frac{\partial^2 v^*}{\partial x^{*2}} + \frac{\partial^2 v^*}{\partial y^{*2}} + 2\frac{\partial \mu^*}{\partial y^*}\frac{\partial v^*}{\partial y^*} + \frac{\partial \mu^*}{\partial x^*}\frac{\partial v^*}{\partial x^*} + \frac{\partial \mu^*}{\partial x^*}\frac{\partial u^*}{\partial y^*} \right)\right] \tag{3.124}$$

For convenience, some of the terms in Equations (3.123) and (3.124) are grouped and renamed as A and B respectively;

$$A^{(n)} = u^{*(n)} + \delta t\left[-\frac{\partial(u^{*2})}{\partial x^*} - \frac{\partial(u^* v^*)}{\partial y^*} + \frac{1}{\mathrm{Re}}\left(\frac{\partial^2 u^*}{\partial x^{*2}} + \frac{\partial^2 u^*}{\partial y^{*2}} + 2\frac{\partial \mu^*}{\partial x^*}\frac{\partial u^*}{\partial x^*} + \frac{\partial \mu^*}{\partial y^*}\frac{\partial v^*}{\partial x^*} + \frac{\partial \mu^*}{\partial y^*}\frac{\partial u^*}{\partial y^*} \right)\right] \tag{3.125}$$

$$B^{(n)} = v^{*(n)} + \delta t\left[-\frac{\partial(u^* v^*)}{\partial x^*} - \frac{\partial(v^{*2})}{\partial y^*} + \frac{1}{\mathrm{Re}}\left(\frac{\partial^2 v^*}{\partial x^{*2}} + \frac{\partial^2 v^*}{\partial y^{*2}} + 2\frac{\partial \mu^*}{\partial y^*}\frac{\partial v^*}{\partial y^*} + \frac{\partial \mu^*}{\partial x^*}\frac{\partial v^*}{\partial x^*} + \frac{\partial \mu^*}{\partial x^*}\frac{\partial u^*}{\partial y^*} \right)\right] \tag{3.126}$$

By using the Equations (3.125) and (3.126), Equations (3.123) and (3.124) can be rearranged as,

$$u^{*(n+1)} = A^{(n)} - \delta t \frac{\partial p^{*(n+1)}}{\partial x^*} \tag{3.127}$$

$$v^{*(n+1)} = B^{(n)} - \delta t \frac{\partial p^{*(n+1)}}{\partial y^*} \tag{3.128}$$

All of the variables in Equations (3.127) and (3.128) are related to a time level. Here A and B terms are associated with time level n while the terms $\frac{\partial p^*}{\partial x^*}$ and $\frac{\partial p^*}{\partial y^*}$ belongs to time level n+1. In other words spatial derivatives of pressure are calculated by using the updated values at same time step. On the other hand spatial derivatives in terms A and B are calculated by using the values obtained from previous time step. Namely, velocity field can be calculated for time level (n+1) once the pressure field is known at that time level.

Using the Equations (3.123), (3.124) and the continuity equation which is written below, it is possible to derive Poisson equation for the pressure values at time level n+1.

$$\frac{\partial u^*}{\partial x^*}+\frac{\partial v^*}{\partial y^*}=0 \tag{3.129}$$

Equation (3.129) is non-dimensionalized continuity equation for two dimensions in Cartesian coordinates. By substituting Equations (3.123) and (3.124) into continuity equation one can get,

$$\frac{\partial u^{*(n+1)}}{\partial x^*}+\frac{\partial v^{*(n+1)}}{\partial y^*}=\frac{\partial A^{(n+1)}}{\partial x^*}-\delta t\frac{\partial^2 p^{*(n+1)}}{\partial x^{*2}}+\frac{\partial B^{(n+1)}}{\partial y^*}-\delta t\frac{\partial^2 p^{*(n+1)}}{\partial y^{*2}}=0 \tag{3.130}$$

After rearranging the expression in Equation (3.130) it is possible to obtain an expression for pressure values at time level n+1, in terms of spatial derivatives of velocity and other unknowns calculated at previous time level n.

$$\frac{\partial^2 p^{*(n+1)}}{\partial x^{*2}}+\frac{\partial^2 p^{*(n+1)}}{\partial y^{*2}}=\frac{1}{\delta t}\left(\frac{\partial A^{(n+1)}}{\partial x^*}+\frac{\partial B^{(n+1)}}{\partial y^*}\right) \tag{3.131}$$

The Equation (3.131) should be discretized before solution. As it is stated above pressure values and velocity values are assigned to different nodes on a cell. For this reason Equation (3.131) can be discretized by central differencing around the cell center as follows,

$$\frac{p_{i+1,j}^{*(n+1)} - 2p_{i,j}^{*(n+1)} + p_{i-1,j}^{*(n+1)}}{(\delta x)^2} + \frac{p_{i,j+1}^{*(n+1)} - 2p_{i,j}^{*(n+1)} + p_{i,j+1}^{*(n+1)}}{(\delta y)^2} = \frac{1}{\delta t}\left(\frac{A_{i,j}^{(n)} - A_{i-1,j}^{(n)}}{\delta x} + \frac{B_{i,j}^{(n)} - B_{i-1,j}^{(n)}}{\delta y} \right) \tag{3.132}$$

In Equation (3.132) i and j indices vary from 1 to i_{max} and j_{max} respectively. By using the boundary values, it is possible to solve this system of equations for pressure unknowns. Pressure matrix for the nodes of problem domain is solved iteratively by using Gauss-Seidel iteration method combined with Successive Over Relaxation (SOR) method. Before applying this iterative method, pressure values are set as zero initially. Iterations for the solution of pressure matrix is terminated when least square of the residual matrix of pressure variables fallen below 0.001. This predetermined tolerance was enough to get desired solutions.

First, pressure unknowns are iteratively solved for the *(n+1)*th time step by using the velocity and viscosity values of the *(n)*th time step. Then both x and y velocity values are calculated for the *(n+1)*th time step by using the pressure values. These updated values for velocities are used in the solution of energy equation. The procedure for updating velocity values with the obtained pressure values are given below.

$$u_{i,j}^{*(n+1)} = A_{i,j}^{n} - \frac{\delta t}{\delta x}(p_{i+1,j}^{*(n+1)} + p_{i,j}^{*(n+1)}) \tag{3.133}$$

$$v_{i,j}^{*(n+1)} = B_{i,j}^{n} - \frac{\delta t}{\delta y}(p_{i,j+1}^{*(n+1)} + p_{i,j}^{*(n+1)}) \tag{3.134}$$

Since, pressure and velocity nodes are aligned in a staggered form it is possible to discretize the spatial derivative of pressure by using central differencing with half mesh width.

After completing the calculation of new velocity and pressure values, the temperature variables will be solved. The rearranged form of the energy equation can be written as follows.

$$\begin{aligned}\frac{\partial\theta}{\partial t^*} &= \frac{1}{\mathrm{Re}\,\mathrm{Pr}}\left(\frac{\partial k^*}{\partial x^*}\frac{\partial\theta}{\partial x^*} + k^*\frac{\partial^2\theta}{\partial x^{*2}} + \frac{\partial k^*}{\partial y^*}\frac{\partial\theta}{\partial y^*} + k^*\frac{\partial^2\theta}{\partial y^{*2}}\right) + \\ &\frac{Br}{\mathrm{Re}\,\mathrm{Pr}}\left[2\mu^*\left(\left(\frac{\partial u^*}{\partial x^*}\right)^2 + \left(\frac{\partial v^*}{\partial y^*}\right)^2 + \left(\frac{\partial u^*}{\partial y^*} + \frac{\partial v^*}{\partial x^*}\right)\right)\right] - u^*\frac{\partial\theta}{\partial x^*} - v^*\frac{\partial\theta}{\partial y^*}\end{aligned} \tag{3.135}$$

By using the calculated temperature variables in the previous time step, it is possible to update temperature values.

When all temperature variables are updated, dimensionless viscosity and thermal conductivity can be calculated. These variables are algebraically related to dimensionless temperature as it is discussed above. The time stepping is continued until difference between local Nusselt values in two consecutive time steps fall below 10^{-3}. This criterion is validated during validation studies.

3.6 Code Validation

Code is written in commercial software MATLAB®. Since the geometry is uncomplicated, no additional algorithm is used for mesh generation. However it is

possible to use less grid points by using mesh stretching. However, simple structured grid is used since it is very easy to transform the physical domain into computational domain. The number of nodes that will be used in longitudinal and transverse directions can be defined by using the user interface before starting solution.

Code validation studies performed by using the analytical and numerical results given in references [28],[62] and [63]. Both velocity profiles and fully developed Nusselt values available in the references are used for comparison. Validation of the Nusselt values will give an idea about the accuracy of temperature distribution obtained from our numerical solver. The available solutions are made by neglecting the effect of axial conduction and transverse convection; for this reason additional runs are required for validation. Furthermore, as a result of the difference in Knudsen number definition, between this study and reference [62], the available results can be compared for Knudsen numbers 0.01, 0.02 and 0.04. In addition to the comparison mesh independence is also tested by making preliminary test runs for different numbers of vertical and longitudinal grid points. This mesh independence study is performed for Knudsen number 0.1 and Brinkman number equal to 0.001 by neglecting the effect of axial conduction. Obtained fully developed Nusselt values and x-velocity profile is compared with the references. As stated previously, in the study of Jeong and Jeong [28] the fully developed Nusselt values are obtained by making analytical solution. On the other hand, Çetin [62] obtained the same results numerically. The only difference in their study is the non-dimensionalization, of Knudsen numbers.

The variation of Nusselt values for different mesh sizes are plotted against axial position in Figure 3.22. The results are obtained for 50 x 300, 80 x 480 and 100 x 600, vertical and longitudinal grid points.

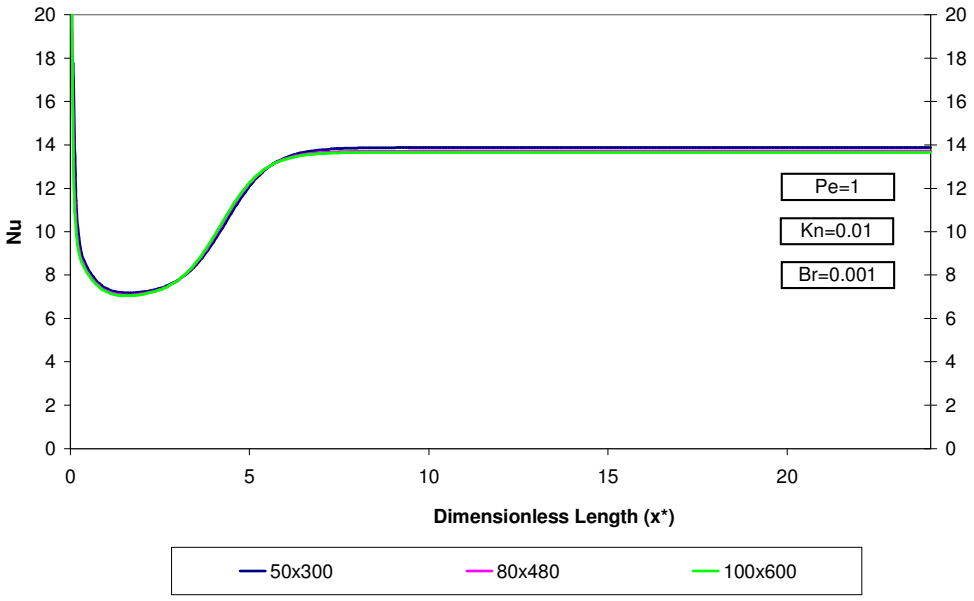

Figure 3.22 Variation of Nusselt number with axial position for different mesh sizes, obtained from constant property solutions by neglecting the axial conduction (Kn=0.01, Pe=1, Br=0.001)

However the difference between results of different mesh sizes can not be clearly seen in Figure 3.22. The fully developed Nusselt values are tabulated in Table 3.1 for different mesh sizes, by comparing them with the results of reference [28] which is also in agreement with the results of [63].

Table 3.1 Fully developed Nusselt numbers, for thermally developing flow for various mesh sizes (Axial conduction is neglected)

Kn=0.01	Nu_{fd}	Nu_{fd}[28]	% difference
50x300	13,868	13,669	1,456
80 x480	13,712		0,315
100 x 600	13,660		-0,066

In addition to the fully developed Nusselt values, also fully developed x-velocity values are compared with the analytically obtained results. The analytical derivation for the velocity profiles in a two dimensional half channel is as follows. First the flow is assumed to be fully developed and only function of y.

$$u^* = f(y) \tag{3.136}$$

Since the flow is fully developed, the vertical components will vanish.

$$v^* = 0 \tag{3.137}$$

The dimensional x-momentum equation given below can be written again according to these assumptions and constant properties.

$$\frac{\partial u}{\partial t} + \frac{\partial (u^2)}{\partial x} + \frac{\partial (uv)}{\partial y} = -\frac{1}{\rho}\frac{\partial p}{\partial x} + \frac{\mu}{\rho}\left(\frac{\partial^2 u}{\partial x^2} + \frac{\partial^2 u}{\partial y^2} + 2\frac{\partial \mu}{\partial x}\frac{\partial u}{\partial x} + \frac{\partial \mu}{\partial y}\frac{\partial v}{\partial x} + \frac{\partial \mu}{\partial y}\frac{\partial u}{\partial y} \right) \tag{3.138}$$

The reduced x-momentum equation will take the following form,

$$\frac{1}{\rho}\frac{\partial p}{\partial x}=\frac{\mu}{\rho}\left(\frac{\partial^2 u}{\partial y^2}\right) \tag{3.139}$$

After simplification of y-momentum equation which is written below,

$$\frac{\partial v}{\partial t}+\frac{\partial (uv)}{\partial x}+\frac{\partial (v^2)}{\partial y}=-\frac{1}{\rho}\frac{\partial p}{\partial y}+ \\ \frac{\mu}{\rho}\left(\frac{\partial^2 v}{\partial x^2}+\frac{\partial^2 v}{\partial y^2}+2\frac{\partial \mu}{\partial y}\frac{\partial v}{\partial y}+\frac{\partial \mu}{\partial x}\frac{\partial v}{\partial x}+\frac{\partial \mu}{\partial x}\frac{\partial u}{\partial y}\right) \tag{3.140}$$

The reduced y-momentum equation will yields,

$$\frac{1}{\rho}\frac{\partial p}{\partial y}=0 \tag{3.141}$$

Then it is showed that pressure is only a function of x. In Equation (3.139) right hand side is only function of y while left hand side is only function of x. Then both right hand side and left hand side of Equation (3.139) should be equal to a constant.

$$\frac{\partial p}{\partial x}=\text{constant} \tag{3.142}$$

$$\frac{\partial^2 u}{\partial y^2}=\text{constant} \tag{3.143}$$

Here assuming a pressure drop Δp through finite tube length Δx. It is possible to write the left hand side of Equation (3.139) as follows,

$$\frac{\Delta p}{\mu \Delta x} = \frac{\partial^2 u}{\partial y^2} \tag{3.144}$$

By using the boundary conditions for the half channel used in the model given in Figure 3. 4. Ordinary differential equation (Equation (3.144)) can be solved. The boundary conditions are defined below, in dimensional form.

$$y = 0 \qquad u = u_s \tag{3.145}$$

$$y = H \qquad u = finite \tag{3.146}$$

Slip velocity u_s is defined earlier, and can be written as follows,

$$u_s = \lambda \left(\frac{\partial u}{\partial y} \right)_{y=0} \tag{3.147}$$

After integrating twice, Equation (3.144) can be written as,

$$u(y) = \frac{\Delta p}{\mu \Delta x} y^2 + c_1 y + c_2 \tag{3.148}$$

The c_1 and c_2 are constants of integration, which can be determined by using boundary conditions.

$$u(y) = \frac{\Delta p}{\mu \Delta x} y^2 - 2\frac{\Delta pH}{\mu \Delta x} y - 8Kn\frac{\Delta pH^2}{\mu \Delta x} \tag{3.149}$$

By using the definition of mean velocity, after integrating velocity field over the channel width,

$$U_{\infty} = \frac{1}{H}\int_{0}^{H} u(y)dy \tag{3.150}$$

Integrated mean velocity is given below,

$$U_{\infty} = \frac{2}{3}\left(-\frac{\Delta p H^2}{\mu \Delta x} - 12Kn\frac{\Delta p H^2}{\mu \Delta x}\right) \tag{3.151}$$

Then dimensionless form of the x-velocity given in Equation (3.149) can be written as follows by using the non-dimensional parameters defined earlier,

$$u^* = \frac{u(y^*)}{U_{\infty}} = \frac{3}{2}\frac{(2y^* - y^{*2} + 8Kn)}{1+12Kn} \tag{3.152}$$

After obtaining the analytical representation for fully developed x-velocity, the analytical results can be compared with the numerical ones. The dimensionless x-velocity profiles obtained by using different mesh sizes are plotted against dimensionless channel width in Figure 3.23.

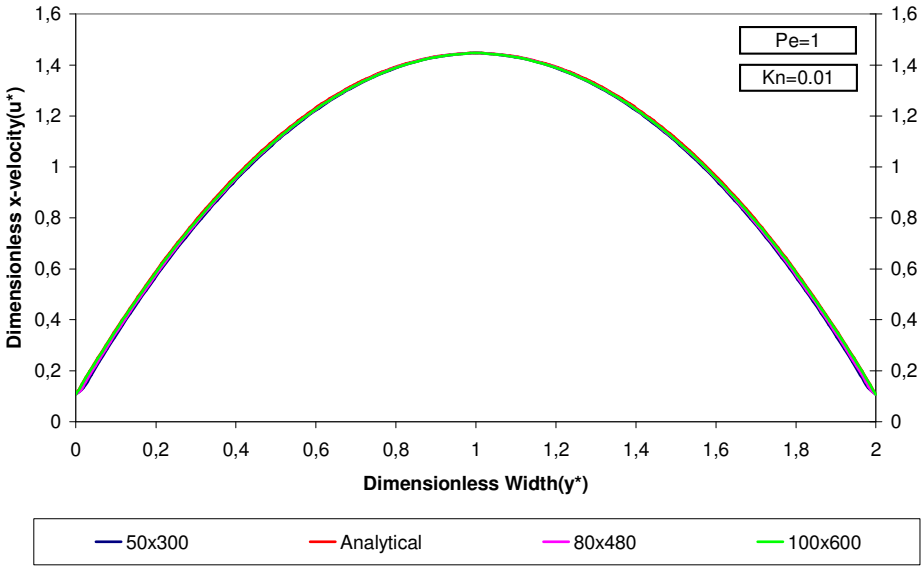

Figure 3.23 Variation of fully developed x-velocity with channel width for different mesh sizes, obtained from constant property solutions (Kn=0.01, Pe=1)

As can be seen from Figure 3.23 the difference between fully developed x-velocity values are negligibly low for different mesh sizes and the plots are overlapped. Since velocity values are not different, the fully developed Nusselt results will be taken as a reference for comparison and 100 grid points used in vertical direction, while 600 grid points are used for the longitudinal direction.

Another comparison is made with the Reference [62] in which fully developed Nusselt values are obtained by neglecting the effects of axial conduction and viscous dissipation. The results are given in comparison in Table 3.2.

Table 3.2 Fully developed Nusselt numbers, for thermally developing flow (Axial conduction and viscous dissipation is neglected)

	Nu_{fd}	Nu_{fd}[62]	% Difference
Kn 0.00	7.541	7.541	0.000
Kn 0.01	6.921	6.925	0.058
Kn 0.02	6.369	6.374	0.078
Kn 0.04	5.441	5.445	0.073

The fully developed Nusselt values obtained from solutions, in which viscous dissipation is included, are tabulated in Table 3.3. These results are compared with the reference [28] in which non-dimensional parameter definition is the same with this study. In these solutions axial conduction is neglected.

Table 3.3 Fully developed Nusselt numbers, for thermally developing flow (Axial conduction is neglected)

Kn	Nu_{fd}	Nu_{fd}[28]	% difference
0.01	13.660	13.690	0.219
0.02	11.208	11.223	0.132
0.04	8.227	8.230	0.042
0.06	6.486	6.486	0.002
0.08	5.348	5.347	-0.015
0.1	4.547	4.547	-0.017

In addition to the slip flow regime also macro scale flow results are taken as a reference. As it is given in Table 3.2 for macro scale laminar flow without viscous dissipation, axial conduction and radial convection, fully developed Nusselt number converges to 7.541

Moreover as mentioned above, fully developed x velocities also can be compared with the analytical solutions, to verify the accuracy of solver. For this purpose the non-dimensional velocity profiles are compared with the analytical results for different Knudsen numbers. The comparison of developed non-dimensional x velocity values are given in Figure 3.24. The dashed lines in the figure are representing the analytical velocity profiles while the solid lines are velocity profiles obtained from numerical solutions.

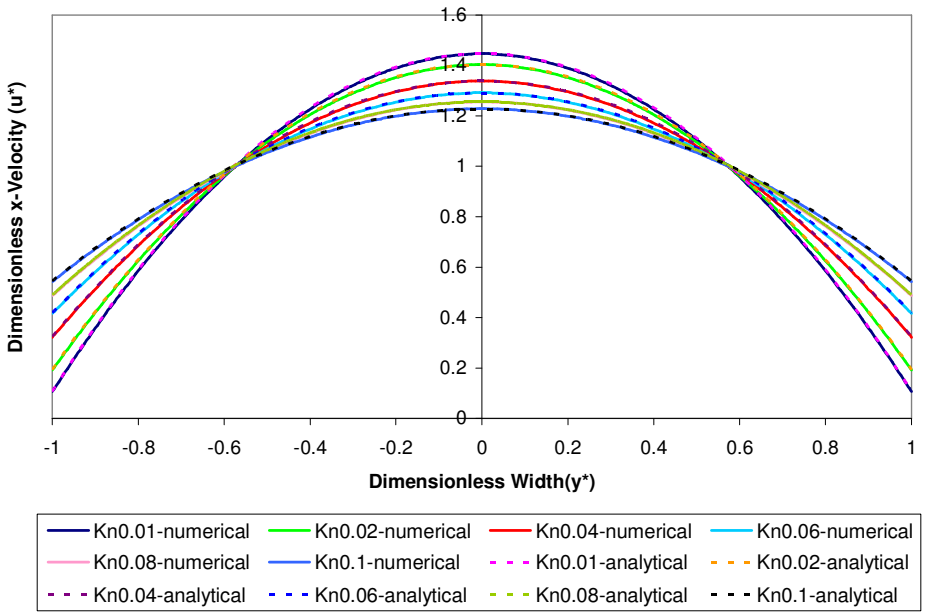

Figure 3.24 Dimensionless fully developed x velocity plotted against dimensionless channel width for various Knudsen numbers. (Analytical and numerical data is used)

Mesh size is determined by trial and using the comparisons for Nusselt number and velocity profiles. In addition to mesh size, time step size also affects the convergence characteristics. To be able to increase the convergence rate, while decreasing the run times, adaptive time stepping algorithm is added into code. This algorithm selects the maximum time step size, satisfying the stability condition. The details of the stability criterion is given in [60]

CHAPTER 4

RESULTS AND DISCUSSION

In this chapter, results obtained from numerical analyses will be presented and discussed in detail. The velocity and temperature distribution is investigated in a micro channel with constant wall temperature. Simultaneously developing flow conditions are analyzed regarding the variation of viscosity and thermal conductivity. Numerical simulations are repeated for different Knudsen numbers, Brinkman numbers and Reynolds numbers in combination. Working fluid is chosen as air. Since air has a definite mean free path at room temperature, by defining the Knudsen number range subject to investigation, hydraulic diameter of the microchannels that will be analyzed is fixed. Another limitation in our analyses is related with the compressibility. The solutions are made by assuming that air is incompressible, for this reason maximum velocity of air is required to be lower than 0.3 Mach for the pressure and temperature range of the analyses. According to these limitations low Reynolds numbers are used in the analyses for the sake of being realistic, which also yield low Péclet numbers. The effect of Reynolds and Péclet number will be discussed in detail in the following sections.

Knudsen numbers are chosen in the 0.1-0.001 range which is the limit values for the slip flow regime. Analyses are repeated for different Knudsen numbers to demonstrate the effect of rarefaction on property variation in slip flow. Similarly different Brinkman numbers are chosen to show the influence of viscous dissipation on property variation in slip flow. Additionally, for two different

Péclet numbers analyses are performed for visualizing the effect of axial conduction.

Dimensionless numbers and expressions are frequently used while presenting the results. The effect of property variation on fluid flow and heat transfer will be expressed in terms of Nusselt number. Variation of heat transfer characteristics with the effects of viscous dissipation, rarefaction, geometric dimensions and axial conduction will be illustrated in terms of local and average Nusselt values. Regarding the non-dimensional momentum and energy equations given below effects of non-dimensional parameters can be analyzed.

$$\frac{\partial u^*}{\partial t^*}+\frac{\partial (u^{*2})}{\partial x^*}+\frac{\partial (u^*v^*)}{\partial y^*}=-\frac{\partial p^*}{\partial x^*}+ \frac{1}{\mathrm{Re}}\left(\frac{\partial^2 u^*}{\partial x^{*2}}+\frac{\partial^2 u^*}{\partial y^{*2}}+2\frac{\partial \mu^*}{\partial x^*}\frac{\partial u^*}{\partial x^*}+\frac{\partial \mu^*}{\partial y^*}\frac{\partial v^*}{\partial x^*}+\frac{\partial \mu^*}{\partial y^*}\frac{\partial u^*}{\partial y^*}\right) \tag{4.1}$$

$$\frac{\partial v^*}{\partial t^*}+\frac{\partial (u^*v^*)}{\partial x^*}+\frac{\partial (v^{*2})}{\partial y^*}=-\frac{\partial p^*}{\partial y^*}+ \frac{1}{\mathrm{Re}}\left(\frac{\partial^2 v^*}{\partial x^{*2}}+\frac{\partial^2 v^*}{\partial y^{*2}}+2\frac{\partial \mu^*}{\partial y^*}\frac{\partial v^*}{\partial y^*}+\frac{\partial \mu^*}{\partial x^*}\frac{\partial v^*}{\partial x^*}+\frac{\partial \mu^*}{\partial x^*}\frac{\partial u^*}{\partial y^*}\right) \tag{4.2}$$

$$\frac{\partial \theta}{\partial t^*}+u^*\frac{\partial \theta}{\partial x^*}+v^*\frac{\partial \theta}{\partial y^*}=\frac{1}{\mathrm{Re}\,\mathrm{Pr}}\left(\frac{\partial k^*}{\partial x^*}\frac{\partial \theta}{\partial x^*}+k^*\frac{\partial^2 \theta}{\partial x^{*2}}+\frac{\partial k^*}{\partial y^*}\frac{\partial \theta}{\partial y^*}+k^*\frac{\partial^2 \theta}{\partial y^{*2}}\right)+ \frac{Br}{\mathrm{Re}\,\mathrm{Pr}}\left[2\mu^*\left(\left(\frac{\partial u^*}{\partial x^*}\right)^2+\left(\frac{\partial v^*}{\partial y^*}\right)^2+\left(\frac{\partial u^*}{\partial y^*}+\frac{\partial v^*}{\partial x^*}\right)\right)\right] \tag{4.3}$$

Here,

$$Br = \frac{\mu_\infty U_\infty^2}{k_\infty (T_i - T_w)} \tag{4.4}$$

$$Pe = \mathrm{Re}\,\mathrm{Pr} \tag{4.5}$$

4.1 Results for Simultaneously Developing Flow

In this section, results will be presented for simultaneously developing flow, by considering both constant and variable thermophysical properties. The results are obtained for Knudsen numbers, 0.01, 0.02, 0.04, 0.06, 0.08, and 0.1. For all the Knudsen numbers analyses are repeated by changing the Brinkman number values. The Brinkman number values used are 0.001, 0.01, 0.1, -0.001, -0.01, 0.1. The analyses are repeated for six different Knudsen and six different Brinkman numbers, with a fixed Péclet number, which is 1. Then to be able to understand the effect of Reynolds and Péclet number, some of the analyses are conducted with a different Péclet number which is equal to 3.57. The plots are given for a few of the parameters used in the analyses for simplicity. Additional plots are available in Appendix A.

The effect of rarefaction can be clearly seen from the velocity values at the wall boundary, which are shown on the vertical axis in Figure 4.1. As the Knudsen number increases, the effect of rarefaction and the slip velocities at the wall increase. Development of the x-velocity is also affected from the rarefaction. The development of x velocity can be seen in Figures 4.2, 4.3 and 4.4. In these figures dimensionless x velocity is plotted against the dimensionless channel width, for the vertical sections taken at different locations. The sections are taken from the positions where dimensionless channel length is equal to 0.8, 4 and 8. The velocity profiles are given for different Knudsen numbers and for the Brinkman

number equal to 0.001. Before investigating the effect of property variation, simultaneously developing flow with constant property will be demonstrated to become familiarized with the nature of simultaneously developing slip flow in microchannels. For this reason all of the given velocity profiles are obtained from constant property solutions. The velocity profiles obtained from variable property solution will be given in comparison with the constant property velocity profiles for various Knudsen, Brinkman and Péclet numbers in the Appendix A.

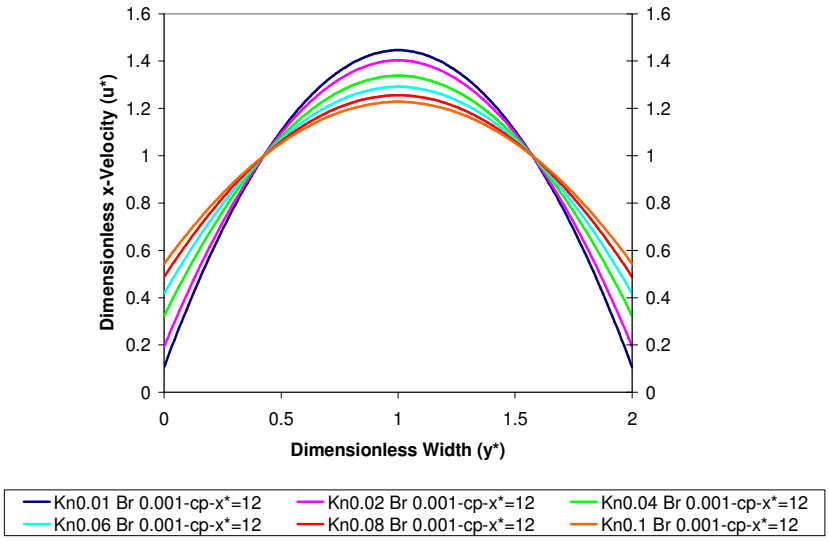

Figure 4.1 Dimensionless, developed x-velocity profile for different Knudsen numbers at the section x*=12, obtained from constant property solutions (Pe=1)

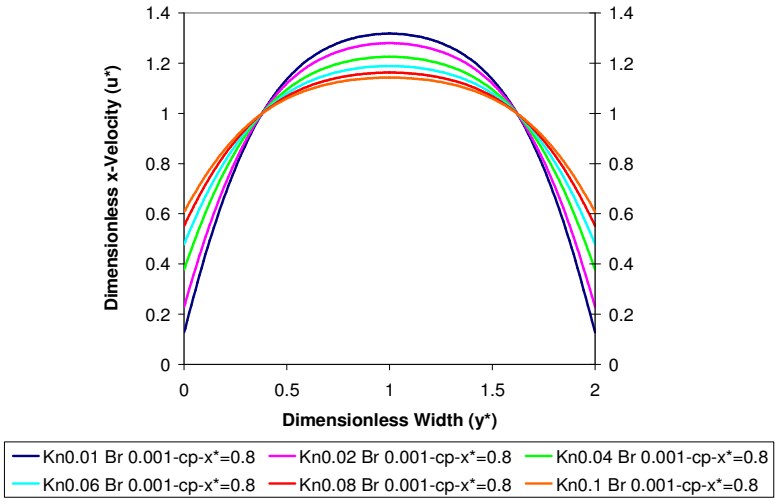

Figure 4.2 Dimensionless x-velocity profile for different Knudsen numbers at the section x*=0.8, obtained from constant property solutions (Pe=1)

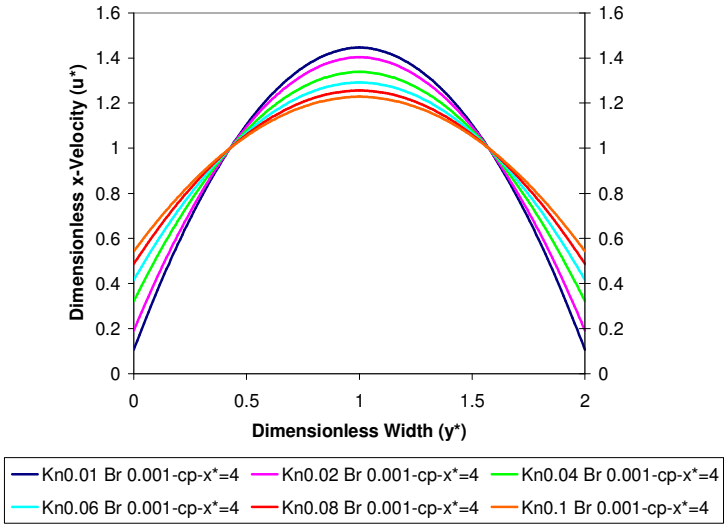

Figure 4.3 Dimensionless x-velocity profile for different Knudsen numbers at the section x*=4, obtained from constant property solutions (Pe=1)

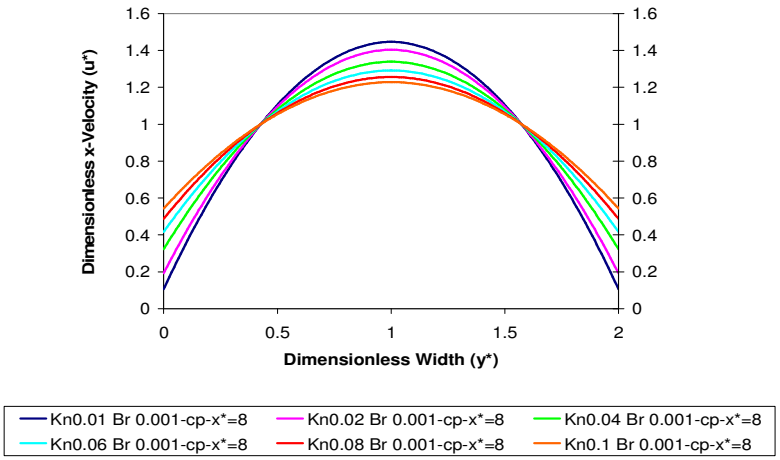

Figure 4.4 Dimensionless x-velocity profile for different Knudsen numbers at the section x*=8, obtained from constant property solutions (Pe=1)

From the Figures 4.2 4.3 and 4.4 it can be understood that, even for the low Reynolds numbers, flow develops rapidly. In Figure 4.3, velocity profiles reach its final form at x*=4 and no further development is observed. As a result of this rapid development in flow, y velocities are equal to zero, for a wide portion of the flow field. The development of y velocities can be demonstrated by using the plots for the sections taken at different locations. The plots are given in Figures 4.5, 4.6 and 4.7. The dimensionless y velocity values are plotted against dimensionless channel width for different Knudsen numbers and for Brinkman number equal to 0.001. As stated above, the velocity profiles are obtained from constant property solutions with a Péclet number of 1.

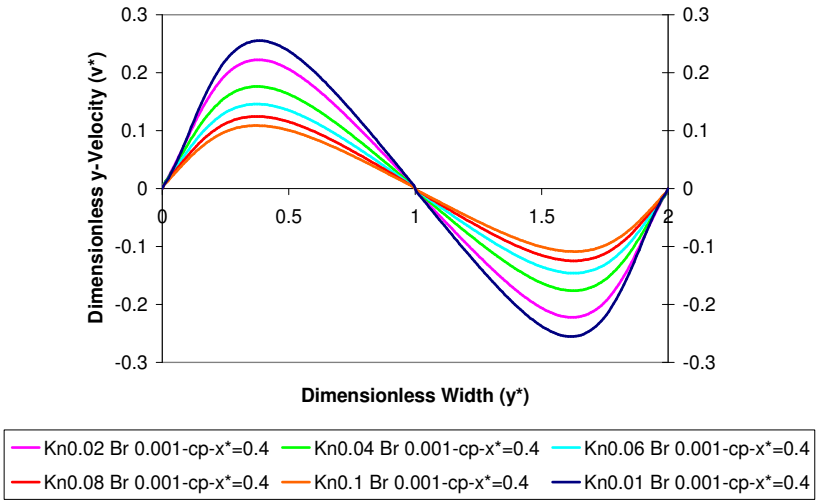

Figure 4.5 Dimensionless y-velocity profile for different Knudsen numbers at the section x*=0.4, obtained from constant property solutions (Pe=1)

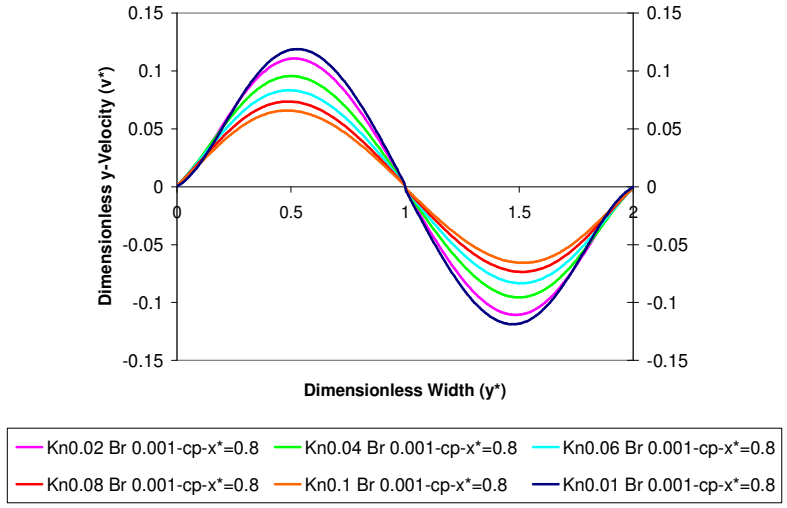

Figure 4.6 Dimensionless y-velocity profile for different Knudsen numbers at the section x*=0.8, obtained from constant property solutions (Pe=1)

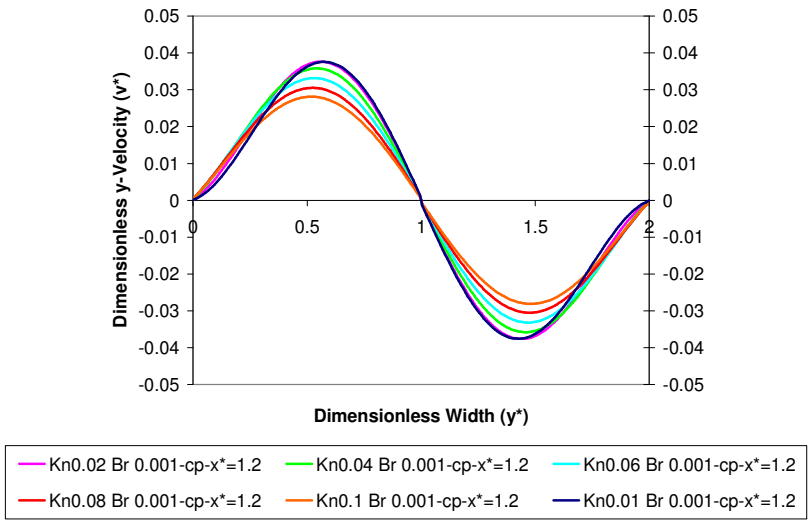

Figure 4.7 Dimensionless y-velocity profile for different Knudsen numbers at the section x*=1.2, obtained from constant property solutions (Pe=1)

As can be seen in Figures 4.5, 4.6 and 4.7, y velocity values are reduced as the dimensionless channel length x* increases. The y velocity values reach zero when flow is developed. In addition to the velocity profiles, temperature profiles for different Knudsen numbers is obtained in the numerical simulations. Temperature profiles, plotted against dimensionless channel width are given at different sections in Figures 4.8, 4.9, 4.10 and 4.11 to visualize the thermal development. All dimensionless temperature profiles given in the figures are obtained from constant property solutions for Brinkman number equal to 0.001 and Péclet number equal to 1.

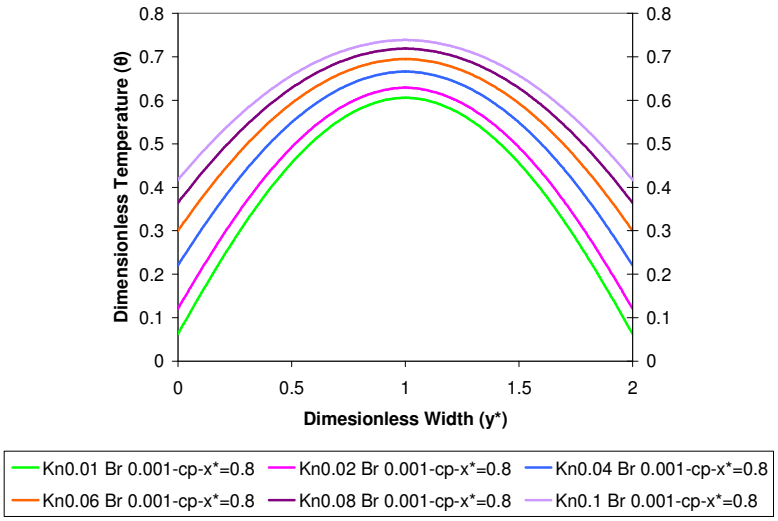

Figure 4.8 Dimensionless temperature profile for different Knudsen numbers at the section x*=0.8, obtained from constant property solutions (Pe=1)

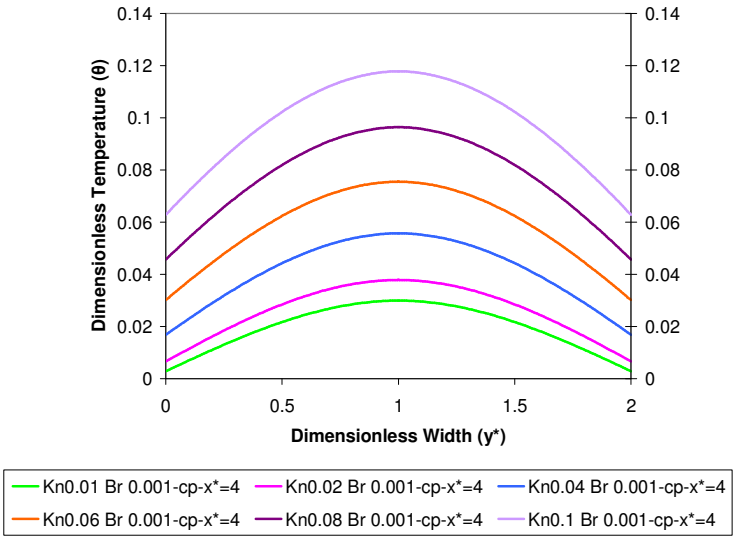

Figure 4.9 Dimensionless temperature profile for different Knudsen numbers at the section x*=4, obtained from constant property solutions (Pe=1)

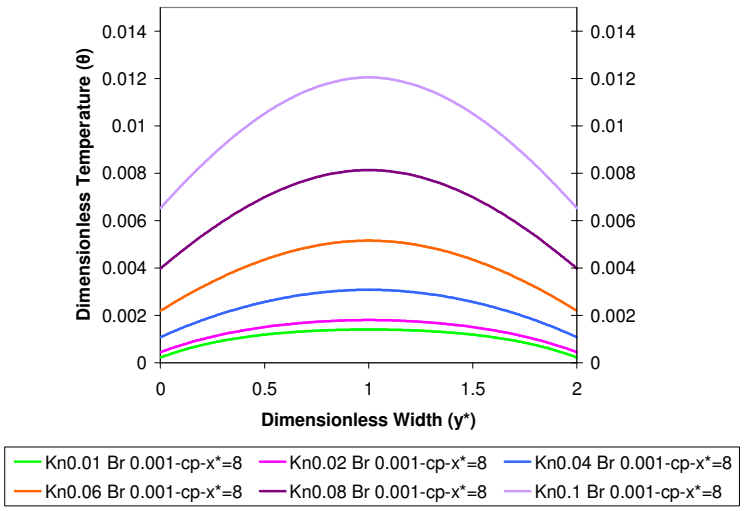

Figure 4.10 Dimensionless temperature profile for different Knudsen numbers at the section x*=8, obtained from constant property solutions (Pe=1)

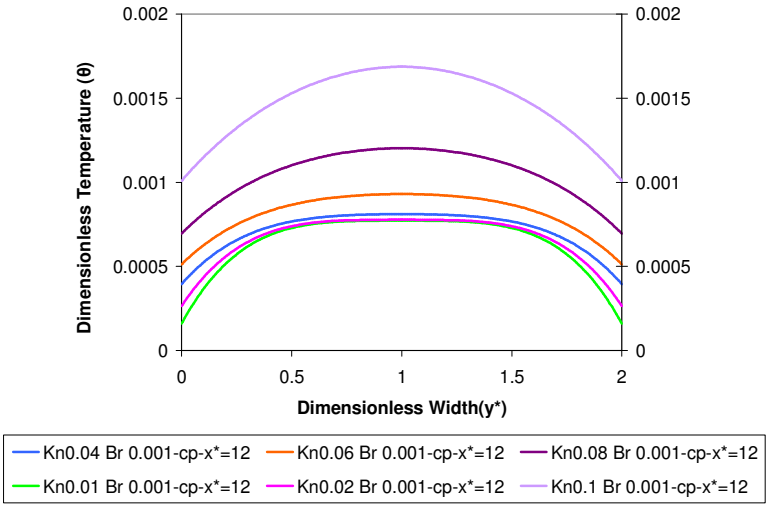

Figure 4.11 Dimensionless temperature profile for different Knudsen numbers at the section x*=12, obtained from constant property solutions (Pe=1)

4.1.1 Constant Property Solutions

The thermal development and variation of temperature profile with rarefaction effect can be seen from Figures 4.8-4.11. Effect of rarefaction is represented by Knudsen number in the non-dimensional solutions. As the Knudsen number increases, the temperature jump and velocity slip at the wall boundaries increases. This is an expected consequence of rarefaction effect. One other important dimensionless parameter is Nusselt number as stated above. Variation of Nusselt number with the axial position will provide detailed information about thermal development, and heat transfer characteristics of the flow. Plot of Nusselt number against the axial direction for constant property solution with Péclet number equal to 1 is given in Figure 4.12. In Figure 4.12 results are presented for different Knudsen numbers in combination with a positive Brinkman number and Péclet number is equal to 1. As it is clear from the definition in Equation (3.25), positive Brinkman numbers indicates a cooling process for the fluid. In other words, fluid enters the microchannel with a higher temperature than the wall has, and cools down. Conversely, negative Brinkman numbers refer to a heating process for the fluid. However, heating process in a microchannel has a singularity as a result of viscous heating. This singular point emerges where the wall and bulk fluid temperatures become equal. At this point there is no heat transfer between the wall and the fluid. Besides, at the downstream of this point, fluid temperature continues rising as a result of viscous heating. Thereafter, the bulk fluid temperature exceeds the wall temperature and cooling process takes place. In Figure 4.13 variation of Nusselt number with axial position, is plotted for a negative Brinkman number for constant property solutions with Péclet number equal to 1.

Considering Figure 4.12 and Figure 4.13, it is possible to see that heat transfer in microchannel reduces with increasing Knudsen number. In other words

rarefaction has a negative effect in heat transfer for both heating and cooling processes.

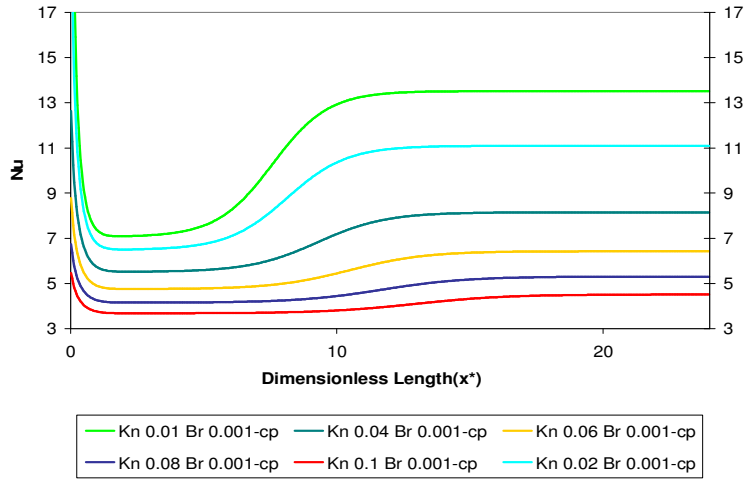

Figure 4.12 Variation of Nusselt number with axial position for different Knudsen and positive Brinkman numbers, obtained from constant property solutions (Pe=1)

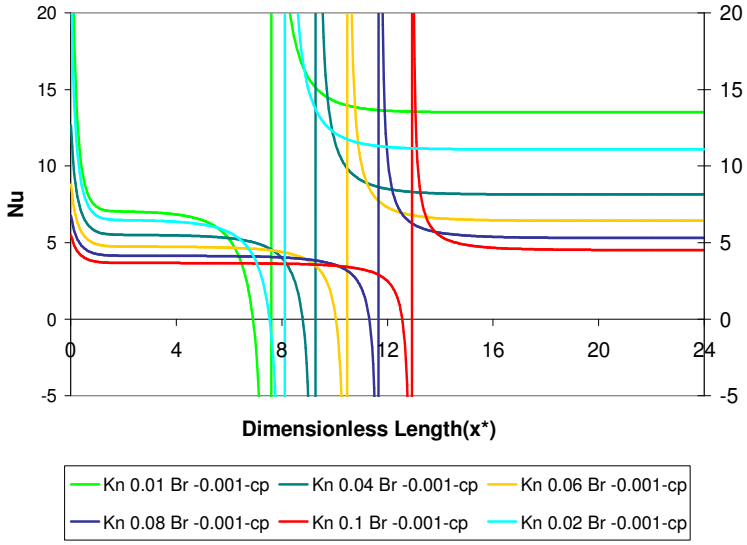

Figure 4.13 Variation of Nusselt number with axial position for different Knudsen and negative Brinkman numbers, obtained from constant property solutions (Pe=1)

The fully developed Nusselt numbers for the constant property solutions with a Péclet number of 1 is given in Table 4.1. The results are tabulated for various Knudsen and Brinkman numbers. Due to the results in Table 4.1 it is possible to say that for both positive and negative Brinkman numbers; fully developed Nusselt numbers converges to the same value. It is possible to say that viscous dissipation has a limited influence on the fully developed region for constant property solutions.

Table 4.1 Fully developed Nusselt numbers, for various Knudsen and Brinkman numbers, obtained from constant property solution (Pe=1)

Kn	Br					
	0.001	0.010	0.100	-0.001	-0.010	-0.100
0.010	13.660	13.660	13.660	13.660	13.660	13.660
0.020	11.208	11.208	11.208	11.208	11.208	11.208
0.040	8.227	8.227	8.227	8.227	8.227	8.227
0.060	6.486	6.486	6.486	6.486	6.486	6.486
0.080	5.348	5.349	5.349	5.349	5.349	5.349
0.100	4.547	4.548	4.548	4.549	4.548	4.548

If the channel has a finite length, in addition to the fully developed Nusselt numbers, also average Nusselt number for the channel become important. In this case channel length is 12 times the channel spacing, for this reason channel averaged Nusselt numbers should also be considered while investigating heat transfer characteristics. Average Nusselt number values for various Knudsen and Brinkman numbers are tabulated in Table 4.2 for constant property solutions with a Péclet number of 1.

As expected, with increasing Knudsen number, in other words with increasing rarefaction effect, channel averaged heat transfer coefficient and Nusselt number will decrease.

For the positive Brinkman numbers, where the fluid is cooled by the wall, local Nusselt number experiences a jump, as it is illustrated in Figure 4.12. This jump is

mainly caused by viscous dissipation. In the beginning of entrance region, as a result of cooling, the bulk fluid temperature starts to decrease. As the bulk temperature of the fluid decreases, the heat transfer rate reduces. The decrease in heat transfer rate together with the viscous heat generation causes a rapid increase in the bulk fluid temperature. This rapid increase in bulk fluid temperature yields higher heat transfer rate which creates a jump in Nusselt value. If the viscous dissipation increases, the jump point will move in the upstream direction. The shift in jump point position for Knudsen number 0.01 can be seen in Figure 4.14 for constant property solutions with a Péclet number of 1. The detailed plots for different Knudsen numbers of variable and constant property solutions are available in Appendix A.

The reason for the migration of jump point is the higher heat generation that increases the bulk fluid temperature earlier and more rapidly. For this reason with the increasing viscous dissipation, thermal entry length reduces. As it can be seen from Figure 4.12 and Figure 4.14, entrance region Nusselt numbers are lower than the fully developed Nusselt numbers for positive Brinkman numbers. Therefore as the Brinkman numbers increases, channel averaged Nusselt numbers will be increased and approximated the fully developed values. This increase in averaged Nusselt values mainly stems from the shortened entrance length. The variation of channel averaged Nusselt numbers can be seen in Table 4.2.

Table 4.2 Channel averaged Nusselt numbers, for various Knudsen and Brinkman numbers, obtained from constant property solution (Pe=1)

Kn	Br					
	0.001	0.010	0.100	-0.001	-0.010	-0.100
0.010	11.820	12.476	13.145	10.262	10.477	13.281
0.020	9.779	10.280	10.784	11.344	10.253	13.270
0.040	7.278	7.602	7.926	7.535	7.910	8.197
0.060	5.798	6.028	6.257	5.803	6.879	6.036
0.080	4.819	4.993	5.166	5.273	5.131	5.168
0.100	4.123	4.260	4.396	3.889	4.561	3.899

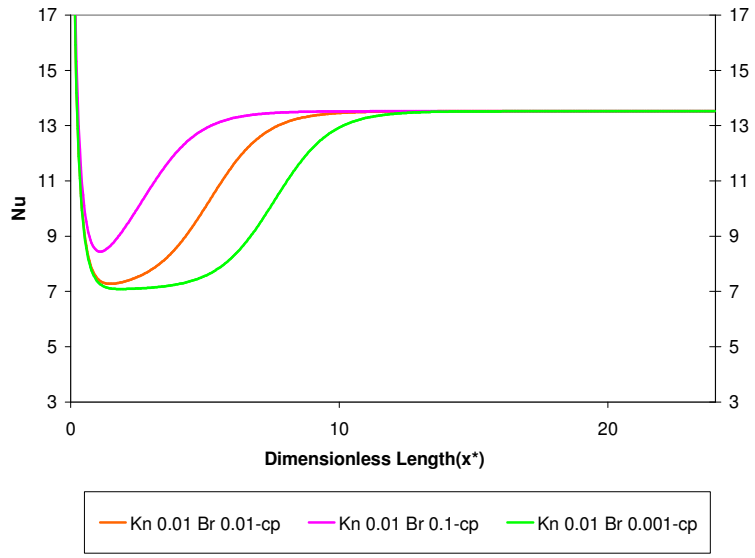

Figure 4.14 Variation of Nusselt number with axial position for different positive Brinkman numbers, obtained from constant property solutions (Kn=0.01, Pe=1)

The channel averaged Nusselt values obtained from analyses of negative Brinkman numbers, are also given in Table 4.2. Unfortunately, the variation of channel averaged Nusselt numbers can not be directly related with the viscous dissipation by using these data. Virtually high heat transfer rates, in the vicinity of singular point create unrealistic channel averages. Therefore, considering channel averaged Nusselt values for negative Brinkman numbers will not be presented beyond this point.

Moreover, from Figure 4.13, it is possible to see the variation of the axial position of the singularity point with Knudsen numbers. Additionally the variation of local Nusselt numbers and the axial position of singularity point with the effect of viscous dissipation can be seen in Figure 4.15 for constant property solutions. As stated above the detailed plots for both constant and variable properties are available in Appendix A.

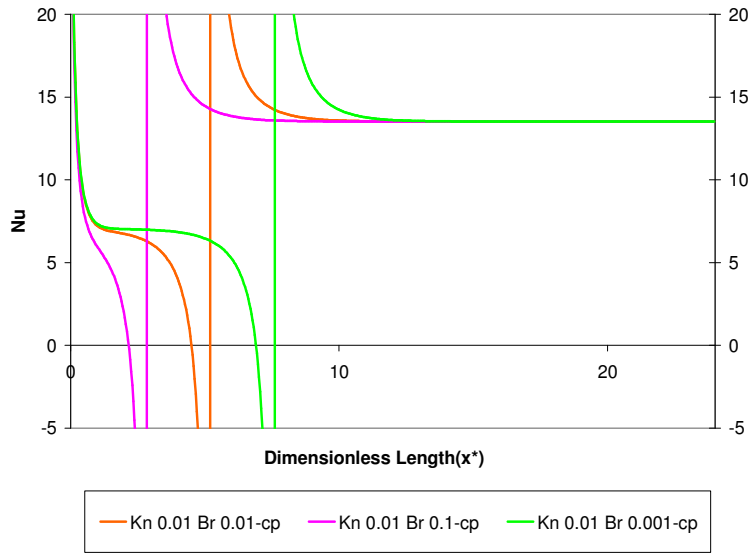

Figure 4.15 Variation of Nusselt number with axial position for different positive Brinkman numbers, obtained from constant property solutions (Kn=0.01, Pe=1)

With increasing Knudsen number, the point of singularity moves in the downstream direction, due to increasing rarefaction and reduced heat transfer rate. On the other hand as the viscous dissipation increases, the bulk fluid temperature will increase more rapidly and will be equalized to the wall temperature earlier. This phenomenon will move the singularity point towards upstream direction as mentioned above. One other parameter that will be discussed is the Péclet number. This dimensionless quantity represents the relative importance of axial conduction in the energy equation. Actually Péclet number is the product of Reynolds and Prandtl number, and Prandtl number is fixed for a definite fluid. Therefore, changing Péclet number for a fluid refers to changing the Reynolds number. The effect of Péclet number, in combination with Knudsen and positive Brinkman number can be seen in Figure 4.16

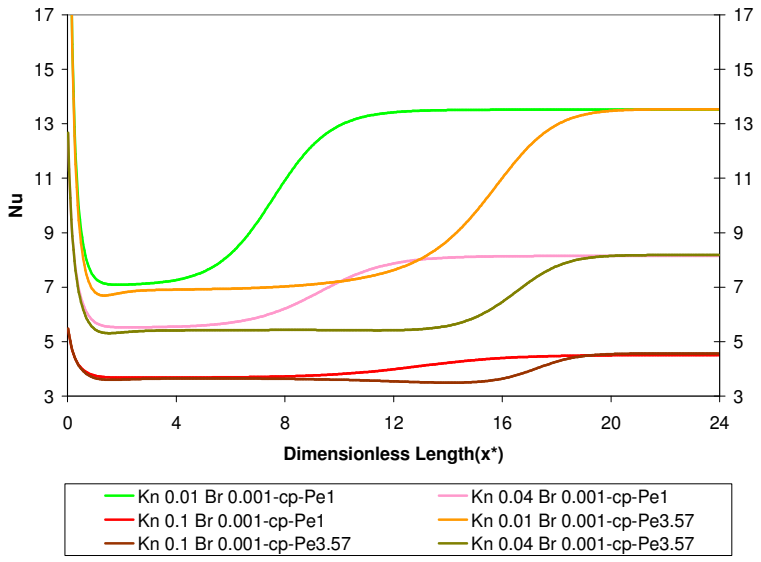

Figure 4.16 Variation of Nusselt number with axial position for various Knudsen numbers, obtained from constant property solutions (Br=0.001, Pe=1, Pe=3.57)

Mainly, the increase in Reynolds number causes an increase in the entrance length. For the positive Brinkman numbers, in other words for the fluid heating process, axial position of the jump in local Nusselt values will move in to the downstream direction with increasing Reynolds number.

For same Knudsen number, fully developed Nusselt numbers, converge to almost same value, regardless of Brinkman Reynolds and Péclet number as expected. Fully developed Nusselt numbers for various Knudsen, Brinkman and two different Péclet numbers are tabulated in Table 4.3. Even though the effect of axial conduction is not obviously decreased with the increase of Péclet number; the small differences observed in fully developed Nusselt values are thought to be caused by the reduced significance of axial conduction term. Effect of Brinkman number in combination with the increased Péclet number can be seen in Figure 4.17.

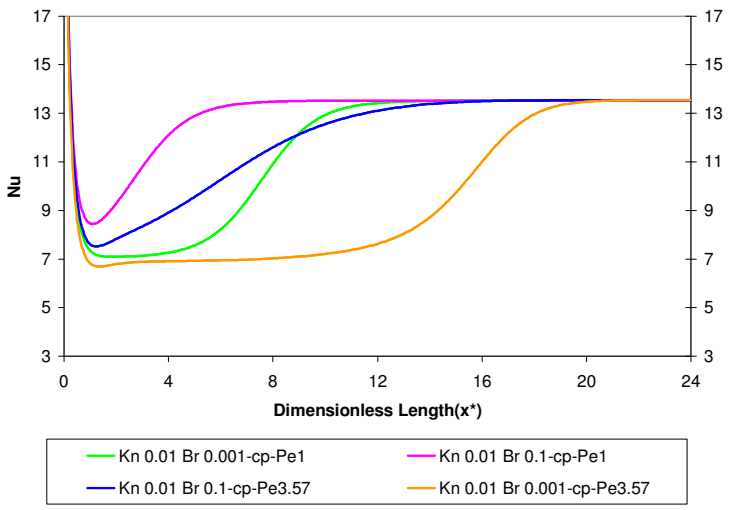

Figure 4.17 Variation of Nusselt number with axial position for various Brinkman numbers, obtained from constant property solutions (Kn=0.01, Pe=1, Pe=3.57)

The channel averaged Nusselt number for two different Péclet and positive Brinkman numbers are also given in Table 4.4. Due to the results of analyses for positive Brinkman numbers, increasing Reynolds number and entrance length causes a substantial decrease in the channel averaged Nusselt values. This decrease is a result of finite channel length and shift in position of jump in Nusselt values.

Table 4.3 Fully developed Nusselt numbers, for various Knudsen and Brinkman numbers, obtained from constant property solution (Pe=1, Pe=3.57)

	Kn	Br			
		0.001	0.100	-0.001	-0.100
Pe=1	0.010	13.660	13.660	13.660	13.660
	0.040	8.227	8.227	8.227	8.227
	0.100	4.547	4.548	4.549	4.548
Pe=3.57	0.010	13.676	13.676	13.676	13.676
	0.040	8.260	8.260	8.260	8.260
	0.100	4.603	4.603	4.603	4.603

Table 4.4 Channel averaged Nusselt numbers, for various Knudsen and positive Brinkman numbers, obtained from constant property solution (Pe=1, Pe=3.57)

	Kn	Br	
		0.001	0.100
Pe=1	0.010	11.820	12.476
	0.040	7.278	7.602
	0.100	4.123	4.260
Pe=3.57	0.010	9.683	12.200
	0.040	6.424	7.454
	0.100	3.915	4.229

The variation of Nusselt number is plotted against axial position in Figure 4.18 for various Knudsen number and two different Péclet number. Similarly, for the negative Brinkman numbers, effect of axial conduction will not be easily understood, with the slight change in Péclet number from 1 to 3.57. However, it is possible to say that increased Reynolds number causes an increase in the entrance length, due to delayed development of the flow. The fully developed Nusselt numbers converge to the same value for the same Knudsen number regardless of the Brinkman and Péclet numbers. The effect of negative Brinkman number in combination with Péclet number can be seen in Figure 4.19. As discussed earlier, increased viscous heating will shift the position of singular point toward upstream direction. Additionally with the increase of Reynolds number, the influence of Brinkman number will become more significant.

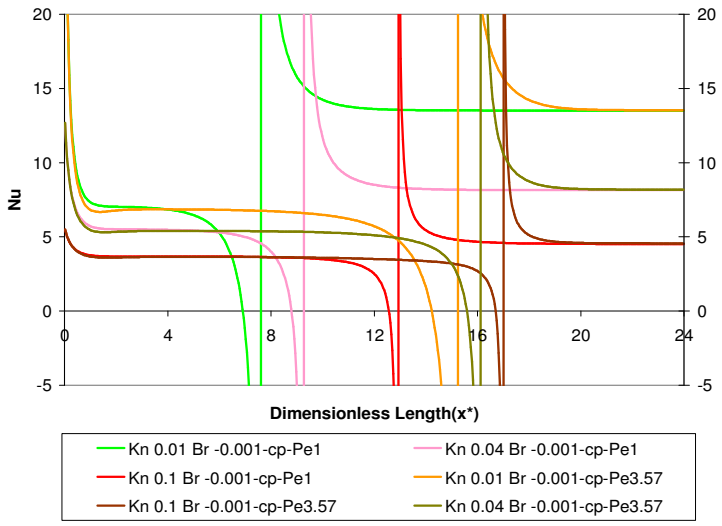

Figure 4.18 Variation of Nusselt number with axial position for various Knudsen numbers, obtained from constant property solutions (Br=-0.001,Pe=1, Pe=3.57)

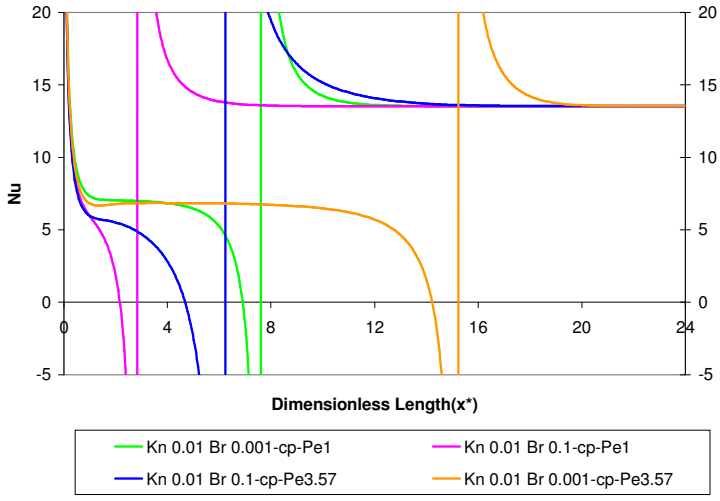

Figure 4.19 Variation of Nusselt number with axial position for various Brinkman numbers, obtained from constant property solutions (Kn=0.01, Pe=1, Pe=3.57)

4.1.2 Variable Property Solutions

After completing the overview about simultaneously developing flow with constant thermophysical properties, in the slip flow regime, property variation effect can be discussed in detail in the following part.

First of all, the effect of rarefaction will be discussed in comparison with the property variation. Then, for each Knudsen number, relative significance of axial conduction and viscous dissipation will be investigated.

In the variable property analyses, the dimensional temperature values for inlet and wall temperature should be defined to non-dimensionalize the thermal conductivity and viscosity. Hence for the fluid heating where Brinkman numbers are positive, the inlet temperature is taken as 444 K and the wall temperature is taken as 296 K. For the second case in which fluid is heated by the wall, wall temperature is taken as 394 K and inlet temperature is taken as 296 K. By using these dimensional values, the property variation range of air is defined.

The axial variation of Nusselt numbers, for various Knudsen numbers, and positive Brinkman numbers obtained from variable and constant property solutions are plotted in Figure 4.22 .The solid lines in the graph denotes the results obtained from constant property solution and a suffix "cp" is added to their labels. The dashed lines in the plots stand for the results of variable property solutions and "vp" is added as a suffix to their label.

In the following parts, the percent difference in local Nusselt values between constant and variable property solutions will be demonstrated frequently. The term will be denoted as “%Δ Nu” and expressed as follows,

$$\%\Delta Nu = \frac{Nu_{vp} - Nu_{cp}}{Nu_{cp}} x100 \tag{4.6}$$

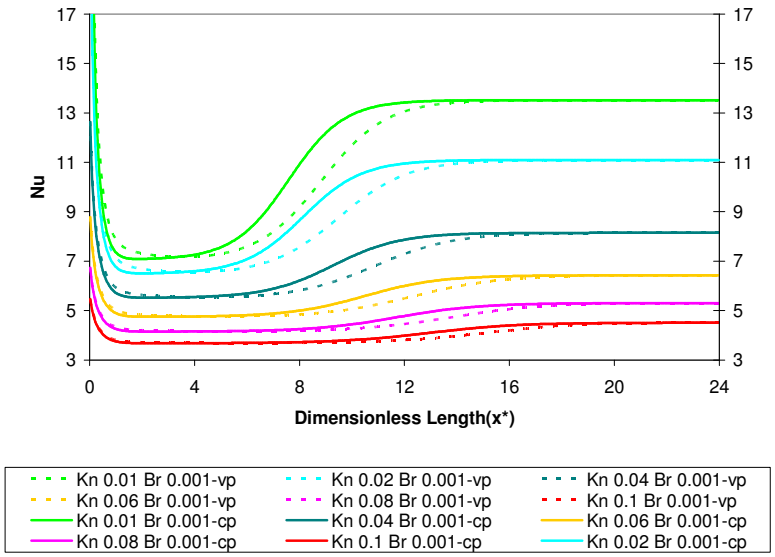

Figure 4.20 Variation of Nusselt number with axial position for various Knudsen numbers, obtained from constant and variable property solutions (Br=0.001, Pe=1)

The difference between variable and constant property solution local Nusselt numbers decreases with increasing Knudsen number as it can be seen in Figure 4.20. Furthermore, the difference is visualized in Figure 4.21 more clearly. In Figure 4.21, the difference between variable and constant property local Nusselt numbers is plotted against axial position.

Basically, the difference between constant and variable property solutions is strongly related to the temperature gradients. For this reason as the rarefaction

increases, the temperature and velocity gradients will be decreased. The decrease in temperature gradients can also be seen from the flattened temperature profiles with increasing Knudsen number in Figures 4.8-4.11.

As can be seen from Figure 4.21, the difference also has a peak value at an axial position, which varies with Knudsen and Brinkman number. The peak value is decreased with increasing rarefaction as a result of reduced temperature gradients. Additionally, the axial position of the peak value, move in to downstream with increasing Knudsen number as a result of retarded decrease of heat transfer rate in the entrance region.

The viscous heat generation and reduced heat transfer rate increases the bulk fluid temperature which yields a jump in heat transfer rates and temperature gradient. Consequently with the variation of Knudsen number, the location of the jump in Nusselt number and peak value for the difference moves to the downstream. Since the fluid cools down, both viscosity and thermal conductivity values will be decreased, which causes a reduced conductive heat transfer and viscous heating. The conductive heat transfer and viscous dissipation are acting in the same way for the bulk temperature rise in the downstream. For this reason variable property solution will experience a delayed jump in local Nusselt values due to reduced viscosity and thermal conductivity.

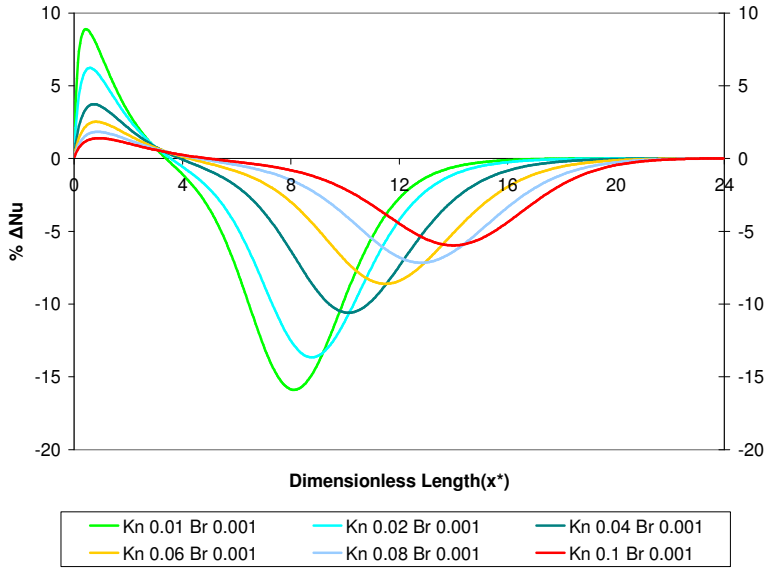

Figure 4.21 Variation of percent difference in Nusselt number between constant and variable property solutions with axial position for various Knudsen numbers (Br=0.001, Pe=1, Pe=3.57)

As can be seen from Figure 4.21 the difference between constant and variable property local Nusselt values may reach 15 %. However the difference reduces to zero for the fully developed flow conditions. Thus it is possible to say that property variation effect is not significant for the fully developed flow. The fully developed Nusselt values are tabulated in Table 4.5 for constant and variable property solutions of various Knudsen and Brinkman numbers. The main reason for the negligible differences between variable and constant property solutions in the fully developed flow can be stated as reduced temperature gradients.

Table 4.5 Fully developed Nusselt numbers, for various Knudsen and Brinkman numbers, obtained from constant and variable property solutions (Pe=1)

	Br					
Kn	cp	vp	cp	vp	cp	vp
	0.001	0.001	0.010	0.010	0.100	0.100
0.010	13.660	13.661	13.660	13.675	13.660	13.810
0.020	11.208	11.209	11.208	11.217	11.208	11.289
0.040	8.227	8.227	8.227	8.230	8.227	8.256
0.060	6.486	6.486	6.486	6.488	6.486	6.500
0.080	5.348	5.348	5.349	5.350	5.349	5.356
0.100	4.547	4.548	4.548	4.549	4.548	4.553

In addition to the fully developed Nusselt numbers, channel averaged Nusselt values for variable and constant property solutions are tabulated in Table 4.6. When both Table 4.6 and Figure 4.21 are considered together it can be said that the difference between constant and variable property solutions may be locally significant but, the positive difference in the early entrance region and negative difference observed in the downstream of entrance region will compensate each other and the average difference become very low. By considering the channel averaged Nusselt values in Table 4.6, it is possible to say that the difference increases with increasing Brinkman numbers. This phenomenon will be discussed in detail in the following parts.

Table 4.6 Channel averaged Nusselt numbers, for various Knudsen and Brinkman numbers, obtained from variable and constant property solutions (Pe=1)

	Br					
Kn	cp	vp	cp	vp	cp	vp
	0.001	0.001	0.010	0.010	0.100	0.100
0.010	11.820	11.529	12.476	12.318	13.145	13.237
0.020	9.779	9.544	10.280	10.147	10.784	10.815
0.040	7.278	7.115	7.602	7.505	7.926	7.918
0.060	5.798	5.679	6.028	5.954	6.257	6.241
0.080	4.819	4.730	4.993	4.933	5.166	5.148
0.100	4.123	4.059	4.260	4.212	4.396	4.379

The Nusselt values are plotted against axial position for variable and constant property solutions of negative Brinkman numbers in Figure 4.22. The plots of Nusselt number for various Knudsen numbers are given in comparison with the property variation effect. Since it is not easy to follow the difference between constant and variable property results from the plot in Figure 4.22, the variation of difference with axial position is given in Figure 4.23. The position of singularity in local Nusselt values changes with the property variation. Moreover percent difference plots are not clear due to the shift in singularity position. For this reason, the peak value of the difference between variable and constant property solutions become infinitely high and has no significance. However, by looking at the Figures 4.22 and 4.23, it is possible to say that, effect of property variation will shifts the position of singular point towards upstream. The main reason for this shift may be the increased bulk fluid temperature as a result of heating. The increase in fluid temperature results in increased thermal conductivity and viscosity. Due to the increased thermal conductivity and viscosity, both

conductive heat transfer rate and viscous heating will be increased. Consequently, the fluid will reach the wall temperature more rapidly than the constant property solution.

Another remarkable point of Figure 4.22 is the variation of the difference between variable and constant property solutions with increasing rarefaction effect. The increased rarefaction effect causes an increase in the difference. The reason for the increased difference may be the decreased convective heat transfer rate with increasing rarefaction. Moreover, as a result of increased thermal conductivity, the conductive heat transfer rate will also be increased, because for the fluid heating case, convective and conductive heat transfer mechanism are counteracting. In other words, heat is diffused to the upstream while fluid is flowing downstream. As a result, with increasing rarefaction, relative significance of conductive heat transfer will be increased while the relative significance of convective heat transfer is decreased. Due to the increase in thermal conductivity, the property variation effect will be emphasized more for high Knudsen numbers.

Similar to the positive Brinkman number analyses results, the fully developed Nusselt numbers for both variable and constant property solutions converge to the same value. The fully developed local Nusselt values for various Knudsen and negative Brinkman numbers are given in Table 4.7 for constant and variable property solutions. As stated above the difference becomes negligible for the fully developed flow as a result of lower temperature gradients.

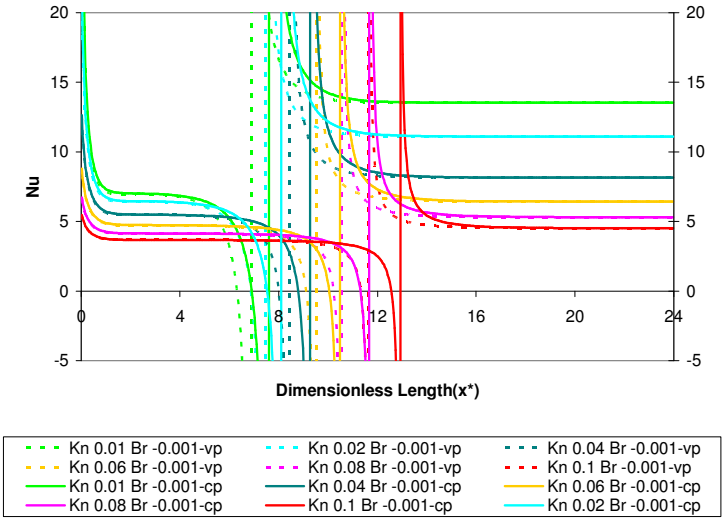

Figure 4.22 Variation of Nusselt number with axial position for various Knudsen numbers, and negative Brinkman numbers, obtained from constant and variable property solutions (Br=-0.001,Pe=1)

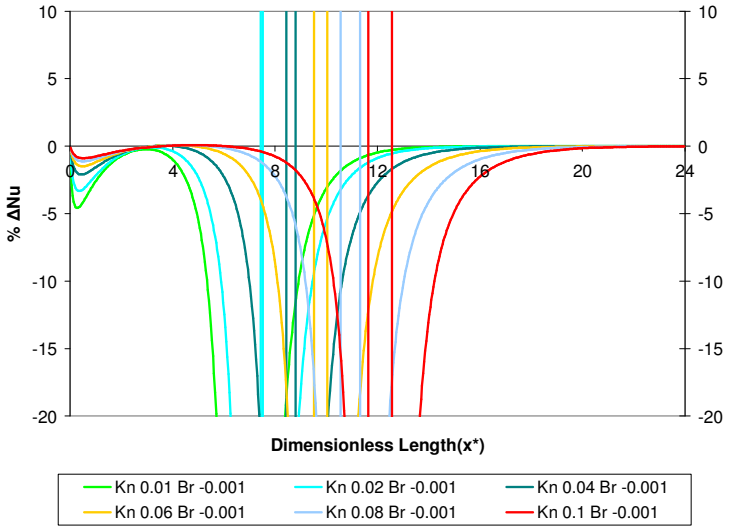

Figure 4.23 Variation of percent difference in Nusselt number between constant and variable property solutions with axial position for various Knudsen numbers (Br=-0.001,Pe=1)

Table 4.7 Fully developed Nusselt numbers, for various Knudsen and Brinkman numbers, obtained from constant and variable property solution (Pe=1)

	Br					
Kn	cp	vp	cp	vp	cp	vp
	-0.001	-0.001	-0.010	-0.010	-0.100	-0.100
0.010	13.660	13.661	13.660	13.668	13.660	13.742
0.020	11.208	11.209	11.208	11.213	11.208	11.253
0.040	8.227	8.227	8.227	8.228	8.227	8.243
0.060	6.486	6.486	6.486	6.487	6.486	6.494
0.080	5.349	5.349	5.349	5.349	5.349	5.352
0.100	4.549	4.548	4.548	4.548	4.548	4.550

As stated previously the channel averaged Nusselt values will not be presented for the negative Brinkman number analyses results, due to singular points.

The variable property effect will be discussed in comparison with viscous dissipation by varying the Brinkman number while Knudsen number and Péclet numbers are fixed. In Figure 4.24, the variation of Nusselt number with axial position is plotted for various positive Brinkman numbers while Knudsen number equal to 0.01 and Péclet number equal to 1. With increasing Brinkman number, length of thermal entrance region increases meanwhile, the position of the jump in Nusselt value, moves towards. The reasons for this shift was discussed in detail, in the previous sections. The difference between variable and constant property solutions can be seen in Figure 4.24. The percent difference in local Nusselt values are plotted against axial position in Figure 4.25Figure 4.27, however they are not so clear and comprehensible.

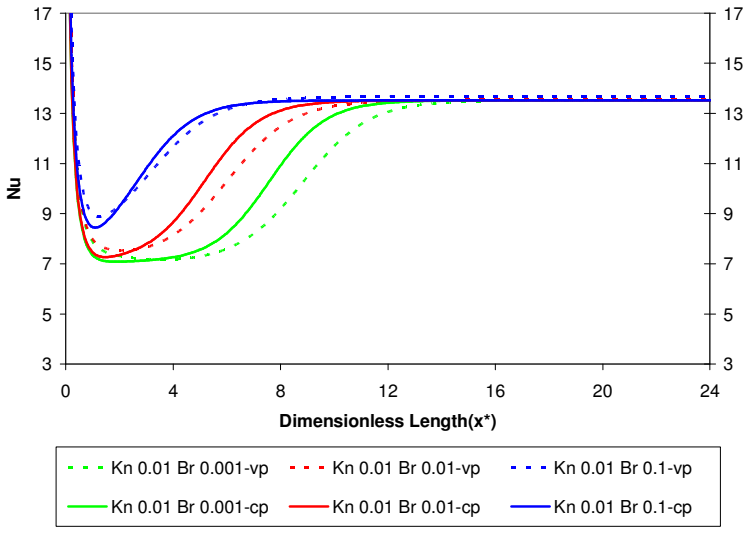

Figure 4.24 Variation of Nusselt number with axial position for various positive Brinkman numbers, obtained from constant and variable property solutions (Kn=0.01, Pe=1)

As it can be seen in Figure 4.25 the positive difference between constant and variable local Nusselt values, in the early entrance region is approximately the same for all the Brinkman numbers. Hence, in the early entrance region; the temperature gradients are inherently independent from the effect of viscous dissipation. On the other hand, in the downstream of entrance region, where the difference between variable property solutions are negative, viscous dissipation is effective. Increasing viscous dissipation has a negative effect on the peak value of the difference between variable and constant property local Nusselt numbers. On the contrary the difference in channel averaged Nusselt values are increasing with increased viscous dissipation. As the fluid enters the channel, the viscosity and thermal conductivity decreases with the decreasing temperature. Additionally, the conductive heat transfer rate is reduced with the reduced thermal conductivity. In the fluid cooling case, the conductive heat transfer assists the convective one.

Hence, the assistance of conductive heat transfer will be weaker for reduced viscous heat generation due to the retarded increase in thermal conductivity. Consequently, the variable property solution experiences a slower development as a result of reduced heat transfer rate and reduced heat generation. For this reason the difference between variable and constant property solutions are increasing with decreased positive Brinkman number. The position of this peak shifts to the downstream with decreasing Brinkman number, which results from the shift in the position of the jump in local Nusselt values. The reason of the shift in jump point position is discussed in previous parts. Since the difference between variable and constant property solutions converges to zero for Brinkman number equal to 0.001 and 0.01 in the fully developed region, there is still a finite difference for the Brinkman number 0.1. The order of difference is 1 % which may be resulted from increased viscous dissipation effect or numerical instability introduced.

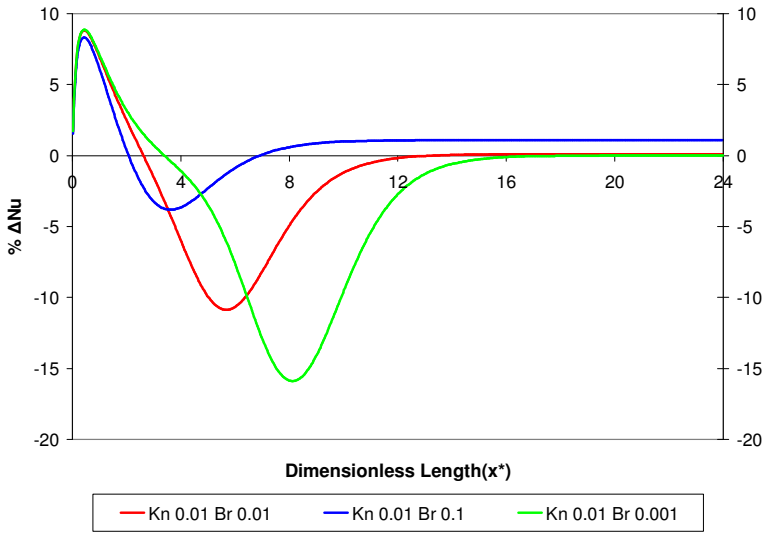

Figure 4.25 Variation of percent difference in Nusselt numbers between constant and variable property solutions with axial position for various positive Brinkman numbers (Kn=0.01, Pe=1)

In the Figure 4.26 the Nusselt values for both variable and constant property solutions for different positive Brinkman numbers with a Knudsen number of 0.04 and Péclet number of 1 is plotted against the axial position. Additionally the percent difference in Nusselt numbers are also plotted against axial position in Figure 4.27. Mainly the curves have the same characteristics with the previous ones in which Knudsen number is equal to 0.01. The dependence of variable property effect on Knudsen number was also discussed in detail previously.

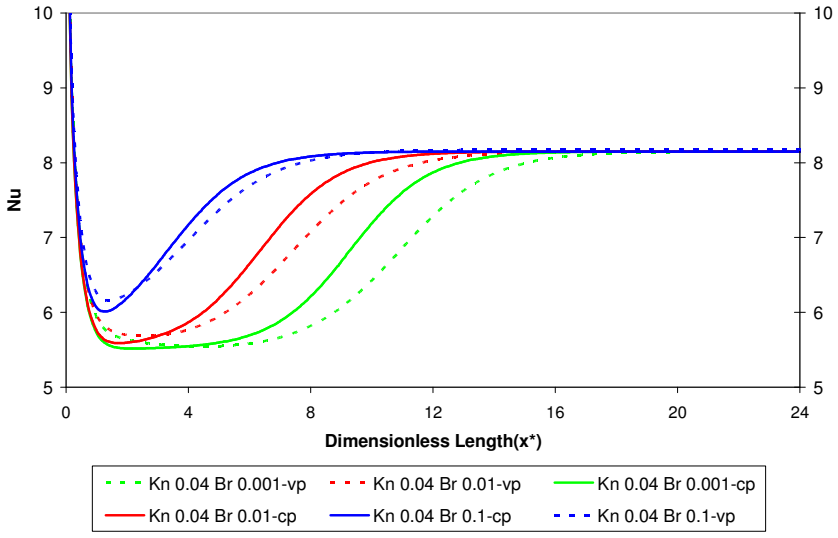

Figure 4.26 Variation of Nusselt number with axial position for various positive Brinkman numbers, obtained from constant and variable property solutions (Kn=0.04, Pe=1)

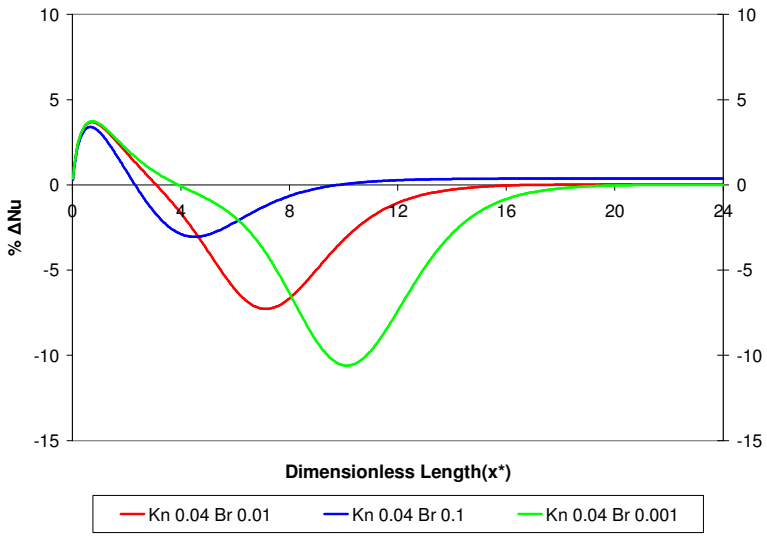

Figure 4.27 Variation of percent difference in Nusselt numbers between constant and variable property solutions with axial position for various positive Brinkman numbers (Kn=0.04, Pe=1)

Similarly the variation of Nusselt values and percent difference is plotted against the axial position in Figure 4.28 and Figure 4.29 respectively. The only difference between previous plots is the values of local Nusselt numbers and the percent differences.

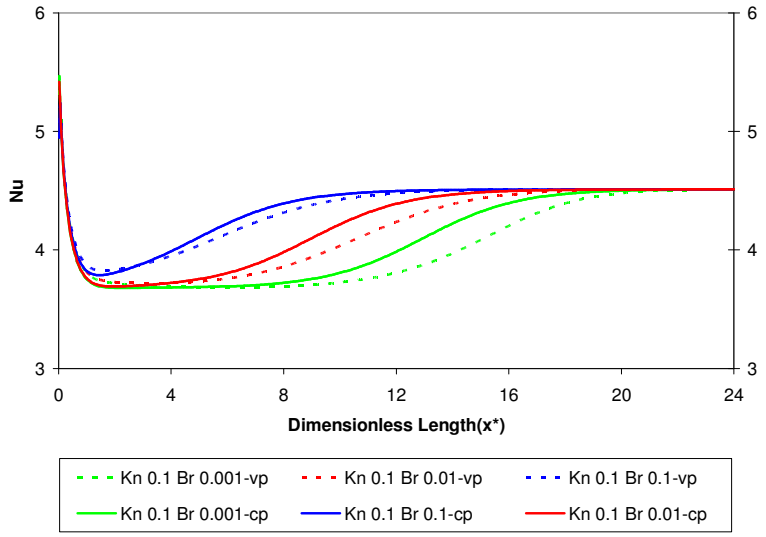

Figure 4.28 Variation of Nusselt number with axial position for various positive Brinkman numbers, obtained from constant and variable property solutions (Kn=0.1, Pe=1)

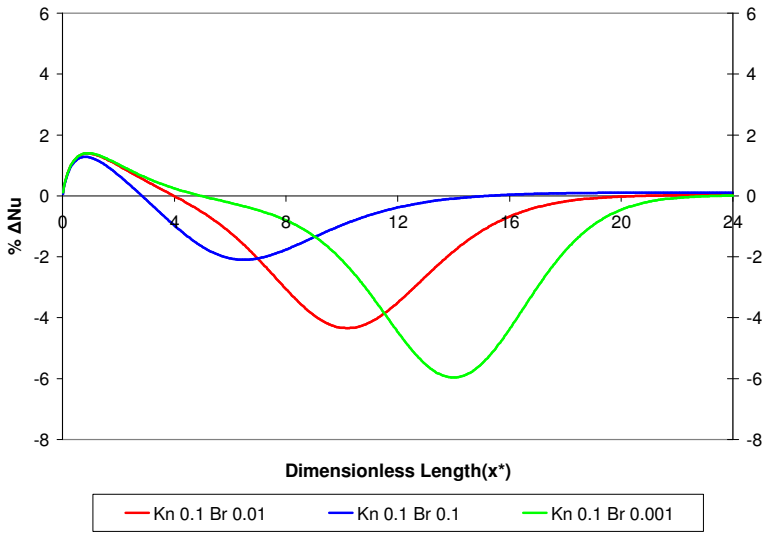

Figure 4.29 Variation of percent difference in Nusselt numbers between constant and variable property solutions with axial position for various positive Brinkman numbers (Kn=0.1, Pe=1)

In addition to the effects of Brinkman and Knudsen number, also Péclet number has an effect on the property variation. In Figure 4.30 the variation of Nusselt values for various Knudsen numbers and two different Péclet number is plotted against axial position. Extra plots covering variation of Nusselt number with axial position for different Knudsen values is available in Appendix A.

As it can be seen from Figure 4.30, increased Péclet number increases the entrance length. Additionally the axial location of the jump in Nusselt values shifted to the downstream direction, as a result of delayed development in velocity and temperature profiles.

The difference between variable and constant property solutions is increased with increased Péclet number as a result of increased temperature gradients. The difference for different Péclet numbers and Knudsen numbers are plotted against axial position in Figure 4.31. Where, the peak value of the difference increases with increasing Péclet number. Moreover it moves to the downstream due to the shifted Nusselt value jump position.

The fully developed Nusselt values for Péclet numbers, 1 and 3.57 are tabulated in Table 4.8. The fully developed values are approximately the same for variable and constant property solutions of different Péclet numbers, whereas there is very little difference due to the decreased axial conduction or increased numerical errors with increasing Péclet number.

According to the results given in Table 4.8, effect of Brinkman number on property variation is emphasized with increasing Péclet number. This increased influence of Brinkman number is a result of increased velocity gradients with increasing Péclet number. On the other hand, as the rarefaction increases, the property variation effect becomes less severe with increasing Péclet number. The reason for reduced effect of property variation is the decreased gradients due to

increased rarefaction. One other reason for the reduced effect of property variation may be the decreased thermal conductivity with decreasing temperature.

As the Péclet number increases, the relative significance of axial conduction decreases, in addition to the decrease in thermal conductivity, the assistance of conductive heat transfer will be also reduced. Both reduced conductive and convective heat transfer will compensate the effect of increased temperature gradients with increased Péclet number. Consequently the property variation effect becomes less emphasized with increased Péclet numbers for high Knudsen values.

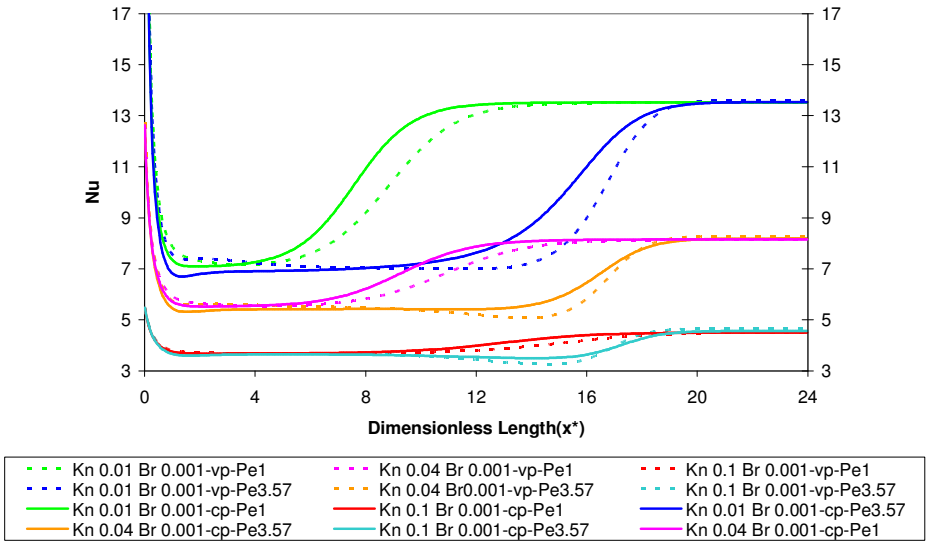

Figure 4.30 Variation of Nusselt number with axial position for various positive Knudsen numbers, obtained from constant and variable property solutions (Br=0.001, Pe=1, Pe=3.57)

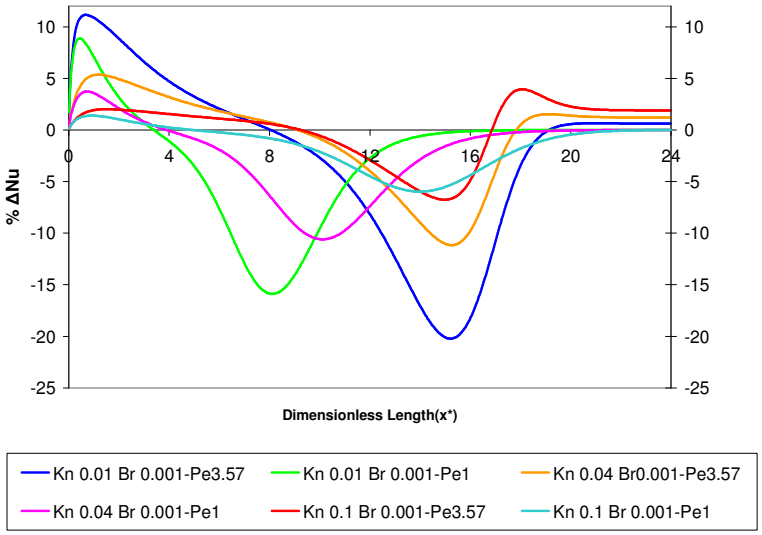

Figure 4.31 Variation of percent difference in Nusselt number between constant and variable property solutions with axial position for various Knudsen numbers (Br=0.001, Pe=1, Pe=3.57)

Table 4.8 Fully developed Nusselt numbers, for various Knudsen and Brinkman numbers, obtained from constant and variable property solutions

		Br			
	Kn	cp	vp	cp	vp
		0.001	0.001	0.100	0.100
Pe=1	0.010	13.660	13.661	13.660	13.810
	0.040	8.227	8.227	8.227	8.256
	0.100	4.547	4.548	4.548	4.553
Pe=3.57	0.010	13.676	13.760	13.676	13.900
	0.040	8.260	8.359	8.260	8.380
	0.100	4.603	4.691	4.603	4.690

In addition to the effect of Knudsen number, the effect of Brinkman number on property variation will also be discussed in combination with Péclet number. In Figure 4.32, the Nusselt numbers for different Péclet and Brinkman numbers are plotted against the axial position while Knudsen number is equal to 0.01. As previously discussed, the thermal entrance region is elongated with decreased positive Brinkman number, due to the reduced viscous heat generation. On the contrary, the difference between variable and constant property solutions is increased with decreasing Brinkman number. The details of this phenomenon are discussed above.

The difference between variable and constant property solutions are plotted against axial position in Figure 4.33 for convenience. As stated above the difference increases with increasing Péclet number, and shifts to the downstream due to the delayed flow development. Detailed plots for different Knudsen and Brinkman numbers are available in Appendix A.

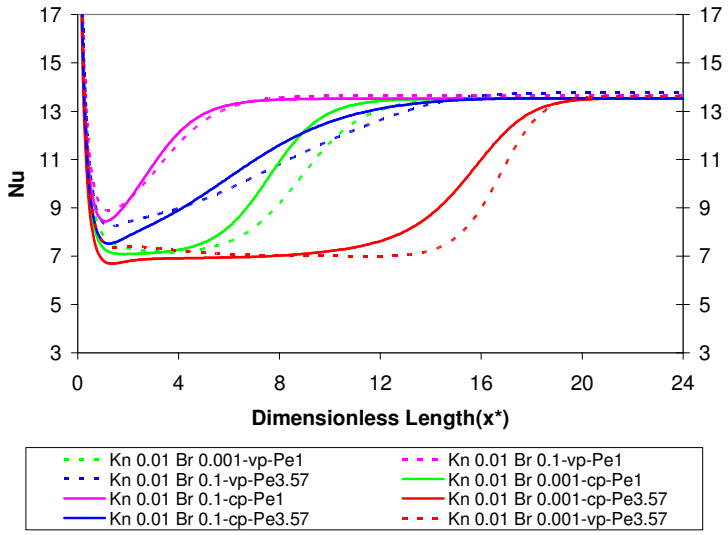

Figure 4.32 Variation of Nusselt number with axial position for various positive Brinkman numbers, obtained from constant and variable property solutions (Kn=0.01, Pe=1, Pe=3.57)

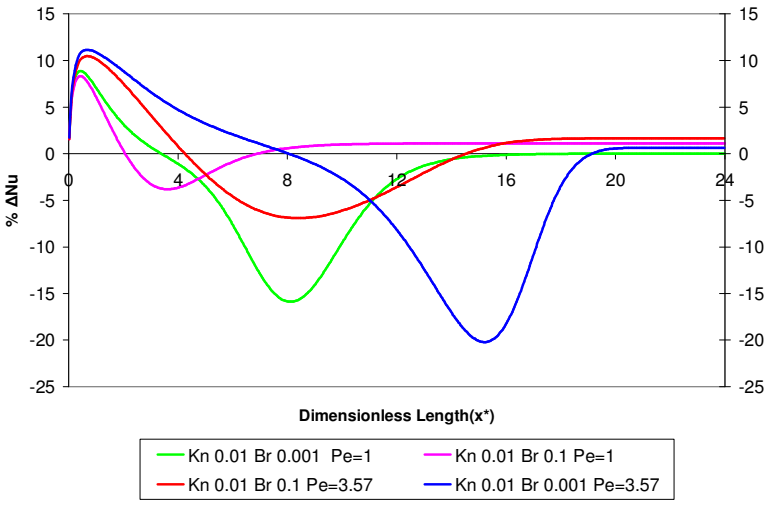

Figure 4.33 Variation of percent difference in Nusselt number between constant and variable property solutions with axial position for various positive Brinkman numbers (Kn=0.01, Pe=1, Pe=3.57)

Effect of variable viscosity and thermal conductivity is discussed above in combination with the effects of Brinkman, Knudsen and Péclet number. In addition to this, Nusselt values and percent difference between variable and constant property solutions are plotted against axial position for various Knudsen, positive Brinkman and Péclet numbers in combination below. The fully developed Nusselt values, for Péclet number 3.57 may differ from the constant properties solution made with a Péclet number of 1. The difference in fully developed Nusselt values is increased with increasing Péclet number for higher Knudsen numbers. For this reason, the difference is thought to be resulting from decreased significance of axial conduction. Moreover the fully developed Nusselt values are higher for the increased Péclet number which can be a consequence of increased convective heat transfer rate.

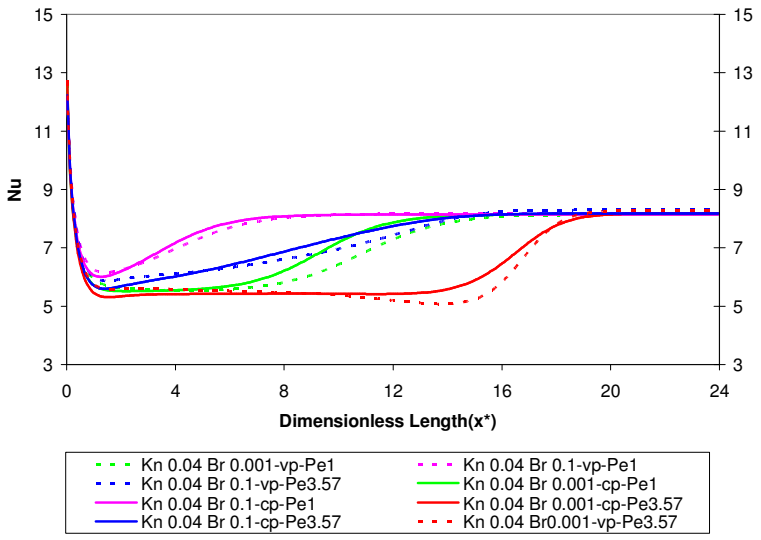

Figure 4.34 Variation of Nusselt number with axial position for various positive Brinkman numbers, obtained from constant and variable property solutions (Kn=0.04, Pe=1, Pe=3.57)

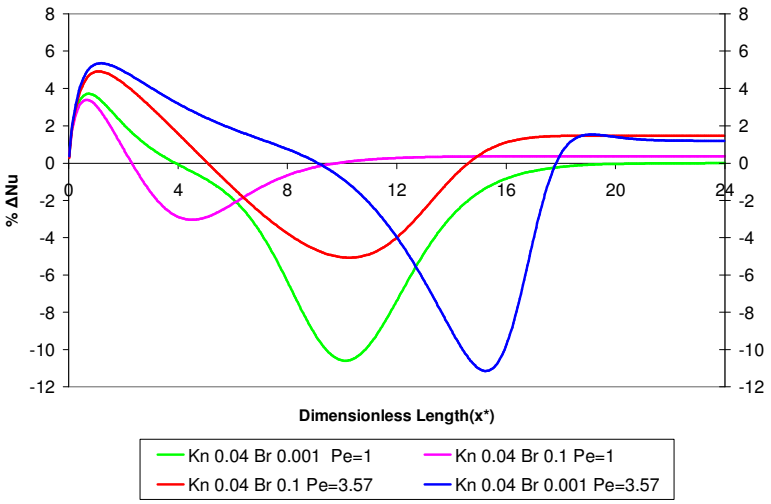

Figure 4.35 Variation of percent difference in Nusselt number between constant and variable property solutions with axial position for various positive Brinkman numbers (Kn=0.04, Pe=1, Pe=3.57)

The reasons of decreasing difference between constant and variable property local Nusselt values with increasing viscous dissipation have been discussed in the previous parts. As a result, only the combined effects of Péclet and Brinkman numbers will be discussed in this part.

Increased Péclet number will cause an increase in the effect of viscous heating as a result of increased velocity gradients. Additionally, as the fluid is cooled in the channel, the viscosity will be reduced which will decrease the effect of viscous dissipation in variable property solutions. Therefore the difference in variable and constant property local Nusselt numbers will not be significantly increased with increasing Péclet number while Brinkman number is held constant.

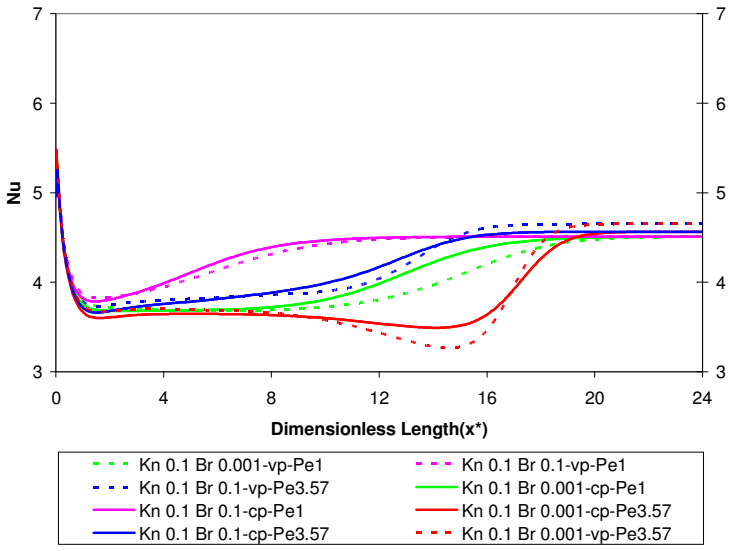

Figure 4.36 Variation of Nusselt number with axial position for various positive Brinkman numbers, obtained from constant and variable property solutions (Kn=0.1, Pe=1,Pe=3.57)

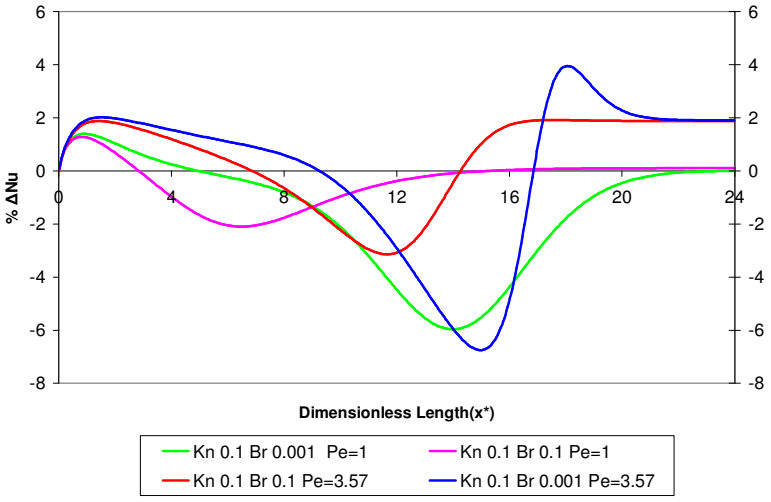

Figure 4.37 Variation of percent difference in Nusselt number between constant and variable property solutions with axial position for positive Brinkman numbers, (Kn=0.1, Pe=1, Pe=3.57)

After completing the discussion about the combined effects of Brinkman, Péclet and Knudsen number on property variation in fluid heating process, the effects of same parameters will be discussed for fluid cooling process. Rarefaction, viscous dissipation and property variation will be discussed in combination, to be able to understand their influence on heat transfer characteristics. The Nusselt numbers obtained from variable and constant property solutions are plotted against axial dimension in Figure 4.38 for negative Brinkman numbers for a fixed Knudsen number. As it can be seen in Figure 4.38, the position of the singular point in variable property solutions is moved to the upstream. Main reason for the shift in position of the singular point is increase in viscosity and thermal conductivity of air with increasing temperature after it enters the channel. The increase in viscosity causes an increase in viscous heating, while the increase in thermal conductivity increases the conductive heat transfer. The conductive heat transfer is heating the upstream of the flow. Due to the increased conductive heat transfer, the fluid temperature reaches the wall temperature faster and earlier with the increased viscous dissipation.

Moreover, the effect of viscous dissipation on property variation can be seen by looking at Figure 4.38. The difference between variable and constant property solutions are decreased with decreasing negative Brinkman number. When viscous dissipation is increased, the fluid is heated more and this will increase the viscosity and thermal conductivity. The increased viscous dissipation due to increased viscosity and increased conductive heat transfer due to increased thermal conductivity will act in opposite directions. As a result of these counteracting mechanisms the difference will be reduced with increasing viscous dissipation. In Figure 4.39 the percent difference between constant and variable property Nusselt values are plotted against the axial position. This plot is not so clear, but it is possible to see the shift in singularity point by looking this plot.

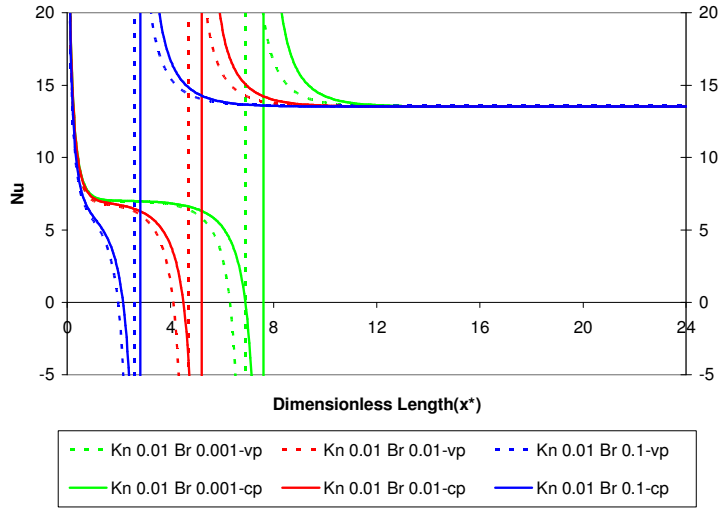

Figure 4.38 Variation of Nusselt number with axial position for various negative Brinkman numbers, obtained from constant and variable property solutions (Kn=0.01, Pe=1)

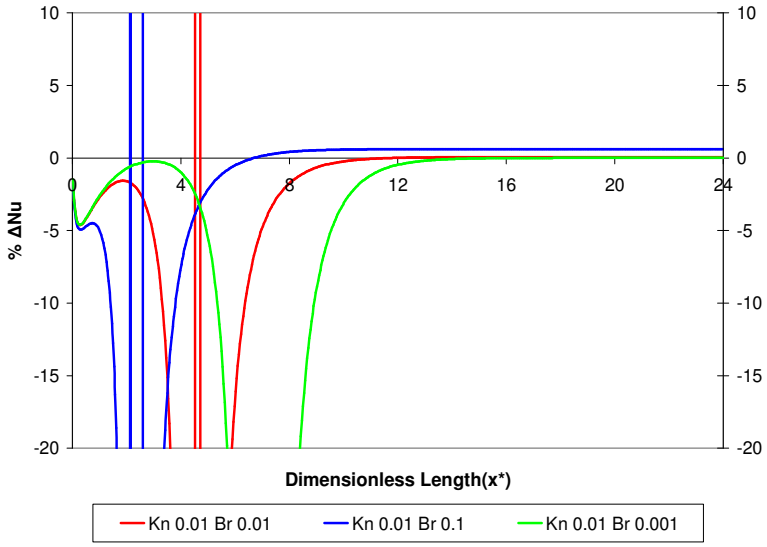

Figure 4.39 Variation of Nusselt difference in Nusselt number between constant and variable property solutions with axial position for negative Brinkman numbers, (Kn=0.1, Pe=1)

In addition to the effect of Brinkman number, also combined effects of Brinkman and Knudsen numbers, on property variation needs to be discussed for heating process. Therefore, both variable and constant property Nusselt numbers are plotted for a Knudsen number of 0.04 and various negative Brinkman numbers, with a Péclet number equal to 1 in Figures 4.40 and 4.41.

By considering Figure 4.40 and Figure 4.41 it is possible to see that the effect of viscous heating on property variation decreases with increased rarefaction. Since the viscous heating is decreasing with increased rarefaction effect, the property variation will be less dependent on viscous dissipation. Furthermore, the viscous dissipation and convective heat transfer rate will be reduced with increased rarefaction and as a result, effect of property variation will be more emphasized, due to increased significance of conductive heat transfer.

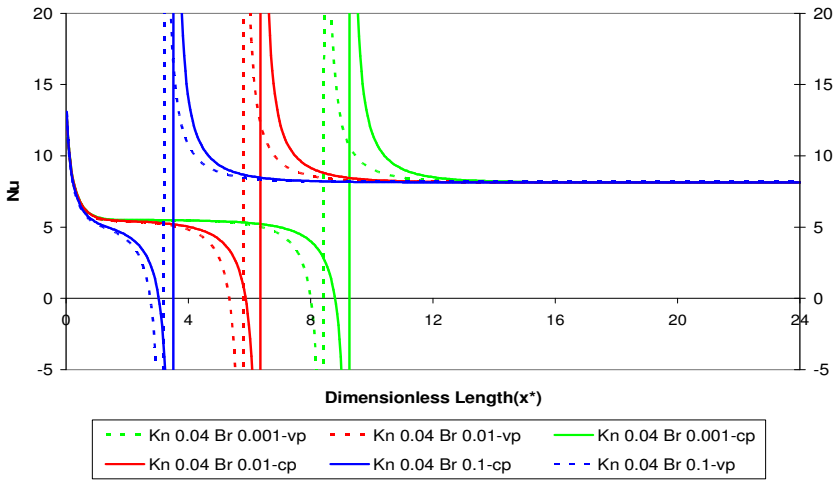

Figure 4.40 Variation of Nusselt number with axial position for various negative Brinkman numbers, obtained from constant and variable property solutions (Kn=0.01, Pe=1)

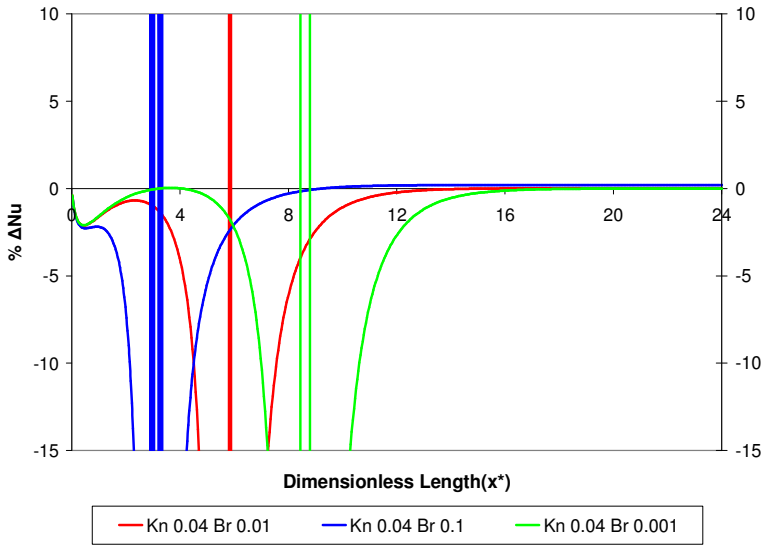

Figure 4.41 Variation of percent difference in Nusselt number between constant and variable property solutions with axial position for negative Brinkman numbers, (Kn=0.04, Pe=1)

Similarly the difference between variable and constant property solutions can be seen in Figure 4.42 and Figure 4.43 for Knudsen number 0.1 and various negative Brinkman numbers with a Péclet number of 1.

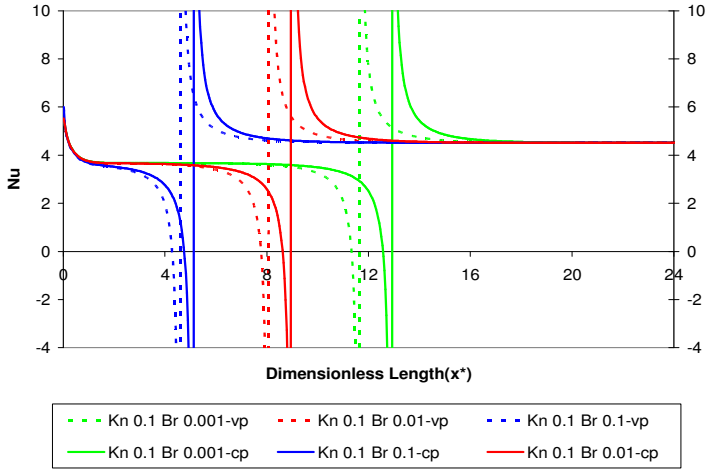

Figure 4.42 Variation of Nusselt number with axial position for various negative Brinkman numbers, obtained from constant and variable property solutions (Kn=0.1, Pe=1)

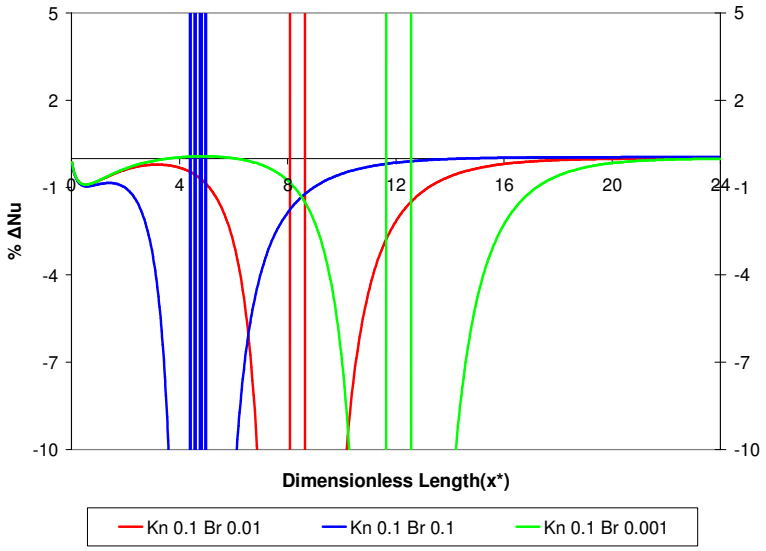

Figure 4.43 Variation of percent difference in Nusselt number between constant and variable property solutions with axial position for negative Brinkman numbers, (Kn=0.1, Pe=1)

After completing the discussions about the combined effects of Knudsen and negative Brinkman numbers on the property variation, the effect of Péclet number will be discussed in detail in the following section.

The variation of Nusselt values for constant and variable property solutions are plotted against the axial position for two different Péclet numbers which are 1, and 3.57.

As discussed before and can be seen from Figure 4.44, the singular point shifts to the downstream with increasing Reynolds number. Similar to the positive Brinkman number cases, with increasing Péclet number, the difference between variable and constant property solutions will be increased. However this is valid for the low Knudsen number flows. Different from the positive Brinkman number case, increasing Péclet number will reduce the difference between constant and variable property solutions with increasing rarefaction for Brinkman number -0.001. As discussed above, the thermal conductivity will be increasing with the heating of the fluid. Moreover, the significance of conductive heat transfer will be reduced with the increased Péclet number. The low viscous dissipation combined with increased Péclet number will reduce the difference resulted from increased conductive heat transfer in variable property solutions. Consequently the difference between Nusselt numbers of variable and constant property solutions will be reduced with increasing Péclet and Knudsen number for low Brinkman numbers. The percent difference is plotted against axial position in Figure 4.45. The shift in position of singular point can also be seen from Figure 4.45.

In brief, Péclet and Knudsen numbers have counteracting effects on the shift in position of singular point, for variable property solutions. Increased rarefaction will retards the heating of fluid by reducing the effect of viscous heating while increased Péclet number will increase effect of viscous dissipation.

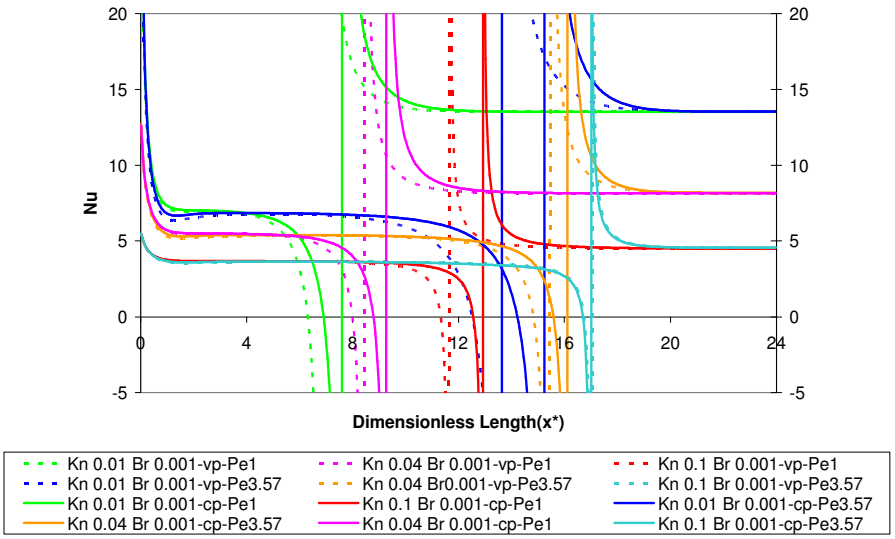

Figure 4.44 Variation of Nusselt number with axial position for various negative Brinkman numbers, obtained from constant and variable property solutions (Kn=0.01, Pe=1, Pe=3.57)

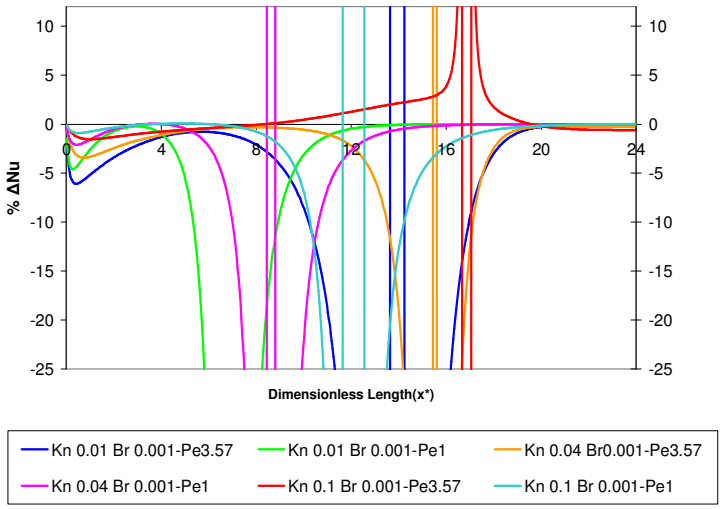

Figure 4.45 Variation of Nusselt difference in Nusselt number between constant and variable property solutions with axial position for negative Brinkman numbers, (Kn=0.1, Pe=1, Pe=3.57)

Fully developed Nusselt numbers will converge to the same values with very little differences for different Péclet numbers. Main reason for these small differences possibly result from increased axial conduction effect. The fully developed Nusselt numbers are tabulated in Table 4.9.

Table 4.9 Fully developed Nusselt numbers, for various Knudsen and Brinkman numbers, obtained from constant and variable property solutions (Pe=1)

		Br			
	Kn	cp	vp	cp	vp
		-0.001	-0.001	-0.100	-0.100
Pe=1	0.010	13.660	13.661	13.660	13.742
	0.040	8.227	8.227	8.227	8.243
	0.100	4.549	4.548	4.548	4.550
Pe=3.57	0.010	13.676	13.664	13.676	13.745
	0.040	8.260	8.238	8.260	8.254
	0.100	4.603	4.691	4.603	4.690

As can be seen from Table 4.9, the difference in fully developed Nusselt values in variable property solutions are increased with the increasing viscous dissipation for the low Knudsen numbers. On the other hand the difference in fully developed Nusselt values due to property variation is decreased with increasing viscous dissipation for higher Knudsen numbers. It is possible to observe the combined effect of Brinkman and Péclet numbers by varying the Péclet and Brinkman numbers while Knudsen number is fixed. In Figure 4.46 the variation of Nusselt values with axial position is plotted for Knudsen equal to 0.01.

The difference between constant and variable property solutions is increased for increasing negative Brinkman number when Knudsen number is equal to 0.01. The reason for the increased difference between constant and variable local Nusselt numbers with decreasing negative Brinkman number is explained above. The difference between variable and constant property solutions are plotted against axial position in Figure 4.47.

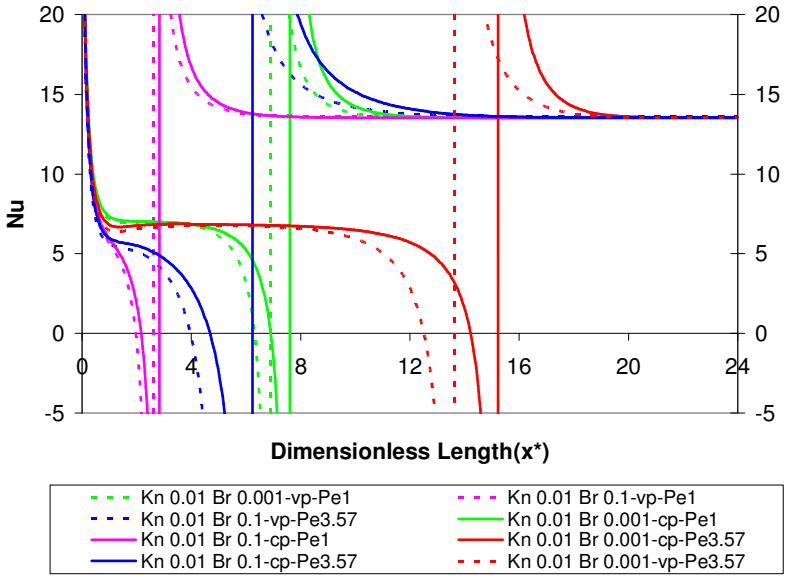

Figure 4.46 Variation of Nusselt number with axial position for various negative Brinkman numbers, obtained from constant and variable property solutions (Kn=0.01, Pe=1, Pe=3.57)

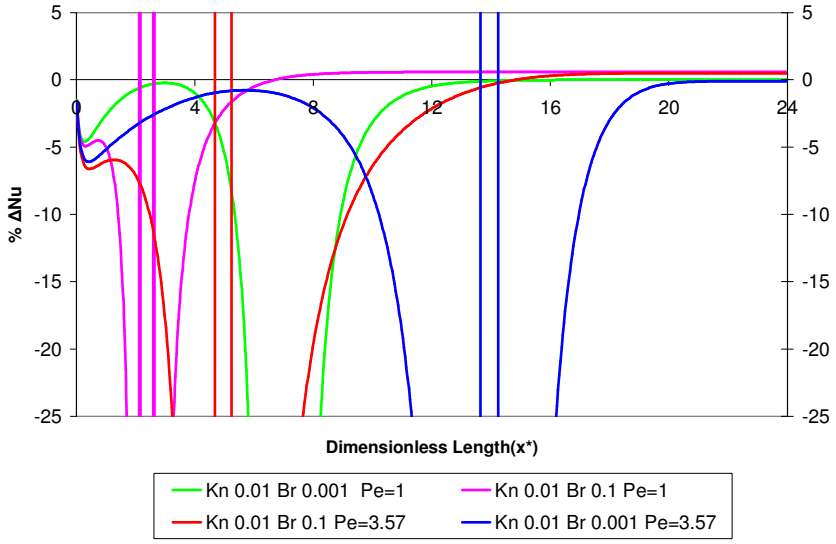

Figure 4.47 Variation of percent difference in Nusselt number between constant and variable property solutions with axial position for negative Brinkman numbers, (Kn=0.1, Pe=1, Pe=3.57)

The local Nusselt values of variable and constant properties are plotted for Knudsen number of 0.04 in Figure 4.48 .With the increase of rarefaction, the relative significance of convective heat transfer is reduced. For this reason, as the viscous dissipation is increased, the difference between constant and variable property solutions will be increased. As stated above, with increased viscous heating the temperature and the thermal conductivity and will be increased. In addition to the increase in conductive heat transfer, the decrease in convective heat transfer will results in a higher drop in heat transfer coefficients. The differences are plotted against axial position in Figure 4.49. Similar results are obtained for Knudsen number 0.1. The increased viscous heating will cause a higher drop in local Nusselt values of variable property solutions with the increased rarefaction. However, the decrease in convective heat transfer combined with low viscous dissipation will result in small differences between constant and

variable property solutions. The plots of Nusselt values and percent difference are given in Figure 4.50 and Figure 4.51 respectively.

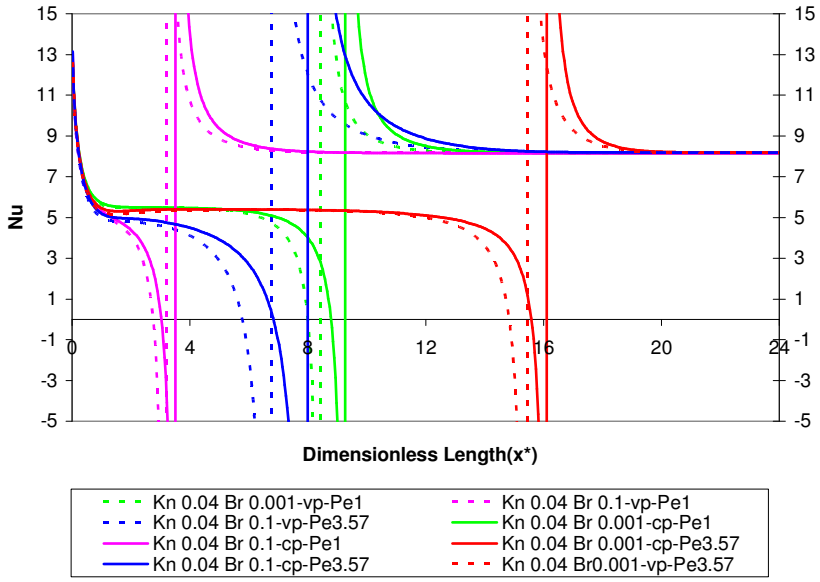

Figure 4.48 Variation of Nusselt number with axial position for various negative Brinkman numbers, obtained from constant and variable property solutions (Kn=0.04, Pe=1, Pe =3.57)

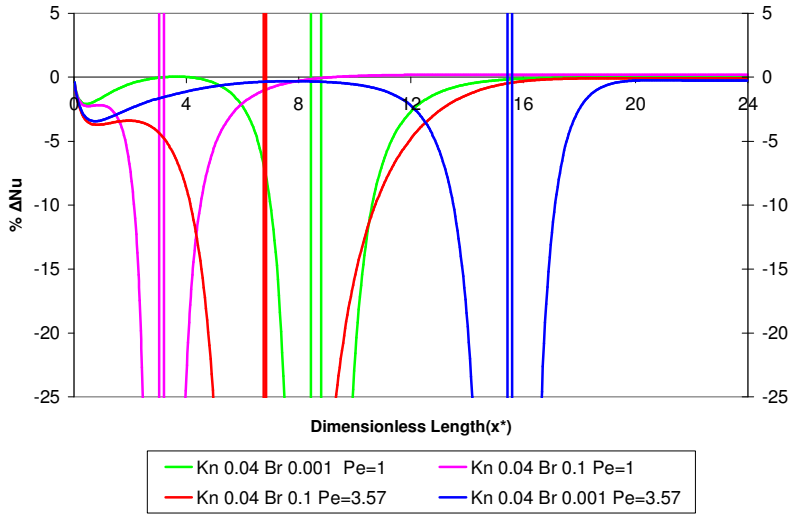

Figure 4.49 Variation of percent difference in Nusselt number between constant and variable property solutions with axial position for negative Brinkman numbers, (Kn=0.1, Pe=1, Pe=3.57)

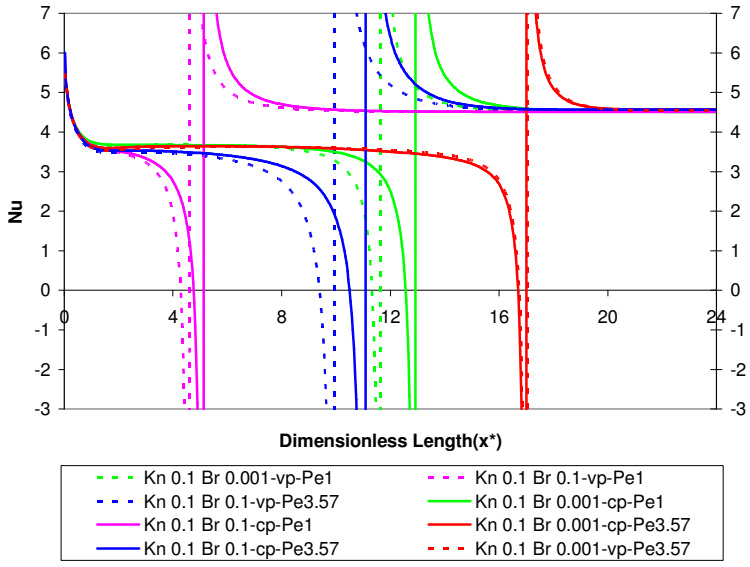

Figure 4.50 Variation of Nusselt number with axial position for various negative Brinkman numbers, obtained from constant and variable property solutions (Kn=0.01, Pe=1, Pe=3.57)

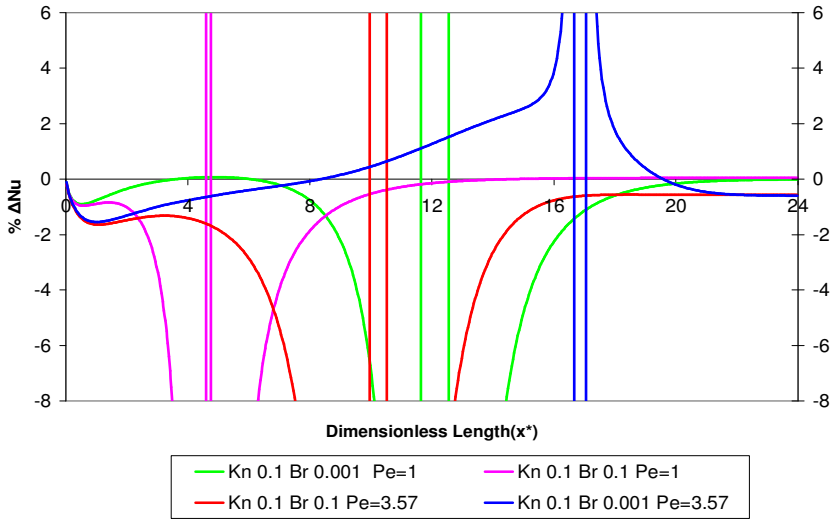

Figure 4.51 Variation of percent difference in Nusselt number between constant and variable property solutions with axial position for negative Brinkman numbers, (Kn=0.1, Pe=1, Pe=3.57)

4.1.3 Entry Length Variations

Both thermal and hydrodynamic entry lengths can be calculated from analyses results. Basically the flow assumed to be hydrodynamically fully developed when centerline axial velocity reaches 0.999 of the fully developed value. Similarly the flow is assumed to be thermally fully developed when dimensionless temperature reaches 0.999 of the fully developed value. The non-dimensional hydrodynamic entry length and thermal entry length values obtained from constant property solutions are tabulated for positive Brinkman numbers and Péclet number equal to 1 in Table 4.10.

Table 4.10 Variation of hydrodynamic and thermal entry length with varying Knudsen numbers and positive Brinkman numbers obtained from constant property solution (Pe=1)

		Br 0.001	Br 0.01	Br 0.1
Kn 0.01	Hydrodynamic entry length	1.39	1.39	1.39
	Thermal entry length	13.62	11.22	8.70
Kn 0.02	Hydrodynamic entry length	1.44	1.44	1.44
	Thermal entry length	15.06	12.46	9.82
Kn 0.04	Hydrodynamic entry length	1.48	1.48	1.48
	Thermal entry length	16.86	13.94	10.90
Kn 0.06	Hydrodynamic entry length	1.50	1.50	1.50
	Thermal entry length	18.50	15.26	11.9
Kn 0.08	Hydrodynamic entry length	1.52	1.52	1.52
	Thermal entry length	20.78	17.42	13.78
Kn 0.1	Hydrodynamic entry length	1.52	1.52	1.52
	Thermal entry length	22.30	18.94	15.14

Increasing rarefaction effect with increasing Knudsen numbers will result in a slightly increased hydrodynamic entry length. However, hydrodynamic entry length is not affected from viscous dissipation effect. For this reason the hydrodynamic entry length does not change for different Brinkman numbers in constant property solutions.

On the other hand thermal entry length depends on both Knudsen and Brinkman numbers. The thermal entry length increases with increasing rarefaction effect as it was discussed earlier, and it decreases with increasing Brinkman numbers. These phenomena were discussed in detail in the previous sections.

In addition to the fluid cooling case in which Brinkman numbers are positive, thermal and hydrodynamic entry length is tabulated for fluid heating case. The non-dimensional thermal and hydrodynamic entry length values are tabulated for various Knudsen and negative Brinkman numbers in Table 4.11.

Table 4.11 Variation of hydrodynamic and thermal entry length with varying Knudsen numbers and negative Brinkman numbers obtained from constant property solution (Pe=1)

		Br- 0.001	Br -0.01	Br -0.1
Kn 0.01	Hydrodynamic entry length	1.39	1.39	1.39
	Thermal entry length	14.86	12.46	10.14
Kn 0.02	Hydrodynamic entry length	1.44	1.44	1.44
	Thermal entry length	15.38	12.78	10.30
Kn 0.04	Hydrodynamic entry length	1.48	1.48	1.48
	Thermal entry length	16.42	14.1	11.26
Kn 0.06	Hydrodynamic entry length	1.50	1.50	1.50
	Thermal entry length	18.98	15.78	12.62
Kn 0.08	Hydrodynamic entry length	1.52	1.52	1.52
	Thermal entry length	20.46	17.1	13.66
Kn 0.1	Hydrodynamic entry length	1.52	1.52	1.52
	Thermal entry length	22.14	18.78	15.18

For the constant property solution, the hydrodynamic entry length does not change with Brinkman number; the values are the same with the positive Brinkman number case. However, thermal entry length values are increasing with increased rarefaction and reduced viscous dissipation effects as discussed above.

Additionally the entry length values for variable property solutions are also calculated. The non-dimensional hydrodynamic and thermal entry length values obtained from variable property solutions are tabulated for various positive Brinkman numbers in Table 4.12.

Table 4.12 Variation of hydrodynamic and thermal entry length with varying Knudsen numbers and negative Brinkman numbers obtained from variable property solution(Pe=1)

		Br 0.001	Br 0.01	Br 0.1
Kn 0.01	Hydrodynamic entry length	1.60	1.60	1.60
	Thermal entry length	15.94	12.98	10.66
Kn 0.02	Hydrodynamic entry length	1.64	1.64	1.64
	Thermal entry length	17.58	14.46	12.82
Kn 0.04	Hydrodynamic entry length	1.68	1.68	1.68
	Thermal entry length	19.42	16.18	14.02
Kn 0.06	Hydrodynamic entry length	1.68	1.68	1.68
	Thermal entry length	20.74	17.58	14.86
Kn 0.08	Hydrodynamic entry length	1.68	1.68	1.68
	Thermal entry length	22.18	19.26	17.22
Kn 0.1	Hydrodynamic entry length	1.68	1.68	1.68
	Thermal entry length	22.9	21.78	17.9

When both Table 4.10 and Table 4.12 considered together it is possible to see that, variation in viscosity with temperature slightly increases the hydrodynamic entry length. However, the increase in hydrodynamic entry length is not affected from variation in viscous dissipation. The hydrodynamic entry length values are the same for a Knudsen number regardless of Brinkman numbers. On the other

hand thermal entry length is increased slightly for variable property solutions. As discussed above, the property variation effect will delay the thermal development for positive Brinkman numbers which will result in higher thermal entry length values. On the contrary for the negative Brinkman numbers, the variation of thermal and hydrodynamic entry length will be different than the fluid cooling case. The variable property results for fluid heating case are tabulated in Table 4.13 for Péclet number equal to 1.

Table 4.13 Variation of hydrodynamic and thermal entry length with varying Knudsen numbers and negative Brinkman numbers obtained from variable property solution(Pe=1)

		Br- 0.001	Br -0.01	Br -0.1
Kn 0.01	Hydrodynamic entry length	1.28	1.28	1.28
	Thermal entry length	13.58	11.50	7.90
Kn 0.02	Hydrodynamic entry length	1.32	1.32	1.32
	Thermal entry length	14.02	11.74	10.42
Kn 0.04	Hydrodynamic entry length	1.36	1.36	1.36
	Thermal entry length	15.46	12.82	10.62
Kn 0.06	Hydrodynamic entry length	1.40	1.40	1.40
	Thermal entry length	17.26	14.30	11.74
Kn 0.08	Hydrodynamic entry length	1.42	1.42	1.42
	Thermal entry length	18.74	15.54	12.54
Kn 0.1	Hydrodynamic entry length	1.42	1.42	1.42
	Thermal entry length	20.58	17.14	13.86

Regarding the values given in Table 4.13, it can be seen that both hydrodynamic and thermal entry length are decreased for variable property solutions. The reasons for this early development are discussed in detail in the previous sections. Moreover, by considering the data available in Table 4.14, it is possible to say that

thermal entry length is affected from variation of Knudsen and Brinkman numbers. In addition to Brinkman and Knudsen numbers also Péclet number has significant effect on hydrodynamic and thermal entry length. The non-dimensional hydrodynamic and thermal entry length values are tabulated in Table 4.14 for different Knudsen and positive Brinkman numbers. The results are given for both constant and variable property solutions obtained for Péclet number equal to 3.57.

Table 4.14 Variation of hydrodynamic and thermal entry length with varying Knudsen numbers and positive Brinkman numbers obtained from variable property solution (Pe=3.57)

		Constant Property		Variable Property	
		Br 0.001	Br 0.1	Br 0.001	Br 0.1
Kn 0.01	Hydrodynamic entry length	1.72	1.72	2.44	2.32
	Thermal entry length	18.74	12.9	19.18	14.86
Kn 0.04	Hydrodynamic entry length	1.88	1.88	2.48	2.38
	Thermal entry length	19.34	14.86	19.20	15.76
Kn 0.1	Hydrodynamic entry length	2.00	2.00	2.34	2.32
	Thermal entry length	20.02	16.46	19.46	16.66

As mentioned above increase in Péclet number increases both thermal and hydrodynamic entry length values. Additionally as discussed earlier the effect of viscosity and thermal conductivity variations become more emphasized with increasing entry length. As can be seen in Table 4.14 the increase in hydrodynamic and thermal entry length due to property variation is increased with

decreasing Brinkman number. Moreover, the difference in entry lengths will be decreased with increasing rarefaction effect as discussed earlier.

Similarly the variation of non-dimensional entry length values are tabulated in Table 4.15 for constant and variable property solutions of fluid heating case.

Table 4.15 Variation of hydrodynamic and thermal entry length with varying Knudsen numbers and negative Brinkman numbers obtained from variable property solution (Pe=3.57)

		Constant Property		Variable Property	
		Br -0.001	Br -0.1	Br -0.001	Br -0.1
Kn 0.01	Hydrodynamic entry length	1.72	1.72	1.51	1.50
	Thermal entry length	18.84	13.24	17.99	11.27
Kn 0.04	Hydrodynamic entry length	1.88	1.88	1.66	1.66
	Thermal entry length	19.4	15.02	19.26	13.88
Kn 0.1	Hydrodynamic entry length	2.00	2.00	1.80	1.80
	Thermal entry length	20.06	16.58	20.06	16.58

As discussed earlier, the entry length will be decreased for variable property solutions in case of fluid heating. Moreover by considering the data available in Table 4.15, it can be said that effect of Brinkman number is less severe on the hydrodynamic entry length than thermal entry length.

4.2 Effect of Flow Parameters on Heat Transfer

Regarding the non-dimensional momentum and energy equations given previously, effects of non-dimensional parameters can be analyzed.

4.2.1 Fluid Cooling Case

For the fluid cooling case in which Brinkman numbers are positive and fluid is cooled by the wall, the thermal conductivity and the viscosity values are decreasing as the fluid proceeds in the channel. For this reason the axial conductive flux will be positive and the transverse conductive flux will be negative. Similarly the axial convective flux will be negative as a result of flow direction and temperature change. On the contrary the transverse convective flux will be positive. Additionally the viscous dissipation terms will be inherently positive as a result of positive Brinkman number. Overall conductive flux will be negative since transverse convective flux is the dominating one. Likewise the overall convective flux will be negative. In this case the right hand side of the Equation (4.3) will be positive as a result of positive viscous dissipation terms. The magnitudes will change with the Brinkman and Péclet numbers; however signs of the terms will remain unchanged. With decreasing temperature in the channel, the decreased thermal conductivity will yield, lower conductive flux in both axial and vertical directions. This will reduce the overall heat transfer rate. The increased Péclet number will reduce the magnitude of the right hand side of Equation (4.3). At the steady state the convective terms will also be reduced. The velocity profile will be changed less than the temperature field, so the temperature gradients will be lowered in axial direction mainly, which results in a later development and elongated entrance length. However the increase of Brinkman number will increase the magnitude of the second term on the right hand side of the Equation (4.3). This will increase the axial gradients and shorten the entrance length. The significance of convective terms will be reduced due to increased slip

velocity and temperature jump at the wall boundaries. The reduced significance of the convective terms will also results in, increased entrance length.

4.2.1.1 The Effect of Thermal Conductivity Variation

The variation of non-dimensional conductivity at an arbitrary crossection is given in Figure 4.52.

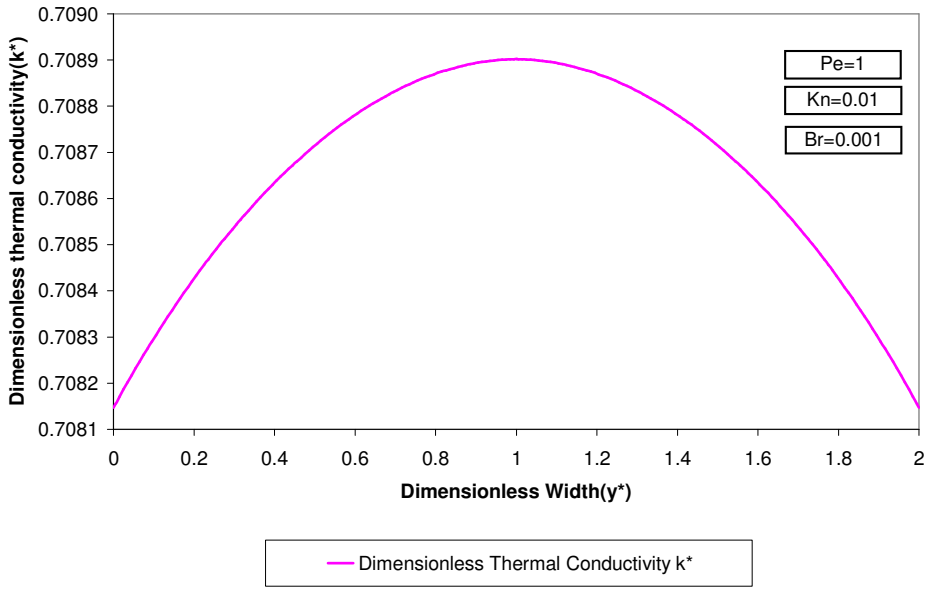

Figure 4.52 Variation of dimensionless thermal conductivity on vertical axis at an arbitrary crossection (Kn=0.01, Pe=1, Br=0.001)

As can be seen, the thermal conductivity is increasing in the positive vertical direction and the dimensionless thermal conductivity values are less than 1 at all locations. As a result, the vertical conductive flux of variable property solution will be less than the constant property solution. Considering the axial variation of

thermal conductivity which is plotted in Figure 4.53, it is possible to say that axial conductive flux of variable property solution will also be reduced as fluid proceed in to downstream. This difference basically results from dimensionless conductivity values which are less than 1. In fluid cooling the axial conductive flux is assisting the axial convective flux as mentioned earlier. For this reason the reduced thermal conductivity will reduce this assistance.

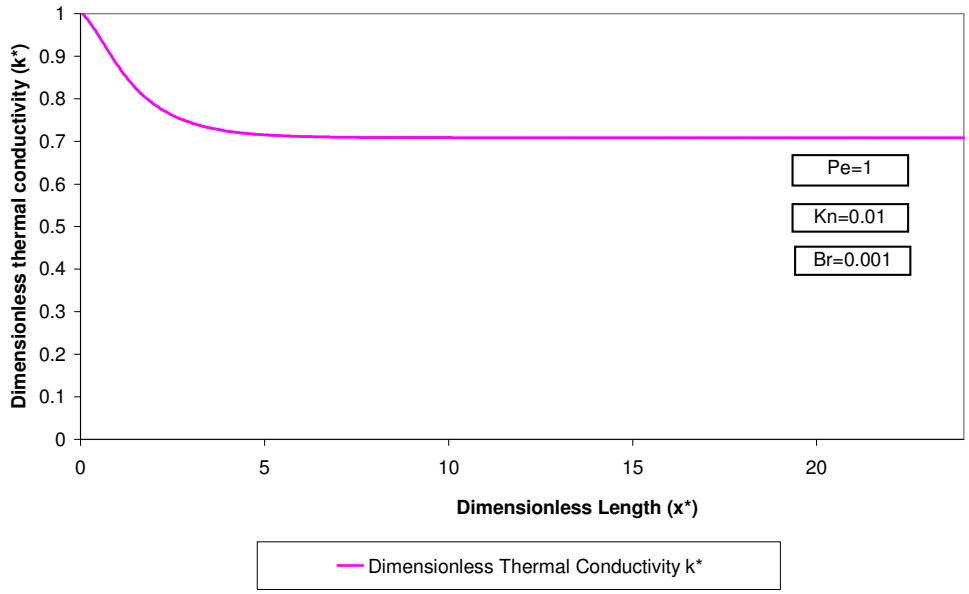

Figure 4.53 Variation of dimensionless thermal conductivity on axial position (Kn=0.01, Pe=1, Br=0.001)

4.2.1.2 The Effect of Viscosity Variation

The variation of dimensionless viscosity with vertical position is plotted in Figure 4.54. Moreover, the variation of dimensionless viscosity with axial position is given in Figure 4.55.

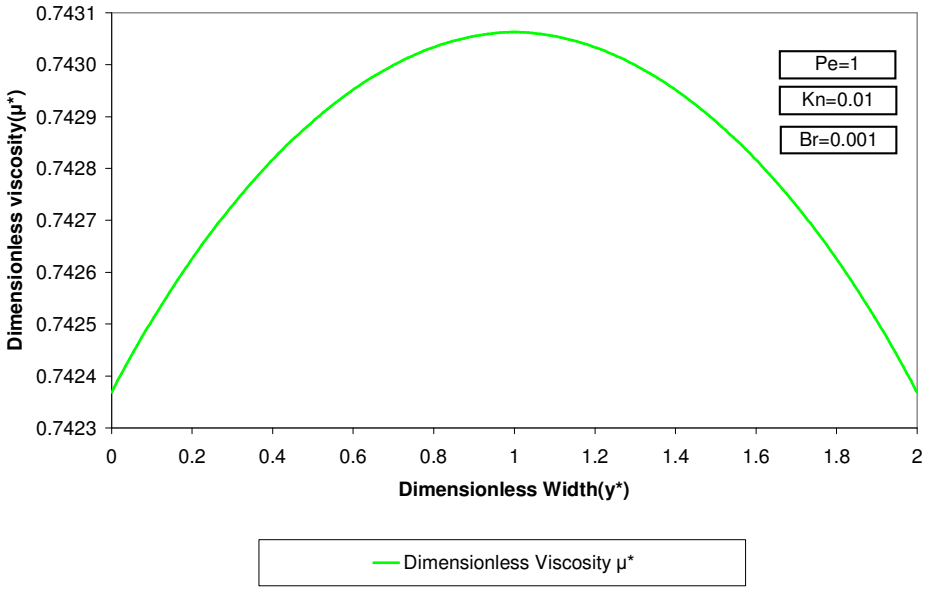

Figure 4.54 Variation of dimensionless viscosity on vertical axis at an arbitrary crossection (Kn=0.01, Pe=1, Br=0.001)

When both Figure 4.54 and Figure 4.55 considered together, it can be seen that viscosity values are both less than 1 in axial and vertical directions. However, the viscosity is increasing in vertical direction while it decreases in the downstream direction. This reduced viscosity values will yield, lower viscous dissipation which will results in reduced viscous dissipation. The reduced viscous dissipation causes a later development of flow. Additionally, the vertical variation of viscosity will cause a distortion in axial velocity profile. For the cooling case, vertical variation of viscosity also induces a vertical velocity which increases the transverse convection. However the effect of viscosity variation is less significant on heat transfer and temperature profile.

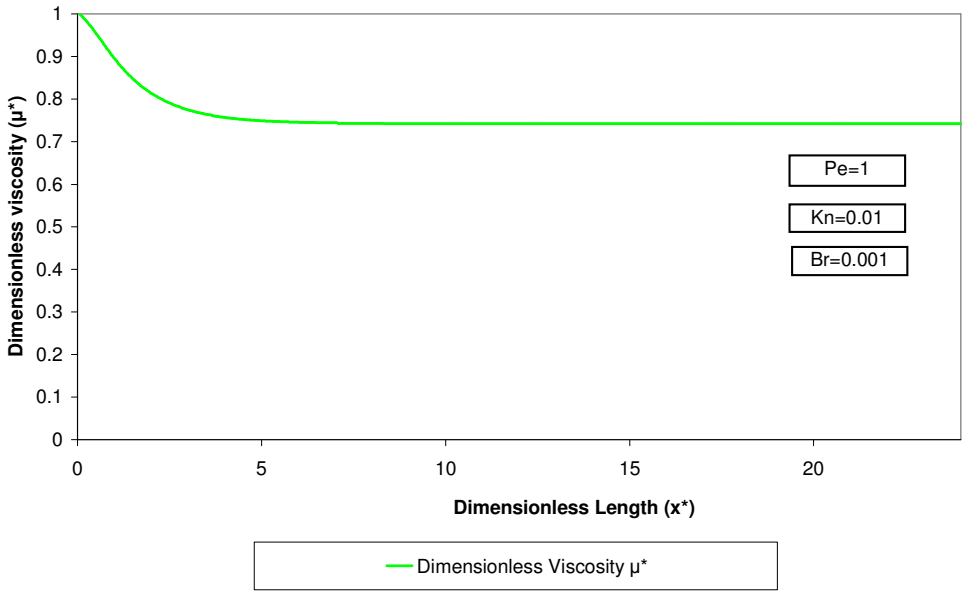

Figure 4.55 Variation of dimensionless viscosity on axial position (Kn=0.01, Pe=1, Br=0.001)

4.2.2 Fluid Heating Case

For the fluid heating case in which fluid is heated by the wall, and the thermal conductivity and viscosity increase as the fluid proceeds in the channel. The axial conductive flux will be negative while vertical conductive flux is positive. On the other hand axial convective flux will be negative and vertical convective flux will be positive. Since axial convective flux and conductive flux are opposite signed, the increase in thermal conductivity will reduce the effect of convective heat transfer. Additionally with increasing Péclet number the magnitudes will be reduced and the effect of conductive heat flux will be reduced. Similarly the effect of viscous heating will be decreased. Due to the decreased significance of viscous dissipation, heating of the fluid and the thermal development will be retarded. As a result of retarded heating the gradients will be lower and the conductive flux

will be lowered for variable property solution. Likewise, the decrease in Brinkman number will also retard the thermal development of flow and reduce the heat transfer for variable property solution.

4.2.2.1 The Effect of Thermal Conductivity Variation

Variation of thermal conductivity in fluid heating case can be seen in Figure 4.56.

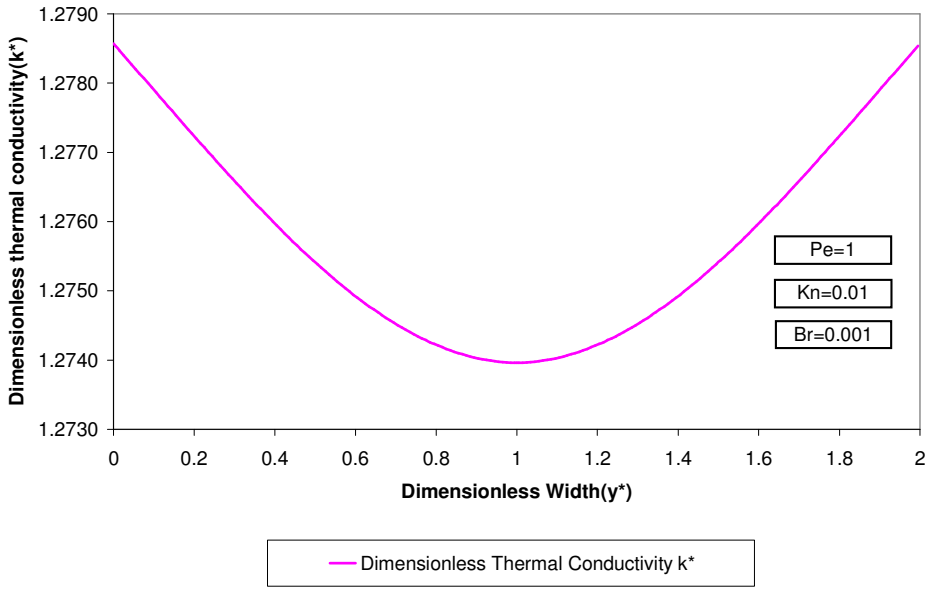

Figure 4.56 Variation of dimensionless thermal conductivity on vertical axis at an arbitrary crossection (Kn=0.01, Pe=1, Br=0.001)

As it can be seen in the plot, the dimensionless thermal conductivity values are higher than 1. The values are decreasing with positive vertical position. Both temperature and thermal conductivity gradients will be negative in positive y direction while these terms will be positive in axial direction. Due to the

dimensionless thermal conductivity values, it can be said that the conductive flux is higher than constant property solution. However, the negative axial conductive flux will have a counteracting effect on overall heat transfer. The axial variation of thermal conductivity is given in Figure 4.57. An as can be seen thermal conductivity is increasing with axial position. Therefore the axial conductive flux will be increased with axial position.

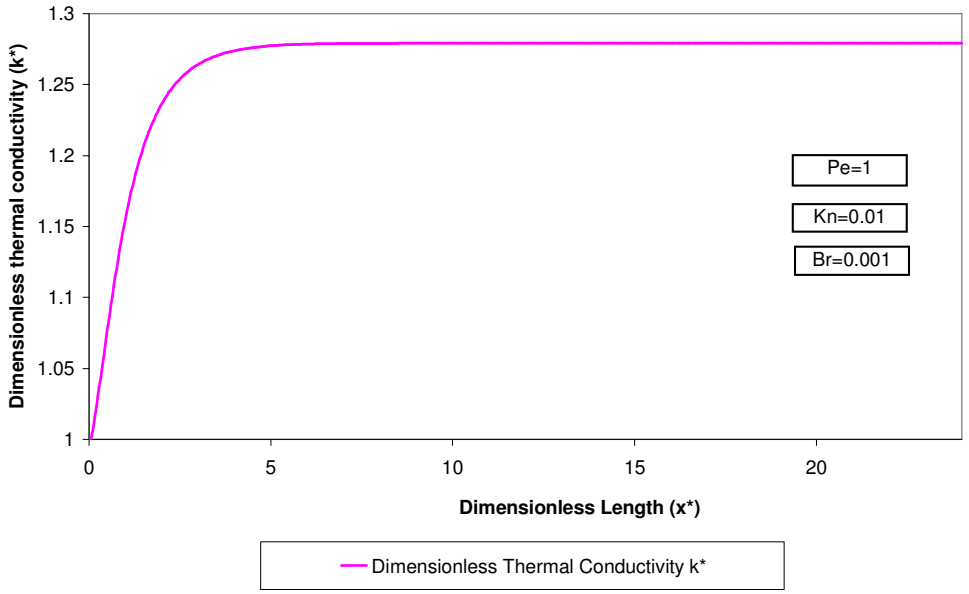

Figure 4.57 Variation of dimensionless thermal conductivity on axial position (Kn=0.01, Pe=1, Br=0.001)

4.2.2.2 The Effect of Viscosity Variation

The variation of dimensionless viscosity with vertical position is plotted in Figure 4.58 for fluid heating case. Moreover, the variation of dimensionless viscosity with axial position is given in Figure 4.59.

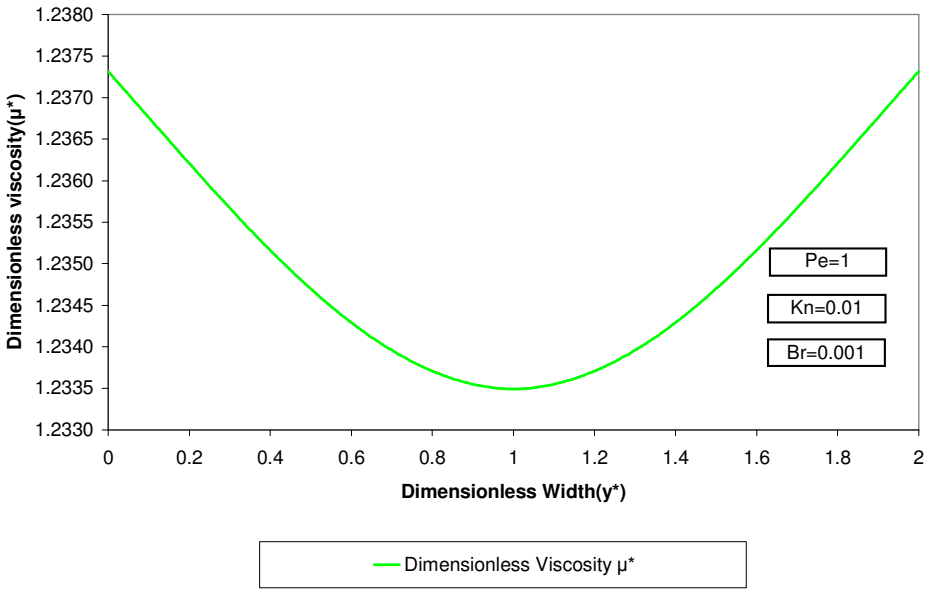

Figure 4.58 Variation of dimensionless viscosity on vertical axis at an arbitrary crossection (Kn=0.01, Pe=1, Br=0.001)

Since all of the viscosity values are higher than 1, this will increase the effect of viscous dissipation. Increased viscous heating will increase the thermal development rate and heating of the fluid. The increase in viscous dissipation will decrease the difference between constant and variable property solutions by reducing the conduction resistance of fluid. Moreover, decreasing viscosity in vertical direction creates an induced vertical velocity component in negative vertical direction. This induced velocity will reduce the transverse convection.

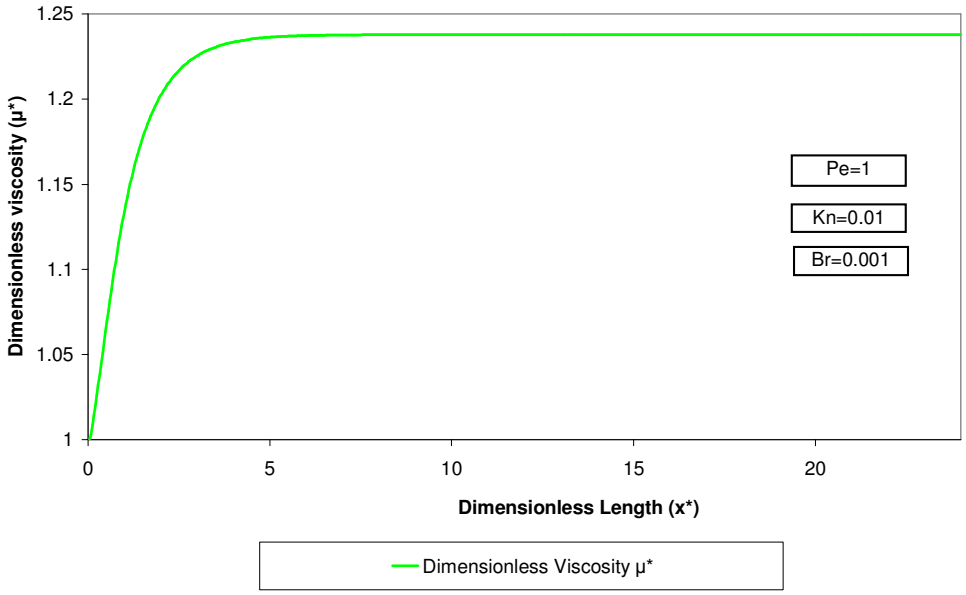

Figure 4.59 Variation of dimensionless viscosity on axial position (Kn=0.01, Pe=1, Br=0.001)

4.2.3 Effect of Knudsen number

With increased Knudsen numbers, the slip velocity and the temperature jump at wall boundaries will be increased. Due to the increase in rarefaction effect, both temperature and velocity gradients will be reduced. This will cause a decrease in viscous heat dissipation, conductive and convective heat transfer. Since the gradients will reduce with increasing rarefaction, the property variation effects will be less significant. Therefore, for fluid cooling case, the difference between constant and variable heat transfer coefficients will be decreasing with increasing rarefaction. However, the difference will be increased for the fluid heating case.

4.2.4 Effect of Péclet number

Péclet number is basically related with the significance of conductive terms and viscous dissipation terms. Increasing Péclet number will reduce the significance of conducive and viscous dissipation terms. The Péclet number is a function of Reynolds number as given in Equation (4.5) and increases only with increasing Reynolds number. The Reynolds increase will reduce the effect of viscous dissipation which causes a delay in the thermal development. Due to the reduced effect of viscous dissipation together with the viscosity and thermal conductivity variation, flow will be developed more slowly for the variable property solution. As a result with increasing Péclet number, the shift in local heat transfer coefficients and Nusselt values will be increased. This increase in shift results from, decreased induced velocity due to decreased conductive flux and viscous dissipation.

4.2.5 Effect of Brinkman number

This dimensionless group defined in Equation (4.4) is only related with the significance of viscous dissipation terms as can be seen from Equation (4.3). Increasing Brinkman number in both heating and cooling flow conditions will reduce the entrance length by decreasing the conduction resistance of the fluid [11]. As a result of increased conductive flux, the entrance length will be reduced. Additionally the significance of Brinkman number will decrease, with increasing Reynolds and Péclet, due to increased channel dimension.

4.3 Dimensionless Groups Related with Typical Applications

In many analyses in the literature, often arbitrary and unrealistic parameters are used to observe the effects of viscous dissipation, axial conduction and

rarefaction. Thus Knudsen, Brinkman and Péclet numbers used in such analyses are rarely encountered in real cases.

The Knudsen numbers used in current the analyses are in the range 0.01 and 0.1. These are theoretically in the slip flow range, however, this Knudsen numbered flows of air will have a characteristic dimension D_h. in the range 6.8μm and 0.68μm meters because the mean free path of air in ambient pressure is 68nm. Even tough these dimensions are smaller than conventional micro channels in heat sinks, they are theoretically applicable.

As an example, an electronic cooling application with micro-heat sink can be considered. In this case the temperature difference can not be higher than 60º C, due to the limits of operation. Moreover, the flow speed of a commercial axial fan that can be used in an electronics cooling application will be in the range of 20 m/s. Also one other constraint for the flow speed is the incompressibility assumption. Therefore the flow speed can not exceed 0.1 Mach for ambient pressure and temperature. Mach = 0.1 corresponds to 34 m/s approximately.

Regarding the hydraulic diameter, temperature difference and flow speed given here, it is possible to calculate Reynolds, Brinkman and Péclet numbers by using the thermophysical properties of air [55].

The thermophysical properties of air is given below for ambient temperature 296 K,

$$\mu = 18.31.10^{-6}\, kg/sm \tag{4.7}$$

$$\rho = 1.19226 kg/m^3 \tag{4.8}$$

$$k = 0.025862 W / mK \tag{4.9}$$

$$\Pr = 0.7127 \tag{4.10}$$

$$6.8.10^{-6} m \le D_h \le 0.68.10^{-6} m \tag{4.11}$$

Here

$$\mathrm{Re} = \frac{\rho U_\infty D_h}{\mu} \tag{4.12}$$

The Reynolds number can be expressed in terms of inlet velocity as follows,

$$0.04427.U_\infty \le \mathrm{Re} \le 0.4427.U_\infty \tag{4.13}$$

For the average velocity of 25 m/s the Reynolds number values will be,

$$1.1 \le \mathrm{Re} \le 11 \tag{4.14}$$

Since Péclet number is product of Reynolds and Prandtl numbers, it will be in the range

$$0.789 \le Pe \le 7.89 \tag{4.15}$$

The upper limit for Péclet number under incompressible fluid assumption and the Knudsen range subject to discussion can be expressed as,

$$Pe \le 0.31551 \cdot 34 \tag{4.16}$$

$$Pe \leq 10 \tag{4.17}$$

Additionally for the given conditions, the realistic Brinkman values can be calculated as follows, by using the thermophysical properties given above,

$$Br = \frac{\mu U_{\infty}^{2}}{k(T_i - T_w)} \tag{4.18}$$

$$Br \leq \frac{18.31 \cdot 10^{-6} U_{\infty}^{2}}{0.025862 \cdot 60} \tag{4.19}$$

Here maximum inlet velocity should be less than 0.1 Mach which is equal to 34 m/s approximately. For this reason upper limit of Brinkman number will be,

$$Br \leq 0.01 \tag{4.20}$$

In the analyses some of the Péclet and Brinkman values are taken beyond these limits to show the effect of these numbers on heat transfer characteristics. Additionally, these numbers are chosen to simulate the extreme conditions

CHAPTER 5

CONCLUSIONS AND RECOMMENDATIONS FOR FUTURE WORK

Effect of variable thermal conductivity and viscosity in single phase flow in microchannels with a constant wall temperature boundary condition is investigated in this study. Microchannel dimensions are chosen to simulate the slip flow regime for air. For this purpose, two-dimensional parallel plate geometry is analyzed. Throughout the analyses, flow is assumed to be laminar and incompressible, while both viscosity and thermal conductivity are assumed to be functions of temperature only. Variation of density and specific heat with temperature is not taken into account in the study. Numerical analyses are performed for variable thermal conductivity and viscosity as well as constant thermal conductivity and viscosity, to be able to understand the difference.

Simultaneously developing flow between parallel plates is investigated numerically by solving pressure and velocity in a coupled manner. Numerical solutions are performed by using finite difference method, due to the simplicity of the geometry. Since our main area of interest is slip flow regime, classical Navier-Stokes equations are solved by imposing slip velocity boundary condition for defining the flow field. Similarly, energy equation is solved by imposing temperature jump boundary condition for defining the temperature field. Besides the pressure velocity coupling, momentum and energy equations are also solved in a coupled manner to be able to take variable thermophysical property effects into account.

Both axial conduction and all terms of viscous dissipation are taken into account while solving the energy equation. The numerical solutions are performed by using the computer code written in MATLAB. Momentum and energy equations are solved in transient form for convenience. The Poisson equation is solved implicitly in each time step to define the pressure field, while all other variables are solved explicitly. The results obtained for velocity field are compared with the analytical solutions, while temperature field is verified by using the analytically calculated Nusselt values for simple cases.

In the analyses, dimensionless variables are varied to be able to observe the effects of viscous dissipation, rarefaction, geometry and axial conduction. The effect of rarefaction is represented non-dimensionally by Knudsen number. The relative significance of viscous dissipation and axial conduction are non-dimensionally represented by Brinkman and Péclet numbers respectively. The non-dimensional parameters used in the analyses are as follows.

- Knudsen numbers: 0.01, 0.02, 0.04, 0.06, 0.08, 0.1
- Brinkman numbers: 0.001, 0.01, 0.1, -0.001, -0.01, -0.1
- Péclet numbers: 1 and 3.57

Since working fluid is air, Prandtl number can not be changed arbitrarily, for this reason Péclet number is varied with Reynolds number. As stated in the previous parts, to be able to non-dimensionalize the variation of viscosity and thermal conductivity with temperature, dimensional inlet and wall temperature values are used. Therefore, for the fluid heating case where Brinkman numbers are negative, wall temperature is taken as 296 K while inlet temperature taken as 394 K. Likewise for the fluid cooling case, inlet temperature is taken as 444 K. Main point of interest of the study is the effect of variable viscosity and thermal conductivity on heat transfer. The conclusions obtained from both constant and variable property solutions, can be summarized as follows,

- As a result of increasing rarefaction, both slip velocity and temperature jump at the wall increases. Due to increased temperature jump and slip velocity, total heat transfer decreases with increasing rarefaction.
- When Nusselt values are plotted against axial position, it is possible to see the jump in Nusselt values for fluid cooling case, resulting from viscous heat dissipation.
- Similarly, Nusselt plots against axial position have a singular point for the fluid heating case which stems from viscous heating.
- This jump and singularity point moves toward downstream with increasing rarefaction, since the effect of viscous dissipation is reduced with increased Knudsen number.
- Increasing positive Brinkman number shifts the jump point position towards upstream while decreasing negative Brinkman number causes a shift in position of singular point towards upstream.
- Constant property solutions converge to the same Nusselt value for fully developed flow regardless of Brinkman number.
- Channel averaged Nusselt values increase with decreasing Knudsen and increasing positive Brinkman numbers. As stated above, total heat transfer will be increased with decreasing rarefaction. Moreover, the channel averaged Nusselt values will be increased with increasing viscous dissipation as a result of early jump in Nusselt values.
- Channel averaged Nusselt values for positive Brinkman numbers, reduce with increasing Péclet number, because of increased entrance length and delayed jump in Nusselt values.
- The difference between constant and variable property solutions decreases with increasing rarefaction for the fluid cooling case.
- The effect of property variation is more emphasized with increasing rarefaction in fluid heating case. Since conductive heat transfer is acting in opposite direction with the convective one in this case, the effect of variable properties become more significant when rarefaction is increased.

- Decreasing negative Brinkman number will reduce the property variation effect, due to increased viscous heating. As stated before, increasing viscous heating increases the conductive heat transfer due to increased thermal conductivity. The effect of increased viscosity will compensate the effect of increased thermal conductivity on heat transfer.
- The difference between constant and variable property solutions are increased with increasing Péclet number except for high Knudsen and low negative Brinkman numbers. On the contrary the difference between constant property and variable property solutions are reduced with increasing Péclet number with for high Knudsen numbers, where Brinkman number is -0.001. This phenomenon is thought to be a result of adverse effect of increased Péclet and Knudsen number on viscous heating.
- The difference between variable and constant property solutions is very little in the fully developed region for both heating and cooling processes. Consequently it is possible to say that, property variation effect is negligible for fully developed flows.
- Effect of property variation is less severe for the flow field than the temperature field.

Air is one of the most common working fluids in single phase heat transfer applications. The temperature differences used in these analyses are higher than the limits of electronics cooling applications, however, these differences can be encountered in different micro applications, such as micro reactors and micro fabrication. It is possible to see from the results that the property variation effect is not substantial for the working fluid and flow conditions that are subjected to investigation, though these results may be used as a guide for validation of the constant property assumptions in slip flow regime.

With the light of the information included in this study it is possible to decide upon the severity of property variation in air flow through microchannels, since it is feasible to make constant property solutions when property variation effect is not significant. This will create an advantage when computation times and complexity of the solution algorithm is considered. It is possible to say that constant property solutions will yield satisfactory results for long channels in which entrance length is small compared to the overall length. Moreover, for shorter channels, which has an overall length comparable with the entrance length for the defined flow conditions, the property variation effect should not be disregarded, especially for low Knudsen numbers. However, constant property assumption may yield satisfactory results for high Knudsen numbered channels. Another important point is the effect of viscous dissipation; the viscous dissipation terms should be included while making variable property solutions, because the effect of viscous heating on property variation is non-negligible and not easily predictable.

Unfortunately variable property effects of air in the slip flow regime are not commonly investigated. For these reasons, comparison of the obtained results with the available literature is limited. However, when obtained results are compared with the variable property solutions of liquid flow in microchannels; it is possible to say that, property variation effect is less significant for the gases. Additionally, the effect of variation in thermal conductivity and viscosity on heat transfer and fluid flow are not contradicting with the available literature in terms of variation of Nusselt values. Furthermore, various studies are available in the literature for the comparison of constant property results. The results are in good agreement with the literature for constant property solutions.

It should be noted that obtaining variable property solutions for different geometry and working fluid combinations for different temperature ranges

would be tedious and time consuming. For this reason, such studies are limited with the flow conditions they are solved for.

One other aspect of investigation of single phase flow in microchannels may be the effect of geometry, which requires three dimensional numerical solutions. Moreover, the variation of density and specific heat with temperature may be taken into account in the numerical solutions. The effect of compressibility should also be discussed in the slip flow regime in combination with the previously discussed issues. Furthermore, the moving boundaries can be imposed to the slip flow analyses and another way of expanding this study may be the inclusion of different type of wall boundaries, such as heat pulse and sinusoidal temperature profile.

REFERENCES

[1] Kandlikar S.G., Grande W.J., "Evolution of microchannel flow passages thermohydraulic performance and fabrication technology", Heat Transfer Engineering, 24, 3-17, (2003)

[2] Gad-el-Hak, M., Flow Physics, in The MEMS Handbook, M. Gad-el-Hak, ed., CRC Press, (2005)

[3] Gad-el-Hak, M., Journal of Fluids Engineering, 121, 5-33, (1999)

[4] Larrode, F. E., Housiadas, C., and Drossinos, Y., Slip-flow heat transfer in circular tubes, Int. J. Heat and Mass Transfer, 43, 2669-2680, (2000)

[5] Maxwell J.C., "On stresses in rarefied gases arising from inequalities of temperature", Philos. Trans. Roy. Soc. Part 1 170, 231–256. (1879)

[6] Yener Y., Kakac S., Avelino M., Okutucu T., "Single phase forced convection in microchannels state-of-the-art-review", Microscale Heat Transfer Fundamentals and Applications in Biological Systems and MEMS, Kluwer Academic Publishers, The Netherlands, (2005)

[7] Smoluchowski M. von, "Über wärmeleitung in verdünnten gasen", Ann. Phys. Chem. 64,101–130 (1898)

[8] Beskok, A., Karniadakis, G. E., Simulation of heat and momentum transfer in complex micro geometries, AIAA J. Thermophysics and Heat Transfer, 8(1994),647-655.

[9] Hadjiconstantinou, N.G., Simek, O., Constant-wall-temperature Nusselt number in micro and nano-channels, Transactions of the ASME, vol. 124, April, 2002.

[10] R.K. Shah, A.L. London, "Laminar Flow Forced Convection in Ducts, Academic Press", New York, (1978)

[11] Tso C.P., Mahulikar S.P., " The use of the Brinkman number for single phase forced convective heat transfer in microchannels", International Journal of Heat and Mass Transfer ,41, 1759-1769, (1998)

[12] Liu J.T., Peng X.F., Wang B.X., " Variable-property effect on liquid flow and heat transfer in microchannels", Chemical Engineering Journal ,141, 346-353, (2008)

[13] Tuckerman, D. B. and Pease, R. F., "Optimized convective cooling using micromachined structure" Journal of Electrochemical Soc.,129, (1982)

[14] Peng, X.F., and Peterson, G.P., "The effect of thermofluid and geometrical parameters on convection of liquids through rectangular microchannels", Int. Journal of Heat and Mass Transfer, 38 (4), 755-758, (1995)

[15] Deisler R.G., "Analytical Investigation of Turbulent Flow in Smooth Pipes with Heat Transfer, with Variable Fluid Properties for Prandtl Number of 1", NACA TN 2242,(1950)

[16] Oskay R., Kakaç S., "Effect of Viscosity Variations on Forced Convection Heat Transfer in Pipe Flow", METU Journal of Pure and Applied Sciences, 6, 211-230,(1973)

[17] Li J., Peterson G.P., Cheng P., "Three-dimensional analysis of heat transfer in a micro-heat sink with single phase flow", International Journal of Heat and Mass Transfer ,47, 4215-4231, (2004)

[18] Gulhane N.P., Mahulikar S.P., " Variations in gas properties in laminar micro-convection with entrance effect", International Journal of Heat and Mass Transfer ,52, 1980-1990, (2009)

[19] Guidice S.P., Nonino C., Savino S., " Efects of viscous dissipation and temperature dependent viscosity in thermally and simultaneously developing laminar flows in microchannels ", International Journal of Heat and Fluid Flow ,28, 15-27, (2007)

[20] Koo J., Kleinstreuer C.," Viscous dissipation effects in microtubes and microchannels", International Journal of Heat and Mass Transfer ,47, 3159-3169, (2004)

[21] Mahulikar S.P., Herwig H., Hausner O., Kock F., "Heat Numerical simulation of 1-D incompressible laminar microflow convection behavior with temperature dependent fluid properties ", PAMM. Proc. Appl. Math. Mech., 4, 488–489 (2004)

[22] Herwig H., Mahulikar S.P., "Variable property effects in single-phase incompressible flows through microchannels ", International Journal of Thermal Sciences ,45, 977-981, (2006)

[23] El-Genk M.S., Yang I.," Numerical analysis of laminar flow in micro-tubes with a slip boundary ", Energy Conversion and Management ,50, 1481-1490, (2009)

[24] Li Z., Huai X., Tao Y., Chen H., " Effects of thermal property variations on the liquid flow and heat transfer in microchannel heat sinks", Applied Thermal Engineering ,27, 2803-2814, (2007)

[25] Incropera F.P., DeWitt D.P., Fundamentals of Heat and Mass Transfer, John Wiley & Sons, New York, (1990)

[26] Wang C.W., Yang R., " A numerical study for slip flow heat transfer", Applied Mathematics and Computation, 173, 1246-1264, (2006)

[27] Barron R.F., Wang X., Ameel T.A., Warrington R.O., "The Graetz problem extended to slip-flow", International Journal Heat Mass Transfer, 40, 1817-1823, (1997)

[28] Jeong H.E. Jeong J.T., " Extended Graetz problem including streamwise conduction and viscous dissipation in microchannel ", International Journal of Heat and Mass Transfer ,49, 2151-2157, (2006)

[29] Çetin B., Yazıcıoğlu A.G., Kakaç S., " Slip-flow heat transfer in microtubes with axial conduction and viscous dissipation – An extended Graetz problem", International Journal of Thermal Sciences,48, 1673-1678, (2009)

[30] Çetin B., Yazıcıoğlu A.G., Kakaç S., " Fluid flow in microtubes with axial conduction including rarefaction and viscous dissipation ", International Communications in Heat and Mass Transfer,35, 335-341, (2008)

[31] Morini G.L., Spiga M., Tartarini P., "The rarefaction effect on the friction factor of gas flow in microchannels", Superlattice and Microstructures, 35,587–599,(2004)

[32] Zhang T.,T., Jia L., Wang Z.C., Li C.,W., " Slip flow characteristics of compressible gaseous in microchannels", Energy Conversion and Management, 50,1676-1681,(2009)

[33] Hong C., Asako P., Lee J.H., " Heat transfer characteristics of gaseous flows in micro-channel with constant heat flux ", International Journal of Thermal Sciences,46, 1153-1162, (2007)

[34] Yu S., Ameel T.A., "Slip-flow heat transfer in rectangular microchannels", International Journal of Heat and Mass Transfer ,44, 4225-4234, (2001)

[35] Tunç G., Bayazıtoğlu Y., "Heat Transfer in rectangular microchannels", International Journal of Heat and Mass Transfer ,45, 765-773, (2002)

[36] Rij v J., Ameel T., Harman T., " The effect of viscous dissipation and rarefaction on rectangular microchannel convective heat transfer", International Journal of Thermal Sciences ,48, 471-481, (2009)

[37] Nizamand H., Renksizbulut M., Saeedi E., " Developing slip-flow and heat transfer in trapezoidal microchannels ", International Journal of Heat and Mass Transfer ,51, 6126-6135, (2008)

[38] Renksizbulut M., Nizamand H., Tercan G., " Slip-flow and heat transfer in rectangular microchannels with constant wall temperature", International Journal of Heat and Mass Transfer ,45, 870-881, (2006)

[39] Worek W.M., Hettiarachchi H.D.M., Golubovic M., Minkowycz, W.J., "Three-dimensional Laminar Slip Flow and Heat Transfer in a Rectengular Microchannel with Constant Wall Temperature", International Journal of Heat and Mass Transfer,51, 5088-5096,(2008)

[40] Patankar, S.V., Numerical Heat Transfer and Fluid Flow. Mc-Graw-Hill, 1980.

[41] Sun W., Kakaç S., Yazıcıoğlu A.G., " A numerical study of single-phase convective heat transfer in microtubes for slip flow ", International Journal of Thermal Sciences,41, 1759-1769, (1998)

[42] Morini G.L., "Viscous heating in liquid flows in micro-channels", International Journal of Heat and Mass Transfer ,48, 3637-3647,(2005)

[43] Kroeker C.J., Soliman H.M., Ormiston S.J., "Three-dimensional thermal analysis of heat sinks with circular cooling micro-channels" International Journal of Heat and Mass Transfer,47, 4733-4744, (2004)

[44] Mishan Y.,Mosyak A., Pogrebnyak E., Hetsroni G., "Effect of developing flow and thermal regime on momentum and heat transfer in micro-scale Heat Sink" International Journal of Heat and Mass Transfer, 50, 3100-3114, (2007)

[45] Lee P.S., Garimella V.S., Liu D., "Investigation of heat transfer in rectangular microchannels", International Journal of Heat and Mass Transfer ,48,1688-1704 ,(2005)

[46] Wang M., Zhixin L., "Simulation of gas flows in microgeometries using the direct simulation monte carlo method", International Journal of Heat and Fluid Flow,25, 975-985,(2004)

[47] Toh, K.C., Chen, X.Y. and Chai, J.C., "Numerical computation of fluid flow and heat transfer in microchannels", International Journal of Heat and Mass Transfer, 45, 5133-5141, (2002)

[48] Morini G.L., "Single-phase convective heat transfer in microchannels: A review of experimental results", International Journal Thermal Science, 43,631–651,(2004)

[49] Hetsroni G., Mosyak A., Pogrebnyak E., Yarin L.P., "Heat transfer in micro-channels: Comparison of experiments with theory and numerical results ", International Journal of Heat and Mass Transfer, 45, 5133-5141, (2002)

[50] Gamrat G., Fevre-Marinet M., Asendrych D., "Conduction and entrance effects on laminar liquid flow and heat transfer in rectangular microchannels", International Journal Heat Mass Transfer, 48, 2943–2954, (2005)

[51] Mokrani O., Bourouga B., Castelain C., Peerhossaini H., "Fluid flow and convective heat transfer in flat microchannels", International Journal Heat and Mass Transfer, 52, 1337-1352, (2009)

[52] Celata G.P., Morini G.L., Marconi V., McPhail S.C., Zummo G., "Using viscous heating to determine the friction factor in microchannels – An experimental validation ", Experimental Thermal and Fluid Science, 40, 1817-1823, (2006)

[53] Mala M.G., Li D., "Flow characteristics of water in microtubes ", International Journal Heat and Fluid Flow, 20, 142-148, (1999)

[54] Lemmon E. W., Jacobsen, R. T., "Viscosity and thermal conductivity equations for nitrogen, oxygen, argon, and air," International Journal of Thermophysics, 25, 21-69, (2004)

[55] Jiji L.M., Heat Convection, Springer-Verlag, Berlin, Heidelberg, NewYork, (2006)

[56] White, F. M., Viscous Fluid Flow, 2nd ed., McGraw-Hill, 1991.

[57] Hernandez, J., Zamora, B., Effects of variable properties and non-uniform heating on natural convection flows in vertical channels, International Journal of Heat and Mass Transfer, 48, 793-807, (2005)

[58] Wang, Q., Yoo, H, Jaluria, Y., Convection in a horizontal rectangular duct under constant and variable property formulations, International Journal of Heat and Mass Transfer, 46, 297-310, (2003)

[59] Anderson Jr., J. D., Computational Fluid Dynamics the Basics with Applications., McGraw-Hill, 1995

[60] Griebel M., Dornseifer T., Neunhoeffer T., Numarical Simulation in Fluid Dynamics, SIAM, 1997

[61] Hirt C., Nichols B., Romero N., SOLA a numerical solution algorithm for transient fluid flows, Technical Report LA-5852, Los Alamos National Laboratory.

[62] Cetin, B., Analysis of single phase convective heat transfer in microtubes and microchannels, Master Thesis in Mechanical Engineering. 2005, Middle East Technical University: Ankara.

[63] Turgay,M.,B., Effect of surface roughness in microchannels on heat transfer, Master Thesis in Mechanical Engineering. 2005, Middle East Technical University: Ankara

APPENDIX A

GRAPHS

The figures which are not presented in Chapter 4 is given here.

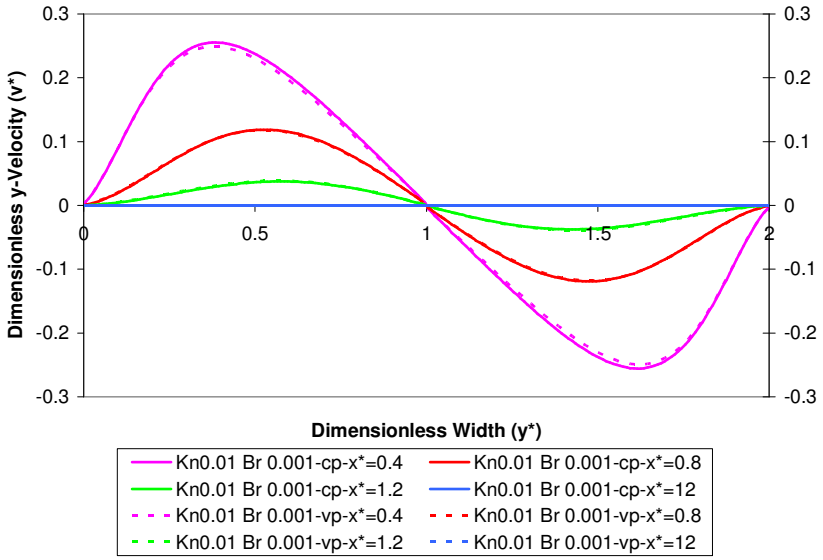

Figure A.1 Variation of dimensionless y-velocity with dimensionless width of the channel (Kn=0.01, Br = 0.001, Pe=1)

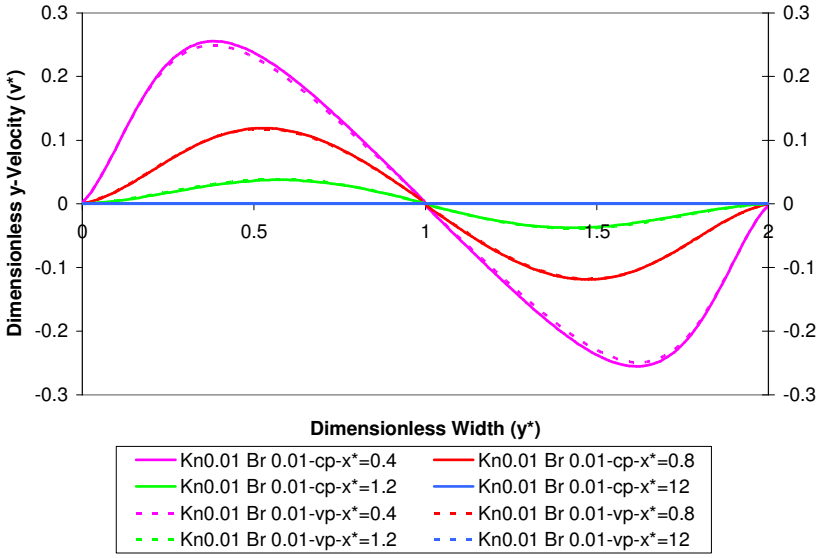

Figure A.2 Variation of dimensionless y-velocity with dimensionless width of the channel (Kn=0.01, Br = 0.01, Pe=1)

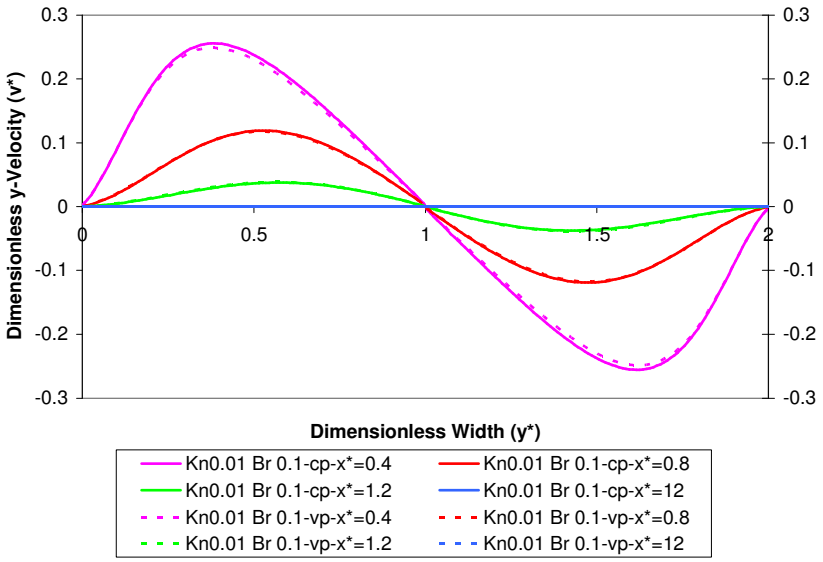

Figure A.3 Variation of dimensionless y-velocity with dimensionless width of the channel (Kn=0.01, Br = 0.1, Pe=1)

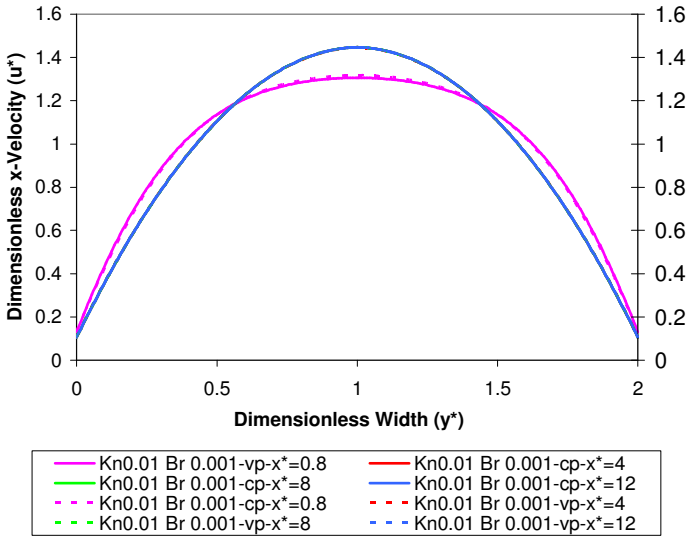

Figure A.4 Variation of dimensionless x-velocity with dimensionless width of the channel (Kn=0.01, Br = 0.001, Pe=1)

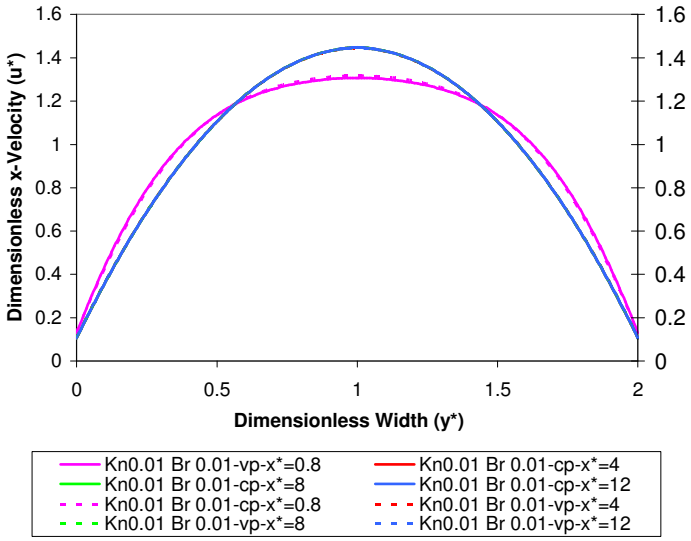

Figure A.5 Variation of dimensionless x-velocity with dimensionless width of the channel (Kn=0.01, Br = 0.01, Pe=1)

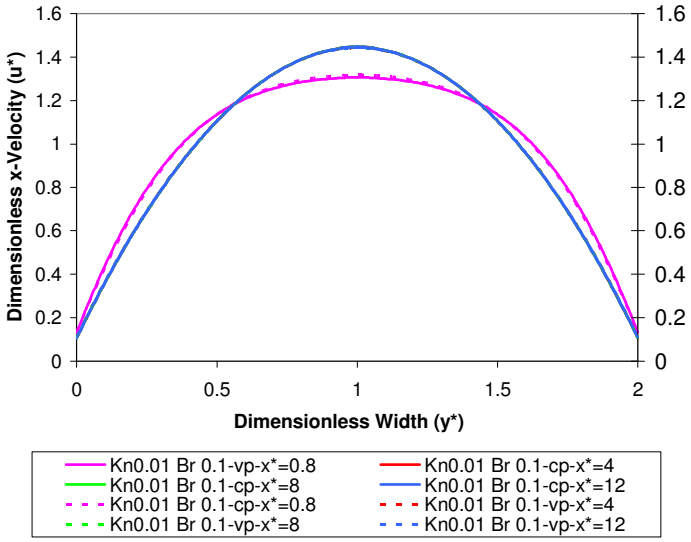

Figure A.6 Variation of dimensionless x-velocity with dimensionless width of the channel (Kn=0.01, Br = 0.1, Pe=1)

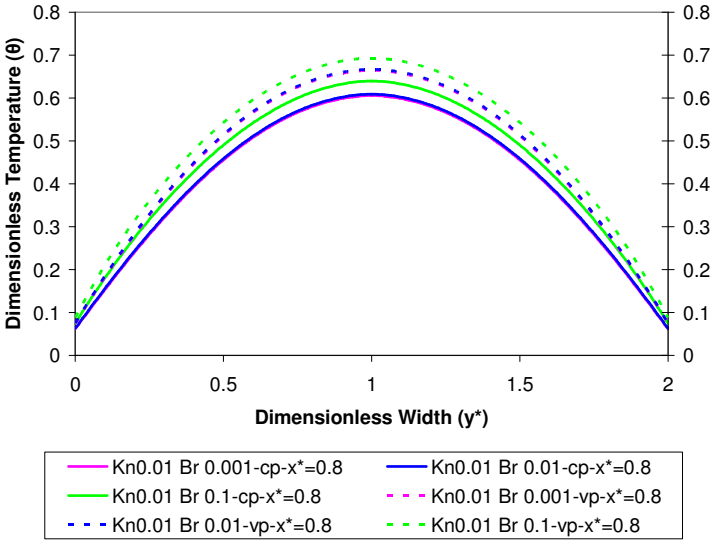

Figure A.7 Variation of dimensionless temperature with dimensionless width of the channel at crossection x*=0.8 for various positive Brinkman numbers (Kn=0.001, Pe=1)

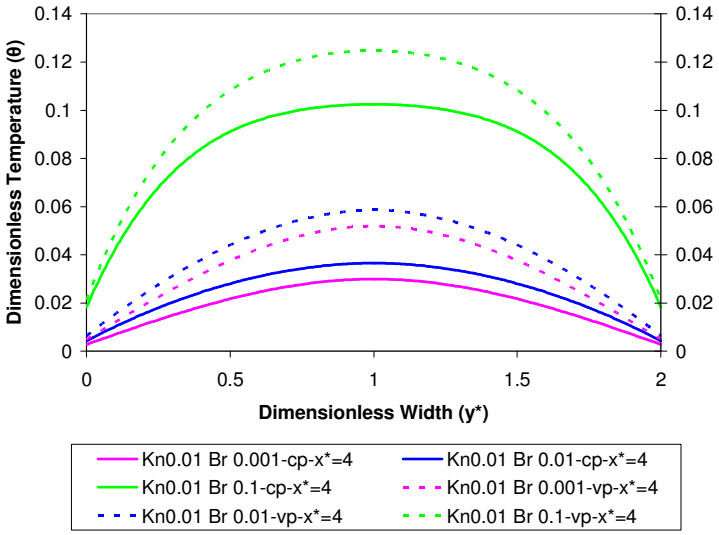

Figure A.8 Variation of dimensionless temperature with dimensionless width of the channel at crossection x*=4 for various positive Brinkman numbers (Kn=0.01, Pe=1)

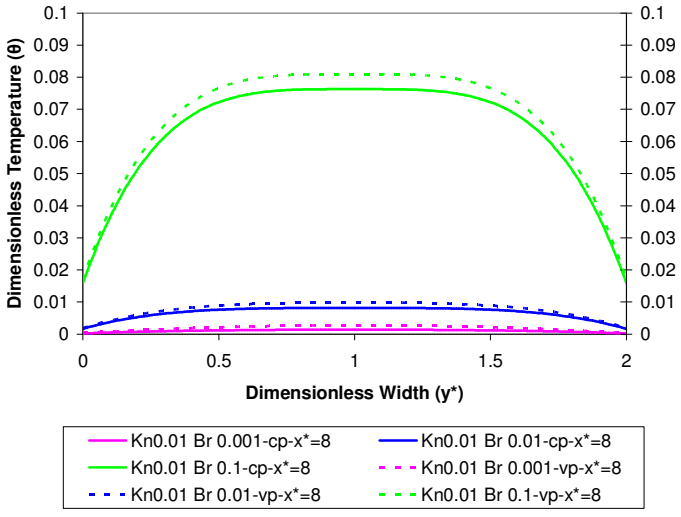

Figure A.9 Variation of dimensionless temperature with dimensionless width of the channel at crossection x*=8 for various positive Brinkman numbers (Kn=0.01, Pe=1)

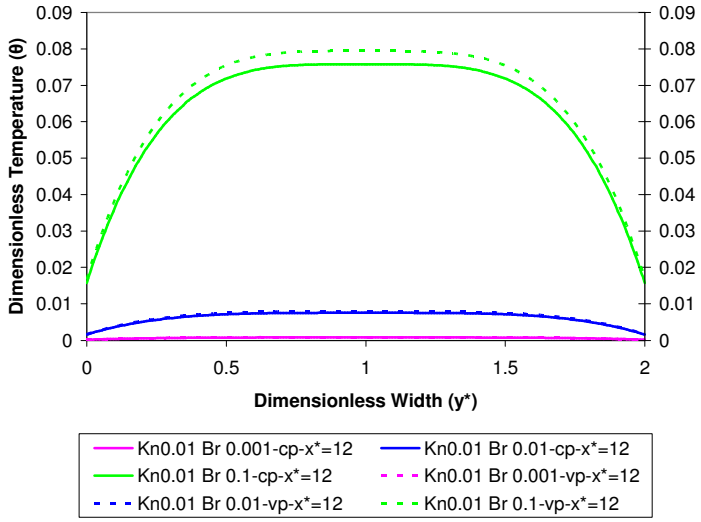

Figure A.10 Variation of dimensionless temperature with dimensionless width of the channel at crossection x*=12 for various positive Brinkman numbers (Kn=0.01, Pe=1)

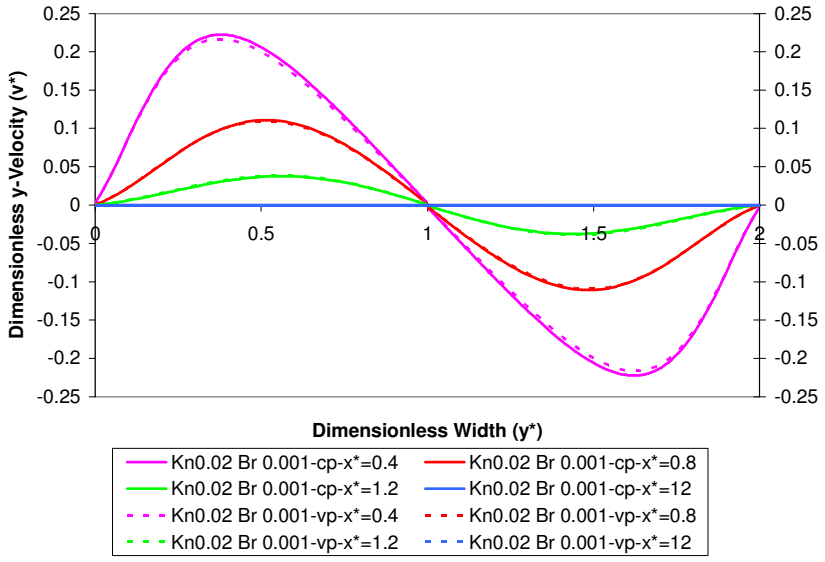

Figure A.11 Variation of dimensionless y-velocity with dimensionless width of the channel (Kn=0.02, Br = 0.001, Pe=1)

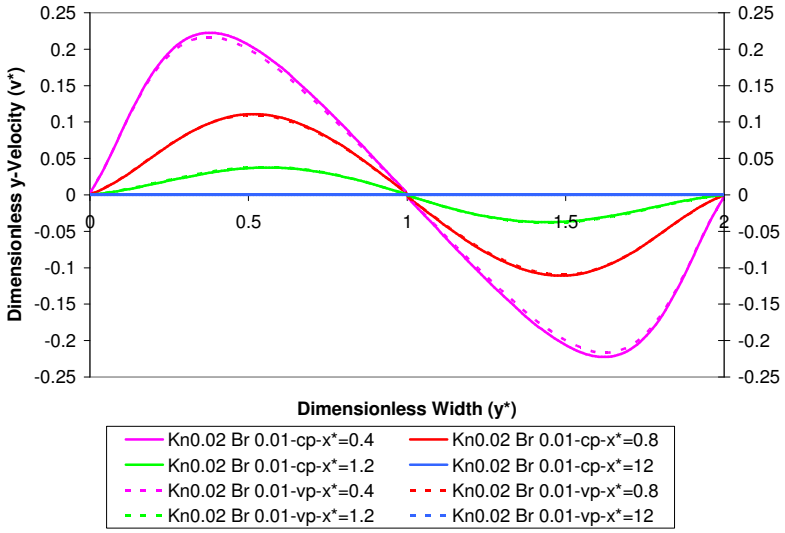

Figure A.12 Variation of dimensionless y-velocity with dimensionless width of the channel (Kn=0.02, Br = 0.01, Pe=1)

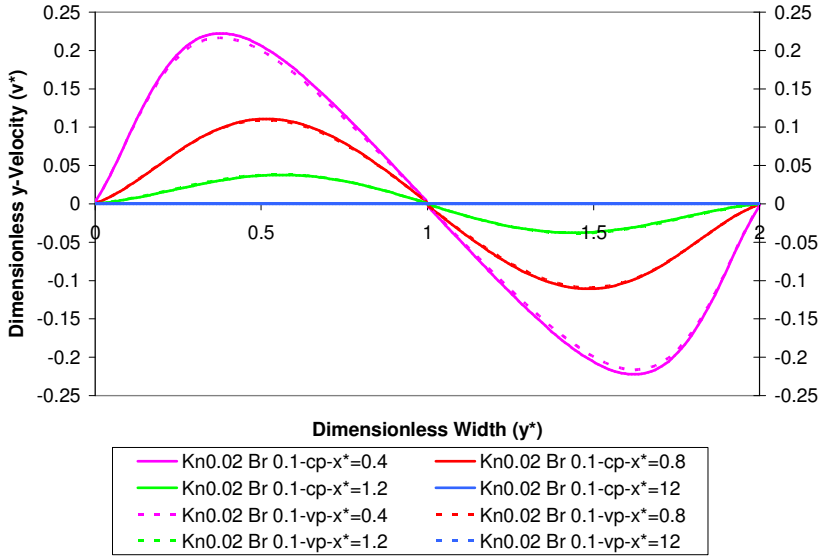

Figure A.13 Variation of dimensionless y-velocity with dimensionless width of the channel (Kn=0.02, Br = 0.1, Pe=1)

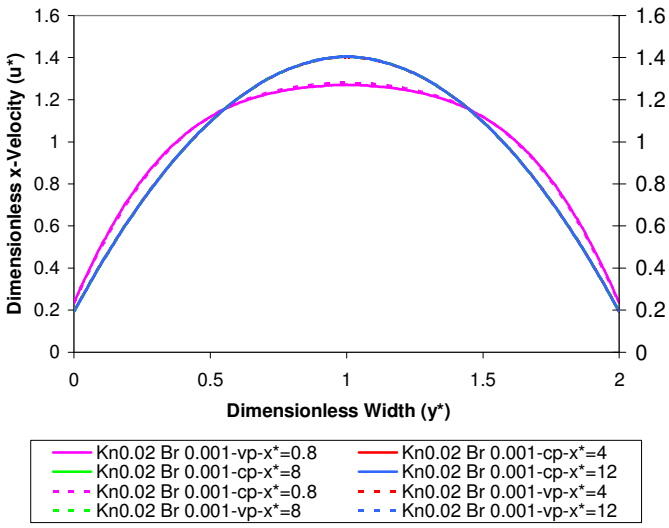

Figure A.14 Variation of dimensionless x-velocity with dimensionless width of the channel (Kn=0.02, Br = 0.001, Pe=1)

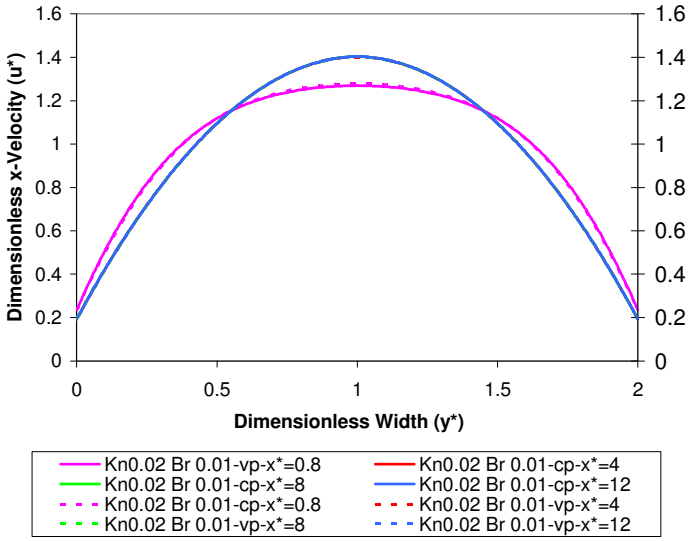

Figure A.15 Variation of dimensionless x-velocity with dimensionless width of the channel (Kn=0.02, Br = 0.01, Pe=1)

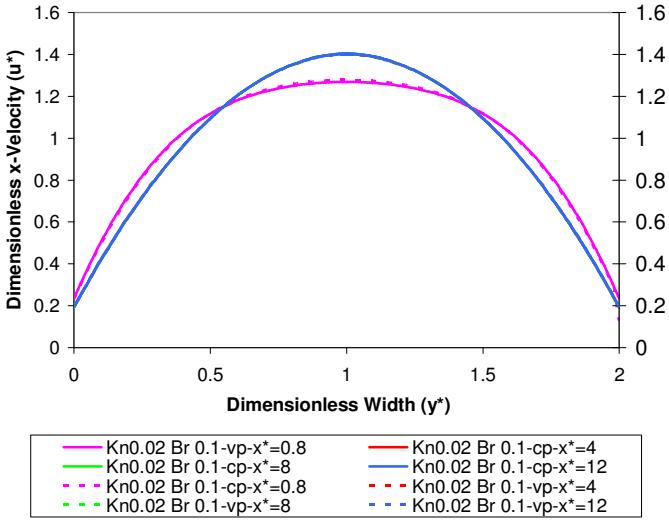

Figure A.16 Variation of dimensionless x-velocity with dimensionless width of the channel (Kn=0.02, Br = 0.1, Pe=1)

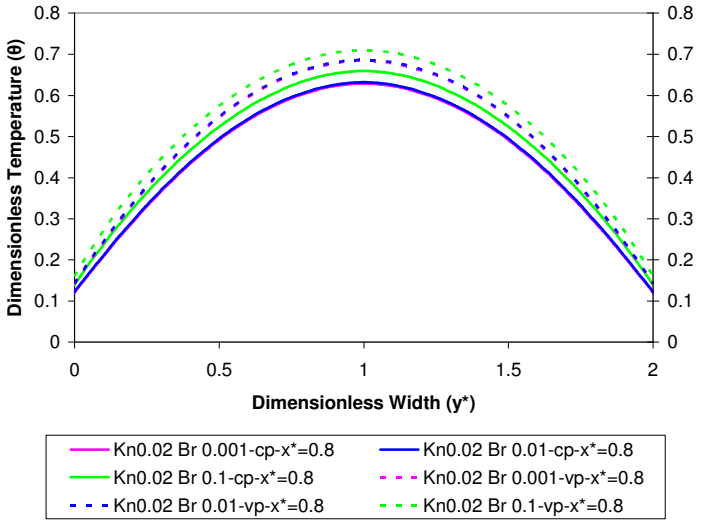

Figure A.17 Variation of dimensionless temperature with dimensionless width of the channel at crossection x*=0.8 for various positive Brinkman numbers (Kn=0.02, Pe=1)

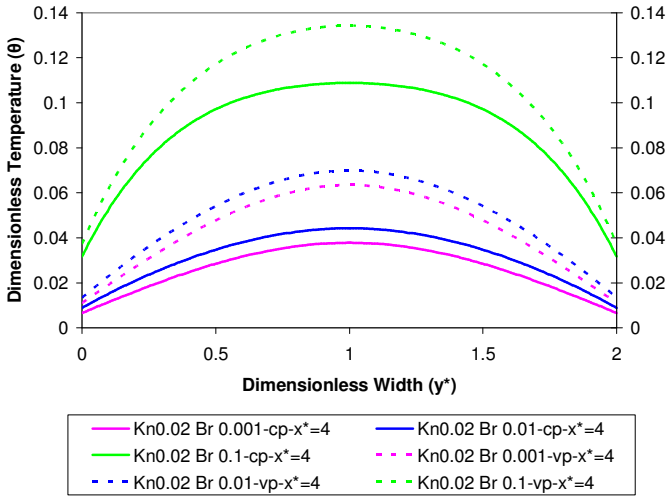

Figure A.18 Variation of dimensionless temperature with dimensionless width of the channel at crossection x*=4 for various positive Brinkman numbers (Kn=0.02, Pe=1)

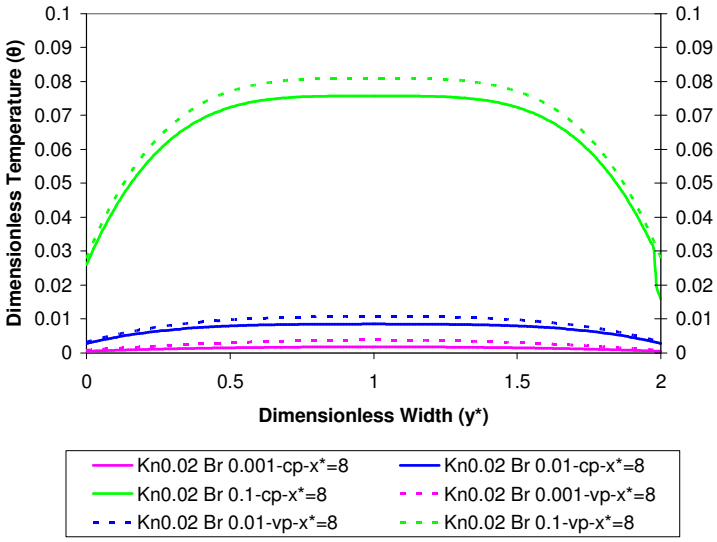

Figure A.19 Variation of dimensionless temperature with dimensionless width of the channel at crossection x*=8 for various positive Brinkman numbers (Kn=0.02, Pe=1)

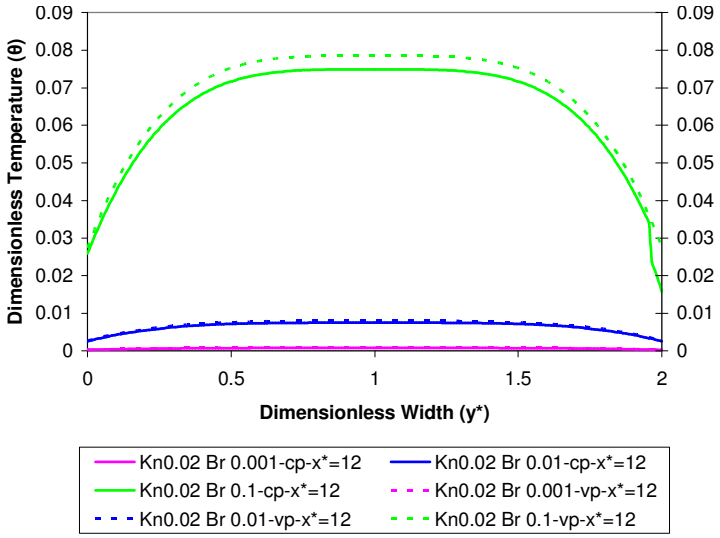

Figure A.20 Variation of dimensionless temperature with dimensionless width of the channel at crossection x*=12 for various positive Brinkman numbers (Kn=0.02, Pe=1)

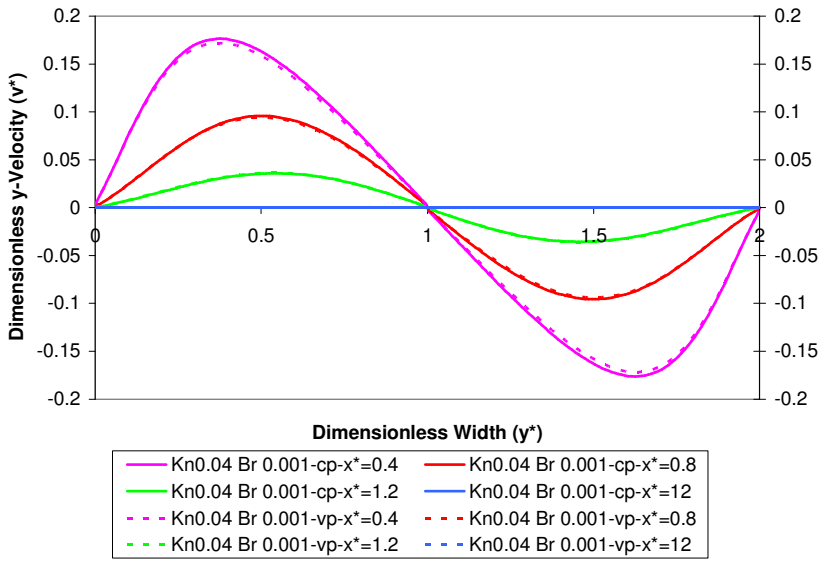

Figure A.21 Variation of dimensionless y-velocity with dimensionless width of the channel (Kn=0.04, Br = 0.001, Pe=1)

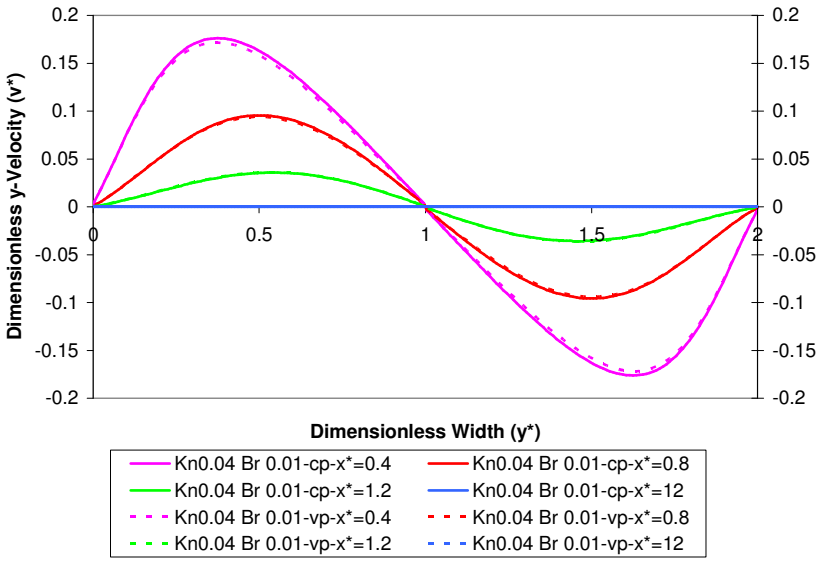

Figure A.22 Variation of dimensionless y-velocity with dimensionless width of the channel (Kn=0.04, Br = 0.01, Pe=1)

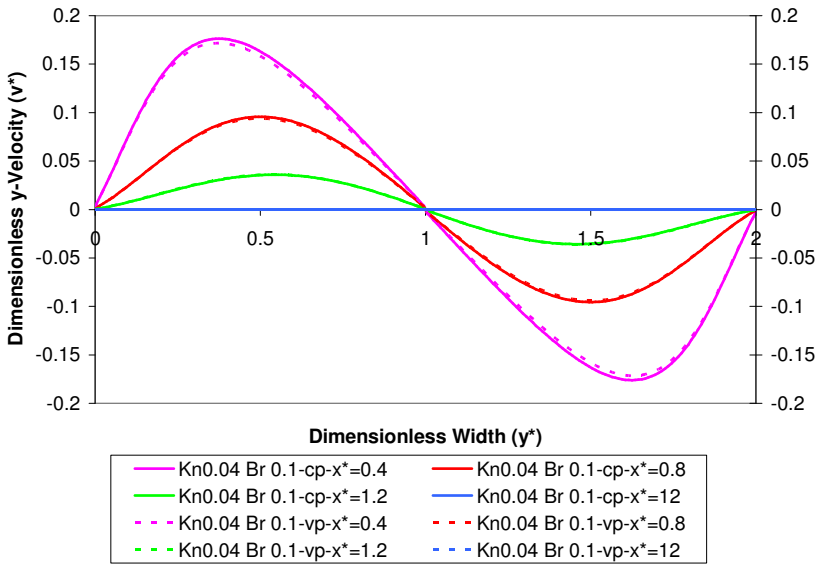

Figure A.23 Variation of dimensionless y-velocity with dimensionless width of the channel (Kn=0.04, Br = 0.1, Pe=1)

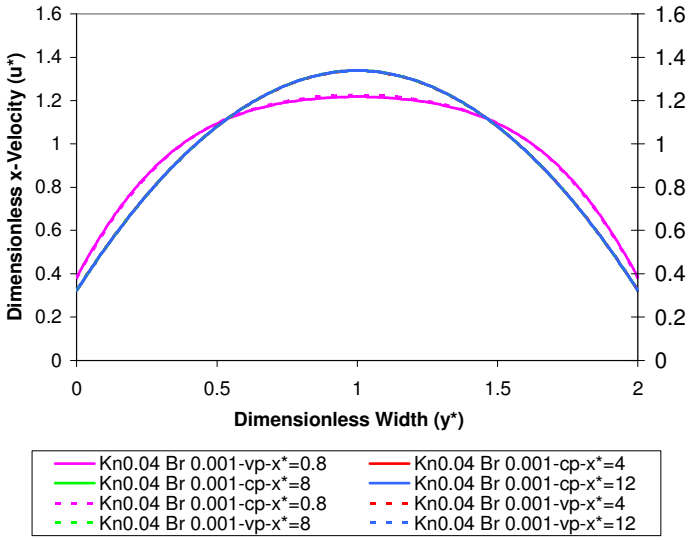

Figure A.24 Variation of dimensionless x-velocity with dimensionless width of the channel (Kn=0.04, Br = 0.001, Pe=1)

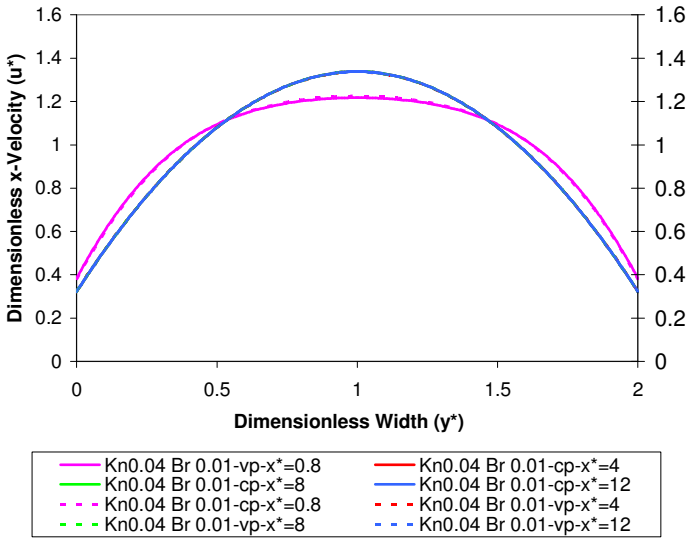

Figure A.25 Variation of dimensionless x-velocity with dimensionless width of the channel (Kn=0.04, Br = 0.01, Pe=1)

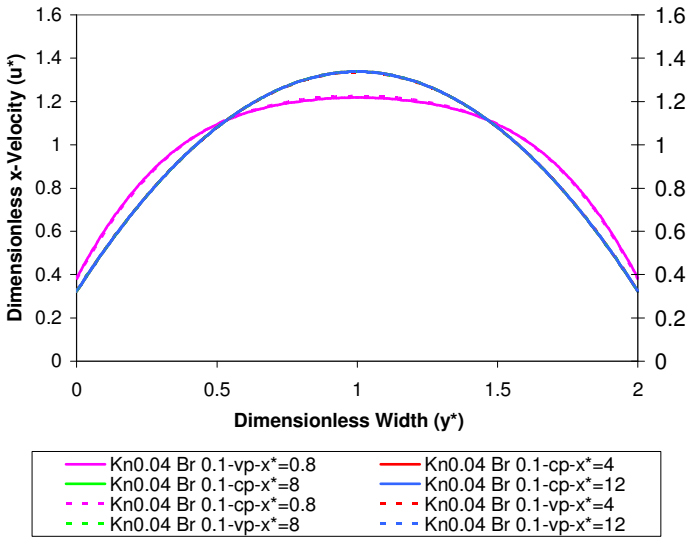

Figure A.26 Variation of dimensionless x-velocity with dimensionless width of the channel (Kn=0.04, Br = 0.1, Pe=1)

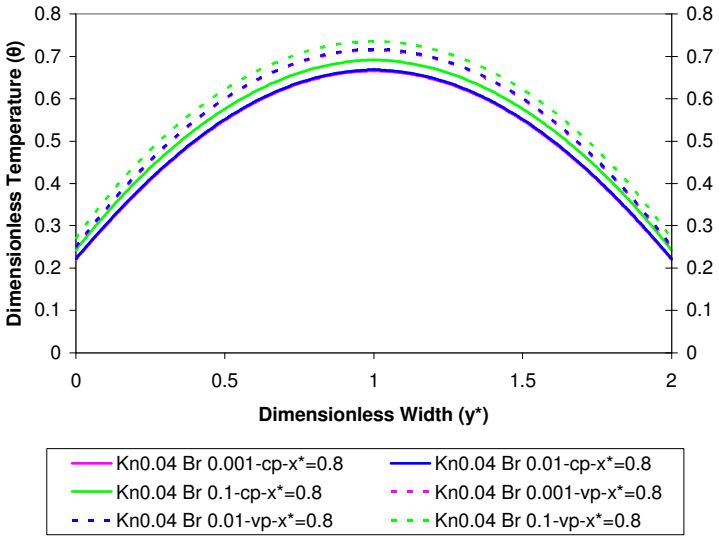

Figure A.27 Variation of dimensionless temperature with dimensionless width of the channel at crossection x*=0.8 for various positive Brinkman numbers (Kn=0.04, Pe=1)

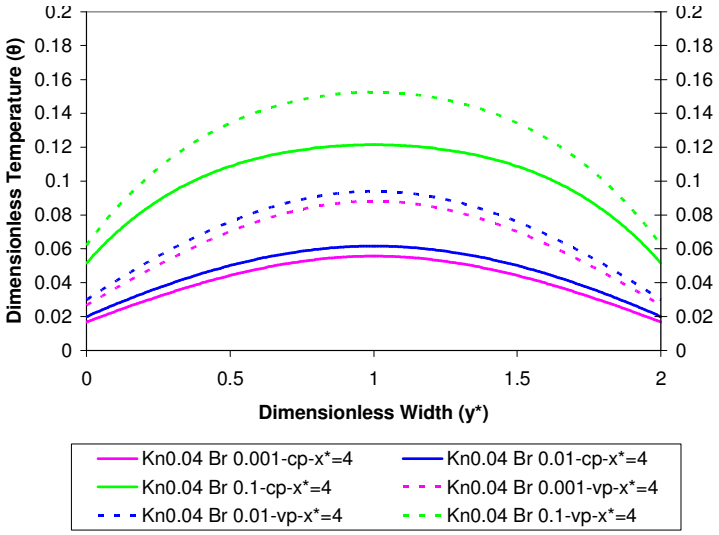

Figure A.28 Variation of dimensionless temperature with dimensionless width of the channel at crossection x*=4 for various positive Brinkman numbers (Kn=0.04, Pe=1)

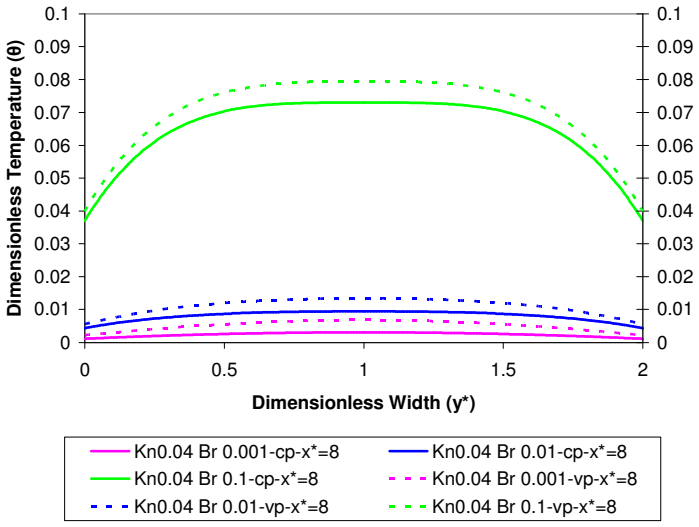

Figure A.29 Variation of dimensionless temperature with dimensionless width of the channel at crossection x*=8 for various positive Brinkman numbers (Kn=0.04, Pe=1)

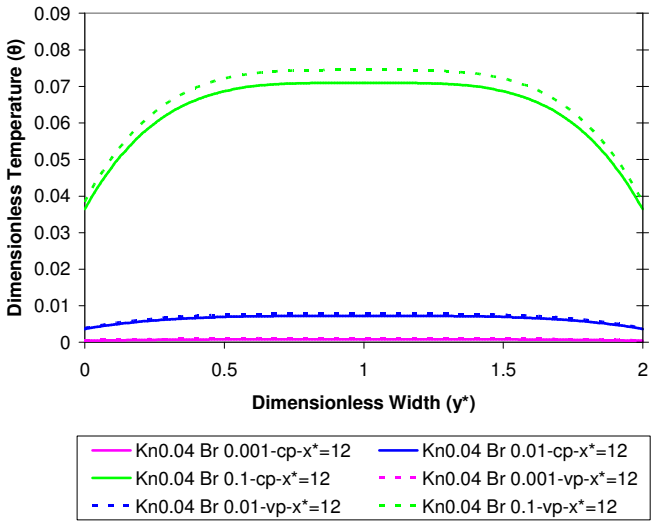

Figure A.30 Variation of dimensionless temperature with dimensionless width of the channel at crossection x*=12 for various positive Brinkman numbers (Kn=0.04, Pe=1)

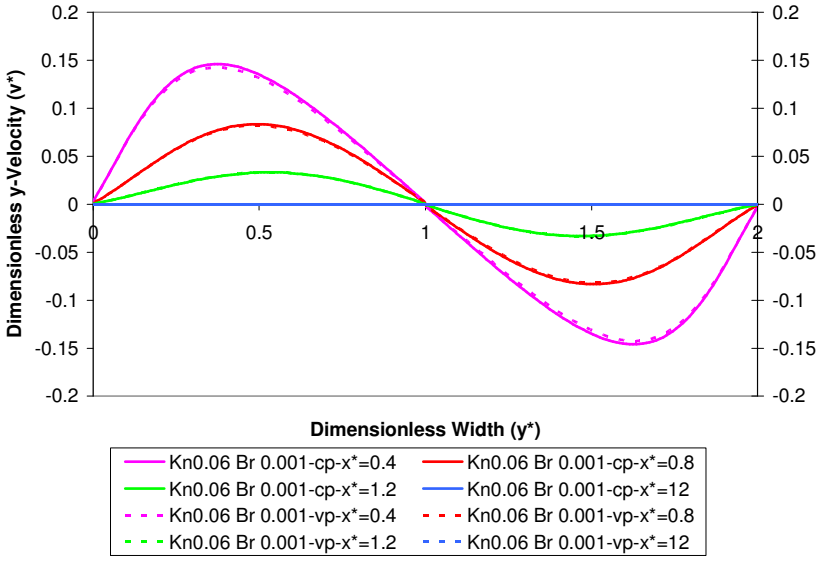

Figure A.31 Variation of dimensionless y-velocity with dimensionless width of the channel (Kn=0.04, Br = 0.001, Pe=1)

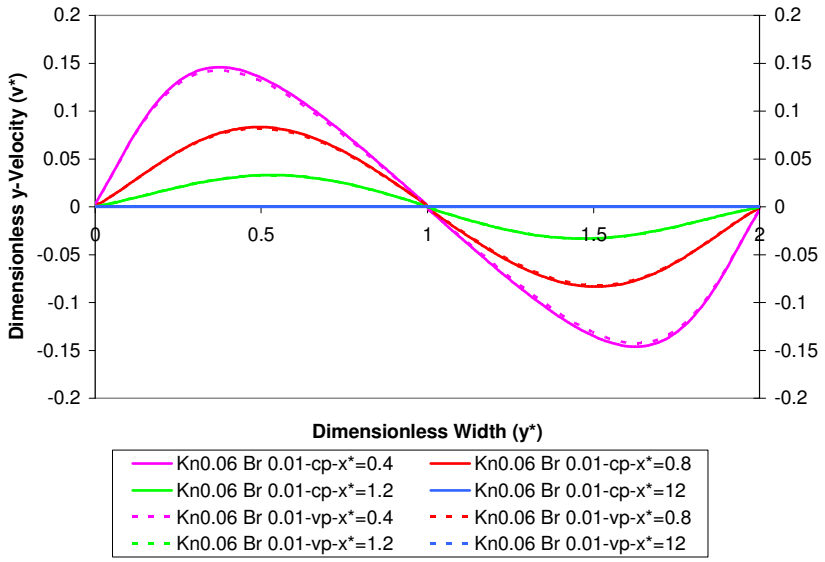

Figure A.32 Variation of dimensionless y-velocity with dimensionless width of the channel (Kn=0.06, Br = 0.01, Pe=1)

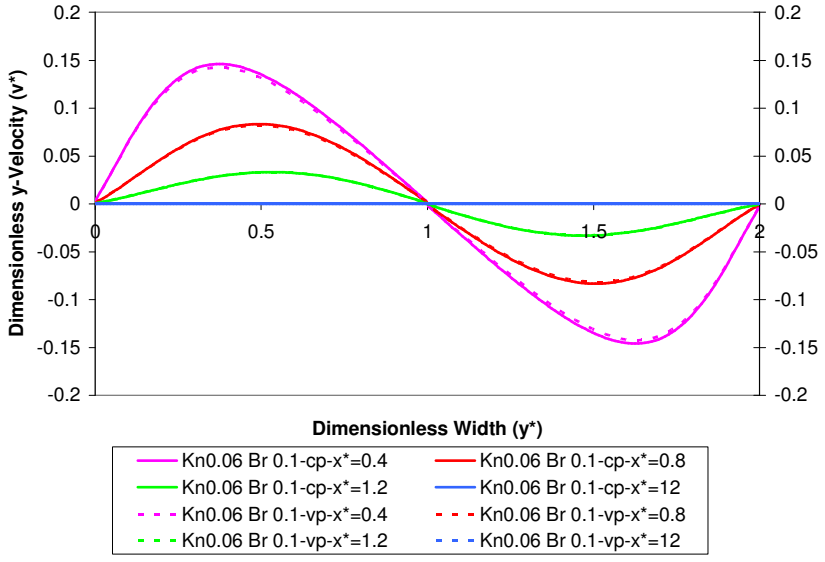

Figure A.33 Variation of dimensionless y-velocity with dimensionless width of the channel (Kn=0.06, Br = 0.1, Pe=1)

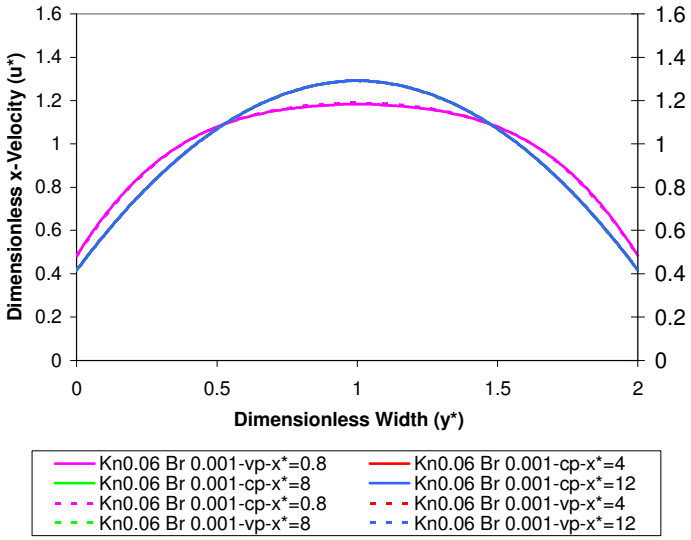

Figure A.34 Variation of dimensionless x-velocity with dimensionless width of the channel (Kn=0.06, Br = 0.001, Pe=1)

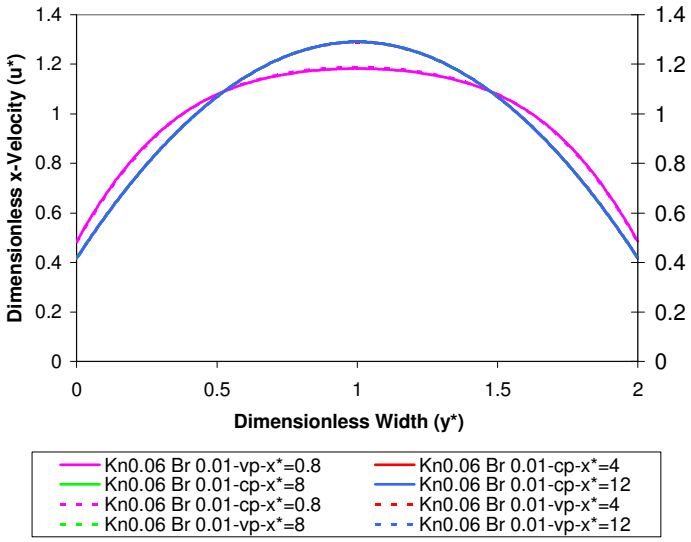

Figure A.35 Variation of dimensionless x-velocity with dimensionless width of the channel (Kn=0.06, Br = 0.01, Pe=1)

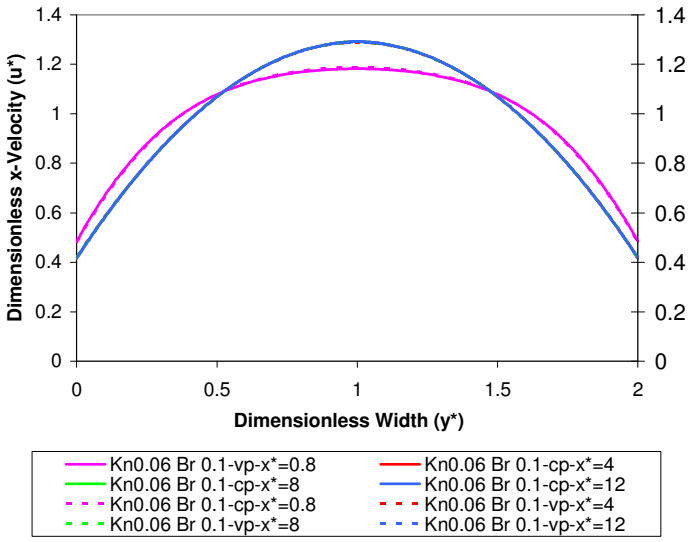

Figure A.36 Variation of dimensionless x-velocity with dimensionless width of the channel (Kn=0.06, Br = 0.1, Pe=1)

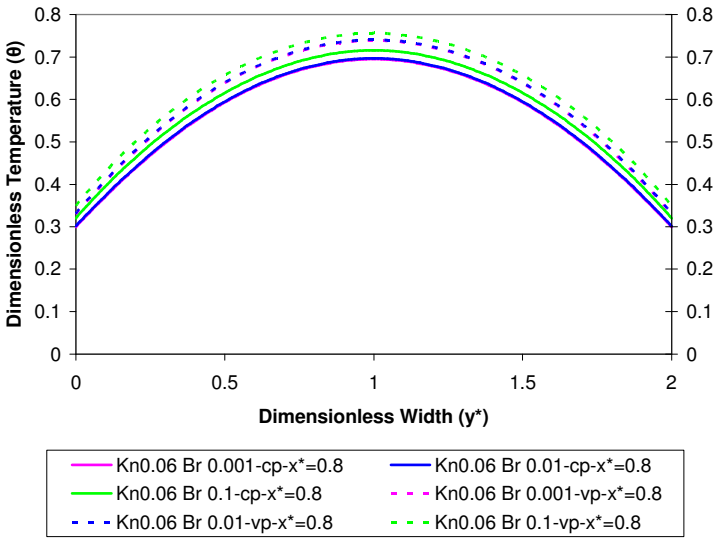

Figure A.37 Variation of dimensionless temperature with dimensionless width of the channel at crossection x*=0.8 for various positive Brinkman numbers (Kn=0.06, Pe=1)

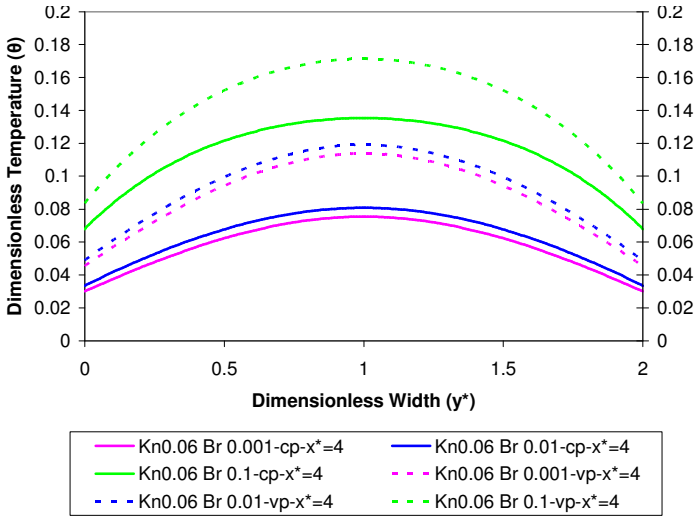

Figure A.38 Variation of dimensionless temperature with dimensionless width of the channel at crossection x*=4 for various positive Brinkman numbers (Kn=0.06, Pe=1)

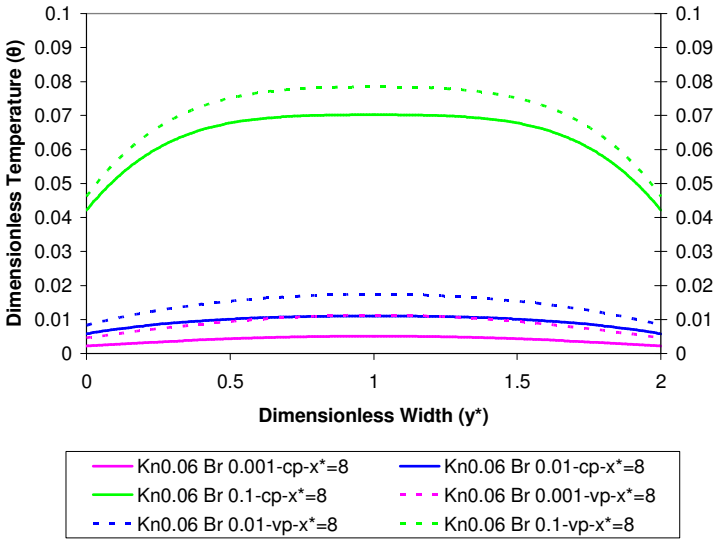

Figure A.39 Variation of dimensionless temperature with dimensionless width of the channel at crossection x*=8 for various positive Brinkman numbers (Kn=0.06, Pe=1)

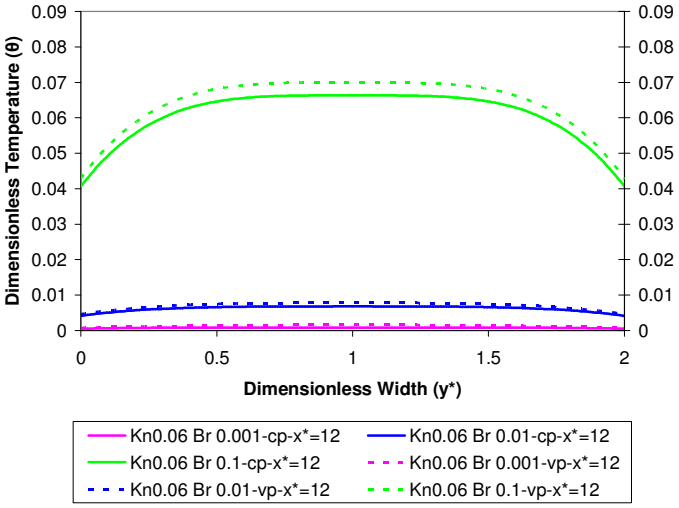

Figure A.40 Variation of dimensionless temperature with dimensionless width of the channel at crossection x*=12 for various positive Brinkman numbers (Kn=0.06, Pe=1)

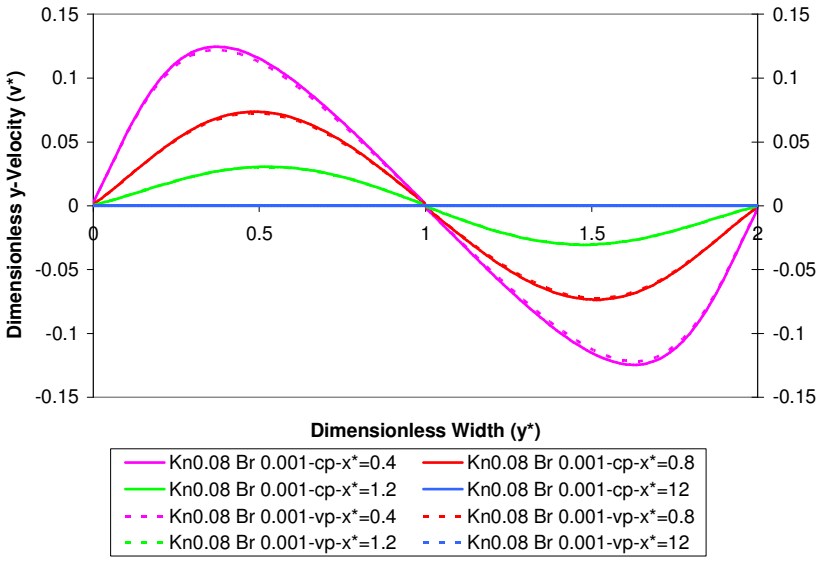

Figure A.41 Variation of dimensionless y-velocity with dimensionless width of the channel (Kn=0.08, Br = 0.001, Pe=1)

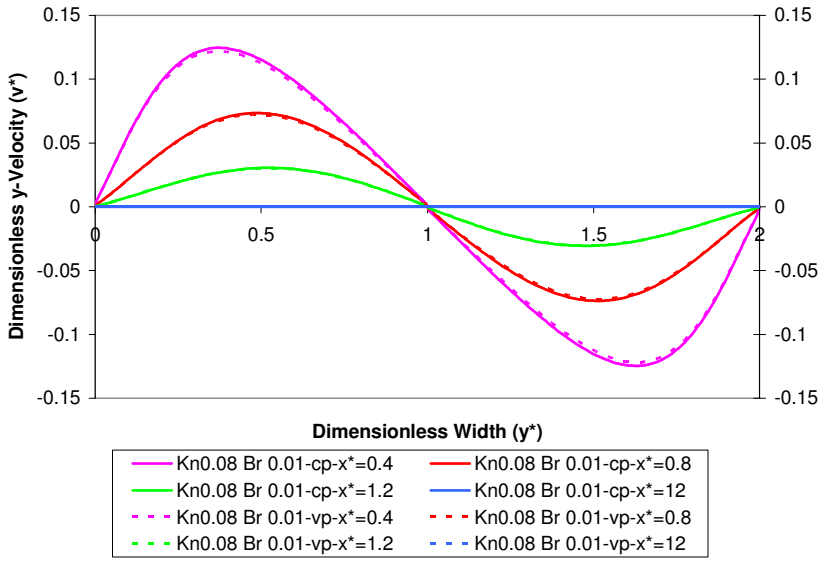

Figure A.42 Variation of dimensionless y-velocity with dimensionless width of the channel (Kn=0.08, Br = 0.01, Pe=1)

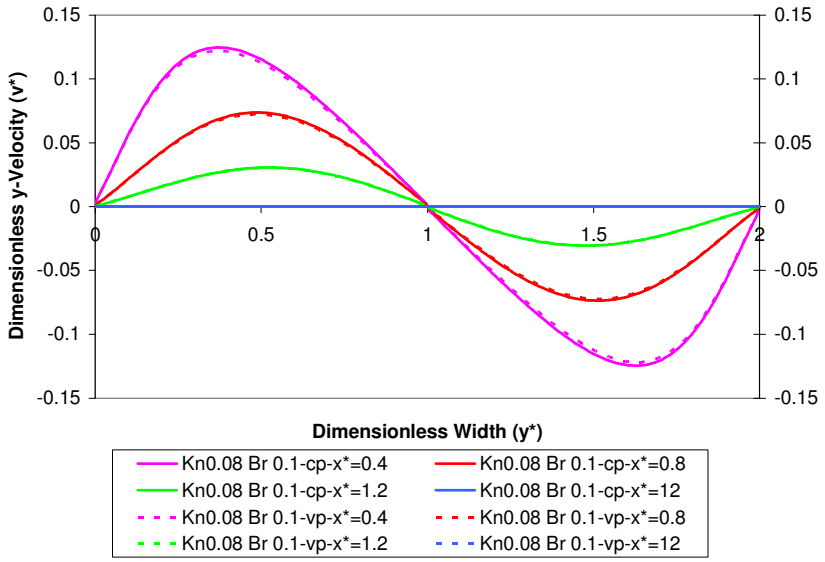

Figure A.43 Variation of dimensionless y-velocity with dimensionless width of the channel (Kn=0.08, Br = 0.1, Pe=1)

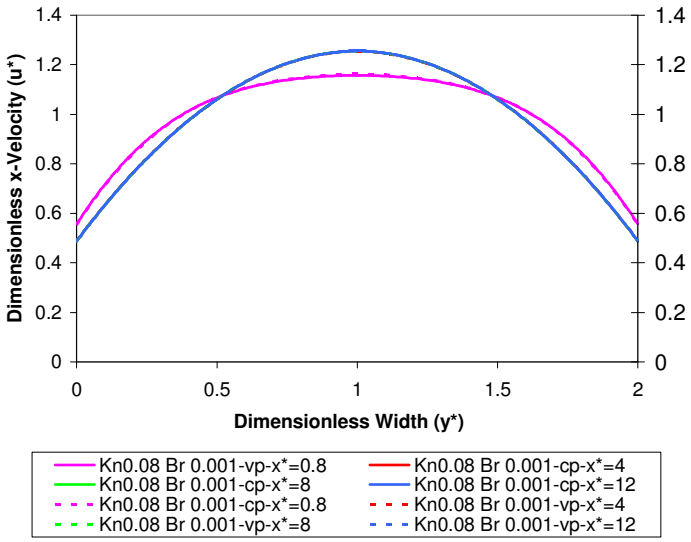

Figure A.44 Variation of dimensionless x-velocity with dimensionless width of the channel (Kn=0.08, Br = 0.001, Pe=1)

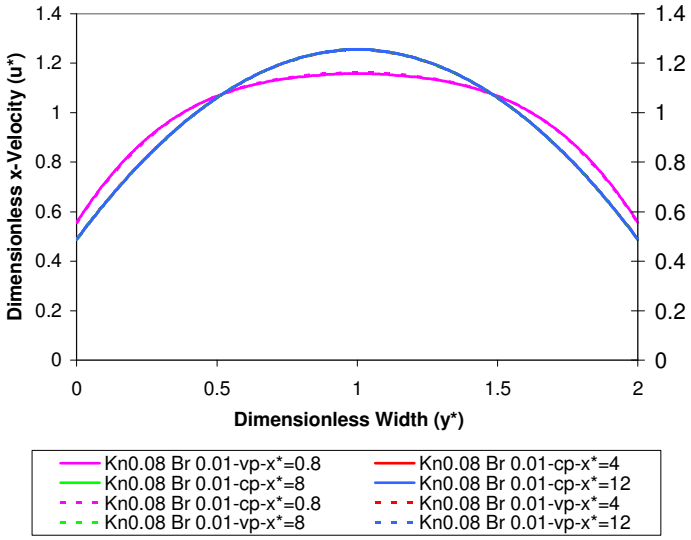

Figure A.45 Variation of dimensionless x-velocity with dimensionless width of the channel (Kn=0.08, Br = 0.01, Pe=1)

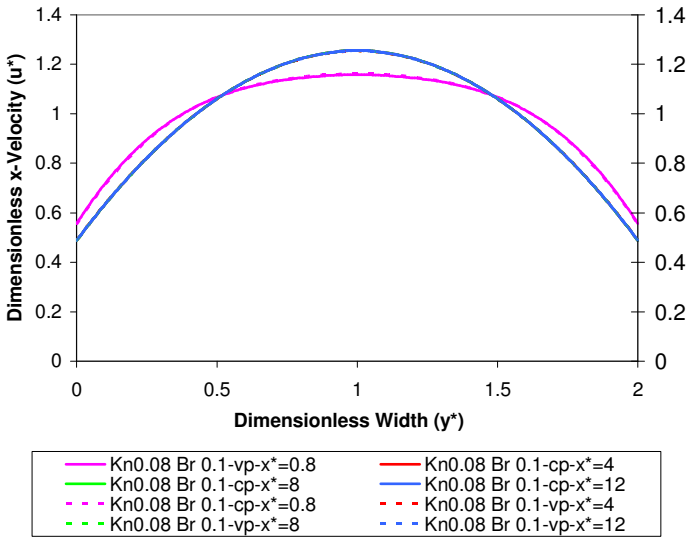

Figure A.46 Variation of dimensionless x-velocity with dimensionless width of the channel (Kn=0.08, Br = 0.1, Pe=1)

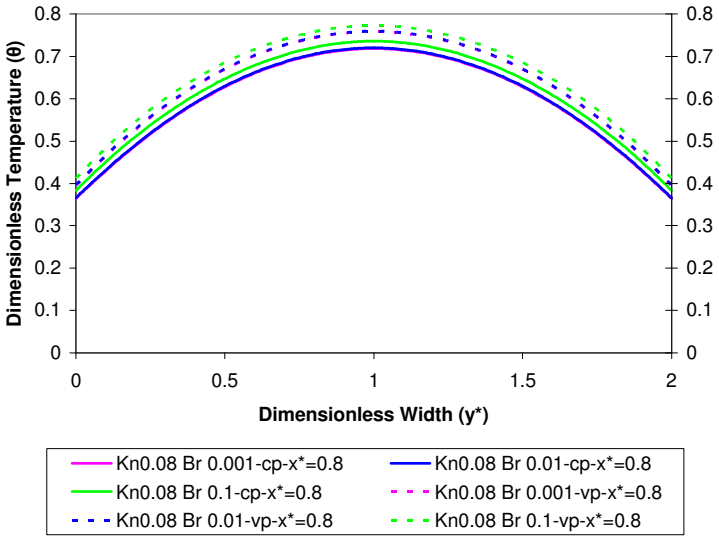

Figure A.47 Variation of dimensionless temperature with dimensionless width of the channel at crossection x*=0.8 for various positive Brinkman numbers (Kn=0.08, Pe=1)

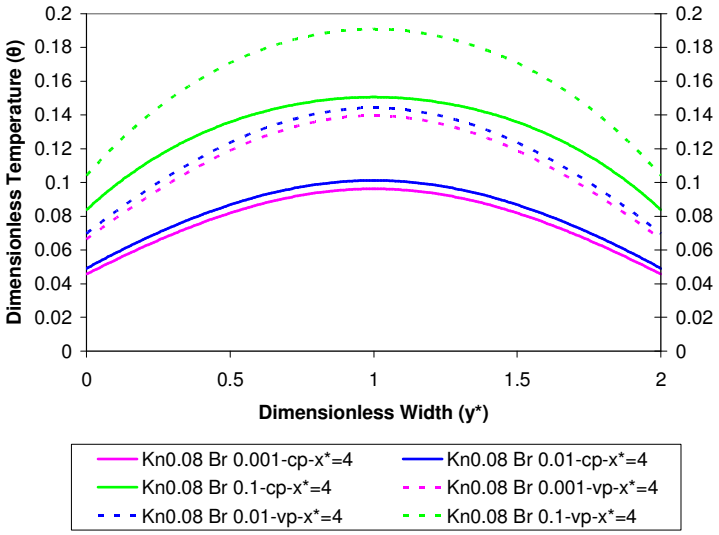

Figure A.48 Variation of dimensionless temperature with dimensionless width of the channel at crossection x*=4 for various positive Brinkman numbers (Kn=0.08, Pe=1)

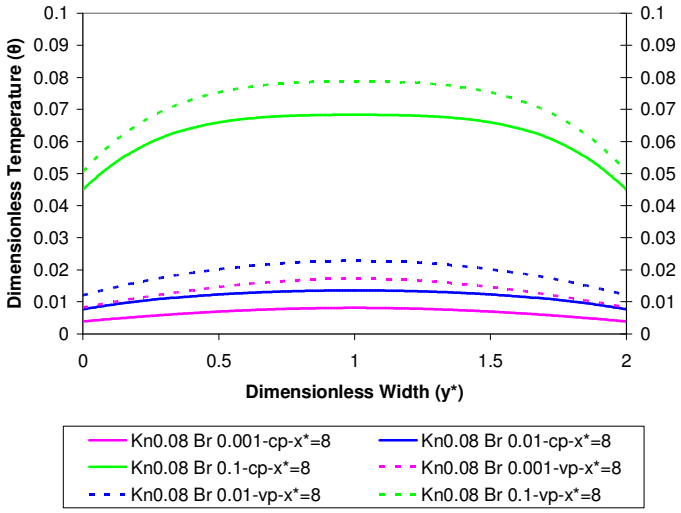

Figure A.49 Variation of dimensionless temperature with dimensionless width of the channel at crossection x*=8 for various positive Brinkman numbers (Kn=0.08, Pe=1)

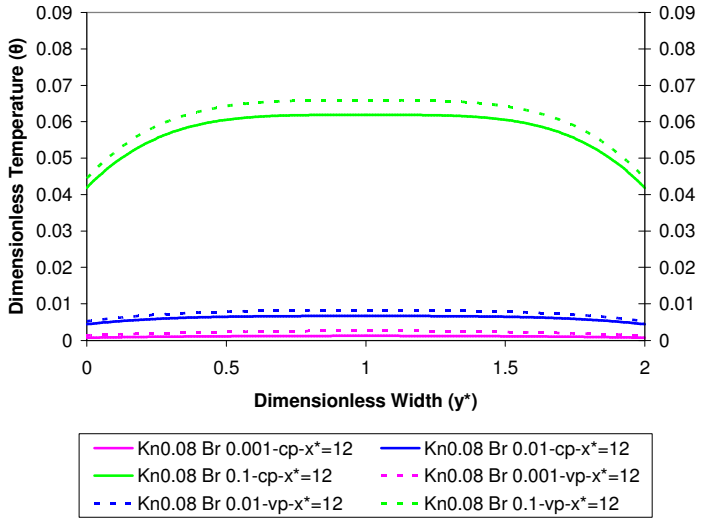

Figure A.50 Variation of dimensionless temperature with dimensionless width of the channel at crossection x*=12 for various positive Brinkman numbers (Kn=0.08, Pe=1)

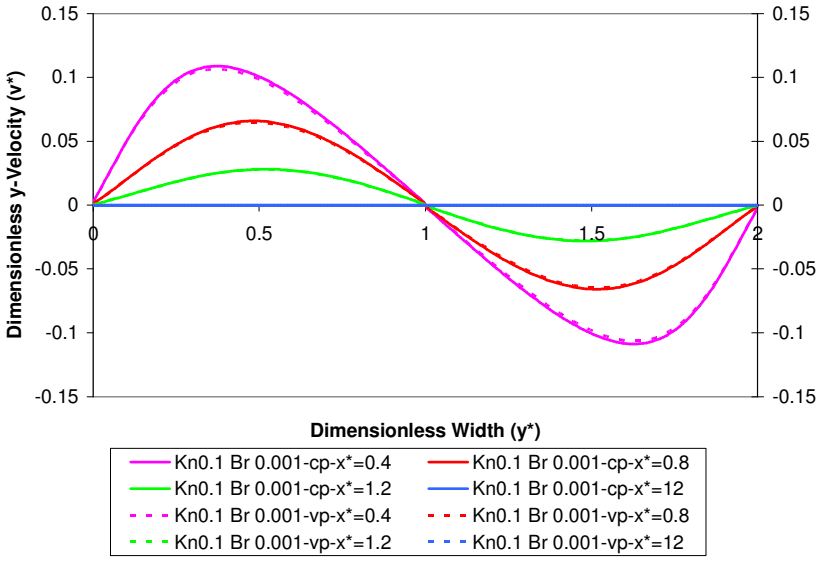

Figure A.51 Variation of dimensionless y-velocity with dimensionless width of the channel (Kn=0.1, Br = 0.001, Pe=1)

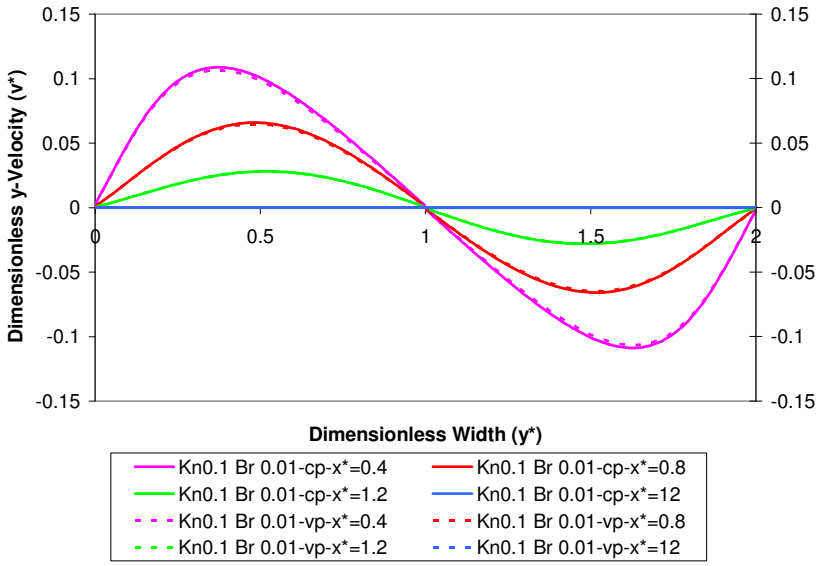

Figure A.52 Variation of dimensionless y-velocity with dimensionless width of the channel (Kn=0.1, Br = 0.01, Pe=1)

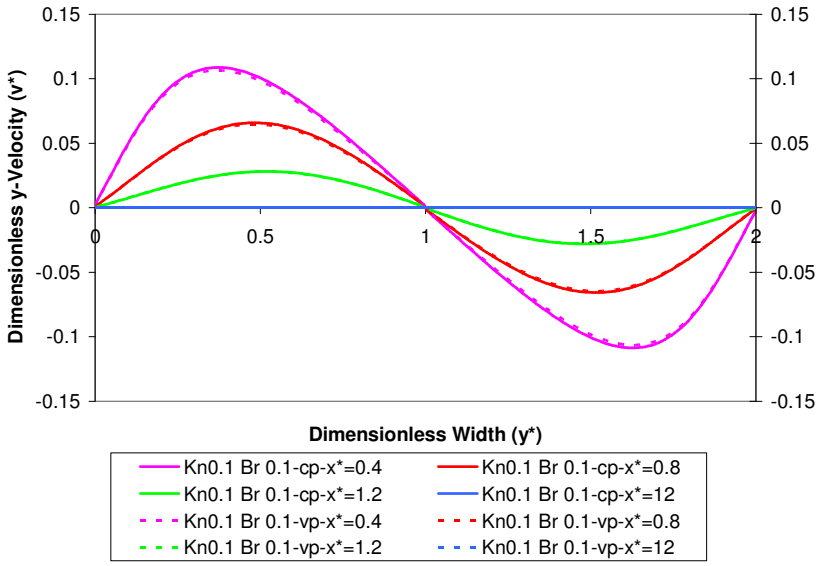

Figure A.53 Variation of dimensionless y-velocity with dimensionless width of the channel (Kn=0.1, Br = 0.1, Pe=1)

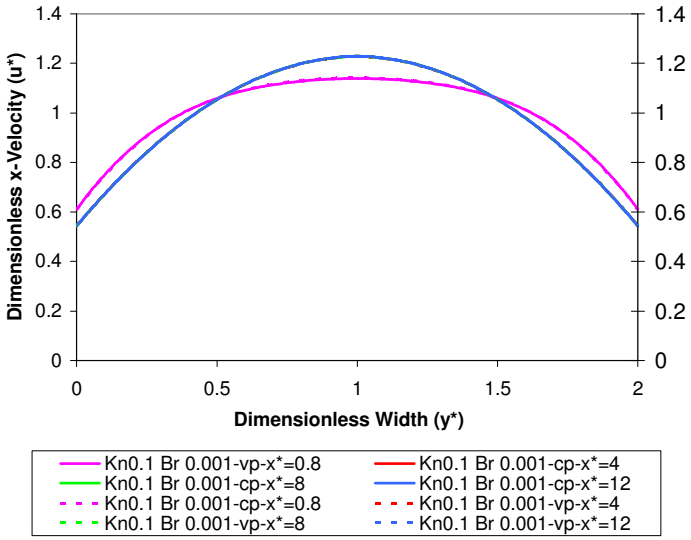

Figure A.54 Variation of dimensionless x-velocity with dimensionless width of the channel (Kn=0.1, Br = 0.001, Pe=1)

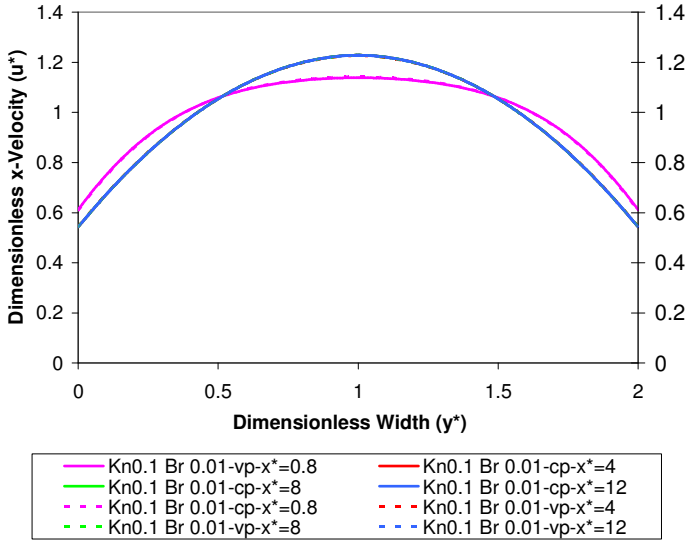

Figure A.55 Variation of dimensionless x-velocity with dimensionless width of the channel (Kn=0.1, Br = 0.01, Pe=1)

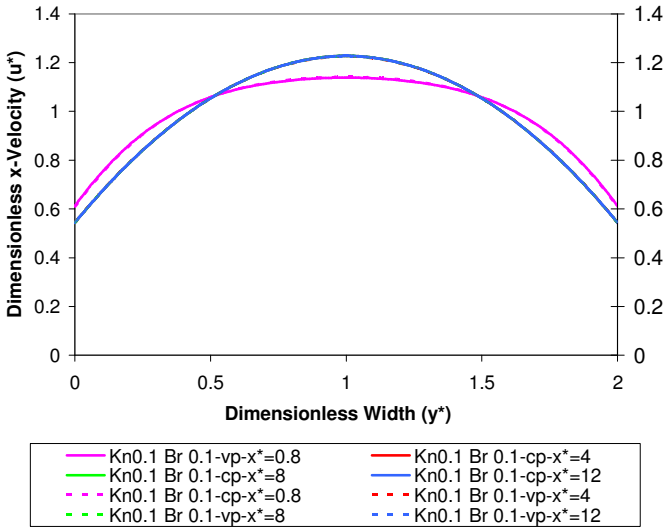

Figure A.56 Variation of dimensionless x-velocity with dimensionless width of the channel (Kn=0.1, Br = 0.1, Pe=1)

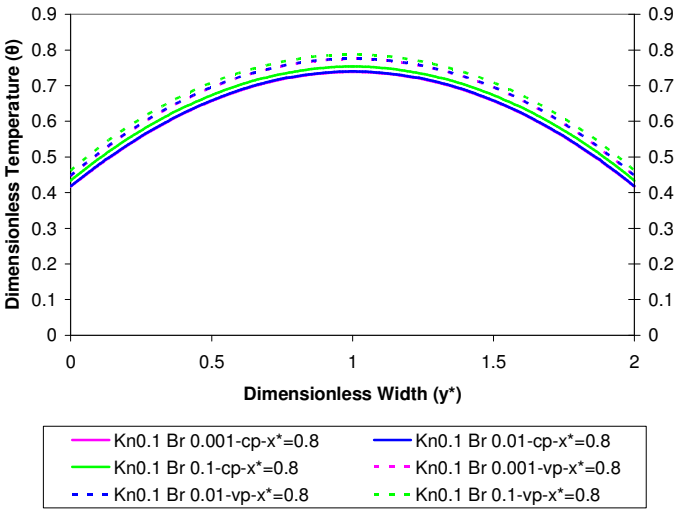

Figure A.57 Variation of dimensionless temperature with dimensionless width of the channel at crossection x*=0.8 for various positive Brinkman numbers (Kn=0.1, Pe=1)

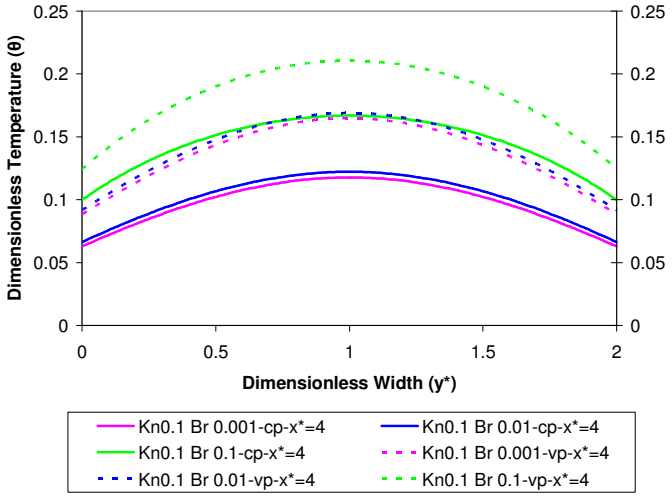

Figure A.58 Variation of dimensionless temperature with dimensionless width of the channel at crossection x*=4 for various positive Brinkman numbers (Kn=0.1, Pe=1)

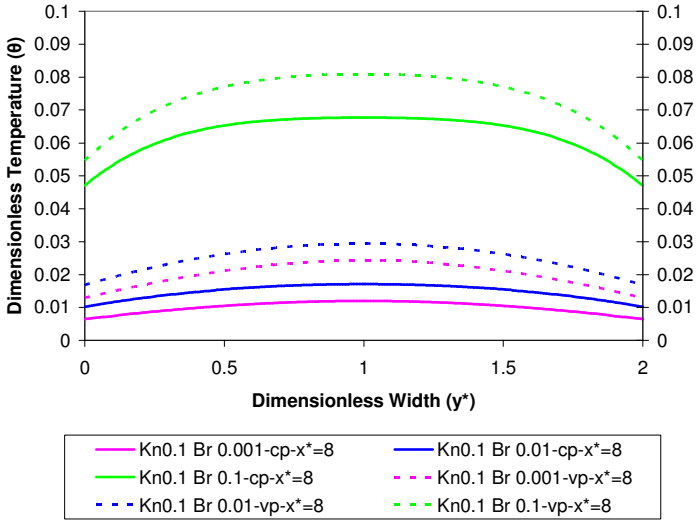

Figure A.59 Variation of dimensionless temperature with dimensionless width of the channel at crossection x*=8 for various positive Brinkman numbers (Kn=0.1, Pe=1)

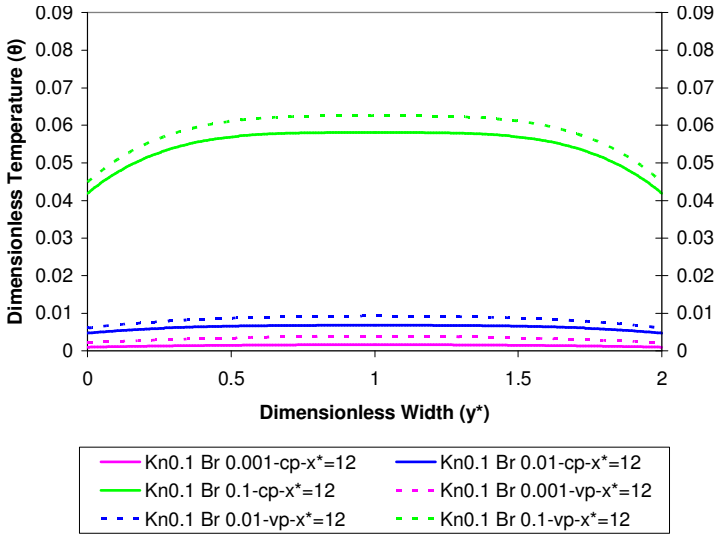

Figure A.60 Variation of dimensionless temperature with dimensionless width of the channel at crossection x*=12 for various positive Brinkman numbers (Kn=0.1, Pe=1)

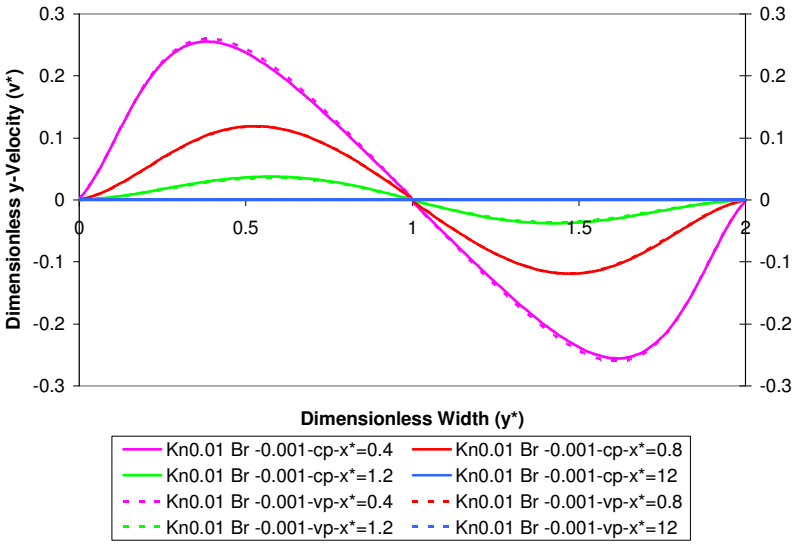

Figure A.61 Variation of dimensionless y-velocity with dimensionless width of the channel (Kn=0.01, Br = -0.001, Pe=1)

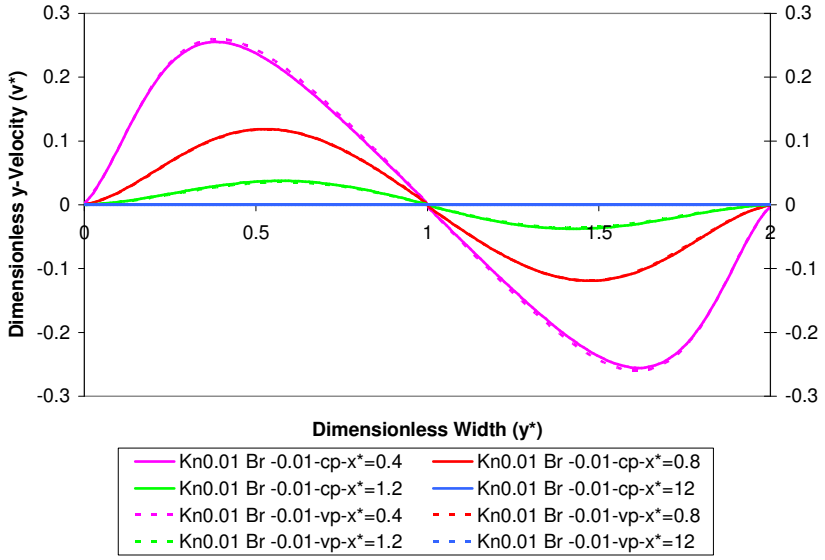

Figure A.62 Variation of dimensionless y-velocity with dimensionless width of the channel (Kn=0.01, Br = -0.01, Pe=1)

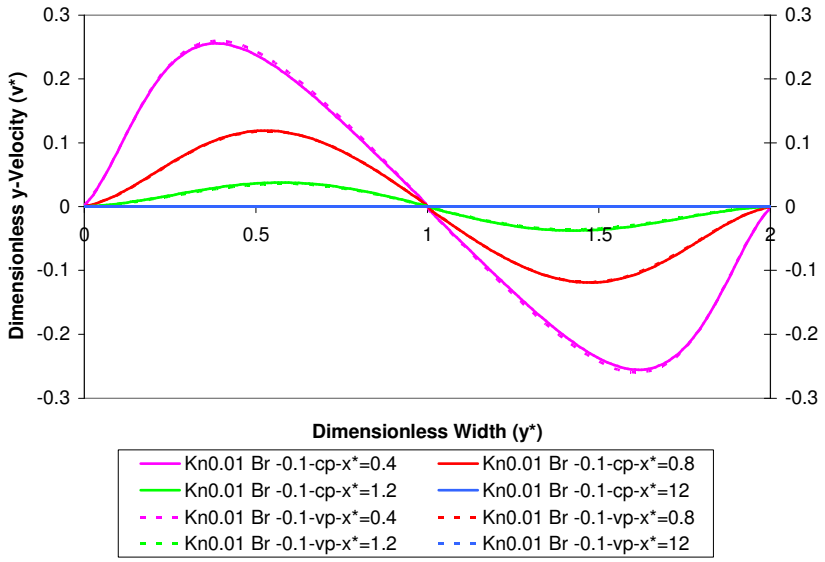

Figure A.63 Variation of dimensionless y-velocity with dimensionless width of the channel (Kn=0.01, Br = -0.1, Pe=1)

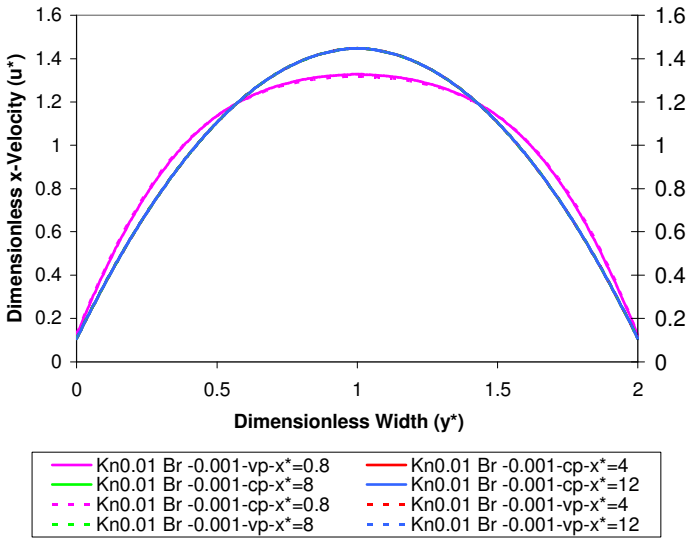

Figure A.64 Variation of dimensionless x-velocity with dimensionless width of the channel (Kn=0.01, Br = -0.001, Pe=1)

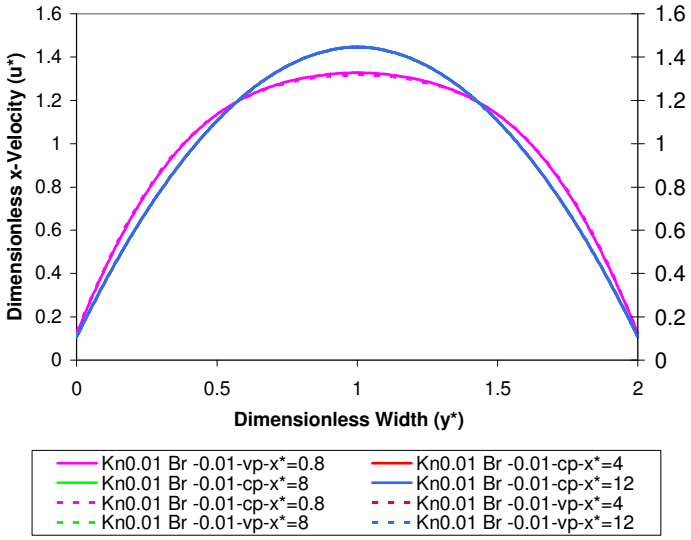

Figure A.65 Variation of dimensionless x-velocity with dimensionless width of the channel (Kn=0.01, Br = -0.01, Pe=1)

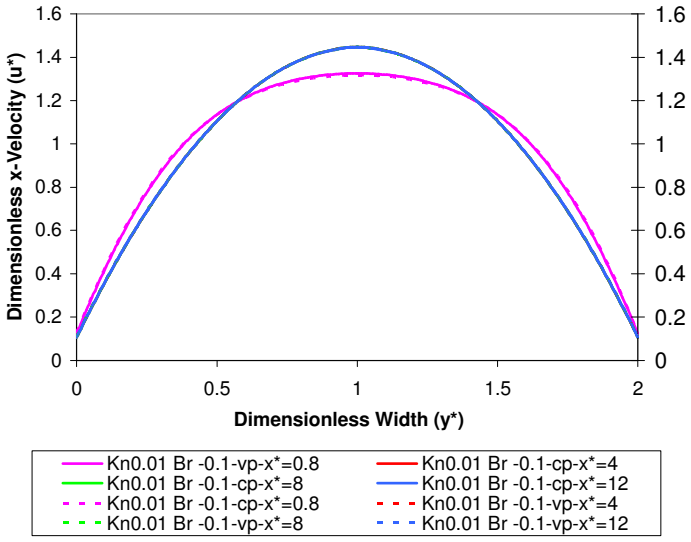

Figure A.66 Variation of dimensionless x-velocity with dimensionless width of the channel (Kn=0.01, Br = -0.1, Pe=1)

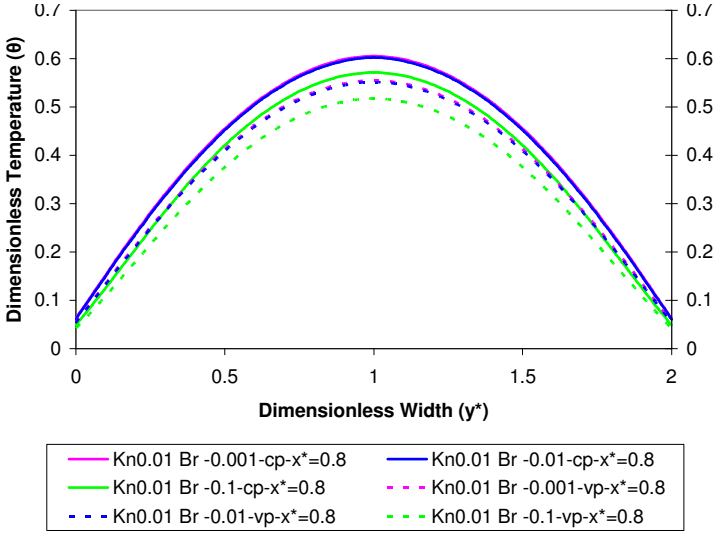

Figure A.67 Variation of dimensionless temperature with dimensionless width of the channel at crossection x*=0.8 for various negative Brinkman numbers (Kn=0.01, Pe=1)

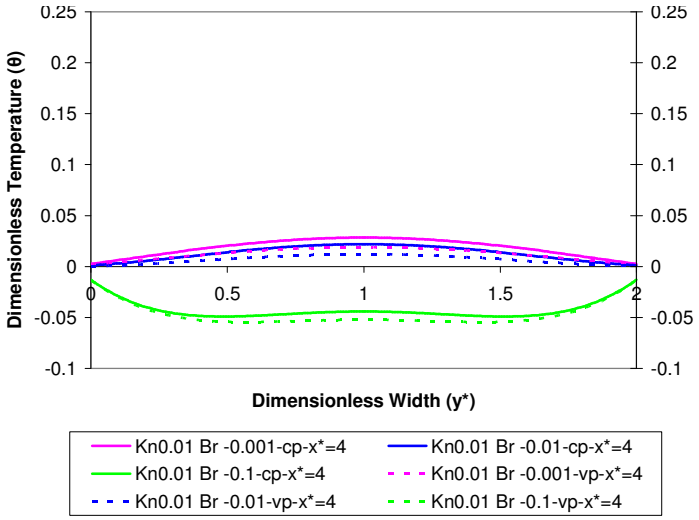

Figure A.68 Variation of dimensionless temperature with dimensionless width of the channel at crossection x*=4 for various negative Brinkman numbers (Kn=0.01, Pe=1)

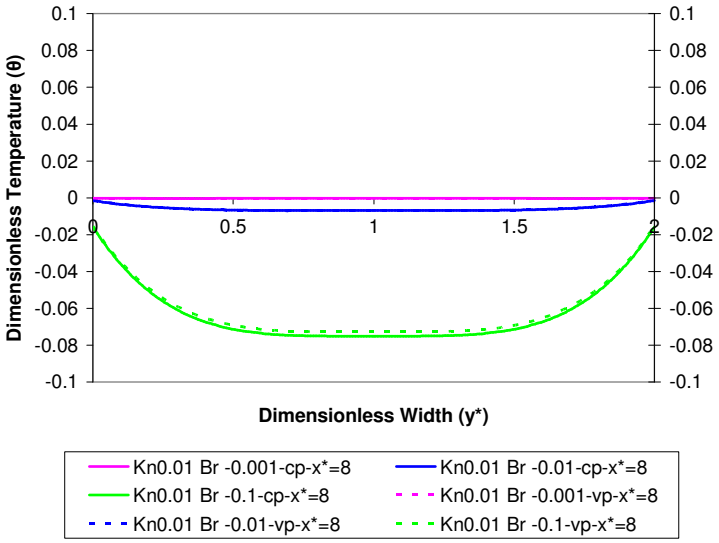

Figure A.69 Variation of dimensionless temperature with dimensionless width of the channel at crossection x*=8 for various negative Brinkman numbers (Kn=0.01, Pe=1)

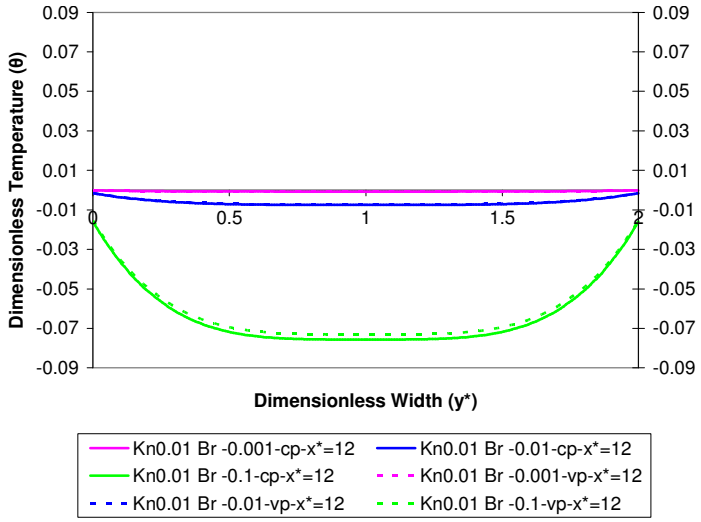

Figure A.70 Variation of dimensionless temperature with dimensionless width of the channel at crossection x*=12 for various negative Brinkman numbers (Kn=0.01, Pe=1)

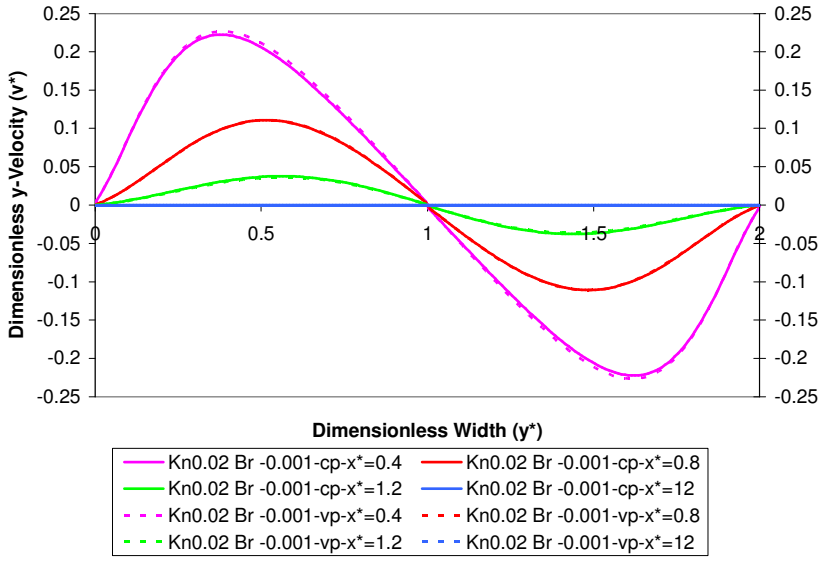

Figure A.71 Variation of dimensionless y-velocity with dimensionless width of the channel (Kn=0.02, Br = -0.001, Pe=1)

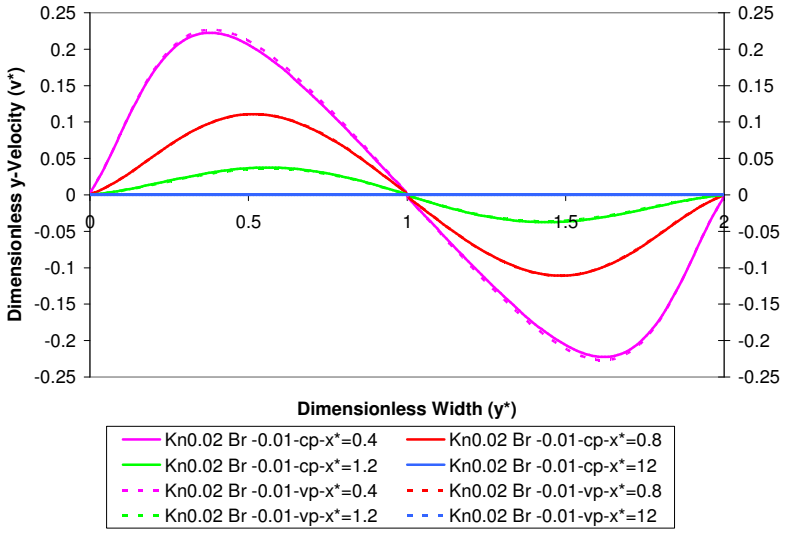

Figure A.72 Variation of dimensionless y-velocity with dimensionless width of the channel (Kn=0.02, Br = -0.01, Pe=1)

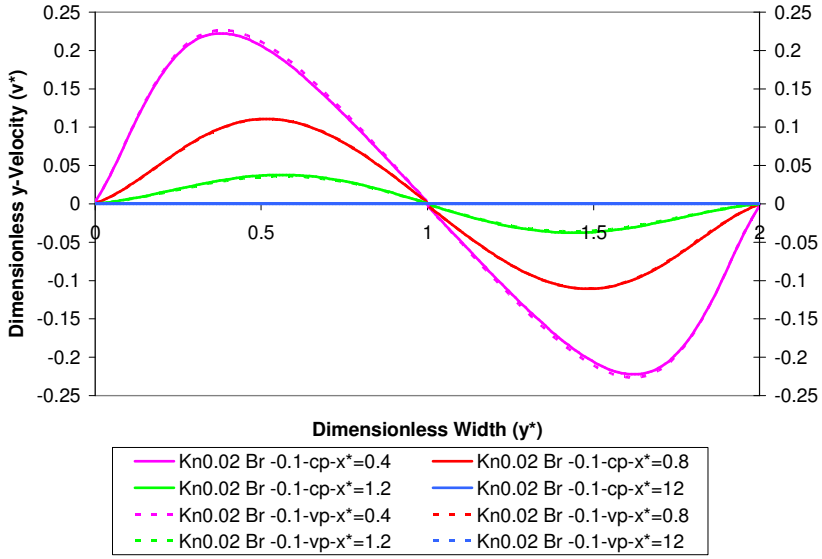

Figure A.73 Variation of dimensionless y-velocity with dimensionless width of the channel (Kn=0.02, Br = -0.1, Pe=1)

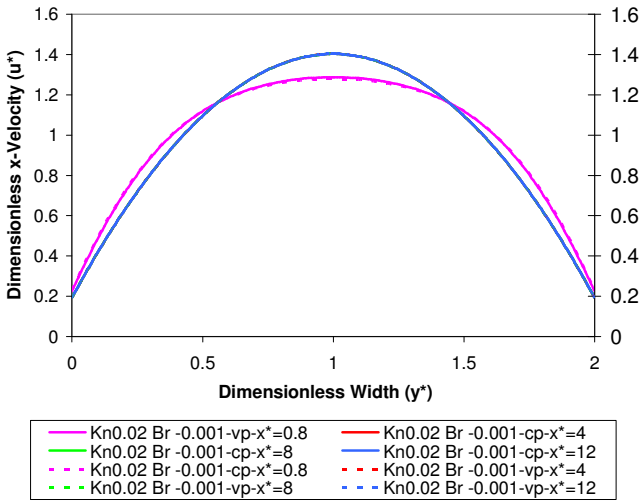

Figure A.74 Variation of dimensionless x-velocity with dimensionless width of the channel (Kn=0.02, Br = -0.001, Pe=1)

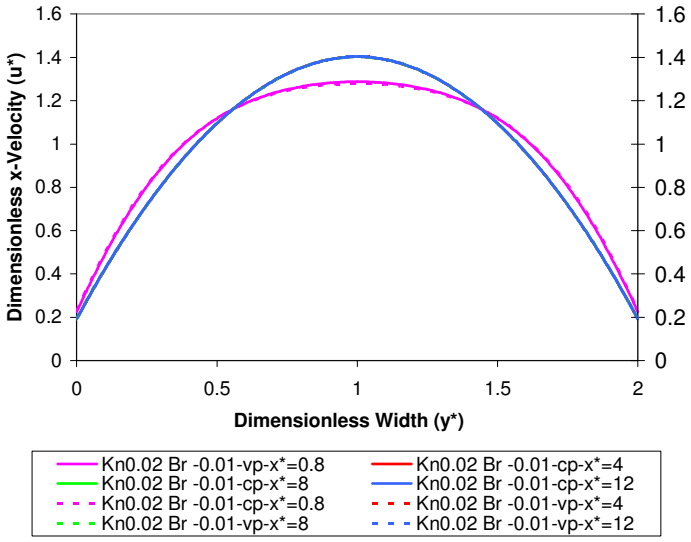

Figure A.75 Variation of dimensionless x-velocity with dimensionless width of the channel (Kn=0.02, Br = -0.01, Pe=1)

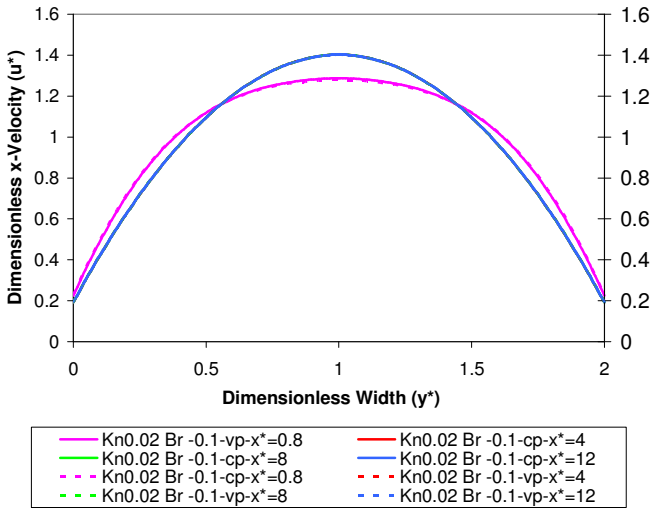

Figure A.76 Variation of dimensionless x-velocity with dimensionless width of the channel (Kn=0.02, Br = -0.1, Pe=1)

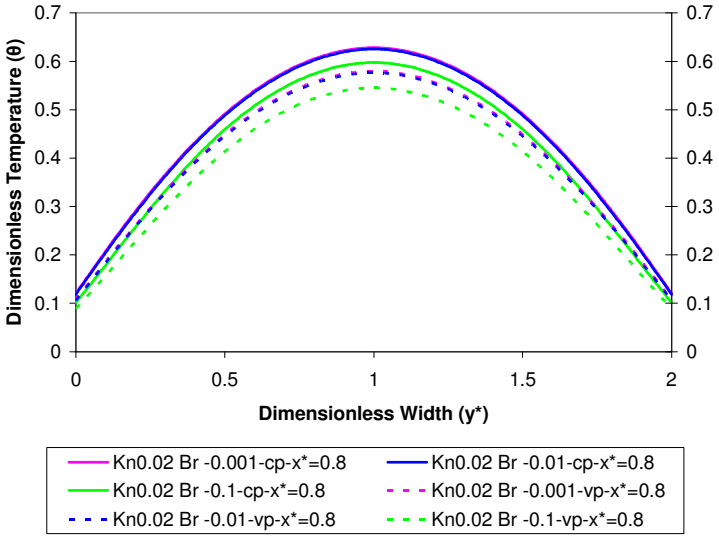

Figure A.77 Variation of dimensionless temperature with dimensionless width of the channel at crossection x*=0.8 for various negative Brinkman numbers (Kn=0.02, Pe=1)

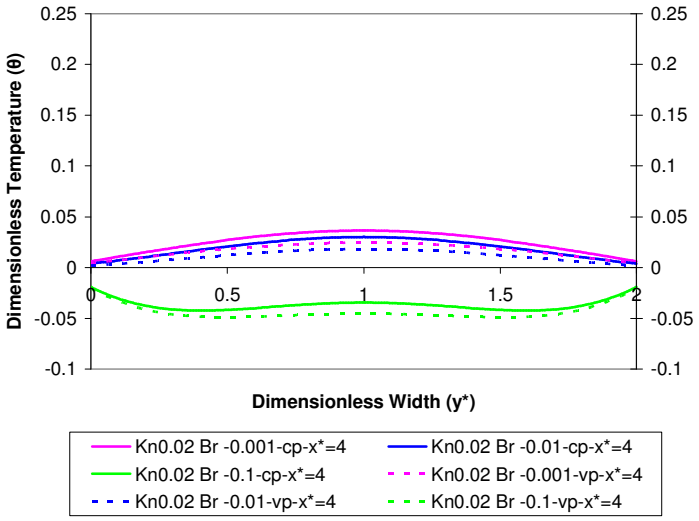

Figure A.78 Variation of dimensionless temperature with dimensionless width of the channel at crossection x*=4 for various negative Brinkman numbers (Kn=0.02, Pe=1)

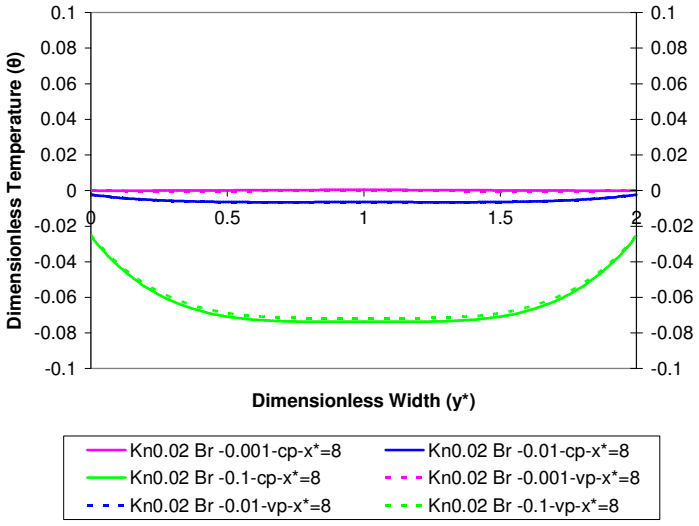

Figure A.79 Variation of dimensionless temperature with dimensionless width of the channel at crossection x*=8 for various negative Brinkman numbers (Kn=0.02, Pe=1)

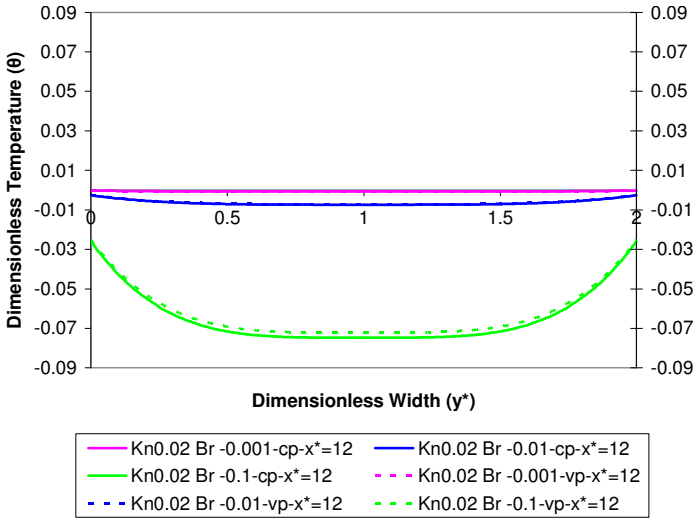

Figure A.80 Variation of dimensionless temperature with dimensionless width of the channel at crossection x*=12 for various negative Brinkman numbers (Kn=0.02, Pe=1)

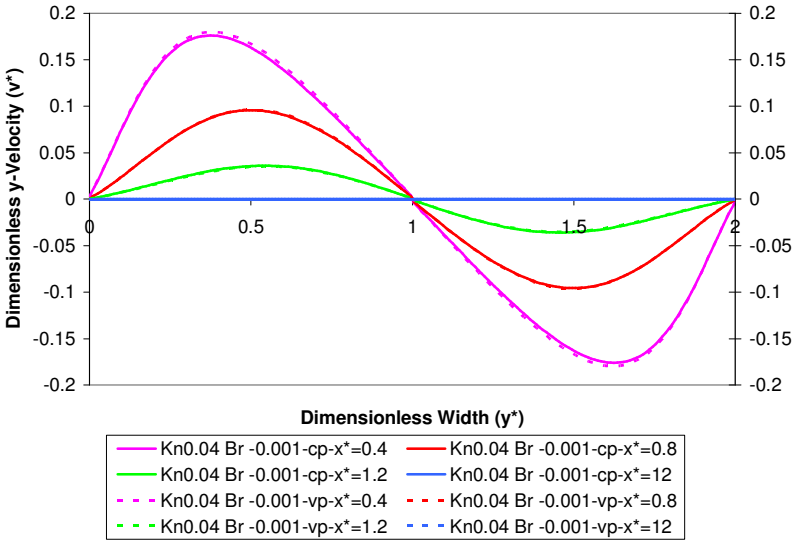

Figure A.81 Variation of dimensionless y-velocity with dimensionless width of the channel (Kn=0.04, Br = -0.001, Pe=1)

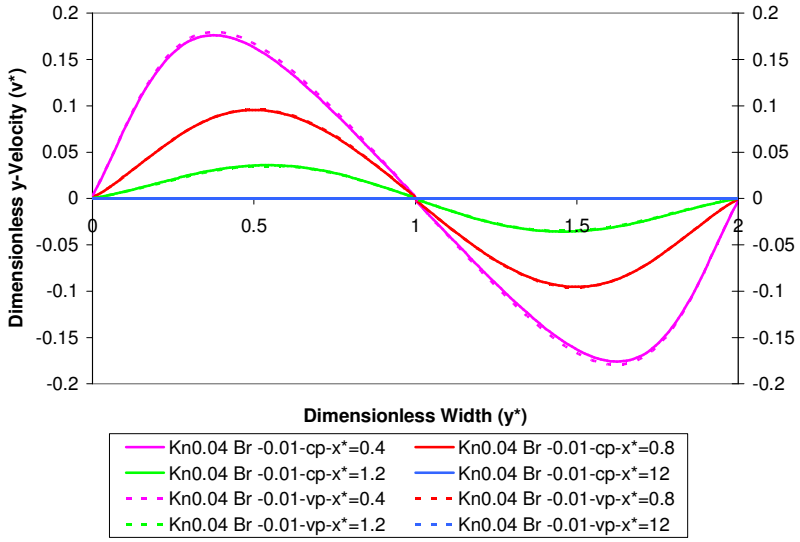

Figure A.82 Variation of dimensionless y-velocity with dimensionless width of the channel (Kn=0.04, Br = -0.01, Pe=1)

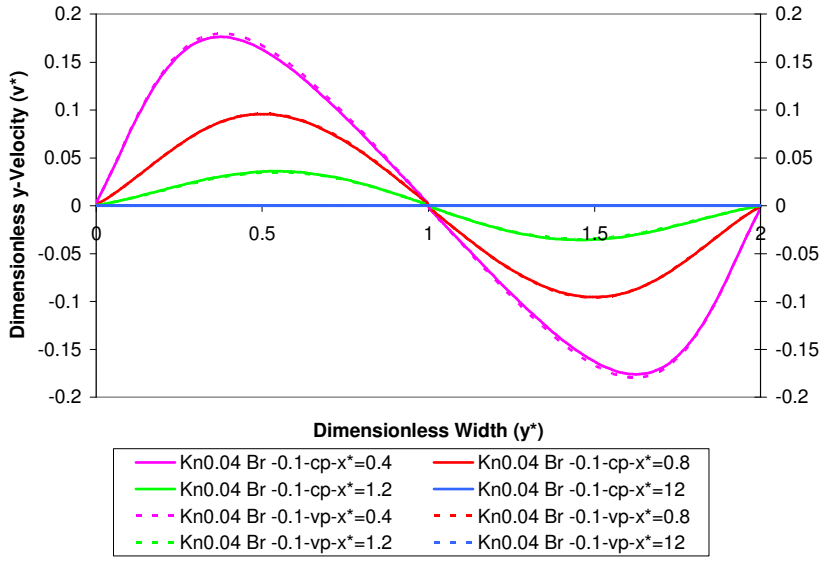

Figure A.83 Variation of dimensionless y-velocity with dimensionless width of the channel (Kn=0.04, Br = -0. 1, Pe=1)

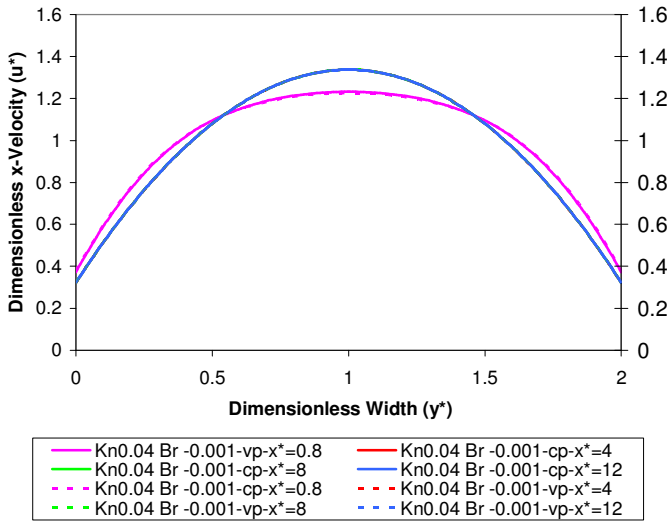

Figure A.84 Variation of dimensionless x-velocity with dimensionless width of the channel (Kn=0.04, Br = -0.001, Pe=1)

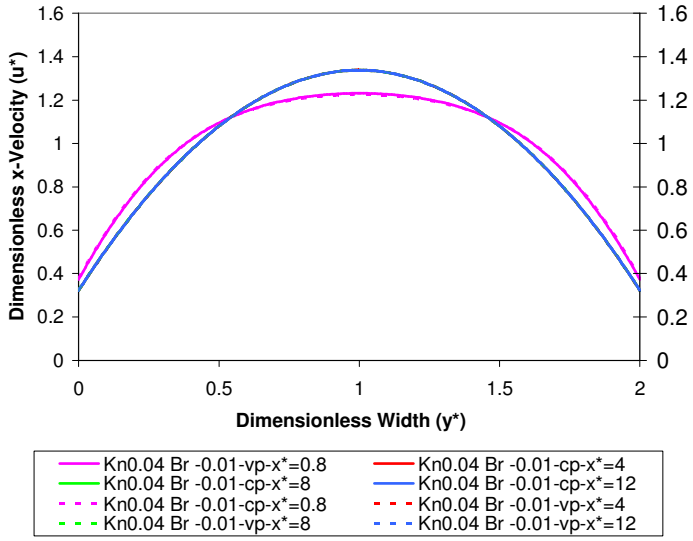

Figure A.85 Variation of dimensionless x-velocity with dimensionless width of the channel (Kn=0.04, Br = -0.01, Pe=1)

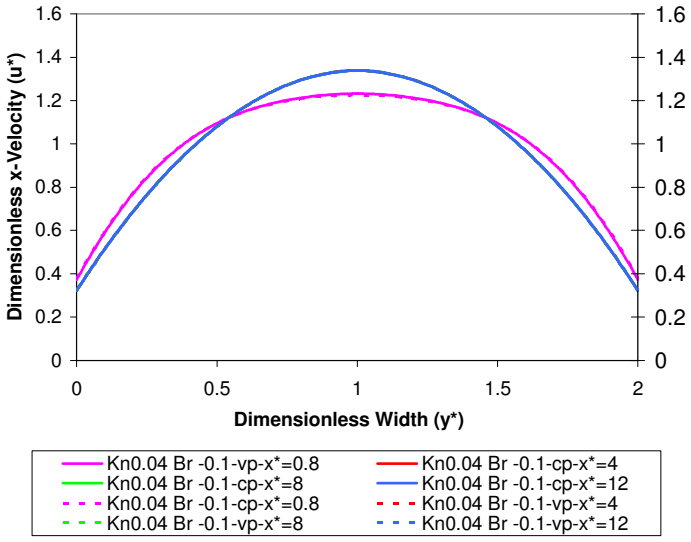

Figure A.86 Variation of dimensionless x-velocity with dimensionless width of the channel (Kn=0.04, Br = -0.1, Pe=1)

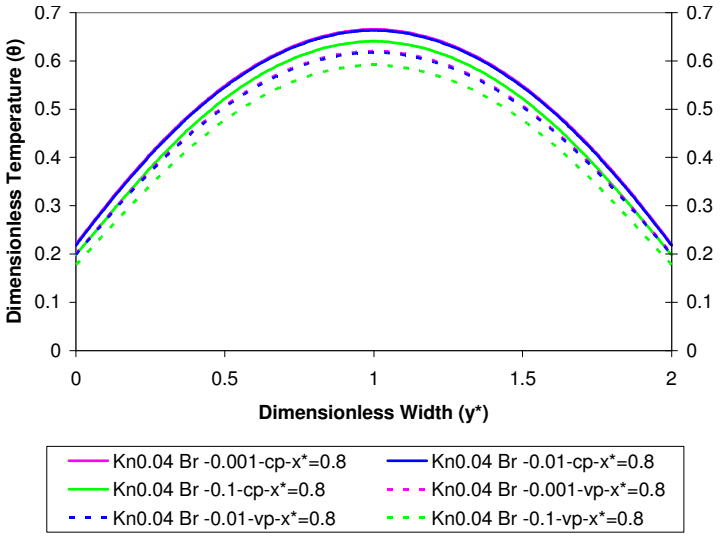

Figure A.87 Variation of dimensionless temperature with dimensionless width of the channel at crossection x*=0.8 for various negative Brinkman numbers (Kn=0.04, Pe=1)

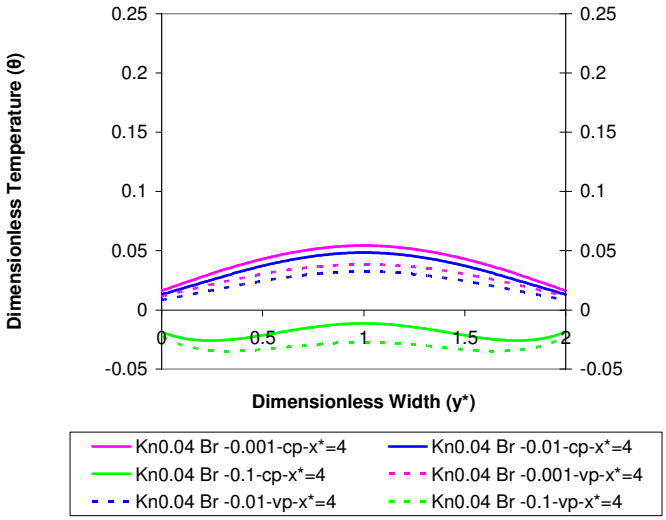

Figure A.88 Variation of dimensionless temperature with dimensionless width of the channel at crossection x*=4 for various negative Brinkman numbers (Kn=0.04, Pe=1)

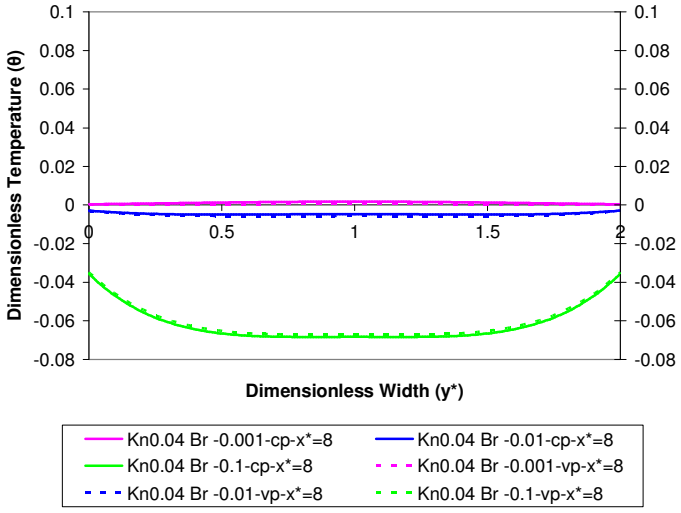

Figure A.89 Variation of dimensionless temperature with dimensionless width of the channel at crossection x*=8 for various negative Brinkman numbers (Kn=0.04, Pe=1)

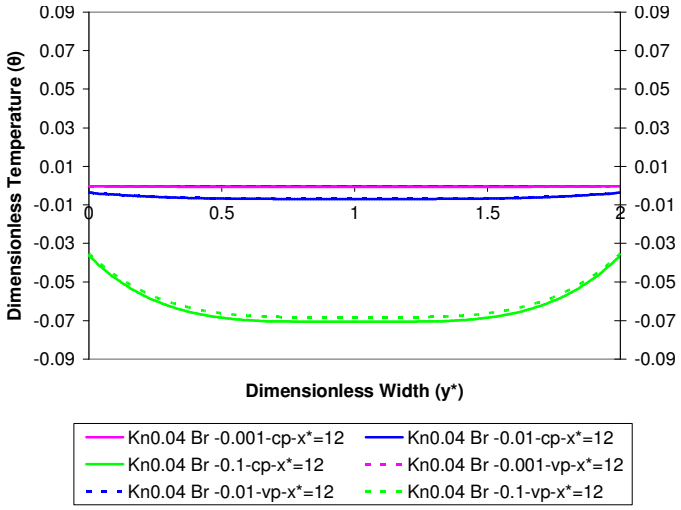

Figure A.90 Variation of dimensionless temperature with dimensionless width of the channel at crossection x*=12 for various negative Brinkman numbers (Kn=0.04, Pe=1)

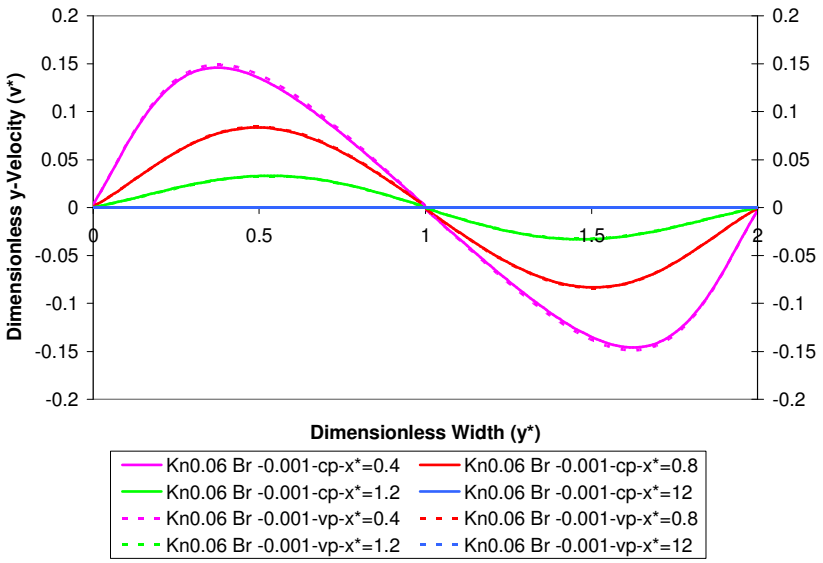

Figure A.91 Variation of dimensionless y-velocity with dimensionless width of the channel (Kn=0.06, Br = -0.001, Pe=1)

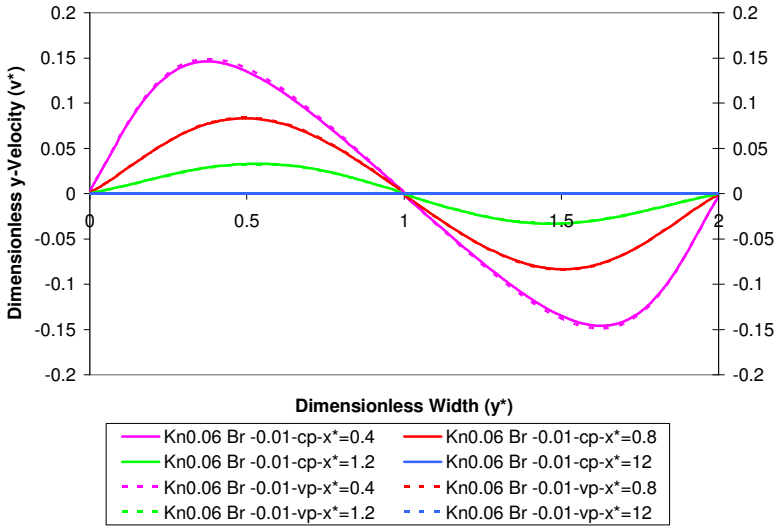

Figure A.92 Variation of dimensionless y-velocity with dimensionless width of the channel (Kn=0.06, Br = -0.01, Pe=1)

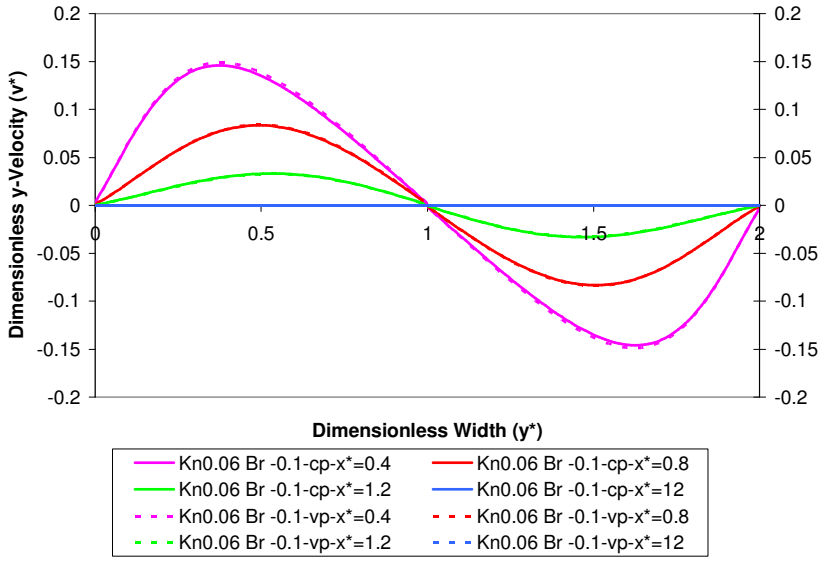

Figure A.93 Variation of dimensionless y-velocity with dimensionless width of the channel (Kn=0.06, Br = -0.1, Pe=1)

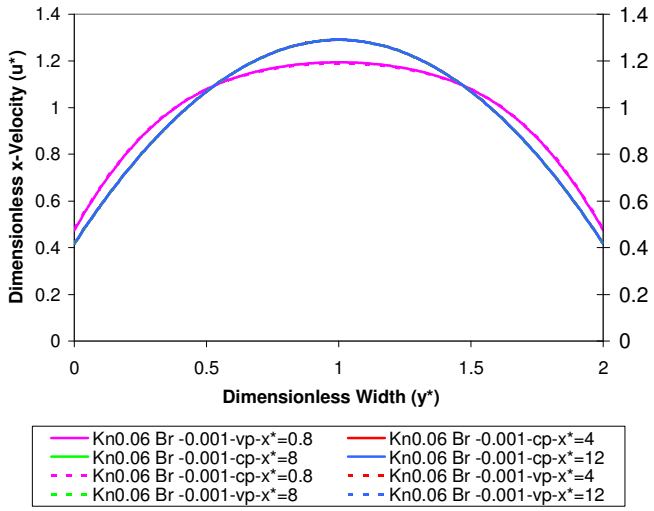

Figure A.94 Variation of dimensionless x-velocity with dimensionless width of the channel (Kn=0.06, Br = -0.001, Pe=1)

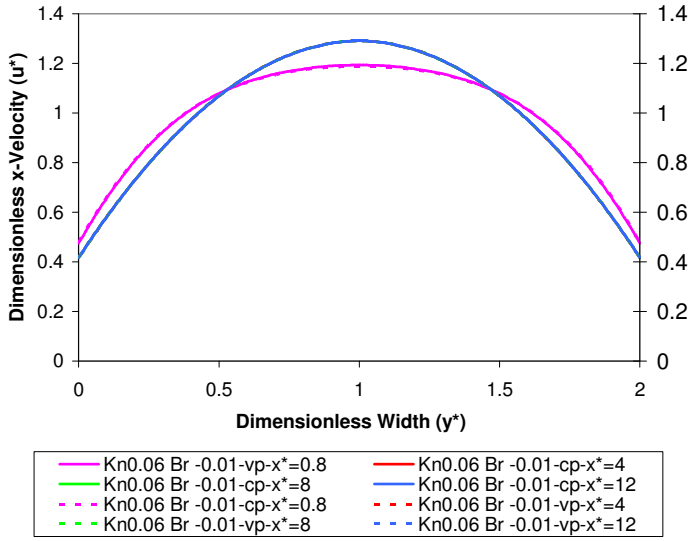

Figure A.95 Variation of dimensionless x-velocity with dimensionless width of the channel (Kn=0.06, Br = -0.01, Pe=1)

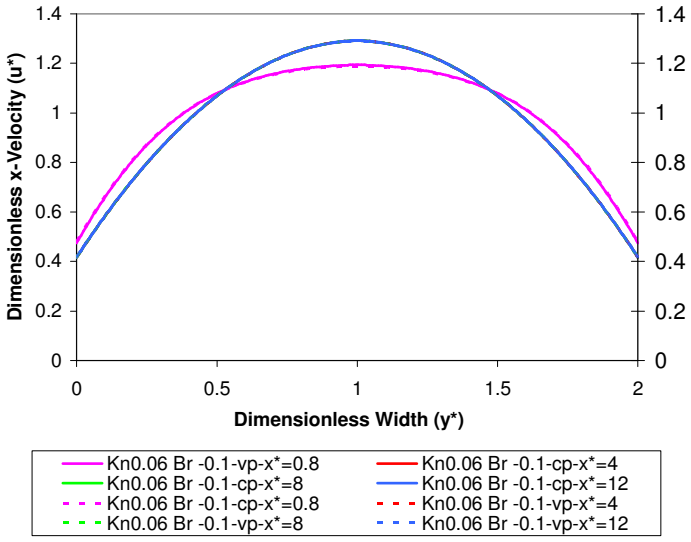

Figure A.96 Variation of dimensionless x-velocity with dimensionless width of the channel (Kn=0.06, Br = -0.1, Pe=1)

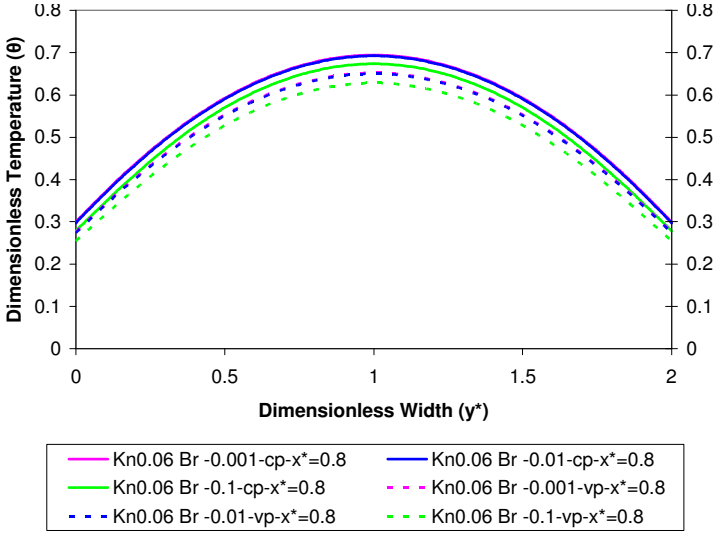

Figure A.97 Variation of dimensionless temperature with dimensionless width of the channel at crossection x*=0.8 for various negative Brinkman numbers (Kn=0.06, Pe=1)

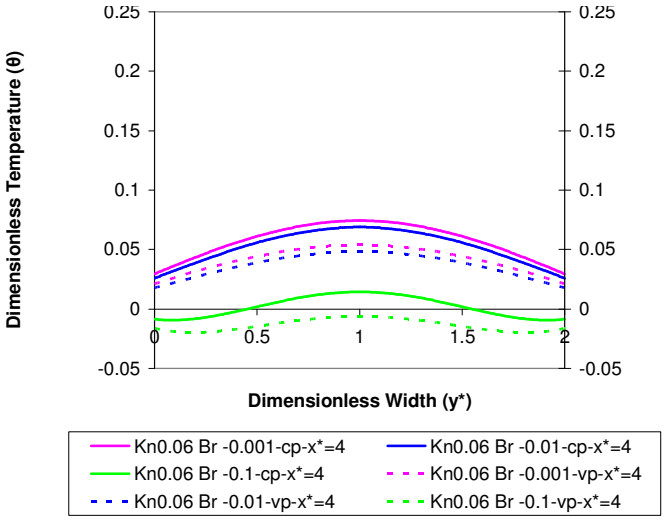

Figure A.98 Variation of dimensionless temperature with dimensionless width of the channel at crossection x*=4 for various negative Brinkman numbers (Kn=0.06, Pe=1)

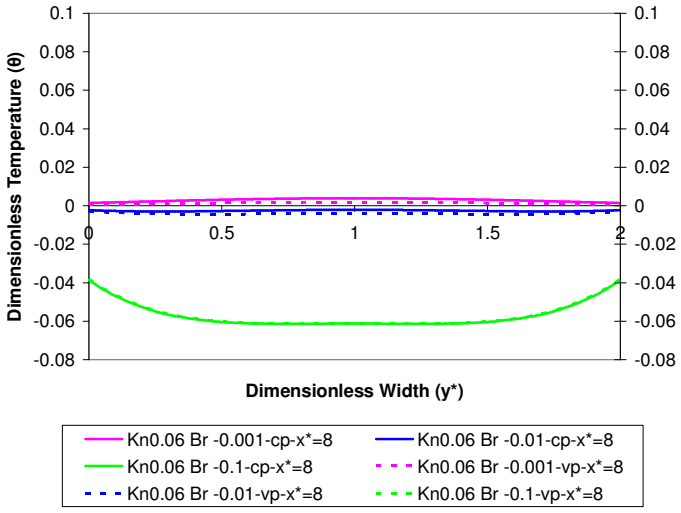

Figure A.99 Variation of dimensionless temperature with dimensionless width of the channel at crossection x*=8 for various negative Brinkman numbers (Kn=0.06, Pe=1)

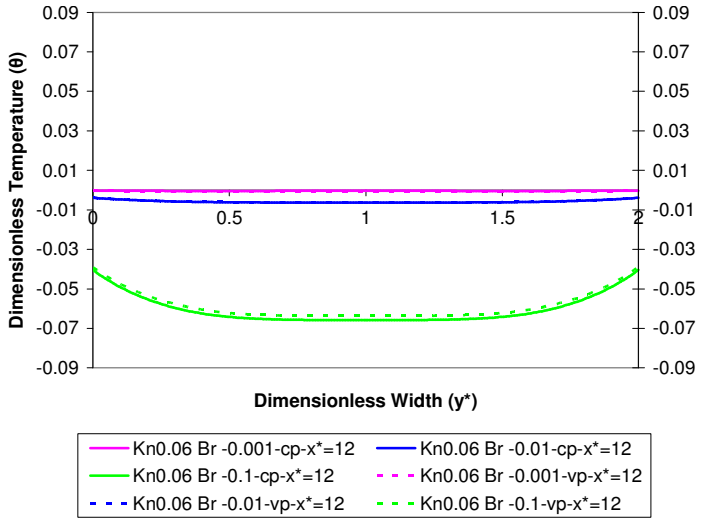

Figure A.100 Variation of dimensionless temperature with dimensionless width of the channel at crossection x*=12 for various negative Brinkman numbers (Kn=0.06, Pe=1)

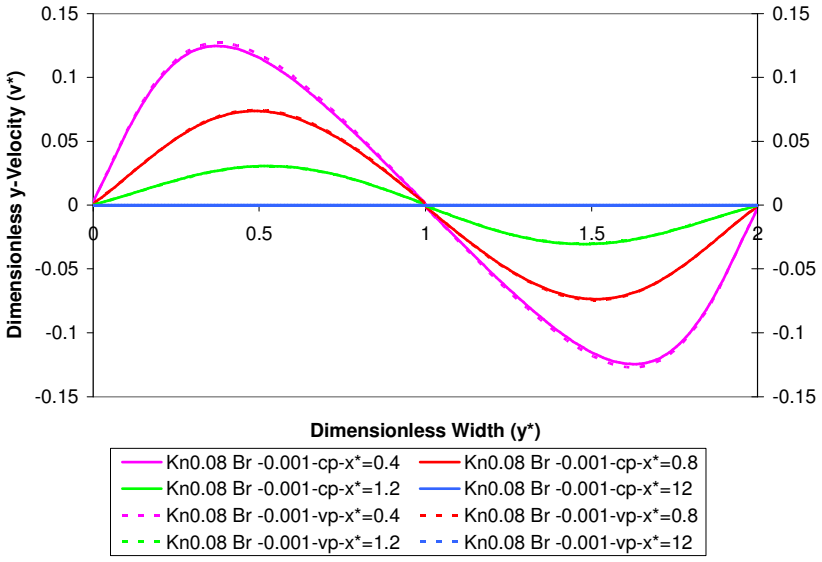

Figure A.101 Variation of dimensionless y-velocity with dimensionless width of the channel (Kn=0.08, Br = -0.001, Pe=1)

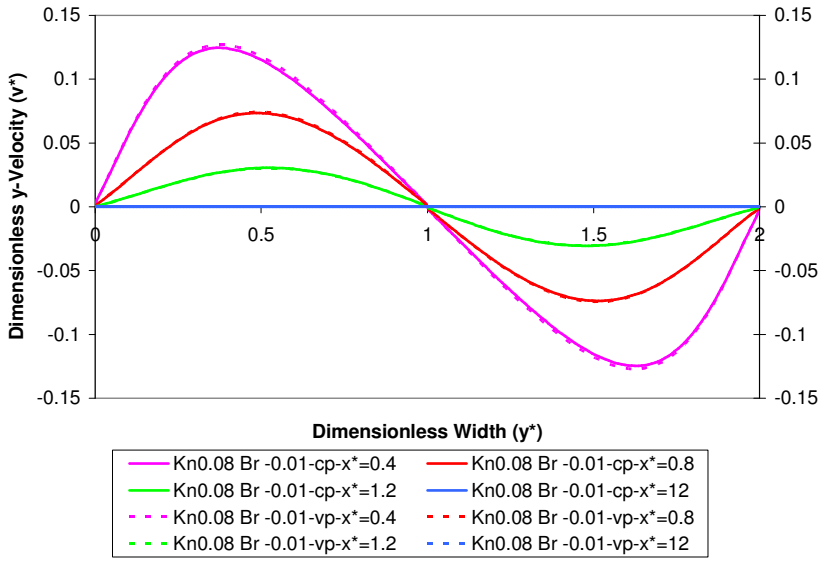

Figure A.102 Variation of dimensionless y-velocity with dimensionless width of the channel (Kn=0.08, Br = -0.01, Pe=1)

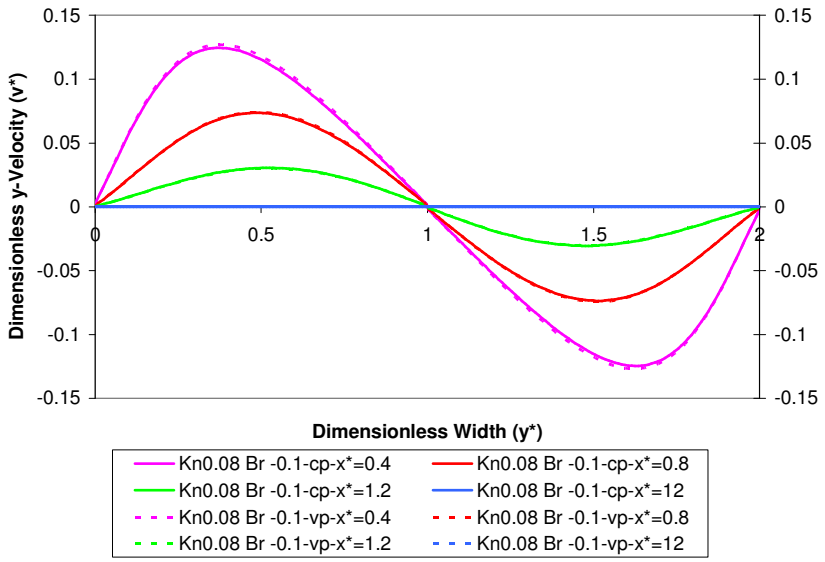

Figure A.103 Variation of dimensionless y-velocity with dimensionless width of the channel (Kn=0.08, Br = -0.1, Pe=1)

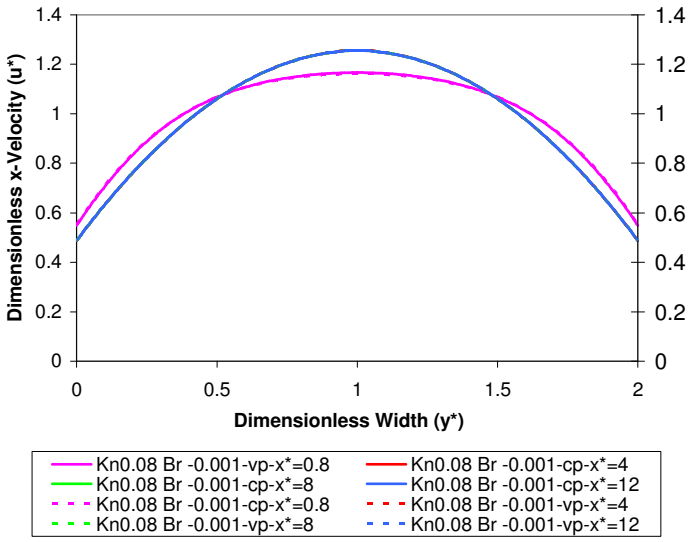

Figure A.104 Variation of dimensionless x-velocity with dimensionless width of the channel (Kn=0.08, Br = -0.001, Pe=1)

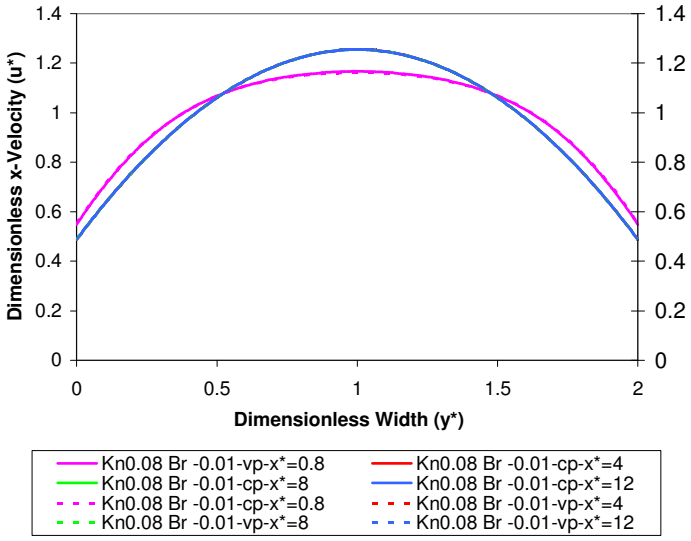

Figure A.105 Variation of dimensionless x-velocity with dimensionless width of the channel (Kn=0.08, Br = -0.01, Pe=1)

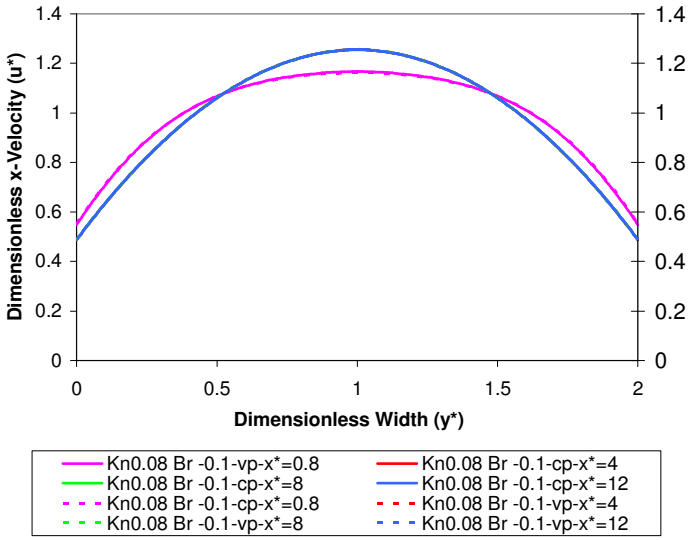

Figure A.106 Variation of dimensionless x-velocity with dimensionless width of the channel (Kn=0.08, Br = -0.1, Pe=1)

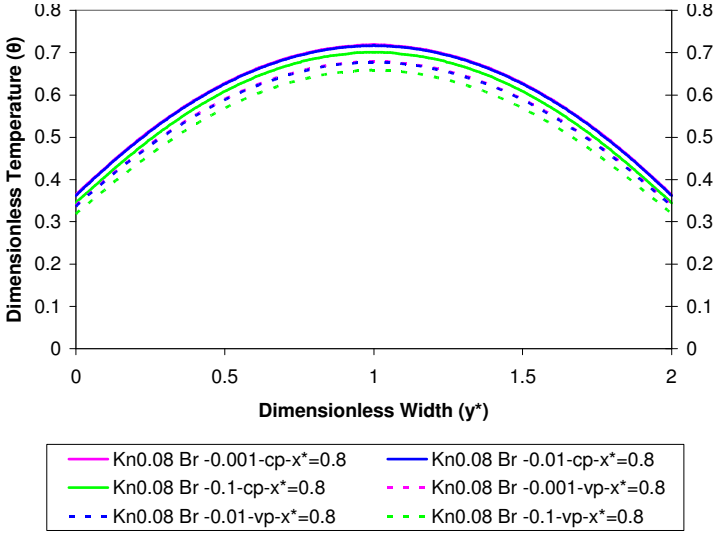

Figure A.107 Variation of dimensionless temperature with dimensionless width of the channel at crossection x*=0.8 for various negative Brinkman numbers (Kn=0.08, Pe=1)

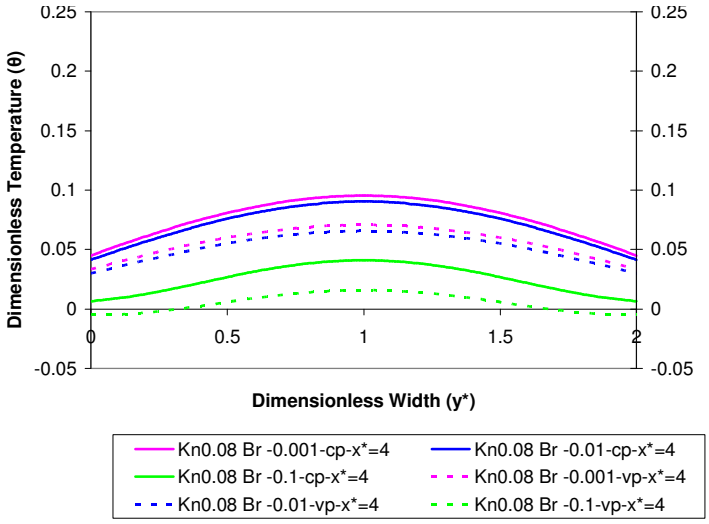

Figure A.108 Variation of dimensionless temperature with dimensionless width of the channel at crossection x*=4 for various negative Brinkman numbers (Kn=0.08, Pe=1)

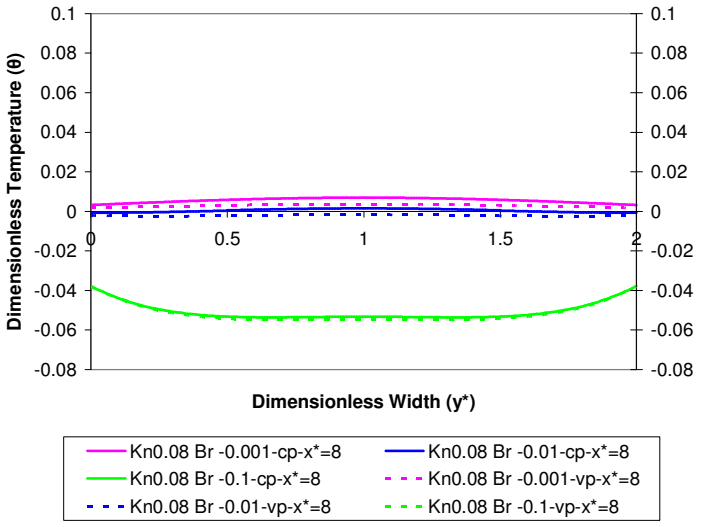

Figure A.109 Variation of dimensionless temperature with dimensionless width of the channel at crossection x*=8 for various negative Brinkman numbers (Kn=0.08, Pe=1)

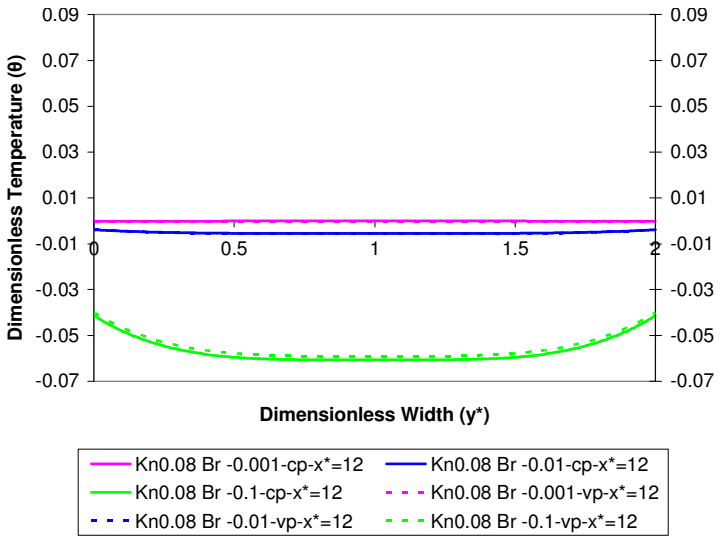

Figure A.110 Variation of dimensionless temperature with dimensionless width of the channel at crossection x*=12 for various negative Brinkman numbers (Kn=0.08, Pe=1)

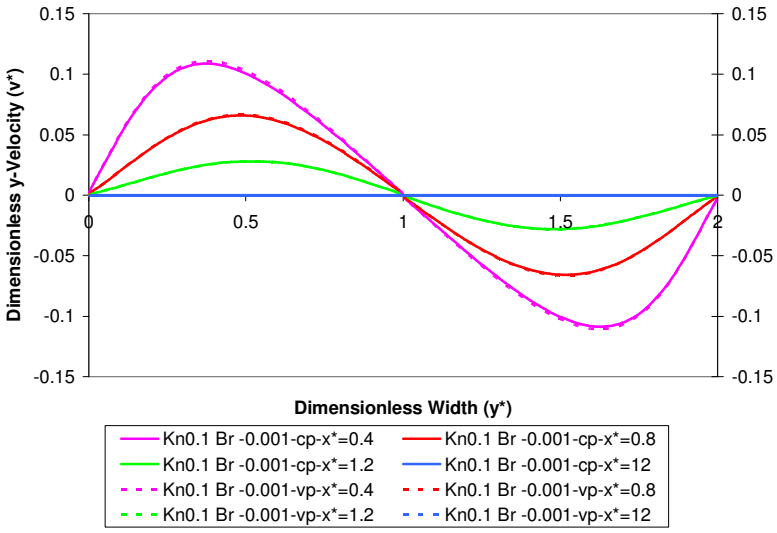

Figure A.111 Variation of dimensionless y-velocity with dimensionless width of the channel (Kn=0.1, Br = -0.001, Pe=1)

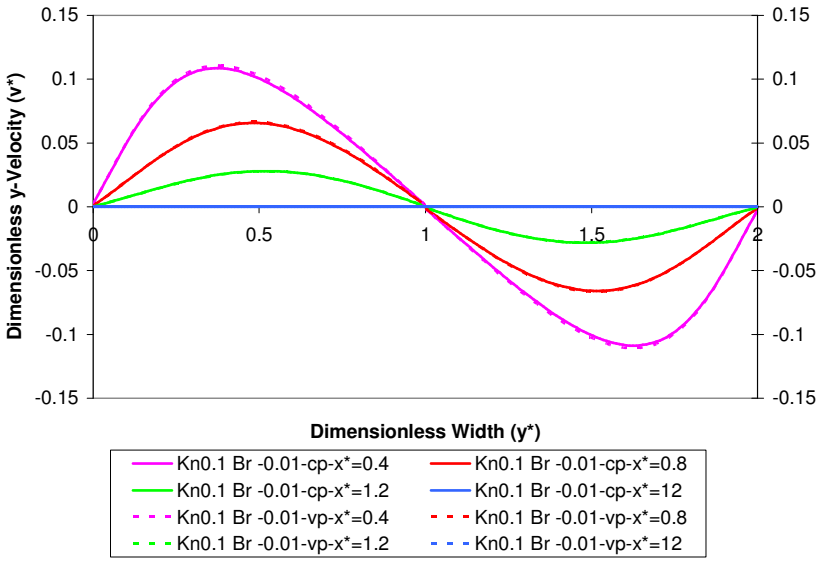

Figure A.112 Variation of dimensionless y-velocity with dimensionless width of the channel (Kn=0.1, Br = -0.01, Pe=1)

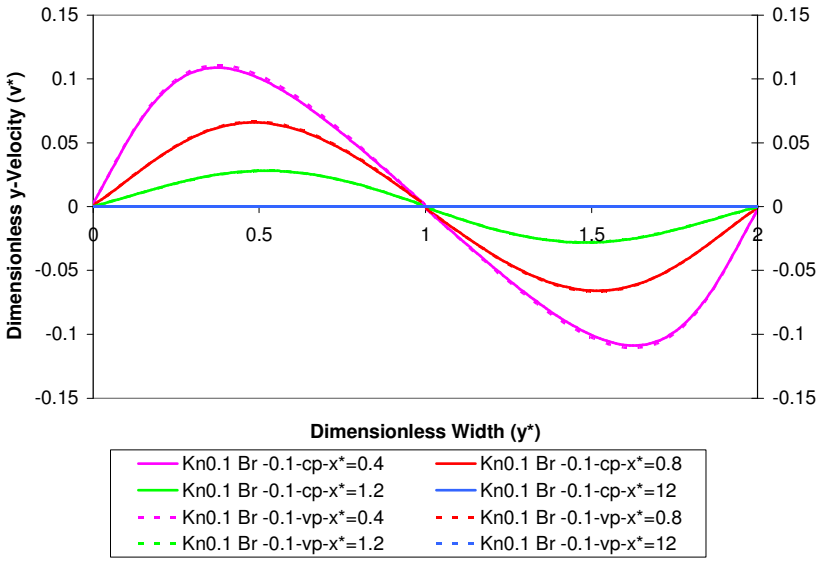

Figure A.113 Variation of dimensionless y-velocity with dimensionless width of the channel (Kn=0.1, Br = -0.1, Pe=1)

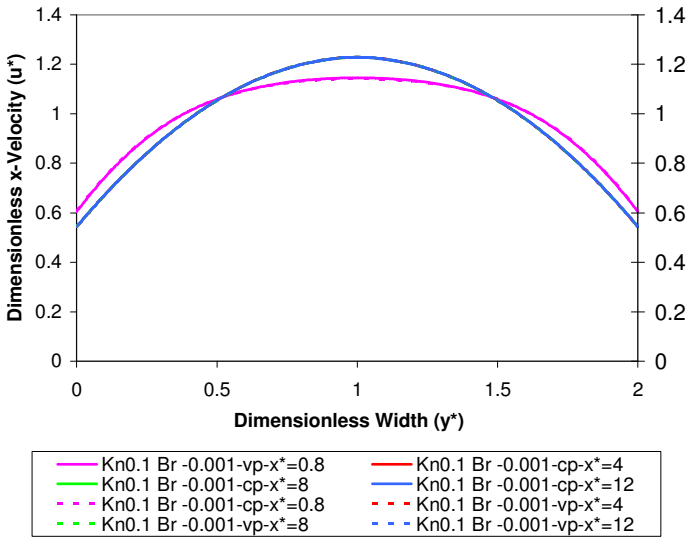

Figure A.114 Variation of dimensionless x-velocity with dimensionless width of the channel (Kn=0.1, Br = -0.001, Pe=1)

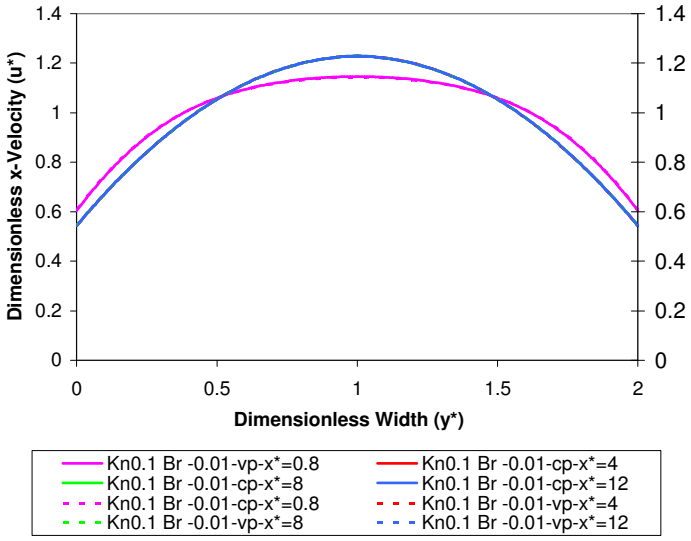

Figure A.115 Variation of dimensionless x-velocity with dimensionless width of the channel (Kn=0.1, Br = -0.01, Pe=1)

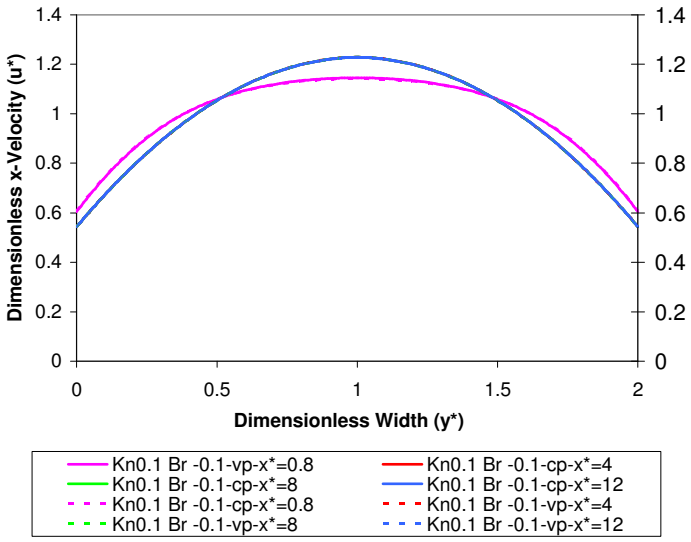

Figure A.116 Variation of dimensionless x-velocity with dimensionless width of the channel (Kn=0.1, Br = -0.1, Pe=1)

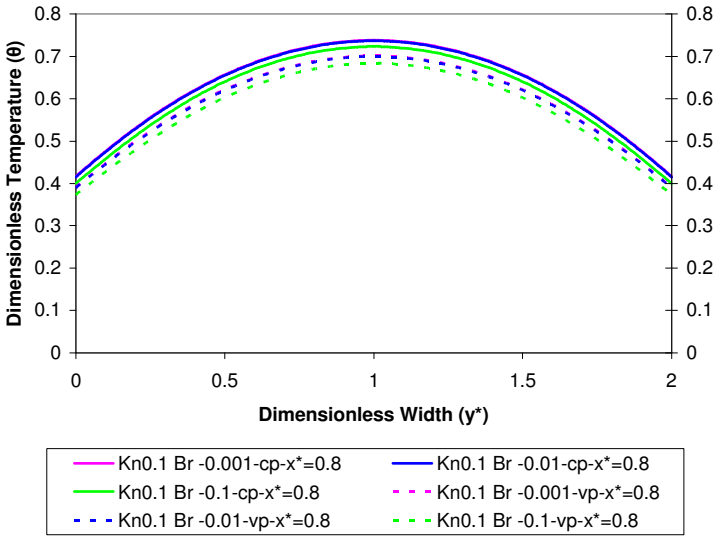

Figure A.117 Variation of dimensionless temperature with dimensionless width of the channel at crossection x*=0.8 for various negative Brinkman numbers (Kn=0.1, Pe=1)

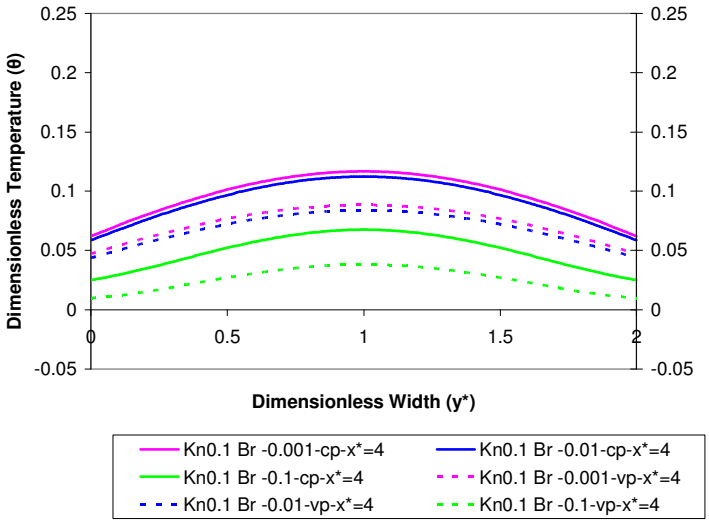

Figure A.118 Variation of dimensionless temperature with dimensionless width of the channel at crossection x*=4 for various negative Brinkman numbers (Kn=0.1, Pe=1)

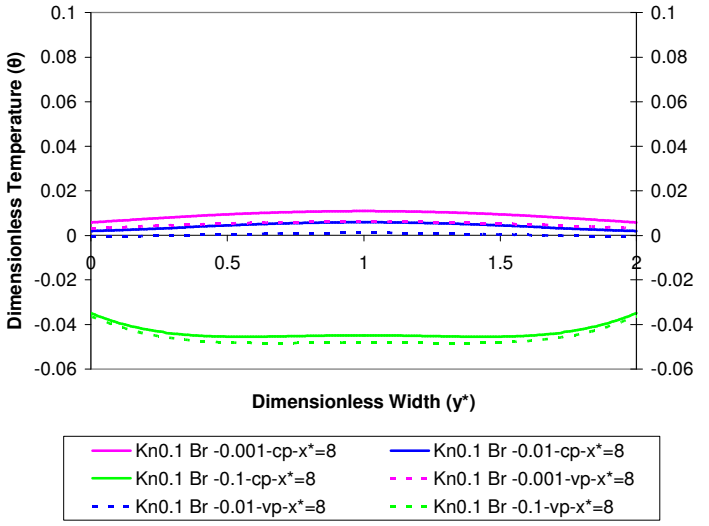

Figure A.119 Variation of dimensionless temperature with dimensionless width of the channel at crossection x*=8 for various negative Brinkman numbers (Kn=0.1, Pe=1)

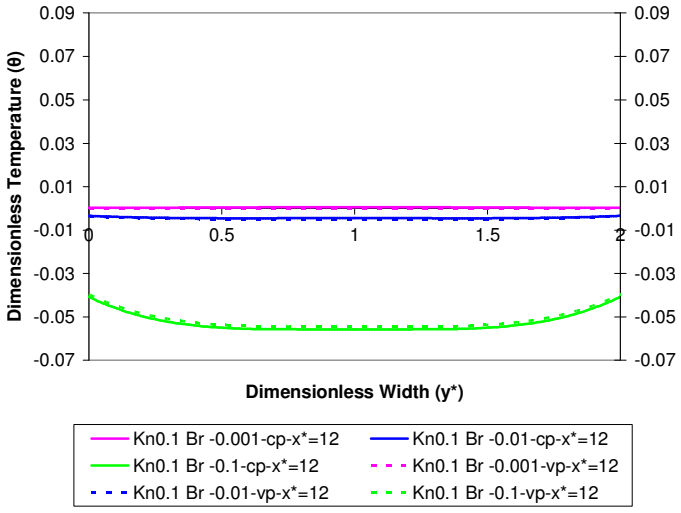

Figure A.120 Variation of dimensionless temperature with dimensionless width of the channel at crossection x*=12 for various negative Brinkman numbers (Kn=0.1, Pe=1)

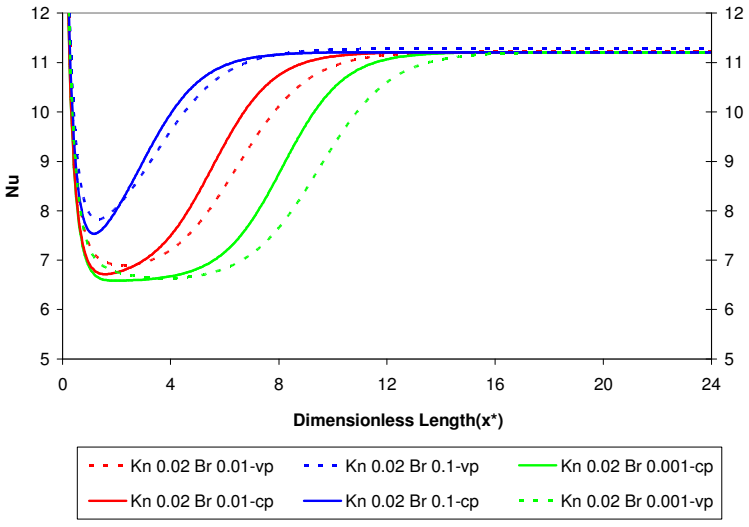

Figure A.121 Variation of Nusselt number with axial position for various positive Brinkman numbers, obtained from constant and variable property solutions (Kn=0.02, Pe=1)

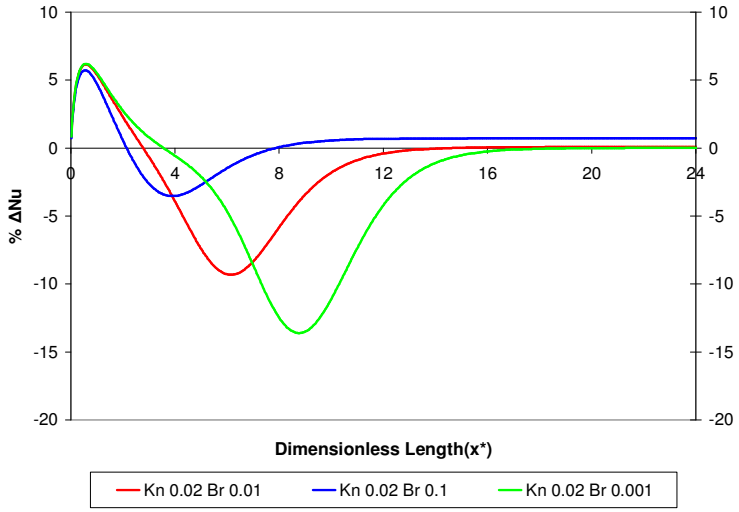

Figure A.122 Variation of percent difference in Nusselt numbers between constant and variable property solutions with axial position for various positive Brinkman numbers (Kn=0.02, Pe=1)

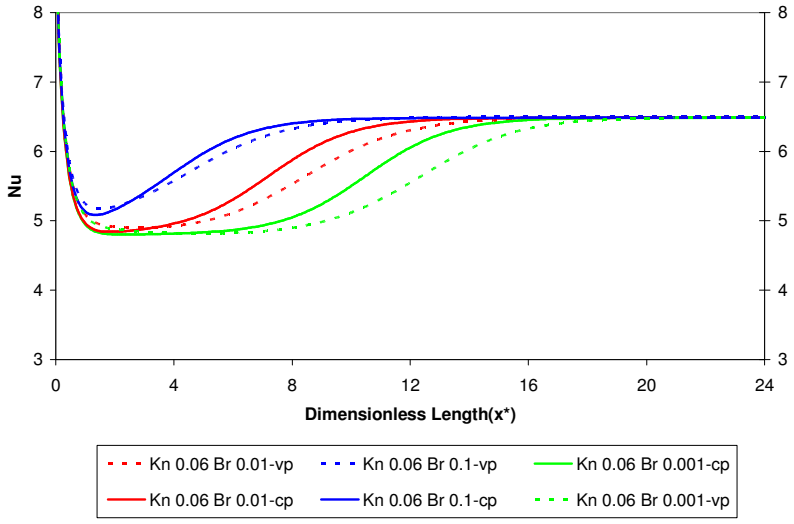

Figure A.123 Variation of Nusselt number with axial position for various positive Brinkman numbers, obtained from constant and variable property solutions (Kn=0.06, Pe=1)

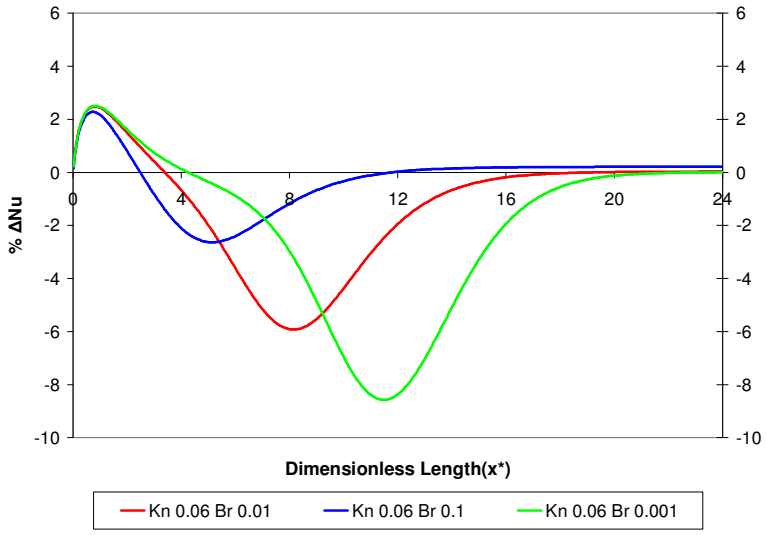

Figure A.124 Variation of percent difference in Nusselt numbers between constant and variable property solutions with axial position for various positive Brinkman numbers (Kn=0.06, Pe=1)

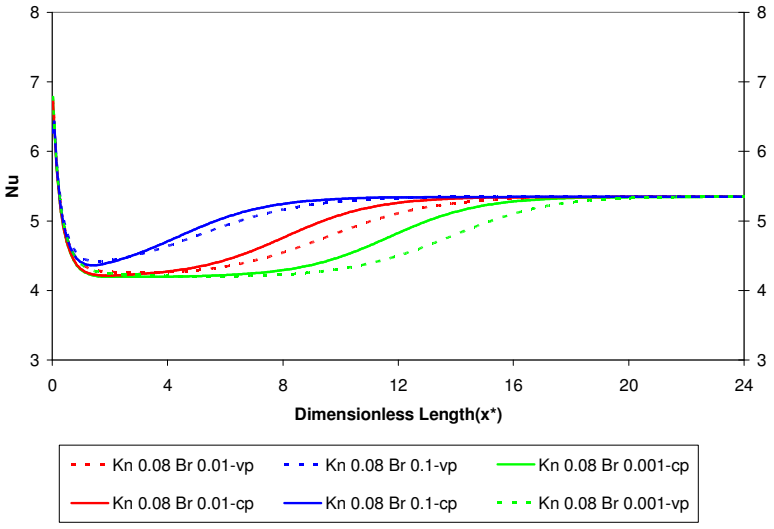

Figure A.125 Variation of Nusselt number with axial position for various positive Brinkman numbers, obtained from constant and variable property solutions (Kn=0.08, Pe=1)

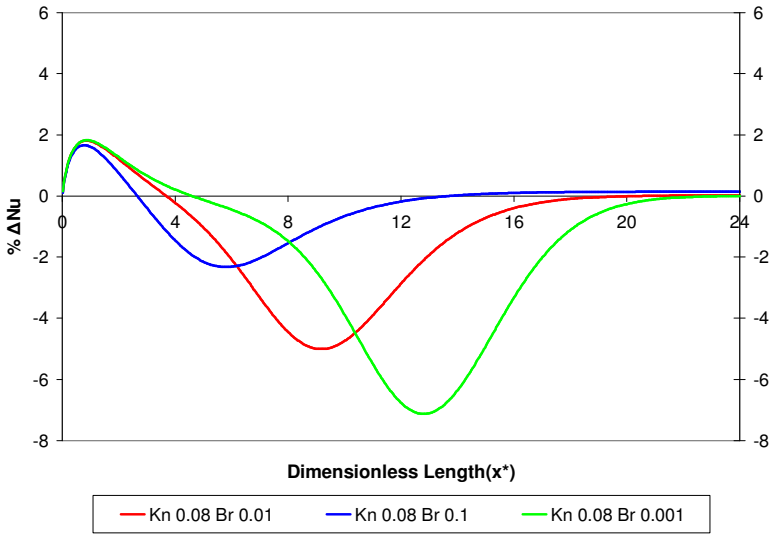

Figure A.126 Variation of percent difference in Nusselt numbers between constant and variable property solutions with axial position for various positive Brinkman numbers (Kn=0.08, Pe=1)

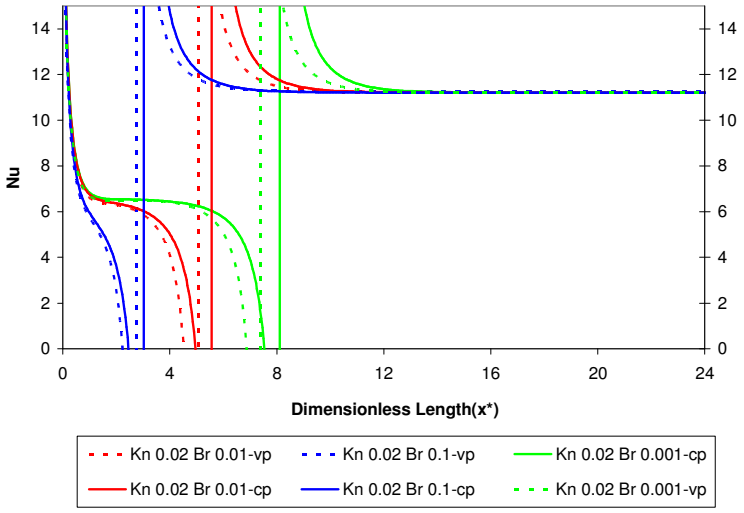

Figure A.127 Variation of Nusselt number with axial position for various negative Brinkman numbers, obtained from constant and variable property solutions (Kn=0.02, Pe=1)

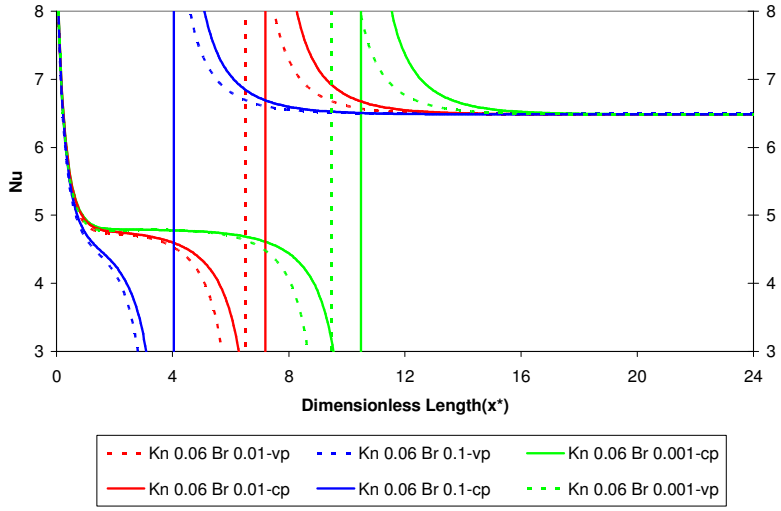

Figure A.128 Variation of Nusselt number with axial position for various negative Brinkman numbers, obtained from constant and variable property solutions (Kn=0.06, Pe=1)

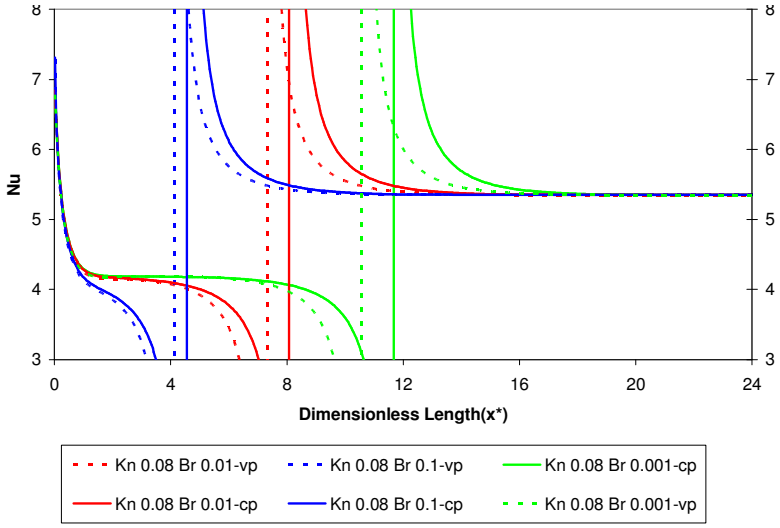

Figure A.129 Variation of Nusselt number with axial position for various negative Brinkman numbers, obtained from constant and variable property solutions (Kn=0.08, Pe=1)